

ALMA MATER STUDIORUM – UNIVERSITY OF BOLOGNA

**DEPARTMENT OF ELECTRIC, ELECTRONIC AND INFORMATION
ENGINEERING “GUGLIELMO MARCONI”**

Ph.D in Electrical Engineering

XXVI CYCLE

Power Electronics,Electrical Machines and Drives (ING-IND/32)

**Grid Connected Doubly Fed Induction
Generator Based Wind Turbine under LVRT**

by

Subramanian Chandrasekaran

Tutor:

Prof. Domenico Casadei

PhD Coordinator:

Prof. Domenico Casadei

March 2014, Bologna, Italy

Acknowledgment

This research project has been carried out at the Department of Electrical, Electronics and Information Engineering at University of Bologna. The financial support provided by “**Erasmus Mundus External Cooperation Window Lot 13 India-INDIA 4EU**” is gratefully acknowledged.

First of all, I would like to express my deep and sincere gratitude to my supervisor **Prof. Domenico Casadei** for his excellent supervision and helps during this work. I would like to thank all my professors at the Department of Electrical Engineering for all their technical, professional and administrative support. I want in special thanks to, **Prof. Claudio Rossi, Prof. Angelo Tani, Prof. Gabriele Grandi, Prof. K. Rajambal** and my Erasmus Coordinator **Livia Mercatelli**.

My PhD work was furthermore Co-supervised by Prof. **Poul Sørensen** in Wind Energy System at Technical University of Denmark (DTU). It is a pleasure for me to take the opportunity to thank all my colleagues in the research group.

My greatest thanks go to the person, who aided me during my final stage of PhD work. I would like to express my deepest gratitude to **Prof. Frede Blaabjerg**, my co supervisor at Aalborg University (Energy Technology), Aalborg, for all his guidance and support as well as teaching me numerous skills of doing scientific work. My colleagues at AAU made me feel so comfortable work with them especially Prof. Francesco Iannuzzo, Wenjie Chen, Yan, Rui, and Milla.

Many thanks go to all my colleagues at Electrical Engineering, who have assisted me during the work of this Ph.D. thesis especially Sanjeevi Kumar, Filippo and Marco Casali.

Finally, I owe my gratitude to my late Appa, my Amma, my brother, my sisters and my family members of everyone especially Manu Shri, Bhaviya Shri, Janesh and Jahnavi, for all their love and support during my personal and professional education.

I want to thank God for his help and his mercy.

“God gave not to us the spirit of dread, but of virtue, and of love, and of soberness”
(Tim. 1,7)

ABSTRACT

This project concentrates on the Low Voltage Ride Through (LVRT) capability of Doubly Fed Induction Generator (DFIG) wind turbine. The main attention in the project is, therefore, drawn to the control of the DFIG wind turbine and of its power converter and to the ability to protect itself without disconnection during grid faults. It provides also an overview on the interaction between variable speed DFIG wind turbines and the power system subjected to disturbances, such as short circuit faults. The dynamic model of DFIG wind turbine includes models for both mechanical components as well as for all electrical components, controllers and for the protection device of DFIG necessary during grid faults. The viewpoint of this project is to carry out different simulations to provide insight and understanding of the grid fault impact on both DFIG wind turbines and on the power system itself. The dynamic behavior of DFIG wind turbines during grid faults is simulated and assessed by using a transmission power system generic model developed and delivered by Transmission System Operator in the power system simulation toolbox Digsilent, Matlab/Simulink and PLECS.

Keywords: Doubly fed induction generators (DFIG); Wind turbine control; Power converter control; Grid faults, LVRT control.

TABLE OF CONTENTS

Chapter 1: INTRODUCTION.....	1
1.1 Background in wind Power.....	1
1.2 Wind Power Market.....	1
1.3 Wind Power Industry.....	3
1.4 References.....	6
Chapter 2: WIND ENERGY CONVERSION SYSTEM (WECS)	10
2.1 Wind Turbine Components.....	10
2.2 Wind Model.....	12
2.3 Wind Speed Distribution.....	15
2.4 Limitations.....	17
2.5 Characteristics of Different Wind Turbine Concepts.....	18
2.6 Market Penetration.....	21
2.7 Variable Speed Wind Turbines versus Fixed Speed Wind Turbines.....	23
2.8 References.....	25
Chapter 3: DYNAMIC MODELLING OF DOUBLY FED INDUCTION GENERATOR (DFIG) WIND TURBINE SYSTEM.....	28
3.1 Aerodynamic Model.....	28
3.1.1 Power Extraction from the Air Stream.....	28
3.2 Variable Speed Wind Turbines (VSWT)	31
3.2.1 Modeling of Variable Speed Wind Turbine.....	32
3.2.1.1 Aerodynamic Wind Turbine Model.....	33
3.2.1.2 Mechanical System.....	33
3.2.1.3 Pitch System.....	35
3.2.1.4 Control of Variable Speed Wind Turbine (VSWT)	36
3.2.1.5 Turbine Speed Control Regions.....	37
3.2.1.6 Regions 1 And 3.....	39
3.2.1.7 Region 2: Maximum Power Tracking.....	39
3.2.1.8 Indirect Speed Controller (ISC)	40
3.2.1.9 Direct Speed Controller (DSC)	42
3.2.1.10 Region 4: Power Control.....	43
3.3 Doubly Fed Induction Generator (DFIG)	43
3.3.1 Power Flow/Operating Modes of DFIG.....	44
3.3.2 Sub-Synchronous Speed Mode.....	44
3.3.3 Super-Synchronous Speed Mode.....	45
3.3.4 Synchronous Speed Mode.....	47

3.3.5 Modeling of DFIG.....	48
3.3.6 Grid Side Control Description.....	54
3.3.7 Grid Model in DFIG System.....	60
3.4 References.....	62

Chapter 4: POWER FLOW ANALYSIS OF DFIG WIND TURBINE SYSTEM.....66

4.1 Introduction.....	66
4.2 System Performance under Rated Wind Speed.....	67
4.3 Maximum Power Point Tracking.....	70
4.4 System Performance under Variable Wind Speed.....	71
4.5 Summary.....	77
4.6 References.....	78

Chapter 5: GRID CODE REQUIREMENTS.....81

5.1 Frequency and Voltage operating Range.....	82
5.2 Reactive Power and Voltage Control Capability.....	83
5.3 Voltage Support.....	84
5.4 Reactive Power Wind Turbine Operation Modes.....	84
5.5 Power Control.....	85
5.6 Active Power Wind Turbine Operation Modes.....	86
5.7 Inertial Response.....	86
5.8 Power System Stabilizer Function.....	87
5.9 Low Voltage Ride Through (LVRT)	88
5.9.1 Voltage dips and LVRT.....	88
5.9.2 Electric Power System.....	89
5.9.3 Origin of Voltage dips.....	90
5.9.4 Voltage dips.....	92
5.9.5 Classification.....	93
5.9.6 Transformer Effect.....	95
5.6.1 Transformer effect in a Wind Farm.....	95
5.7 References.....	97

Chapter 6: LOW VOLTAGE RIDE THROUGH (LVRT) CAPABILITY OF DFIG WIND TURBINE.....100

6.1 Improved Control Strategies Implementation.....	101
6.2 LVRT Strategies with Hardware Implementation.....	102
6.3 Performance of the DFIG during Voltage Dips with an Active Crowbar.....	103
6.3.1 Crowbar Protection Circuit.....	103
6.3.2 Development of the Crowbar Circuit.....	103
6.3.3 Modeling of the Active Crowbar.....	105
6.4 Synthetic Control and Protection Strategy.....	106
6.4.1 Hysteresis Control of the Crowbar.....	106
6.4.2 Demagnetization of DFIG under Grid Voltage Dips.....	107

6.4.3 Requirements and Strategies.....	108
6.5 Simulation Results.....	108
6.6 Summary.....	113
6.7 Dynamic Voltage Restorer (DVR)	114
6.7.1 Control Methods.....	115
6.7.2 Simulation Results.....	117
6.7.3 Measurement Results.....	119
6.7.4 Summary.....	121
6.8 Vector Proportional Integral (VPI) Controller.....	122
6.8.1 Dynamic behaviour of the DFIG System.....	123
6.8.2 VPI Controller Synthesis.....	125
6.8.3 Simulation Results.....	128
6.8.4 Summary.....	132
6.9 Hardware Implementation and Experimental Results.....	133
6.9.1 Case 1(Steady State Condition)	134
6.9.2 Case 2(Unbalanced Grid Supply)	135
6.9.3 Derivation of Current References for DFIG Wind Turbine.....	136
6.9.3.1 Instantaneous Active and Reactive Power Control (IARC)	136
6.9.3.2 Positive and Negative Sequence Compensation (PNSC)	136
6.9.3.3 Average Active and Reactive Power Control (AARC)	137
6.9.3.4 Balanced Positive Sequence (BPS)	137
6.9.4 Case 1.....	138
6.9.5 Case 2.....	141
6.9.6 Summary.....	144
6.10 References.....	145

**Chapter 7: ELECTRICAL SIMULATION MODELS-IEC 61400-27-1:
DFIG WIND TURBINE (TYPE 3)153**

7.1 Wind Turbines.....	155
7.1.1 Scope.....	155
7.1.2 Wind Turbine Model Interface.....	156
7.2 Generic Modular Structure.....	157
7.3 Type 3.....	157
7.3.1 Definition of Type 3(DFIG)	157
7.3.2 Model Specification of Type 3.....	158
7.3.3 Linearised Aerodynamic Model.....	160
7.3.4 Mechanical Models.....	161
7.3.5 Asynchronous Generator Model.....	162
7.3.6 Electrical Equipment.....	164
7.4 Control Models.....	164
7.4.1 Pitch Control Emulator Model.....	164
7.4.2 P Control Model Type 3.....	165
7.4.3 Q Control Model.....	167
7.4.4 Current Limitation Model.....	171
7.4.5 Pitch Angle Control Model.....	172
7.4.6 Grid Protection Model.....	173

7.5 Simulation Results.....	174
7.5.1 steady State Analysis.....	174
7.5.2 LVRT Analysis.....	174
7.6 Summary.....	178
7.7 References.....	179
Chapter 8: SUMMARY.....	181
ANNEXURE I.....	182
ANNEXURE II.....	188
ANNEXURE III.....	191

CHAPTER 1

INTRODUCTION

For centuries the winds have been used to grind grain and although present applications powered by the wind have other purposes than grinding grain, almost any wind powered machine -no matter what job it does -is still called a *windmill*. In the 1920's and 1930's, before electric wires were stretched to every community, small wind generators were used to power lights and appliances. At the instance of the growth in the world-wide infrastructure with widely distributed electrical power, the use of wind generators has been almost suspended for several decades. Among others, a consequence of the oil shock of the 1970's is that the global energy policy of today is towards renewable energy resources and for that reason, the windmill has become its renaissance. This chapter introduces the reader to the trends in modern wind turbine development in annual capacity, installed capacity and wind turbine manufacturer companies.

1.1 BACKGROUND IN WIND POWER

Today, modern energy industry faces a growing awareness regarding the impact of conventional power generation on the environment. An issue such as limited fossil fuel reserves, climate change due to C_{O_2} emissions, brings to attention alternative technologies to generate electricity in a more sustainable manner [1]. As global energy demand is constantly rising, there is a great responsibility for society to develop the green technologies for reducing its impact on the environment. In the trend of diversifying the energy market, wind power is the most rapidly growing sector. After the oil crisis from three decades ago, wind power industry started to flourish. Since then wind turbine technology improved rapidly and it soon took the title of champion from all renewable sources of energy.

1.2 WIND POWER MARKET

During 2012, almost 45 GW of wind power capacity began operation, increasing global wind capacity 19% to almost 283 GW [2] (See Figure: 1). It was another record year for wind power, which again added more capacity than any other renewable technology despite policy uncertainty in key markets [3]. The top 10 countries accounted for more than 85% of year-end global capacity, but the market continued to broaden [4]. Around 44 countries added capacity during 2012, at least 64 had more than 10 MW of reported capacity by year's end, and 24 had more than 1 GW in operation [5]. From the end of 2007 through 2012, annual growth rates of cumulative wind power capacity averaged 25% [6].

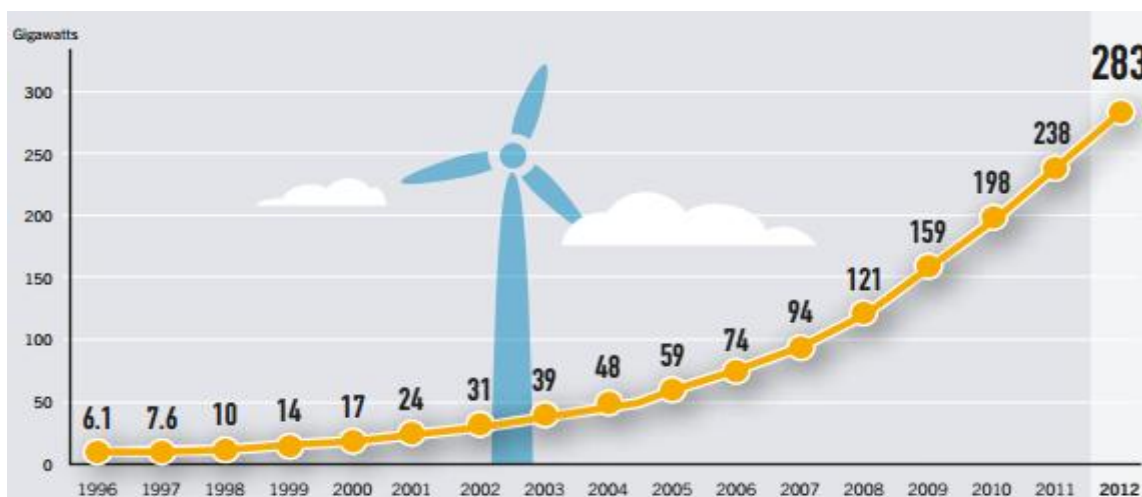


Figure: 1. Wind Power Global Capacity, 1996–2012.

For the first time since 2009, the majority of new capacity was installed in the OECD, due largely to the United States [7]. Developing and emerging economies are moving firmly into the mainstream, however. The United States and China together accounted for nearly 60% of the global market in 2012, followed distantly by Germany, India, and the United Kingdom [8]. Others in the top 10 for capacity added were Italy, Spain, Brazil, Canada and Romania [9]. The EU represented about 27% of the world market and accounted for just over 37% of total global capacity (down from 40% in 2011)[10].

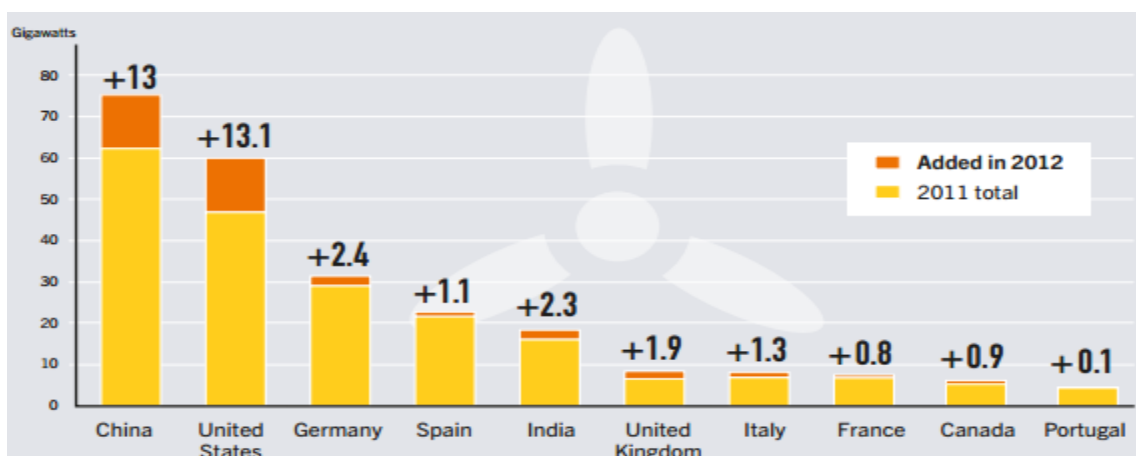


Figure: 2. Wind Power Capacity and Additions, Top 10 Countries, 2012.

The United States had its strongest year yet and was the world's top market in 2012[11] (See Figure: 2). U.S. installations nearly doubled relative to 2011, with almost 64% of the 13.1 GW added coming on line in the year's final quarter [12]. The strong market was driven by several factors including increased domestic manufacturing of turbine parts and technology improvements that are increasing efficiency and driving down costs; most important,

however, was the expected expiration of the federal Production Tax Credit [13]. Wind power represented as much as 45% of all new electric generating capacity in the United States, outdoing natural gas for the first time, and the 60 GW operating at year's end was enough to power the equivalent of 15.2 million U.S. homes [14]. The leading states for capacity added were Texas (1.8 GW), with more than 12 GW in operation, California (1.7 GW), and Kansas (1.4 GW), and 15 states had more than 1 GW in operation by year's end [15].

The European Union passed the 100 GW milestones in 2012, adding a record 11.9 GW of wind capacity for a total exceeding 106 GW [16]. Wind power came in second for electric capacity added (26.5%), behind solar PV (37%) and ahead of natural gas (23%); by year's end, wind accounted for 11.4% of total EU electric capacity [17]. Despite record growth, there is concern that the EU lags on its National Renewable Energy Action Plan (NREAP) targets, and that 2012 additions do not reflect growing economic and policy uncertainty (most capacity was previously permitted and financed) [18]. Some emerging markets are poised for significant growth, but grid connectivity and economic issues pose challenges to future development in much of Europe, as do land issues arising from having so much capacity on shore [19].

1.3 WIND POWER INDUSTRY

During 2005–2009, turbine prices increased in response to growing global demand, rising material costs, and other factors; since then, however, growing scale and greater efficiency have combined to improve capacity factors and reduce costs of turbines as well as operations and maintenance [20]. Oversupply in global turbine markets has further reduced prices, benefitting developers by improving the cost-competitiveness of wind power relative to fossil fuels. However, the industry has been challenged by downward pressure on prices, combined with increased competition among turbine manufacturers, competition with low-cost gas in some markets, and reductions in policy support driven by economic austerity [21]. Relative to their 2008 peak, turbine prices fell by as much as 20–25% in western markets and more than 35% in China before stabilising in 2012 [22].

The costs of operating and maintaining wind farms also dropped significantly due to increased competition among contractors and improved turbine performance [23]. As a result, onshore wind-generated power is now cost competitive with or cheaper than conventional power in some markets on a per kilowatt-hour basis (including some locations in Australia, India, and the United States), although new shale gas in some countries is making it more difficult for wind (and other renewable) to compete with natural gas [24]. Offshore wind remains at least twice as expensive as onshore [25].

The world's top 10 turbine manufacturers captured 77% of the global market and, as in 2011, they hailed from China (4), Europe (4), India (1), and the United States (1). Vestas (Denmark), the top manufacturer since 2000, surrendered its lead to GE Wind (third in 2011), which blew ahead due mainly to the strong U.S. market [26]. Siemens moved from ninth to third, followed by Enercon (Germany) and Suzlon Group (India), both of which moved up one spot relative to 2011 [27]. Other top companies were Gamesa (Spain) and Goldwind, United Power, Sinovel, and Mingyang (all China); both Goldwind and Gamesa dropped out of the top five [28] (See Figure 3).

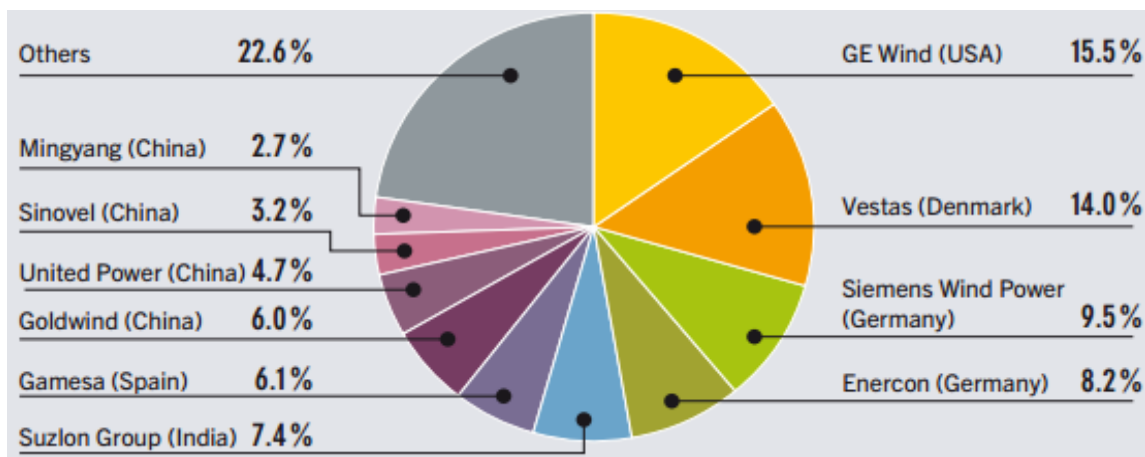


Figure: 3. Market Shares of Top 10 Wind Turbine Manufacturers, 2012.

According to Global Wind Energy Council more than 160 GW of installed capacity has been achieved by the end of 2009 around the world. Also a total power increase of 35% is accomplished in the year 2009 in the world. Thus a new record per annum of installed wind power capacity has been reached, summing up in 38 GW around the world. Europe accounts for 50% of the total amount of installed Wind Power around the world [29]. Figure 4 shows the continuously growing trend of wind power installations inside European Union. This reference scenario shows that with installations of up to 300 GW by the year 2030, EU will have a 21% to 28% wind market penetration [30].

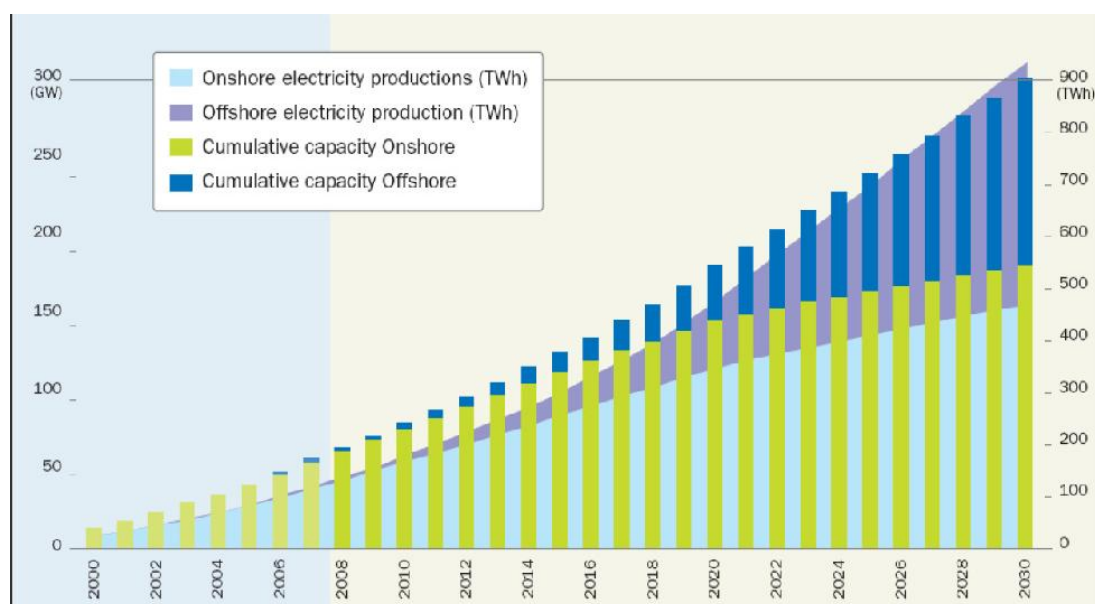


Figure: 4. EU Wind Power Forecast for 2030.

Along with the increasing demands for wind power, the turbine technologies are improving and thus equipment costs are reducing. Because the wind industry is a well established power house on the renewable market, its prices per kWh are comparable with prices of the conventional energy generations. Unlike gas, coal and oil resources which in future will become scarce, and for which the technologies became mature decades ago, the wind energy is abundant and new improvements on aerodynamics and power electronic devices are still to come. Therefore by 2030 electricity production from wind will inevitably become cheaper than any other source of energy, currently having a high market share [31].

There is a good correlation between wind turbines costs and their sizes. Unlike solar panels, which remain at the same price regardless of array size, wind turbines become cheaper with increased system size. The practical explanation is that the power delivered by the wind turbine depends on the square of the rotor diameter. Figure 5 shows the evolution of wind turbine size with respect to year of production. It is seen that in the last 20 years the rotor diameter has increased by a factor of 10. Today state-of-the-art wind turbines, with 126 m rotor diameter, produce 5 to 6 MW of power [32-33].

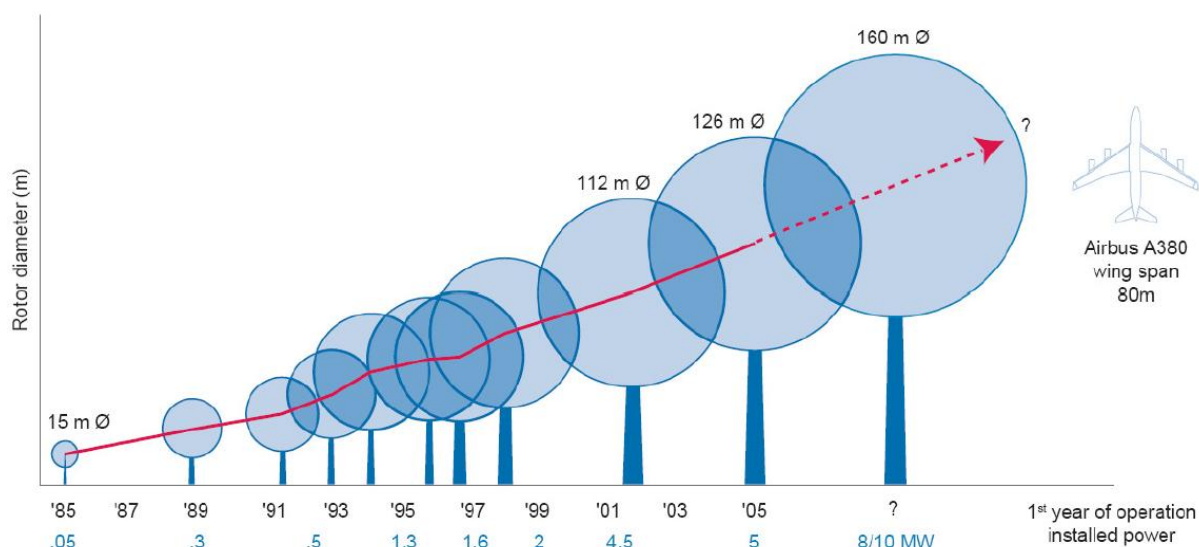


Figure 5. Increase of wind turbine size over the years.

In order to better control more and more wind power fed into the network, these MW range wind turbines are usually connected together either onshore or offshore to form a wind farm. However, including larger (hundreds of MW) wind farms into the grid, will raise the wind power penetration to a point at which it will have a significant impact on power system operation. Already some regulatory tasks needed for system stability, are being performed by wind power plants. With the ever increasing of wind power in the energy mix, Transmission System Operator (TSO) is forced to impose new requirements on the wind farms for the well-functioning of the power system network.

1.4 REFERENCES

[1] European Commission "20 20 by 2020 Europe's climate change opportunity", 2008, Brussels.

[2] A total of 44,799 MW was added in 2012, bringing the year-end total to 282,587 MW, according to Global Wind Energy Council (GWEC), Global Wind Report – Annual Market Update 2012 (Brussels: April 2013); 44,951 MW added for total of 285,761 MW from Navigant's BTM Consult, International Wind Energy Development: World Market Update 2012 (Copenhagen: March 2013); 44,712 MW added from C. Ender, "Wind Energy Use in Germany – Status 31.12.2012," DEWI Magazine (German Wind Energy Institute), February 2013, p. 31. Up 19% (18.7%) based on data for 2011 and 2012 from GWEC, op. cit. this note, and from Navigant's BTM Consult, op. cit. this note. Figure 18 based on GWEC, op. cit. this note, and on Navigant's BTM Consult, op. cit. this note.

[3] Key markets with policy uncertainty included the United States, Europe (Spain, Italy, France, Portugal, the U.K.), Asia (India, Japan), and Australia.

[4] Estimate of 86% based on GWEC, op. cit. note 1, and on Navigant's BTM Consult, op. cit. note 1.

[5] Figures of 44, 64, and 24 countries from GWEC, op. cit. note 1; 24 also from Navigant's BTM Consult, op. cit. note 1. The 24 countries include 15 in Europe, four in the Americas, three in Asia, plus Australia and Turkey. Note that GWEC has 79 countries in its database, per GWEC, personal communication with REN21, April 2013, and that there are 100 countries or regions with wind power capacity, per World Wind Energy Association (WWEA), World Wind Energy Report 2012 (Brussels: May 2013).

[6] Estimate of 24.9% from Navigant's BTM Consult, op. cit. note 1; 24.7% from GWEC, op. cit. note 1.

[7] GWEC, op. cit. note 1.

[8] The United States added 13,131 MW, per American Wind Energy Association (AWEA), "AWEA U.S. Wind Industry Annual Market Report, Year Ending 2012" (Washington, DC: April 2013), Executive Summary. It was followed by China (12,960 MW), Germany (2,415 MW), India (2,336 MW), and the United Kingdom (1,897 MW), per GWEC, op. cit. note 1, and Navigant's BTM Consult, op. cit. note 1. Note that data from both sources agree for all countries except the U.K., which added 1,958 MW according to Navigant's BTM Consult.

[9] Additions were Italy (1,273 MW), Spain (1,122 MW), Brazil (1,077 MW), Canada (935 MW), and Romania (923 MW), per GWEC, op. cit. note 1. Rankings are the same with only slight differences in added capacity, per Navigant's BTM Consult, op. cit. note 1. Mexico was in the top 10 according to WWEA, op. cit. note 4.

[10] Share of the global market was 26.6% and share of total global capacity was 37.5%, based on data from GWEC, op. cit. note 1; share of global market was 28.5% and share of the global total was 38.5%, based on data from Navigant's BTM Consult, op. cit. note 1.

[11] AWEA, op. cit. note 7. Figure 19 based on various sources throughout this section.

[12] The United States added 13,131 MW in 2012, according to AWEA, op. cit. note 7; 6.8 MW were added in 2011, per AWEA, "Annual industry report preview: supply chain, penetration grow," Wind Energy Weekly, 30 March 2012.

[13] Vince Font, “AWEA Reports 2012 the Strongest Year on Record for U.S. Wind Energy, Continues Success Uncertainty,” RenewableEnergyWorld.com, 23 October 2012.

[14] Wind accounted for more than 45% of U.S. electric capacity additions in 2012 (based on 12,799 MW of wind capacity added), per U.S. Energy Information Administration (EIA), “Wind Industry Brings Almost 5,400 MW of Capacity Online in December 2012,” www.eia.gov/electricity/monthly/update/?scr=email, viewed 25 April 2013. Wind was nearly 41% and natural gas accounted for 33% of U.S. capacity additions in 2012, based on data from U.S. Federal Energy Regulatory Commission, Office of Energy Projects, “Energy Infrastructure Update for December 2012” (Washington, DC: 2013). Wind accounted for 42% (based on preliminary 13,124 MW added), according to AWEA, “4Q report: Wind energy top source for new generation in 2012; American wind power installed new record of 13,124 MW,” Wind Energy Weekly, 1 February 2013. The United States ended 2012 with 60,007 MW, per AWEA, op. cit. note 7.

[15] Texas added 1,826 MW, followed by California (1,656 MW), Kansas (1,440 MW), Oklahoma (1,127 MW), and Illinois (823 MW), per AWEA, “4Q report...,” op. cit. note 13; more than 12 GW in Texas and 15 states from AWEA, op. cit. note 7.

[16] China added an estimated 12,960 MW of capacity in 2012, from Chinese Wind Energy Association (CWEA), with data provided by Shi Pengfei, personal communication with REN21, 14 March 2013; from GWEC, op. cit. note 1; and from Navigant’s BTM Consult, op. cit. note 1. Note that 15,780 MW of capacity was brought into operation (including capacity previously installed), per China Electricity Council, with data provided by Pengfei, op. cit. this note. Share of world market was about 27% in 2012, down from 43% in 2011 and 49.5% in 2010, per GWEC, op. cit. note 1. Decline relative to 2009–2011 based on data from GWEC, op. cit. note 1.

[17] Shruti Shukla, GWEC, personal communication with REN21, 13 February 2013; Zoë Casey, “The Wind Energy Dragon Gathers Speed,” Wind Directions, June 2012, pp. 32, 34.

[18] CWEA, op. cit. note 15.

[19] Figure of 75,324 MW installed by year-end from GWEC, op. cit. note 1, and from CWEA, op. cit. note 15. About 14.5 GW of installed capacity was not yet officially operating at year’s end, based on data from CWEA and from China Electricity Council, provided by Pengfei, op. cit. note 15; most of the capacity added in 2012 was feeding the grid, per Steve Sawyer, GWEC, personal communication with REN21, 2 April 2013. Note that the process of finalising the test phase and getting a commercial contract with the system operator takes time, accounting for delays in reporting. The difference is explained by the fact there are three prevailing statistics in China: installed capacity (turbines installed according to commercial contracts); construction capacity (constructed and connected to grid for testing); and operational capacity (connected, tested, and receiving tariff for electricity produced). Liming Qiao, GWEC, personal communication with REN21, 26 April 2013.

[20] Figures of 100.4% and 37%, and exceeding nuclear from China Electricity Council, provided by Pengfei, op. cit. note 15.

[21] CWEA, op. cit. note 15; 14 with more than 1 GW from GWEC, op. cit. note 1.

[22] The EU added 11,895 MW for a total of 106,041 MW, from European Wind Energy Association (EWEA), *Wind in Power: 2012 European Statistics* (Brussels: February 2013); new record from GWEC, “Release of Global Wind Statistics: China, US vie for market leader position at just over 13 GW of new capacity each” (Brussels: 11 February 2013). All of Europe added 12,744 MW for a total of 109,581 MW, from EWEA, *op. cit.* this note. Accounting for closings and repowering, the EU’s net capacity increase was lower, *per idem*.

[23] EWEA, *op. cit.* note 21. Wind’s share of capacity added was up from 21.4% in 2011, and its share of total electric generating capacity in 2012 was up from 2.2% in 2000 and 10.4% in 2011.

[24] NREAP targets for end-2012 totaled 107.6 GW, from EWEA, *op. cit.* note 21, and from Shruti Shukla, GWEC, personal communication with REN21, 13 February 2013. Market in 2012 does not reflect growing uncertainty because most capacity was previously permitted and financed, *per EWEA, op. cit.* note 21.

[25] Some emerging markets are spurred by rapid increases in electricity demand, a desire for independence from Russian gas, good wind resources, and new support policies, from Tildy Bayar, “Can Emerging Wind Markets Compensate for Stagnating European Growth” *RenewableEnergyWorld.com*, 25 January 2013, and from EWEA, “Eastern Winds: Emerging European Wind Power Markets” (Brussels: February 2013); challenges from Steve Sawyer, GWEC, personal communication with REN21, 4 September 2012.

[26] Germany installed 2,415 MW in 2012, EWEA, *op. cit.* note 21; year-end total of 31,315 MW (31,035 MW onshore plus 280 MW offshore) and highest additions since 2002 or 2003 based on data from German Federal Ministry for the Environment, Nature Conservation and Nuclear Safety (BMU), “Renewable Energy Sources 2012,” data from Working Group on Renewable Energy- Statistics (AGEE-Stat), provisional data (Berlin: 28 February 2013), p. 18. Much of the capacity added was for repowering: 1,433 MW of new turbines replaced 626 MW of old ones, *per* “German wind sector strong again in 2012,” *RenewablesInternational.net*, 1 February 2012.

[27] The United Kingdom added 1,897 MW (854 MW offshore) for a total of 8,445 MW, from EWEA, *op. cit.* note 21, and from GWEC, *op. cit.* note 1. It added 1,958 MW for a total of 9,113 MW, according to Navigant’s BTM Consult, *op. cit.* note 1.

[28] Italy added 1,273 MW for a total of 8,144 MW; Spain added 1,122 MW for a total of 22,796 MW; Romania added 923 MW for a total of 1,905 MW; and Poland added 880 MW for a total of 2,497 MW, all from EWEA, *op. cit.* note 21. Italy added 1,272 MW for a total of 7,998 MW, and Spain added 1,112 MW for a total of 22,462 MW, from Navigant’s BTM Consult, *op. cit.* note 1.

[29] EWEA, *op. cit.* note 21.

[30] India added an estimated 2,336 MW in 2012 for a year-end total of 18,421 MW, from GWEC, *op. cit.* note 1. This compares with about 3 GW installed during 2011, from GWEC, *Global Wind Report: Annual Market Update 2011* (Brussels: March 2012).

[31] Steve Sawyer, GWEC, personal communication with REN21, 5 December 2012; Natalie Obiko Pearson, “India Wind Investment May Stall on Tax-Break cut, Industry Says,” *Bloomberg News*, 2 April 2012, at www.businessweek.com.

[32] Asia (almost entirely China and India) added 15,510 MW in 2012, and North America (not including Mexico) added 14,059 MW, per GWEC, op. cit. note 1. Europe (not including Russia or Turkey) added 12,238 MW (EU-27 added 11,895 MW), per EWEA, op. cit. note 21. Note that Europe lost its position as top regional installer in 2012, per Navigant's BTM Consult, op. cit. note 1.

[33] Brazil added an estimated 1,077 MW in 2012 for a total of 2,508 MW and 4 million, from GWEC, op. cit. note 1, and from Associação Brasileira de Energia Eólica, Boletim Mensal de Dados do Setor Eólico – Público," January 2013, p. 2, at www.abeeolica.org.br. The strong market in Brazil has attracted European developers as subsidies decline at home, per Vittorio Perona, Grup BTG Pactual SA, cited in Stephan Nielsen, "Cheapest wind energy spurring renewable deals in Brazil," RenewableEnergyWorld.com, 29 January 2013.

CHAPTER 2

WIND ENERGY CONVERSION SYSTEM (WECS)

2. INTRODUCTION

The aim of this chapter is to provide the basic concepts to understand a wind energy conversion system and the way it must be operated to be connected to the utility grid. It covers general background on wind turbine knowledge, different topology of WECS, not only related to the electrical system, but also to the mechanical and aerodynamics characteristics of wind turbines [1-10].

2.1 WIND TURBINE COMPONENTS

The entire system of a grid connected wind turbine includes several components, which contribute with their specific function in the energy conversion process from wind energy into electrical energy. Figure 2.1 illustrates the main components of a modern wind turbine, which are to a greater or lesser extent common for all wind turbine concepts.

The Figure 2.1 illustrates from left to right the aero dynamical and mechanical part of the wind turbine (aerodynamic rotor and gearbox), the electrical system (generator, power electronic interface and transformer) and finally its connection to the grid [11-15]. An interaction with the control system is indicated as well. The different turbine components can be subsumed under four main groups.

1. Mechanical and aero dynamical components:

- Rotor effective wind
- Turbine rotor
- Blade pitching mechanism
- Drive train (flexible shaft, bearings)
- Emergency breaks
- Gear
- Tower

2. Electrical components

- Generator types
 - ❖ Squirrel cage induction generator
 - ❖ Wound rotor induction generator
 - ❖ Doubly-fed induction generator
 - ❖ Permanent magnet synchronous generator
 - ❖ Electrical excited synchronous generator

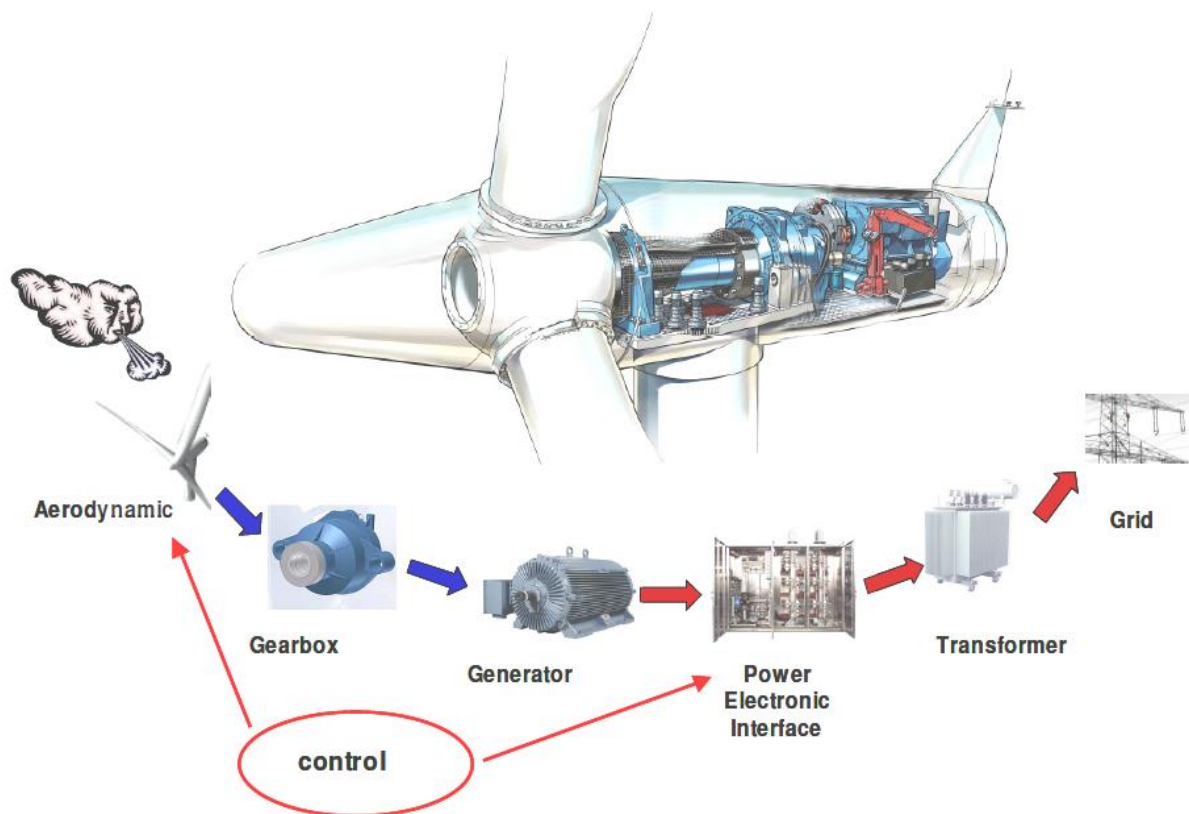


Figure: 2.1. Wind turbine components [Risø/DNV 2007].

- Power electronic interface
 - ❖ Soft starter
 - ❖ Capacitor bank
 - ❖ Static VAR compensator
 - ❖ Frequency converter
- Protection system
- Transformer
- Cable

3. Control system

- Converter controller
- Blade angle controller
- Overall controller (TSO demand)

The fourth main group, called “grid components” contains components, which do not directly belong to the wind turbine itself; however, when the impact of wind turbines with the power system is investigated the grid components play a major role.

4. Grid components – interacting with grid connected wind turbines

- Conventional power plants (synchronous generators)
- Frequency and voltage controller
- Consumer load
- Transformer
- Cable
- Bus bars

2.2 WIND MODEL

Wind simulation plays an important task in wind turbine modeling, particularly for power quality analysis of wind farm and their interaction with the grid to which they are connected. The wind models describe the fluctuations in the wind speed, which cause the fluctuations in the power production of the wind turbines. A wind model has been developed to support studies of the dynamic interaction between large wind farms and the grid to which they are connected, and to support improvement of the electric design of wind turbines as well as grid connection [1, 2, 3].

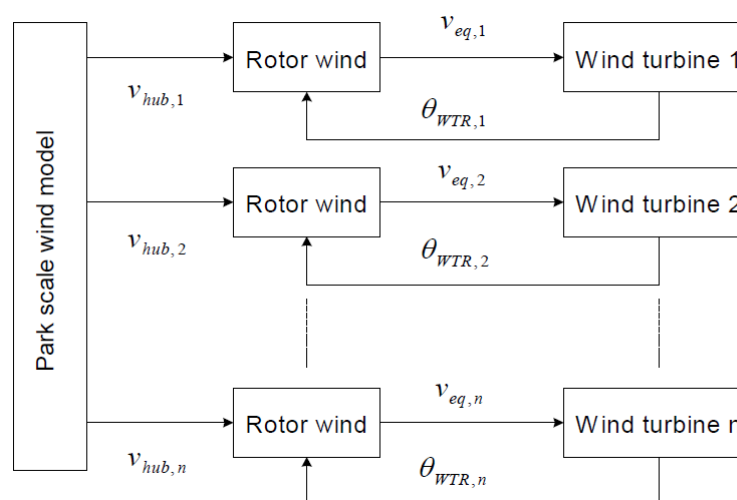


Figure: 2.2. Structure of the wind model.

The wind model is based on a power spectral description of the turbulence, which includes the (park scale) coherence between wind speeds at different wind turbines in a wind farm, together with the effect of rotational sampling of the wind turbine blades in the rotors of the individual wind turbines. Both the spatial variations of the turbulence and the shadows behind the wind turbine towers are included in the model for rotational sampling. The model is verified using measured wind speeds and power fluctuations from wind turbines. The park scale coherence is included, because it ensures realistic fluctuations in the sum of the power from all wind turbines, which is important for estimating the maximum power and power standard deviation of the wind farm.

The effect of the rotational sampling is included because it is a very important source to the fast power fluctuations during continuous operation of the wind turbine. The fast fluctuations are particularly important to assess the influence of the wind turbines on the flicker levels in the power system. The structure of the wind model is shown in Fig. 2.2. It is built into two steps. The first step of the wind model is the park scale wind model, which simulates the wind speeds v_{hub} in hub height at each wind turbine, taking into account the park scale coherence. The second step of the wind model is the rotor wind model, which includes the influence of rotational sampling and the integration along the wind turbine blades as they are rotating. The rotor wind model provides an equivalent wind speed v_{eq} that is conveniently used as input to a simplified aerodynamic model of the wind turbine.

2.2.1 PARK SCALE WIND MODEL

The park scale wind model is assumed to be independent of the operation of the wind farm. The park wind model does not include the effects of wakes in the wind farm, but the mean wind speed and turbulence intensity could be modified to account for these effects. A new method for simulation of park scale wind speeds, the complex cross spectral method, is applied, which directly generates a single time series at the position of each wind turbine. One of the advantages of the new method is that it does not produce more data than what is needed. Due to the data reduction, the new method also reduces the computation time considerably.

2.2.2 ROTOR WIND MODEL

The rotor wind model describes the influence of rotational sampling and integration along the wind turbine blades as the blades rotate. The model for the wind field includes turbulence as well as tower shadow effects. The effects of wind shear and yaw error are not included in the model, because they only have a small influence on the power fluctuations [1],[4,5,6]. The wind speed model provides an equivalent wind speed for each wind turbine, which can be used together with a simple, C_P - based aerodynamic model, and still include the effect of rotational sampling of the blades over the rotor disk.

The equivalent wind speed is essentially a weighted average of the wind speed along the blades. The weighting ensures that the equivalent wind speed applied to a simple aerodynamic function will result in the same aerodynamic torque on the main shaft as the real wind speed distributed along the blades. The equivalent wind model is composed by a deterministic module for mean wind speed and cyclic variations like tower shadow simulation and a stochastic module for turbulence simulation. The two modules are added together in order to get the total equivalent wind, as shown in Fig. 2.3.

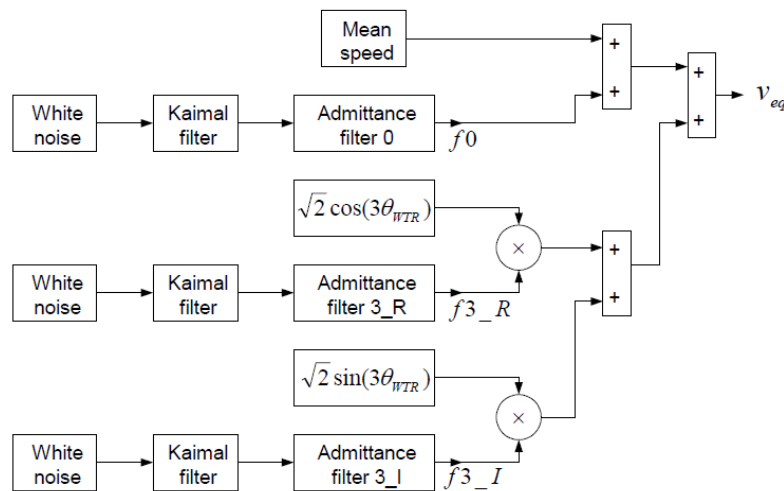


Figure: 2.3. Block diagram of the rotor wind model.

The mean speed is included as a part of the deterministic module. The turbines rotor position θ_{WTR} is fed back from the mechanical model. Three times θ_{WTR} accounts for the interference from the 3rd harmonic from tubular towers in upwind turbines. The white noise represents the source of the turbulence. In the turbulence model, only three components, 0th harmonic component and real and imaginary part of 3rd harmonic component are included. The Kaimal filter is to convert a white noise signal to a signal with a normalized Kaimal spectrum [7,8,9]. The Kaimal spectrum has been selected as it is commonly used to represent the turbulence for wind turbine design. The parameters in the Kaimal filter can be modified to account for the different wind speed, turbulence intensities and turbulence length scales. The admittance filters take into account the structure of the turbulence in terms of the coherence between two points in the rotor plane.

The parameters in the admittance filters can be modified to account for different wind speeds and rotor disk radiuses. Today most wind turbines are constructed with a rotor upwind of the tower to reduce the tower interference of the wind flow. Early wind turbines often had lattice tower, but because of the visual impact, tubular towers are the most common today. The tubular towers have more effect on the flow than lattice tower. Neglecting the effect of the blade bending, the tower shadow effects can be added to contributions from the turbulence.

2.3 WIND SPEED DISTRIBUTION

2.3.1 SHORT TERM WIND DISTRIBUTION

The short term wind speed, for instance describing both the micro-scale air flow and the hourly varying macro-scale air flow, could be generated by the empirical model described in [10, 11, and 12]. The empirical model uses the spectral power density $S(f_{wind})$ calculated for different wind frequency components f_{wind} . The spectral power density of the wind is given by:

$$s(f_{wind}) = \frac{\frac{h}{\bar{V}_{wind}} \cdot \sigma_{wind}^2}{f_m \left(1 + \frac{3}{2 \cdot f_m} \left(f_{wind} \cdot \frac{h}{\bar{V}_{wind}} \right) \right)^{\frac{5}{3}}} \quad (2.1)$$

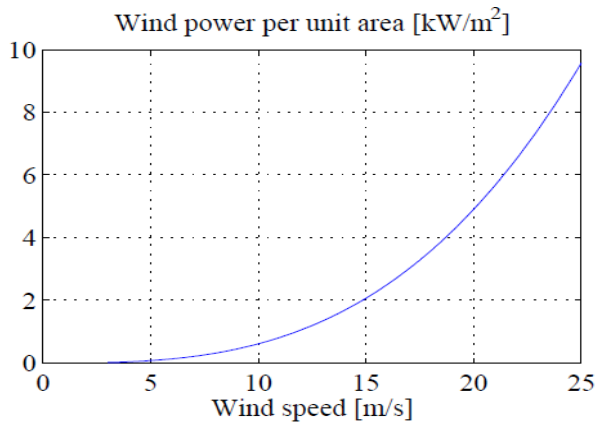


Figure: 2.4. Power in the wind per unit area.

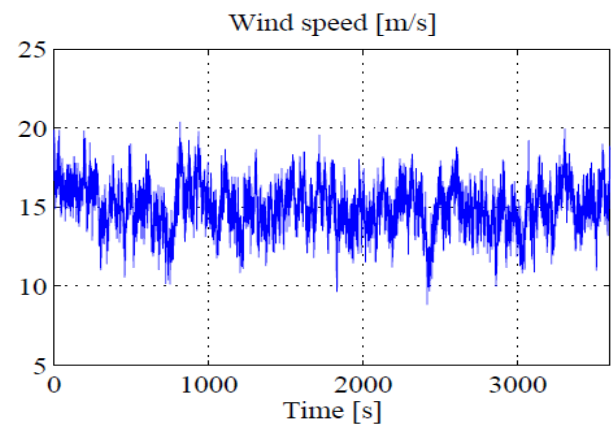


Figure: 2.5. Short term wind speed/Average wind speed is 15 m/s.

where \bar{V}_{wind} is the average wind speed in the considered frequency spectrum, h is the height above ground, f_m is a fluctuation constant (assumed to be 0.06) and σ_{wind} is the wind speed standard deviation given by the turbulence times the average wind speed. Using the wind power spectrum calculated for the different frequency components, the hourly wind speed can be modeled by:

$$v_{wind} = \bar{V}_{wind} + \sqrt{2} \cdot \sum_{i=f_{wind,min}}^{f_{wind,max}} \sqrt{s(f_{wind,i}) \cdot \Delta f_{wind}} \cdot \cos(2 \cdot \pi \cdot f_{wind,i} \cdot t + \beta_i) \quad (2.2)$$

where β_i is a random number between 0 and 2π and Δf_{wind} is the frequency spacing between the considered wind frequencies. Fig. 2.5 shows the wind speed, generated by (2.2) with a turbulence of 0.1, a mean wind speed of 15 m/s and a height above ground of 80 meters.

2.3.2 ANNUAL WIND SPEED DISTRIBUTION

Besides the hourly wind speed described by (2.2), a model of the annual distribution of the hourly average wind speed is needed. The hourly average wind speed distribution throughout the year is often modeled by the Weibull distribution function given by [13]:

$$P(\bar{V}_{wind,c,a}) = \frac{c}{a^c} \cdot \bar{V}_{wind}^{c-1} \cdot e\left(\frac{\bar{V}_{wind}}{a}\right)^c \quad (2.3)$$

where V_{wind} is the wind speed range in which the wind distribution is evaluated. The constants c and a are parameters in the distribution function. Table I shows standard values of the factors a and c for different site classifications. Having the parameters in the Weibull distribution, the annual average wind speed v_{wind} can then be calculated by:

$$v_{wind} = \Gamma\left(\frac{1}{c} + 1\right) \cdot a \quad (2.4)$$

where $\Gamma(1/c + 1)$ is the generalized gamma function of $1/c$ [14]. Using (2.4), with the parameters from Table I gives an annually average wind speed of 7.5 m/s for typical

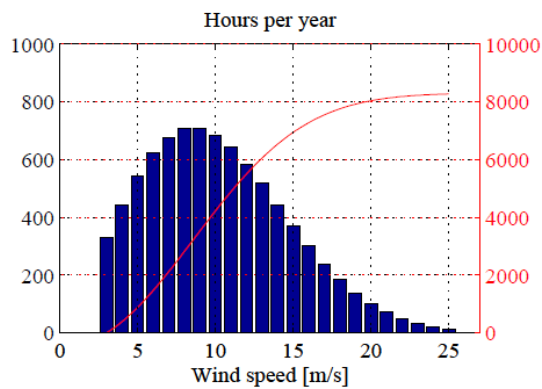


Figure: 2.6. Annual wind distribution for an on-shore site.

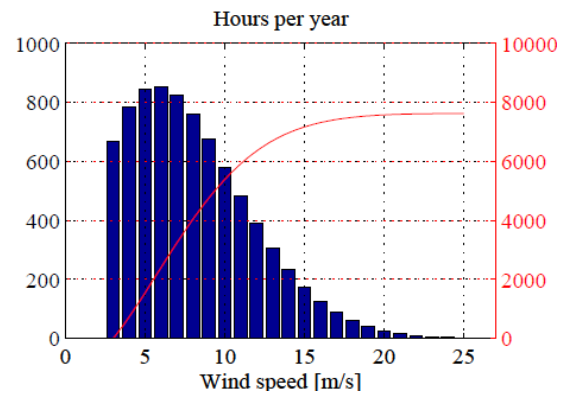


Figure: 2.7. Annual wind distribution for an off-shore site.

on-shore turbines (IEC III) and 10.1 m/s for a high-wind off shore site (IEC I). Fig. 2.6 and 2.7 show the wind distribution for a typical on-shore site and an off-shore site respectively. Although factors as reliability and intervals between maintenance may influence the annual energy production it is assumed that the availability of the turbine is 100% and hence, according to the wind distributions in Fig. 2.6 and Fig. 2.7, an on-shore turbine is producing power 7757 hours per year while an off-shore turbine is producing power 8122 hours per

year. (Assuming a cut-in wind speed of 3 m/s and a cut-out wind speed of 25 m/s). The accumulated hours of operation is shown on the right axis of Fig. 2.6 and Fig. 2.7.

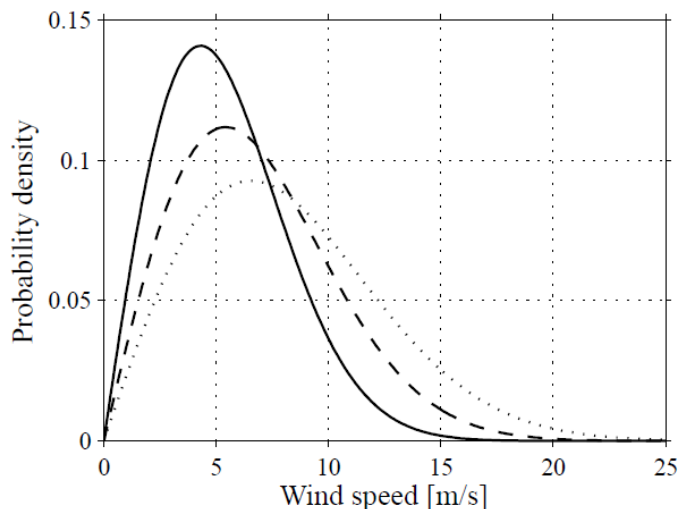


Figure: 2.8. Probability density of the Rayleigh distribution. The average wind speeds are 5.4 m/s (solid), 6.8 m/s (dashed) and 8.2 m/s (dotted).

In Fig. 2.8, the wind speed probability density function of the Rayleigh distribution is plotted. The average wind speeds in the figure are 5.4 m/s, 6.8 m/s, and 8.2 m/s. A wind speed of 5.4 m/s correspond to a medium wind speed site in Sweden [15], while 8–9 m/s are wind speeds available at sites located outside the Danish west coast [16].

2.4 LIMITATIONS

As described above, models exist for both the micro-scale air flow and the hourly varying macro scale air flow. However, to utilize the information in such detailed wind models in the prediction of the annual energy production requires quite good knowledge of the dynamics both in the pitch control system and in the power converter control system. For that reason the wind speed is only modeled as an hourly average, described by (2.4). A justification of this limitation can be found in [17] where it is stated that the error obtained by omitting the turbulent wind component is within a few percent, provided that the turbulent component is within a reasonable range.

TABLE:2.1. Wind Distribution Parameters.

Site classification	Parameter a	Parameter c	Annual average wind speed [m/s]
IEC I site	11.38	2	10.1
IEC II site	9.60	2	8.5
IEC III site	8.46	2	7.5
IEC IV site	6.77	2	6.0

Since the beginnings of wind turbine development (~1980) until today (2013), where wind energy is seen as a mature technology and has become an important participant in the power generation branch, various wind turbine concepts and designs have been developed. The marketable wind turbine concepts can be distinguished by different electrical design and control and can be classified by their speed range (variable speed, fixed speed) and power controllability (stall, pitch control) [18]. In the following, a general overview about different wind turbine concepts. Then the characteristics of different wind turbine concepts are presented and their market penetration is evaluated. Finally the wind turbine concepts are assessed in respect to their controllability, grid code accomplishment and future market prospects.

2.5 CHARACTERISTICS OF DIFFERENT WIND TURBINE CONCEPTS

Four different wind turbine concepts have predominated the global market in the last decade [1]. These concepts are thus introduced in the following. For the sake of uniformity the same classification of concepts as presented in [18] and [19, 20, 21] is made.

Type A: Fixed speed wind turbine concept – Danish concept

Figure 2.9 shows the widely used and most conventional turbine concept. A stall or active stall controlled aerodynamic rotor is coupled via gearbox to a squirrel cage induction generator (SCIG), which in turn is directly (by transformer) connected to the power grid. A capacitor bank provides reactive power compensation and improved grid compatibility during grid connection is facilitated by means of a soft starter.

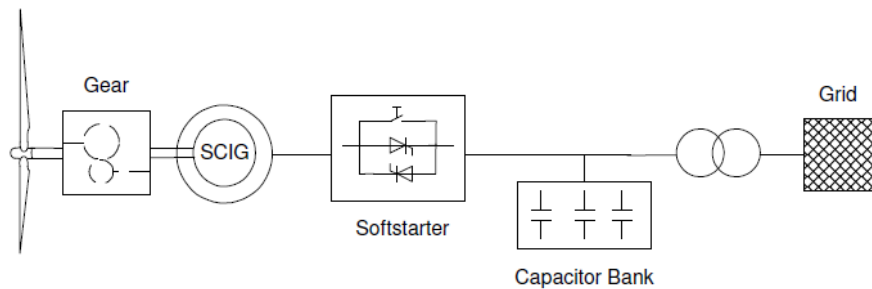


Figure: 2.9. Squirrel cage induction generator concept with gearbox and “direct” grid connection–Type A.

Due to its direct grid connection the generator operates at fixed speed. However, the slip of the generator allows very small speed variations and softens the torque-speed characteristic. Frequently, the generator is equipped with a pole changeable stator (e.g. 4-poles and 6-poles), so that the generator can operate at two speeds, which leads to a better aerodynamic utilization of the turbine at higher wind speeds. The turbine concept excels in its cheap and simple design and robustness, while however its controllability is relatively poor.

Type B: Variable speed wind turbine with variable rotor resistance

A slightly more advanced wind turbine concept is sketched in Figure 2.10. The turbine setup is in principle the same as for Type A; however, now a wound rotor induction generator (WRIG) with external rotor resistance is used, which allows variable speed operation in a limited range of about 10 % above synchronous speed. The external rotor resistance enforces a higher slip, which on the one side enables variable speed operation but on the other hand increases ohmic losses, which are dumped in the resistance. As this also increases the reactive power demand of the generator a capacitor bank is used for this type as well. As the turbine operates with variable speed it is advisable to use pitch control instead of stall control for limitation of aerodynamic power above rated wind speed.

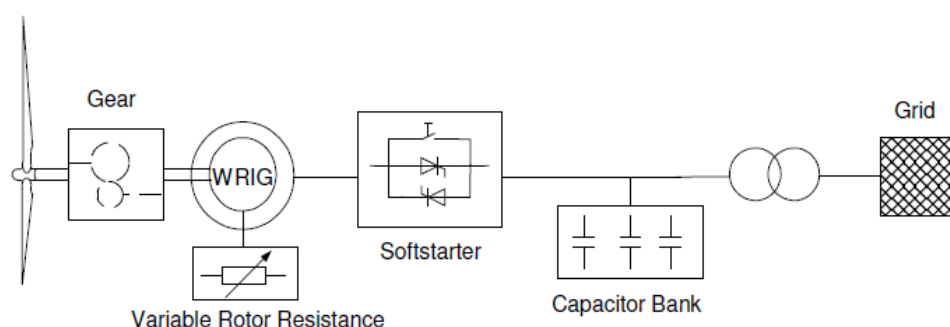


Figure: 2.10. Wound rotor induction generator concept with variable rotor resistance - Type B.

Type C: Doubly-fed induction generator wind turbine

Figure 2.11 shows the doubly-fed induction generator wind turbine concept, the most popular generator concept for wind turbines at the present time. The pitch-controlled aerodynamic rotor is coupled via gearbox to the generator. The doubly Fed Induction Generator (DFIG) provides variable speed operation by means of a partial-scale frequency converter in the rotor circuit. A wound rotor induction generator is used, in order to couple the converter via slip rings to the rotor. Depending on the converter size this concept allows a wider range of variable speed of approximately $\pm 30\%$ around synchronous speed [18, 21].

Moreover, the converter system provides reactive power compensation and smooth grid connection. As the frequency converter only transmits the rotor power it can be designed for typically 25 % - 30 % of the total turbine power. This makes the turbine concept very attractive from an economic point of view compared to turbines with full-scale converter.

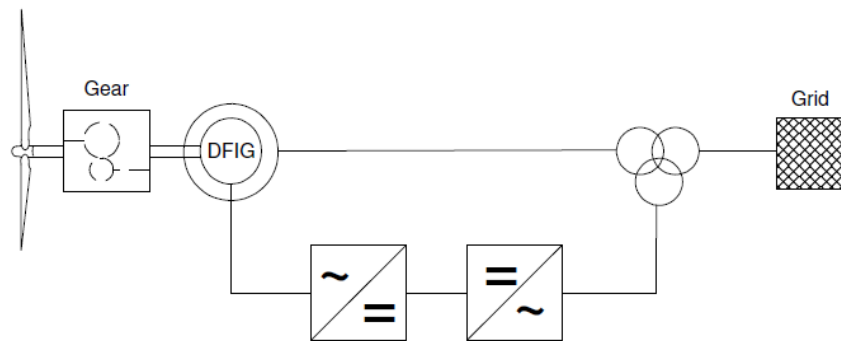


Figure: 2.11. Doubly-fed induction generator concept with partial-scale frequency converter – Type C.

Type D: Variable speed wind turbine with full-scale frequency converter

Type D, illustrated in Figure 2.12, represents the variable speed, pitch controlled wind turbine concept with the generator connected to a full-scale frequency converter. The full-scale frequency converter provides variable speed over the entire speed range of the generator. At the same time the converter guarantees reactive power compensation and smooth grid connection. The generator can optionally be an asynchronous or synchronous generator.

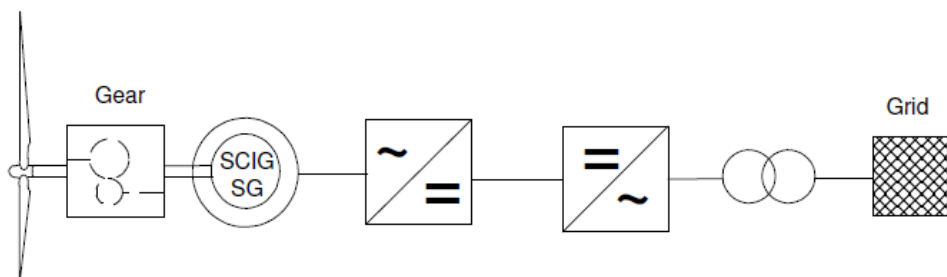


Figure: 2.12. Induction or synchronous generator concept in combination with gearbox and full-scale frequency converter – Type D.

A modification of this turbine concept is sketched in Figure 2.13. If a multi pole synchronous generator is used instead of an induction generator, the generator can be built to operate at low speeds, so that a gearbox can be omitted. This reduces weight, losses and maintenance requirements. The generator can be excited electrically by a DC system (DCSG) or by means of permanent magnets (PMSG).

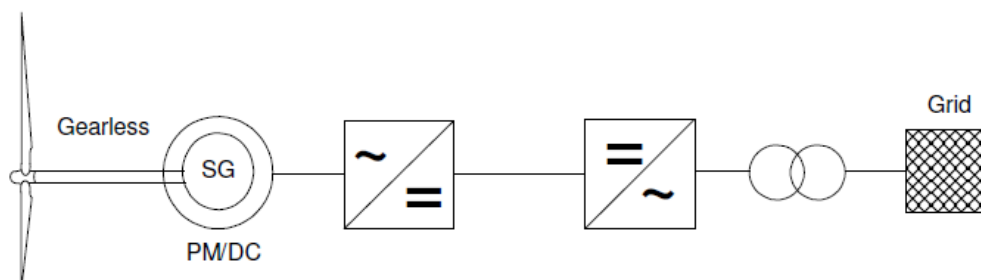


Figure: 2.13. Gearless synchronous generator concept with full-scale converter - Type D.

A resume of the wind turbine concept classification is given in Table 2.2, where the most important attributes of the wind turbine types are summarized and an assignment to the corresponding speed range is given.

Table: 2.2.Wind Turbine Concept Classification

Blade angle control	stall/active stall control		pitch control			
Speed control	fixed speed		variable speed			
Grid connection	direct grid connection		direct grid connection	partial scale converter	full scale converter	
Drive train	gear	gear	gear	gear	gear	gearless
Generator	SCIG	SCIG with pole changeable stator winding	WRIG with variable rotor resistance	DFIG	DCSG/PMSG SCIG	Multipole DCSG/PMSG
Speed range	n_{rated} (~2% slip)	$n_1 ; n_2$ (~2% slip)	$1 - 1.1 \cdot n_{syn}$ (~10% slip)	$0.7 - 1.3 \cdot n_{syn}$ (~ ±30% slip)	$0 \dots 1 \cdot n_{rated}$	$0 \dots 1 \cdot n_{rated}$
	TYPE A		TYPE B	TYPE C	TYPE D	

2.6 MARKET PENETRATION

The most favoured technology among the four different introduced wind turbine concepts has changed within the last decade. In [18-30] a detailed investigation of the wind turbine concept market penetration and its development over 10 years from 2004-2013 is presented and the most interesting outcomes are summarized here.

Table: 2.3.Wind turbine concept market penetration - world market share of yearly installed wind power during 2004 – 2013.

Year \ Concept	2004	2005	2006	2007	2008	2009	2010	2011	2012	2013
Type A (%)	69.5	62.7	53.5	39.6	40.8	39.0	30.6	27.8	19.2	24.7
Type B (%)	16.2	23.4	27.0	17.8	17.1	17.2	15.2	5.2	3.1	2.2
Type C (%)	0.0	0.1	3.1	26.5	28.1	28.2	37.3	46.7	59.8	54.8
Type D (%)	14.3	13.7	16.3	16.1	14.0	15.6	16.9	20.3	17.9	18.3
Installed power [%] (22 suppliers)	1161	1092	1483	2345	3788	4381	7175	7242	8084	8247
Total world market share of top 22 suppliers [%]	85.7	95.7	96.2	92.7	94.0	96.3	100.0	97.4	100.0	97.7

Table 2.3 shows the results of the investigation of [18-25], which is based on data provided by BMT Consults. The table reflects the market penetration of the four wind turbine types A-D from the top 22 wind turbine market suppliers over the years from 2004 to 2013. The total world market share of these 22 suppliers is listed as well. As this value is higher than 85 % for each year, it means that the statistical significance of the data collection is reliable.

The market penetration of the wind turbine types A-D in the years 2004-2013 is also shown graphically in Figure 2.14.

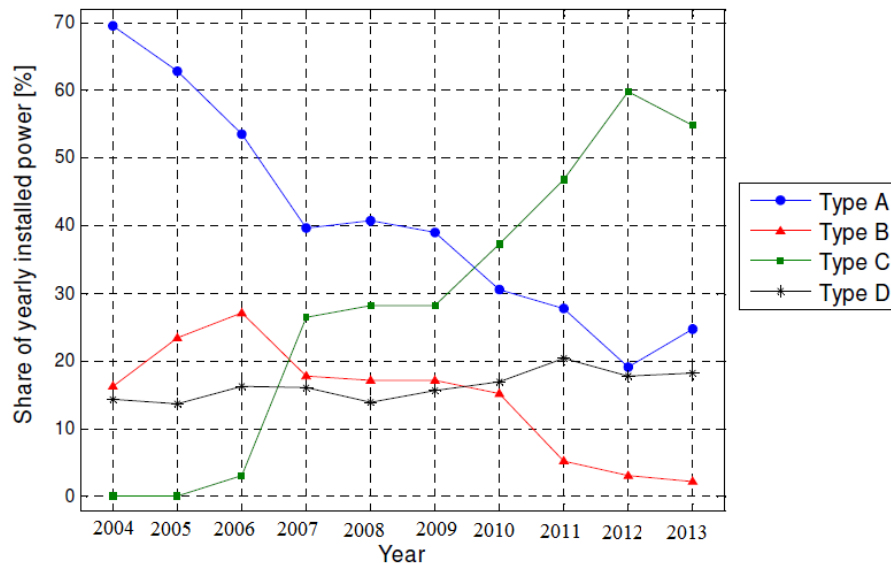


Figure 2.14. World market share of yearly installed wind power during 2004-2013 of the four different wind turbine concepts Type A-D.

During the years 2004-2013 the fixed speed wind turbine concept (Type A) was the predominating wind turbine technology, which was due to the simplicity and robustness of the system. However, from 2005 the DFIG wind turbine (Type C) gained an increasing market penetration, while the demand of Type A and B continuously decreased. The doubly-fed induction generator became thus the most used generator concept, and remains the primary choice for variable speed wind turbines of 1.5 MW and above. This is confirmed by the investigations of [18], which assessed a market share of approximately 50 % for the doubly-fed generator on the Europe market in the years 2002-2005. The market penetration of the variable speed wind turbine concept with full-scale frequency converter – Type D – shows no considerable changes during these considered 10 years, as illustrated in Figure 2.14. However, [18] predicates a share of 44 % of yearly new installed wind turbines with synchronous generators in Europe for 2012 and 2013, because of the high market penetration of the ENERCON concept on the German market. For the coming years an increasing trend of Type D wind turbines can therefore be expected, due to their good control and grid support capabilities.

2.7 VARIABLE SPEED WIND TURBINES VERSUS FIXED SPEED WIND TURBINES

In the previous chapter it has been shown that fixed speed wind turbines were the most installed wind turbines in the early 1990s. The major advantages of this concept are its simplicity and robustness, as standard asynchronous generators can be used and power electronics can be omitted causing economical benefits and reducing maintenance requirements. However, its drawbacks are uncontrollable reactive power consumption, higher mechanical stress and limited power quality control [18-41]. Fixed speed wind turbines are generally equipped with stall control, which implies again simplicity and robustness as no blade bearings or pitch system needs to be installed. On the other hand, stall control causes higher mechanical stresses and requires stronger blades, brakes and bearings. Moreover, a fixed blade angle entails losses in energy capture, as the point of maximum aerodynamic efficiency cannot be approached for any wind speed.

A possibility to achieve power control for fixed speed wind turbines at high wind speeds is active stall control. A very slow control adjusts the pitch angle to larger angles of attack and smoothes the power limitation. In contrast to this, variable speed wind turbines are generally equipped with pitch control. It is not advisable to combine pitch control with fixed speed generators as this would lead to large inherent power fluctuations at high wind speeds since the pitch mechanism reacts too slowly during fast wind speed changes. However, variable speed operation assures, that sudden power surplus of wind gusts is temporarily buffered in rotational energy of the turbine until the pitch control limits the excess power. At partial load variable speed operation assures that maximum aerodynamic efficiency can be adjusted for any wind speed.

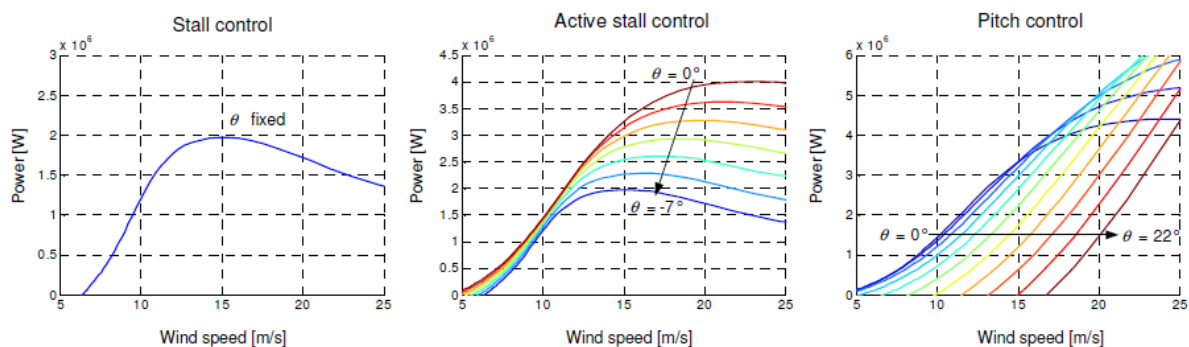


Figure: 2.15. Wind turbine power curves versus wind speed for stall control, active stall control and pitch control.

At wind speeds above rated wind speed the pitch control changes the pitch angle in order to limit the power to its rated value. In both operational modes variable speed pitch controlled wind turbines achieve a better energy capture compared to stall controlled wind turbines. Finally, the power curves of stall wind turbine, active stall wind turbine and pitch controlled wind turbine plotted for different pitch angle values can be compared in Figure 2.15. As indicated in the figure pitch control works in the opposite direction as active stall control.

Variable speed pitch control wind turbines have become the predominating technology for wind turbines, which is confirmed by the investigations of [21] and [14]. As investigated in [18] 92 % of the new installed wind turbines in 2005 were variable speed wind turbines. The main advantages are the increased power capture, reduced mechanical stress and minor acoustical noises as well as better controllability.

The drawbacks of the variable speed pitch controlled concept are additional losses due to additional components as e.g. power electronics and pitch system, which in turn leads to higher capital costs of the system. However, it can be expected, that due to improved developments, costs for power electronics will further decrease in the future. The main trend in wind turbine technology is recently also influenced by other factors. Especially in countries with high wind power penetration, wind power grid integration issues are very important in terms of which wind turbine concept can be applied.

Wind power grid integration addresses at the one hand power control capability of wind turbines, which means that wind turbines must curtail or adjust their power output in order to contribute to the dispatch of power production and consumption. At the other hand grid codes require fault ride-through and reactive power supply from wind turbines. Thus, the controllability of wind turbine in terms of grid compatibility and compliance of grid connection standards has a great impact on future development.

Due to this reason variable speed wind turbines using a frequency converter, as represented by wind turbine type C, will be the relevant technologies on the future market and they are therefore considered in the present PhD work. As fixed speed wind turbines or variable speed wind turbines without power electronics are assessed to be incapable of fulfilling grid code requirements, these wind turbine concepts will withdraw from the market and will not be included in the investigations of the present work. The following chapters focus on (i) the doubly-fed induction generator concept and control – Type C, and (ii) Low Voltage Ride Through (LVRT) Capability.

2.8 REFERENCES

- [1] P. Sørensen, A. Hansen, L. Janosi, J. Bech, B. Bak-Jensen, "Simulation of interaction between wind farm and power system", Risø-R-1281(EN), Risø National Laboratory, Dec. 2001.
- [2] P. Sørensen, A. D. Hansen, P. A. C. Rosas, "Wind models for simulation of power fluctuations from wind farms," *Journal of Wind Engineering and Industrial Aerodynamics*, vol. 90, pp. 1381-1402, Dec. 2002.
- [3] P. A. C. Rosas, P. Sørensen, H. Bindner, "Fast wind modeling for wind turbines," *Proc. of the Wind Power for the 21 Century: EUWER Special Topic Conference and Exhibition*, pp. 184-187, Sept. 2000.
- [4] S. Heier, "Grid integration of wind energy conversion systems", John Wiley & Sons Ltd, Chichester, 1998.
- [5] J. G. Slootweg, H. Polinder, W. L. Kling, "Dynamic modeling of a wind turbine with direct drive synchronous generator and back to back voltage source converter and its control," *Proc. of the European Wind Energy Conference*, pp. 1014-1017, July 2001.
- [6] T. Burton, D. Sharpe, N. Jenkins, E. Bossanyi, "Wind energy handbook", John Wiley & Sons Ltd, Chichester, 2001.
- [7] Z. Chen, E. Spooner, "Grid power quality with variable speed wind turbines," *IEEE Trans. on Energy Conversion*, vol. 16, no. 2, pp. 148-154, June 2001.
- [8] International Electro technical Commission, *Electromagnetic Compatibility (EMC) --- Part 4: Testing and measurement techniques --- Section 15: Flicker meter --- Functional and design specifications*, IEC 61000-4-15, International Electro technical Commission, Geneva, Switzerland, Nov. 1997.
- [9] S. K. Salman, A. L. J. Teo, "Windmill modeling consideration and factors influencing the stability of a grid-connected wind power-based embedded generator," *IEEE Trans. on Power Systems*, vol. 18, no. 2, pp. 793-802, May 2003.
- [10] S. K. Salman, A. L. J. Teo, "Improvement of fault clearing time of wind farm using reactive power compensation," *Proc. of 2001 IEEE Porto Power Tech Conference*, vol. 2, pp. 6/1-6/6, Sept. 2001.
- [11] V. Akhmatov, H. Knudsen, "Modelling of windmill induction generators in dynamic simulation programs," *Proc. of International Conference on Electric Power Engineering*, pp. 108, Aug. /Sept. 1999.
- [12] I. Boldea, S.A. Nasar, "The induction machine handbook", CRC Press, Boca Raton, 2002.
- [13] F. H. Li, D. Q. Zhu, "The electric machine", The Science Press, Beijing, third edition, 2002.
- [14] J. D. Gao, X. H. Wang, F. H. Li, "Analysis of alternative current electric machine system", The Qinghua Press, Beijing, 1993.
- [15] Y. K. He, "Computer simulation of alternative current electric machinery", The Science Press, Beijing, 1990.

- [16] J. Chen, "Mathematic model and speed-regulating system of alternative current electric machinery", The National Defense Industry Press, Beijing, 1989.
- [17] M. Chomit, J. Bendl, L. Schreier, "Extended vector control of doubly fed machine under unbalanced power network conditions," Proc. of the International Conference on Power Electronics, Machines and Drives, pp. 329-334, June 2002.
- [18] N. Mohan, T. M. Undeland, W.P. Robbins, "Power electronics – converters, applications, and design", John Wiley & Sons Inc, USA, third edition, 2003.
- [19] A. M. Trzynadlowski, "Introduction to modern power electronics", John Wiley & Sons Inc, New York, 1998.
- [20] P. Giroux, G. Sybille, H. Le-Huy, "Modeling and simulation of a distribution STATCOM using simulink's power system blockset," Proc. of the 27th Annual Conference of the IEEE Industrial Electronics Society, vol. 2, pp. 990-994, Nov./ Dec., 2001.
- [21] Flemming Abrahamsen, "Energy optimal control of induction motor drives", PhD thesis, Aalborg University, 9220 Aalborg East, February 2000. ISBN: 87-89179-26-9.
- [22] AESO. Wind power facility -technical requirements (draft for stake holder comment). Technical report, Alberta electric system operator, August 2004.
- [23] Gunnar Christensen, Erik Both, and Preben Østergaard Sørensen. Mekanik. Laboratoriet for teknisk fysik, ISBN: 87-503-7583-0, 1990.
- [24] L. L. Freris. Wind energy conversion systems. Prentice Hall, ISBN: 0-13-960527-4, November 1990.
- [25] Clemens Jauch, Poul Sørensen, and Birgitte BakJensen, "International review of grid connection requirements for wind turbines", Nordic Wind Power Conference, Vol. I, March 2004.
- [26] R. Kelly and J. Llamas, "Determination of viscous and coulomb friction by using velocity responses to torque ramp inputs". IEEE International Conference on Robotics and Automation, Vol. 3:pp. 1740–1745, May 1999.
- [27] Erwin Kreyszig, "Advanced engineering mathematics". John Wiley & sons, Inc, 7th ed., ISBN: 0-471-59989-1, 1993.
- [28] W. E. Leithead, "Dependence of the performance of variable speed wind turbines on the turbulence, dynamics and control". IEE Proceedings of Generation, Transmission and Distribution, Vol. 137 No. 6:pp. 403–413, November 1990.
- [29] A. D. McIver, P. Freere, and D. G. Holmes, "Grid connection of a variable speed wind turbine using a matrix converter", Fuel and Energy Abstracts, Vol. 36, No. 4:274, July 1995.
- [30] Ned Mohan, Tore M. Undeland, and William P. Robbins, "Power electronics". John Wiley & Sons, ISBN: 0-471-58408-8, 1995.
- [31] NECA. National electricity code. Technical report, NECA, 2003.
- [32] E. ON Netz. Netzanschlussregeln hoch-und h^ochspannung. Technical report, E. ON Netz GmbH, Beyreuth, Germany, August 2003.
- [33] E. ON Netz. Netzanschlussregeln hoch-und h^ochspannung. Technical report, E. ON Netz GmbH, Beyreuth, Germany, August 2006.

- [34] C. Pelchen, C. Schweiger, and M. Otter, "Modeling and simulating the efficiency of gearboxes and of planetary gearboxes", Proceedings of 2th International Modelica Conference, Vol. I: pp. 257–266, March 2002.
- [35] Gilberto C. D. Sousa, Bimal K. Bose, John Cleland, Ronald J. Spiegel, and P. Jeffrey Chappell, "Loss modeling of converter induction machine system for variable speed drives". Proceeding of the 1992 Industrial Electronics, Control, Instrumentation, and Automation, Vol. I:pp. 114–120, November 1992.
- [36] Scottish Hydro Electric SP Transmission & Distribution, "Guidance note for connection of wind farms". Technical report, Scottish Hydro Electric, December 2002.
- [37] Elkraft System. Vindmøller tilsluttet net med spændinger over 100 kv. Technical report, Eltra forskrift TF 3.2.6, November 2004.
- [38] Hansen M.H., Hansen A.D., Larsen T. J., Øye S., Sørensen P., Fuglsang P., "Control design for a pitch regulated, variable speed wind turbine", Risø report R-1500, Risø National Laboratory, Denmark, 2005.
- [39] John F. Walker and Nicholas Jenkins, "Wind energy technology". John Wiley & Sons, ISBN: 0-471-96044-6, 1997.
- [40] S.E. Zocholl. Induction motors Part I. Technical report, Schweitzer Engineering Laboratories, Inc.
- [41] S.E. Zocholl. Induction motors Part II. Technical report, Schweitzer Engineering Laboratories, Inc.

CHAPTER 3

DYNAMIC MODELLING OF DOUBLY FED INDUCTION GENERATOR (DFIG) WIND TURBINE SYSTEM

3.1 AERODYNAMIC MODEL

Wind turbine power production depends on the interaction between the wind and the turbine rotor. The blades of a wind turbine rotor extract some of the energy flow from air in motion, convert it into rotational energy, and then deliver it via a mechanical drive unit to the generator.

3.1.1 POWER EXTRACTION FROM THE AIR STREAM

The actuator disk theory explains in a very simply way the process of extracting the kinetic energy in the wind, based on energy balances and the application of Bernoulli's equation. The rotor wind capturing energy is viewed as a porous disk, which causes a decrease in momentum of the airflow, resulting in a pressure jump in the faces of the disk and a deflection of downstream flows as shown in Figure 3.1. The theory of momentum is used to study the behavior of the wind turbine and to make certain assumptions. The assumptions are that the air is incompressible, the fluid motion is steady, and the studied variables have the same value on a given section of the stream tube of air.

The power contained in the form of kinetic energy in the wind crossing at a speed V_v , surface A_1 , is expressed by

$$P_v = \frac{1}{2} \rho A_1 V_v^3 \quad (3.1)$$

Where ρ is the air density.

The wind turbine can recover only a part of that power:

$$P_t = \frac{1}{2} \rho \pi R^2 V_v^3 C_p \quad (3.2)$$

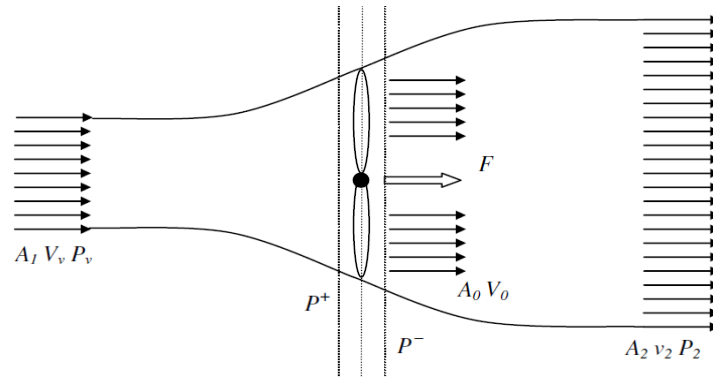


Figure: 3.1. Schematic of fluid flow through a disk-shaped actuator.

where R is the radius of the wind turbine and C_p is the power coefficient, a dimensionless parameter that expresses the effectiveness of the wind turbine in the transformation of kinetic energy of the wind into mechanical energy. For a given wind turbine, this coefficient is a function of wind speed, the speed of rotation of the wind turbine, and the pitch angle. C_p is often given as a function of the tip speed ratio, λ , defined by

$$\lambda = \frac{R\Omega_t}{V_v} \quad (3.3)$$

where R is the length of the blades (radius of the turbine rotor) and Ω_t is the angular speed of the rotor.

The theoretical maximum value of C_p is given by the Betz limit:

$$C_{P-theo-max} = 0.593 = 59.3\%$$

The rotor torque is obtained from the power received and the speed of rotation of the turbine:

$$T_t = \frac{P_t}{\Omega_t} = \frac{\rho\pi R^2 V_v^3 C_p}{2\Omega_t} = \frac{\rho\pi R^3 V_v^2}{2\lambda} C_p = \frac{\rho\pi R^3 V_v^2}{2} C_t \quad (3.4)$$

where C_t is the coefficient of torque. The coefficients of power and torque are related by the equation

$$C_p(\lambda) = \lambda \cdot C_t(\lambda) \quad (3.5)$$

Using the resulting model of the theory of momentum requires knowledge of the expressions for $C_p(\lambda)$ and $C_t(\lambda)$. These expressions depend mainly on the geometric characteristics of the blades. These are tailored to the particular site characteristics, the desired nominal power and control type (pitch or stall), and operation (variable or fixed speed) of the windmill.

The calculus of these curves can only be done by means of aero elastic software such as Bladed or by experimental measurements. From these curves, it is interesting to derive an analytical expression. This task is much easier than obtaining the curves themselves. Without analytical expression, it would save in table form a number of points on the curves and calculate the coefficient corresponding to a given λ (pitch angle) by means of a double interpolation. The analytical expression for $C_p(\lambda)$ or $C_t(\lambda)$ may be obtained, for example, by

polynomial regression. One typical expression that models these coefficients will be described in the next section. Figure 3.2 shows an example of $C_p(\lambda)$ and $C_t(\lambda)$ curves for a pitch regulated wind turbine. The power and torque of the turbine are shown in Figure 3.3. The wind speed V_v of precedent equations is not real; it is a fictitious homogeneous wind. It's a wind, expressed as a point of the area swept by the wind turbine, but the wind must be traceable torque T_t near the field that produced the true wind speed incident on the entire area swept by the rotor.

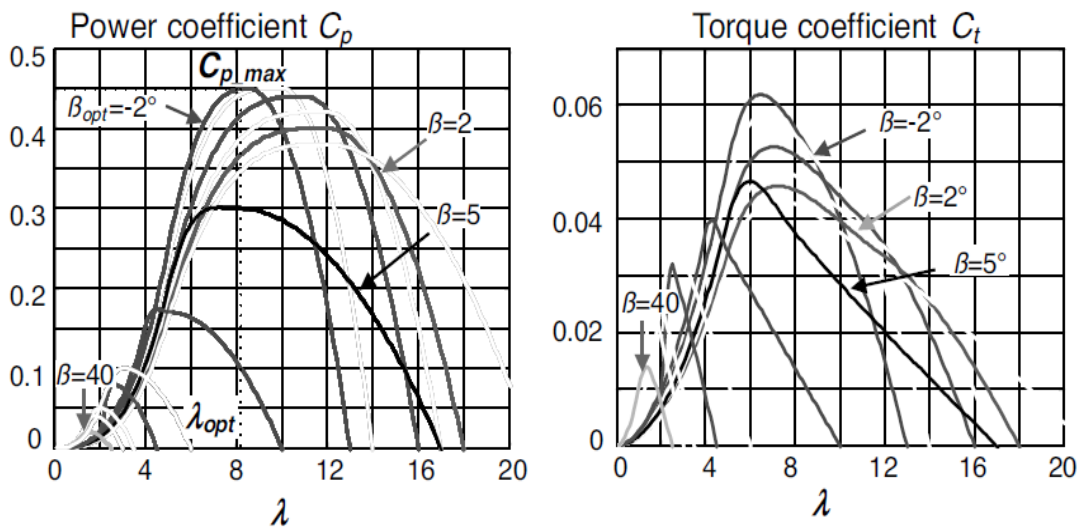


Figure: 3.2. Curves of coefficients of power and torque of a pitch regulated wind turbine, for different pitch angles β .

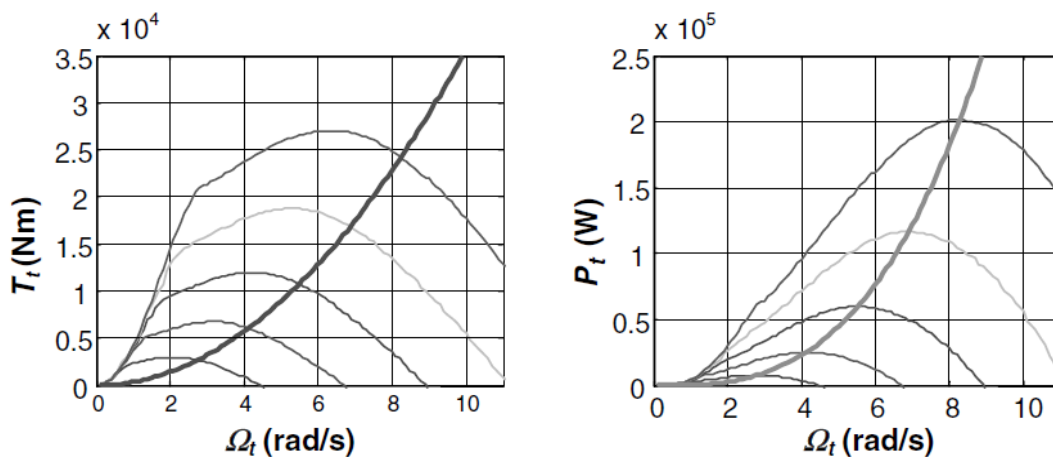


Figure: 3.3. Curves of power and torque of a pitch regulated wind turbine.

3.2 VARIABLE SPEED WIND TURBINES (VSWT)

Figure 3.4 shows the nacelle layout of a Nordex N80 (2.5 MW nominal power), 2.5MW variable speed wind turbine [1-14]. One must appreciate the big differences between the fixed speed and the variable speed wind turbines; it is a technological evolution from the first one. An increase in size equals an increase in mechanical efforts, and the variable speed and the power control provide the tools to do this without risks. The major differences between them are:

- Power control is by means of pitchable blades.
- Doubly fed induction generator and power converters provide variable speed.

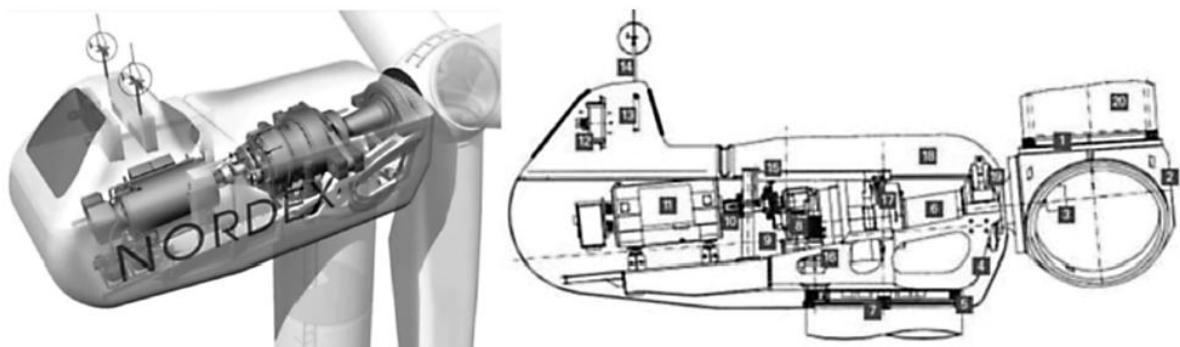


Figure:3.4. Nordex variable speed pitch regulated wind turbine. (Source: Nordex).

The main components of the nacelle and rotor are:

- (1) Pitch bearing,
- (2) Rotor hub,
- (3) Pitch drive,
- (4) Framework,
- (5) Yaw adjustment bearing,
- (6) Main rotor shaft,
- (7) Yaw brakes,
- (8) Gearbox,
- (9) Holding brake,
- (10) Coupling to generator,
- (11) Generator,
- (12) Cooler for the generator,
- (13) Cooler for the gearbox,
- (14) Wind sensors,
- (15) On-board crane,
- (16) Yaw drive mechanism,
- (17) Support of the gearbox,
- (18) Nacelle fiberglass housing,
- (19) Rotor bearing, and
- (20) Stem of the rotor blade.

3.2.1 MODELING OF VARIABLE SPEED WIND TURBINE

The following subsections will explain the basic models and control for the DFIG wind turbine [15-20].

The proposed wind turbine model is composed of the following systems:

- Aerodynamic model, evaluates the turbine torque T_t as a function of wind speed V_v and the turbine angular speed Ω_t .
- Pitch system, evaluates the pitch angle dynamics as a function of pitch reference β_{ref} .
- Mechanical system, evaluates the generator and turbine angular speed (Ω_t and ω_m) as a function of turbine torque and generator torque T_{em} .
- Electrical machine and power converters transform the generator torque into a grid current as a function of voltage grid.
- Control system, evaluates the generator torque, pitch angle and reactive power references as a function of wind speed and grid voltage.

Figure 3.5 shows the interaction between the different subsystems.

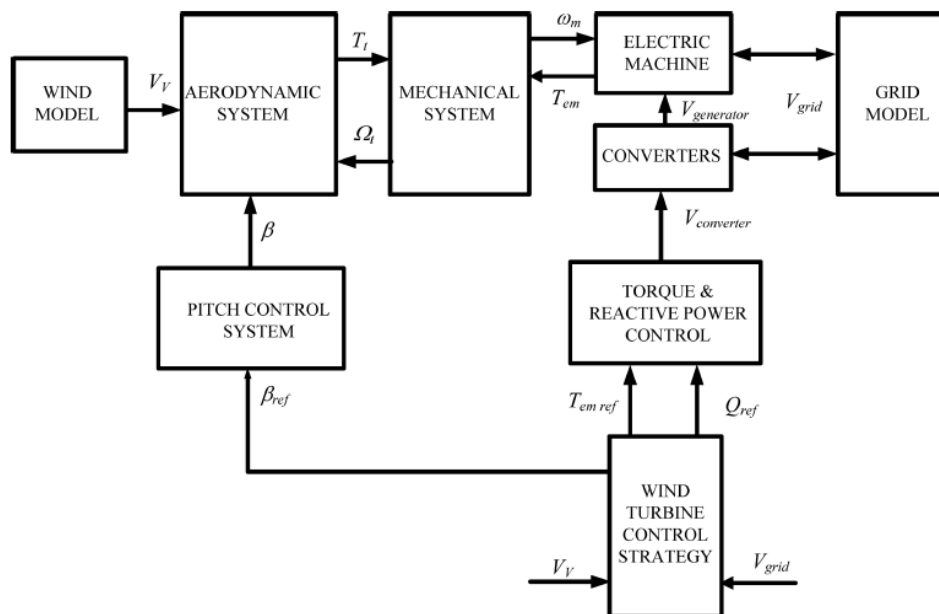


Figure: 3.5. Block scheme of a DFIG wind turbine model.

3.2.1.1 AERODYNAMIC WIND TURBINE MODEL

The aerodynamic wind turbine model represents the power extraction of the rotor, calculating the mechanical torque as a function of the air flow on the blades [21-30]. The wind speed can be considered as the averaged incident wind speed on the swept area by the blades with the aim of evaluating the average torque in the low speed axle.

The torque generated by the rotor has been defined by the following expression:

$$T_t = \frac{\rho \pi R^3 V_v^2}{2} C_t \quad (3.6)$$

The most straightforward way to represent the torque and power coefficient C_p is by means of analytical expressions as a function of tip speed ratio (λ) and the pitch angle (β). One expression commonly used, and easy to adapt to different turbines, is

$$C_p = k_1 \left(\frac{k_2}{\lambda_i} - k_3 \beta - k_4 \beta^{k_5} - k_6 \right) \left(e^{\frac{k_7}{\lambda_i}} \right) \quad (3.7)$$

$$\lambda_i = \frac{1}{\lambda + k_8} \quad (3.8)$$

With the tip speed ratio,

$$\lambda = \frac{R \Omega_t}{V_v} \quad (3.9)$$

3.2.1.2 MECHANICAL SYSTEM

The mechanical representation of the entire wind turbine is complex. The mechanical elements of a wind turbine and the forces suffered or transmitted through its components are very numerous. It is therefore necessary to choose the dynamics to represent and the typical values of their characteristic parameters. The first is the resonant frequency of the power train. The power transmission train is constituted by the blades linked to the hub, coupled to the slow shaft, which is linked to the gearbox, which multiplies the rotational speed of the fast shaft connected to the generator. For the purpose of this simulation model, representing the fundamental resonance frequency of the drive train is sufficient and a two mass model, as illustrated in Figure 3.6, can then model the drive train.

The second resonance frequency is much higher and its magnitude is lower. All the magnitudes are considered in the fast shaft. Inertia J_t concerns the turbine side masses, while J_m concerns those of the electrical machine. These inertias do not always represent exactly the turbine and the electrical machine. If the fundamental resonance frequency comes from the blades, part of the turbine inertia is then considered in J_m .

The stiffness and damping coefficients, K_{tm} and D_{tm} , define the flexible coupling between the two inertias. As for the inertias, these coefficients are not always directly linked to the fast shaft but to the fundamental resonance, which may be located somewhere else. D_t and D_m are the friction coefficients and they represent the mechanical losses by friction in the rotational movement. The turbine rotational speed and driving torque are expressed in the fast shaft by

$$\Omega_{t-ar} = N\Omega_t$$

$$T_{t-ar} = T_t / N$$

where N is the gearbox ratio.

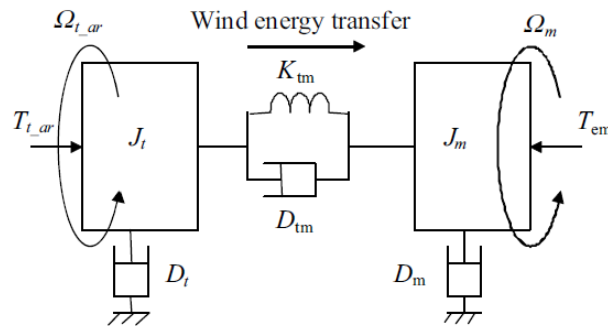


Figure: 3.6. Two mass mechanical model.

Next

$$J_t \frac{d\Omega_{t-ar}}{dt} = T_{t-ar} - D_t \Omega_{t-ar} - T_{em}$$

$$J_m \frac{d\Omega_m}{dt} = T_{em} - D_m \Omega_m + T_{em} \quad (3.10)$$

$$\frac{dT_{em}}{dt} = K_{tm} (\Omega_{t-ar} - \Omega_m) + D_{tm} \left(\frac{d\Omega_{t-ar}}{dt} - \frac{d\Omega_m}{dt} \right)$$

The model can be simplified by neglecting the damping coefficients (D_t , D_m , and D_{tm}), resulting in a model with two inertias (J_t and J_m) and the stiffness (K_{tm}). The resulting transfer function relating the generator torque and speed presents a pole at ω_{01} pulsation and a zero ω_{02} pulsation:

$$\omega_{01} = \sqrt{K_{tm} \frac{J_t + J_m}{J_t J_m}} \quad (3.11)$$

$$\omega_{02} = \sqrt{\frac{K_m}{J_t}} \quad (3.12)$$

The pole has a frequency in the range between 1 and 2 hertz for a multi megawatt wind turbine.

3.2.1.3 PITCH SYSTEM

The controller is designed for rotating all the blades at the same angle or each of them independently. This independent regulation gives more degrees of freedom to the control system. This particular operation would reduce the stresses in the blades. The independent regulation of blades is an important innovation that will bring more intelligence into the control system of wind turbines. In studying a dynamic control system, a blade pitch involves many torques and forces .

The representation of this torques requires modeling the structural dynamics of the blade, the behavior of the air around the blades, or the inclusion of friction in the bearings. Moreover, regulation of the speed of rotation around the longitudinal axis of the blades has a bandwidth much greater than that of the control of the angle itself. Given these last two observations, the most standard approach is to represent the loop control, the rate of change of pitch angle, and a linear system of first order containing the main dynamics of the actuator (hydraulic or electric). In fact, when modeling the pitch control, it is very important to model the rate of change of this angle .

Indeed, given the effort sustained by the blades, the variation of the pitch must be limited. It is limited to about 10°/s during normal operation and 20°/s for emergencies. Regulation of the blade angle is modeled as shown in Figure 3.7, by a PI controller that generates a reference rate of change of pitch; this reference is limited and a first order system gives the dynamic behavior of speed control of pitch variation. The pitch angle itself is then obtained by integrating the variation of the angle.

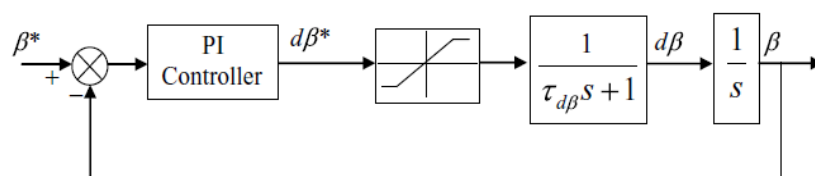


Figure: 3.7. Pitch system and control model.

3.2.1.4 CONTROL OF VARIABLE SPEED WIND TURBINE (VSWT)

Control of a variable speed wind turbine is needed to calculate the generator torque and pitch angle references in order to fulfill several requirements:

- Extract the maximum energy from the wind.
- Keep the turbine in safe operating mode (power, speed, and torque under limits).
- Minimize mechanical loads in the drive train.

Design of this strategy is a very complicated task strongly related with the aerodynamic and mechanical design of the turbine, and indeed only known by the manufacturers. In this section only the aspects related to the energy extraction and speed–power control will be treated. Figure 3.8 shows a general control scheme for the VSWT, where the two degrees of freedom are the generator torque and the pitch angle [31-39].

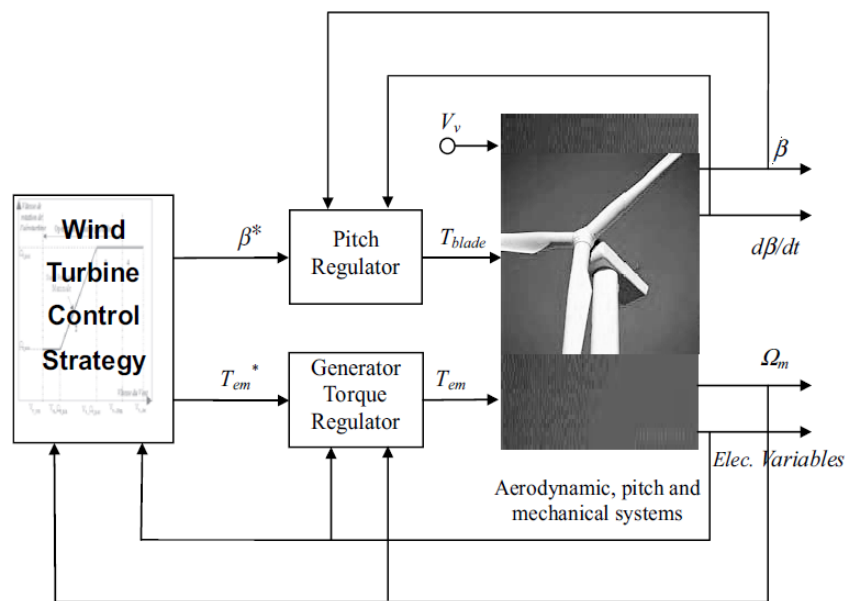


Figure:3.8. Pitch regulated variable speed wind turbine control scheme.

This control is independent of the generator technology and can be simulated without modeling the electrical machine, power converters, and their associated controls just including the torque dynamics as a first-order system. Moreover, for DFIG based wind turbines this limitation also serves to limit the slip of the electrical machine and therefore the voltage must provide the rotor converter. The following subsections describe the wind turbine control strategy and the control objectives.

3.2.1.5 TURBINE SPEED CONTROL REGIONS

The wind turbine control strategy most commonly used is illustrated in Figure 3.9 and consists of four operation zones:

1. Limit the minimum speed of operation.
2. Follow the curve of maximum power extraction from variable speed operation with partial load.
3. Limit the maximum speed at partial load operation.
4. Limit the maximum operating speed at rated power output.

Figure 3.10 shows the wind turbine speed as a function of the wind speed. The minimum speed limit is explained by the fact that we must prevent the turbine from rotating at speeds corresponding to the resonant frequency of the tower. This resonance frequency is about 0.5 Hz and a rotational speed too small can excite it. Moreover, for DFIG based turbines this limitation also serves to limit the sliding of the electrical machine, and hence the rotor voltage, and therefore the voltage that must provide the drive rotor. The imposition of a maximum speed can also be explained by the limitation of sustained efforts by the blades. Indeed, a rotation speed too high can cause inertial loads unbearable by the blades and the turbine shaft. Also, the linear speed of the tip of the blade must be limited.

For DFIG based turbines, this limitation responds to the desire to limit the slip but also the maximum power that passes through the rotor and therefore by the rotor converter and network. With this strategy, the power to operate the converters will be around 30% of the rated power of the electric generator.

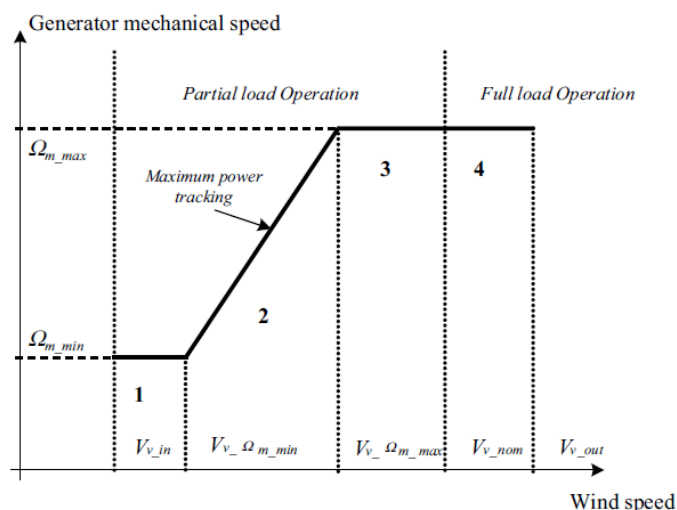


Figure: 3.9. Wind turbine control strategy based on four speed regions.

Therefore, the wind generator starts to run at the wind speed connection (cut-in wind speed) with a rotating speed Ω_{t-min} . When the wind speed becomes more important, it reaches the maximum aerodynamic performance operating in Zone 2. As wind speed increases, the rotation speed also increases until the maximum rotation speed Ω_{t-max} . The wind generator then operates in Zone 3. When wind speed reaches its nominal value, the generator works at the rated mechanical power and the energy captured for higher wind speeds should be

regulated at this nominal value. Zone 4 corresponds to operation at full load. Here, the mechanical power can be limited either by varying the pitch or by torque control. Typically, the electromagnetic torque is maintained at nominal value and adjusts the pitch angle to keep the turbine at maximum speed and rated power. Figure 3.10 shows the torque and power in different operation modes .

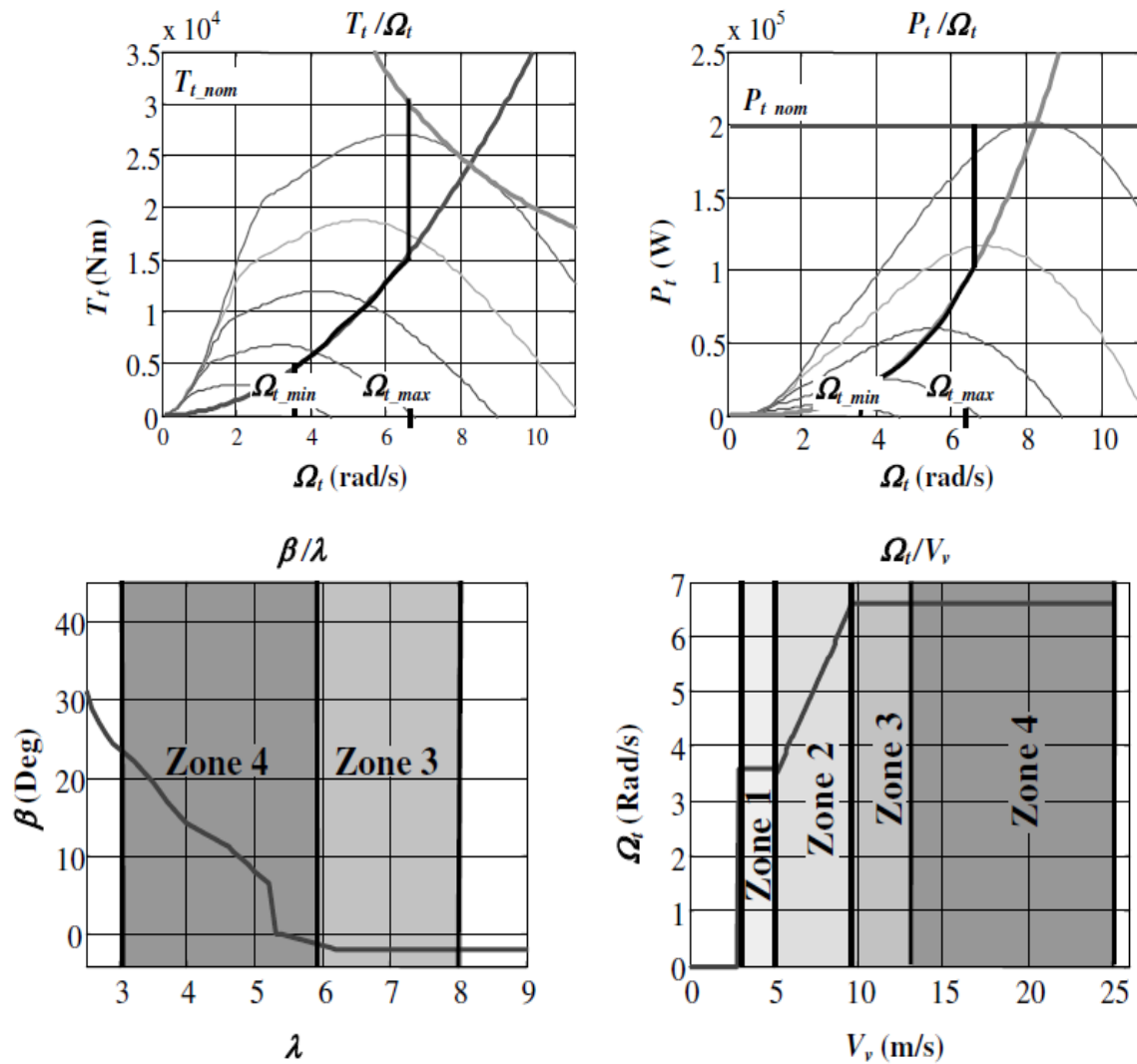


Figure: 3.10. Curves of power and torque of a pitch regulated wind turbine.

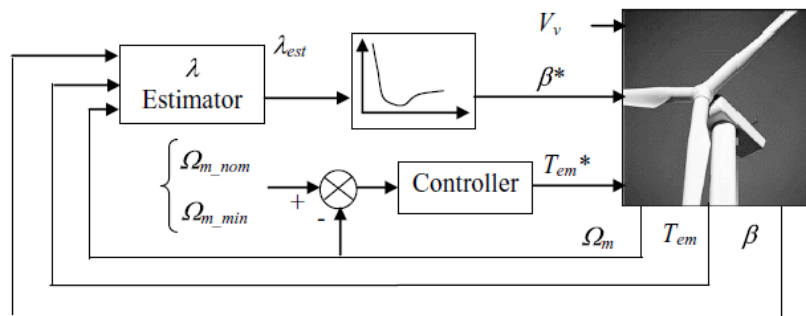


Figure: 3.11. Control schemes for regions 1 and 3.

3.2.1.6 REGIONS 1 AND 3

Minimum and Maximum Speed Control The main objective is to maintain a constant speed of rotation of the turbine at its minimum value in Zone 1 and its nominal value in Zone 3. Regarding energy efficiency, maximization is not as high a priority as in Zone 2, where the speed of the turbine may evolve to maintain a specific speed λ_{opt} corresponding to the maximum power coefficient C_{p-max} . Here, the generator operates at constant speed. The specific speed λ varies with wind speed. Depending on the shape of the curves of power coefficient parameterized by the pitch angle, it might be interesting to vary this angle to optimize aerodynamic performance. It is therefore interesting to plot the curve representing the optimum blade angle, giving it a maximum power coefficient for a given λ . The reference pitch of maximum energy efficiency is λ , a given specific speed obtained from this curve. See Figure 3.11.

3.2.1.7 REGION 2: MAXIMUM POWER TRACKING

In this operation region, the objective of the speed control is to follow the path of maximum power extraction. In the literature, different methods are proposed to regulate the wind turbine at partial load following the maximum power extraction trajectory. Two different types of controllers have been considered; one consists of taking as the electromagnetic torque reference the electromagnetic torque related to the maximum power curve of Figure 3.10 for each turbine rotational speed value and using the dynamically stable nature of the VSWT around this curve. This controller is called the indirect speed controller (ISC). The second controller generates the optimal turbine rotational speed (this is linked to the optimal tip speed ratio) for each wind speed value, and uses this as the turbine rotational speed reference. Then, it controls the turbine rotational speed with a regulator. It is called the direct speed controller (DSC).

3.2.1.8 INDIRECT SPEED CONTROLLER (ISC)

It can easily be shown that the WT is dynamically stable around any point of the maximum power curve of Zone 2 of Figure 3.10. This means that for any rotational speed variation around a point in the maximum power curve, the VSWT naturally goes back to its operating point.

Imagine that the VSWT is operating at point a of the curve in Figure 3.12a, the wind speed and the electromagnetic torque being fixed. If the turbine rotational speed is reduced to $\Omega_{t,b}$, the operating point passes to point b , and the turbine torque is then $T_{t,b}$. The electromagnetic torque is fixed to its preceding value corresponding to $T_{t,a}$, so $T_{t,b}$ is higher than T_{em} , and the turbine rotational speed increases until it is again stabilized around the $\Omega_{t,a}$ value.

Considering this stability property, the aerodynamic torque T_t can be kept in the maximum power curve in response to wind variations, if the electromagnetic torque T_{em} is controlled in a way to follow this curve. Actually, imagine that the VSWT is operating at point a of the curve in Figure 3.12b.

When the wind speed value increases from V_{v1} to V_{v2} , the operating point becomes b , and the turbine torque becomes $T_{t,b}$. The controller provides the electromagnetic torque corresponding to the maximum power curve (point c), which is smaller than $T_{t,b}$. This makes the turbine rotational speed increase until it reaches the equilibrium point c .

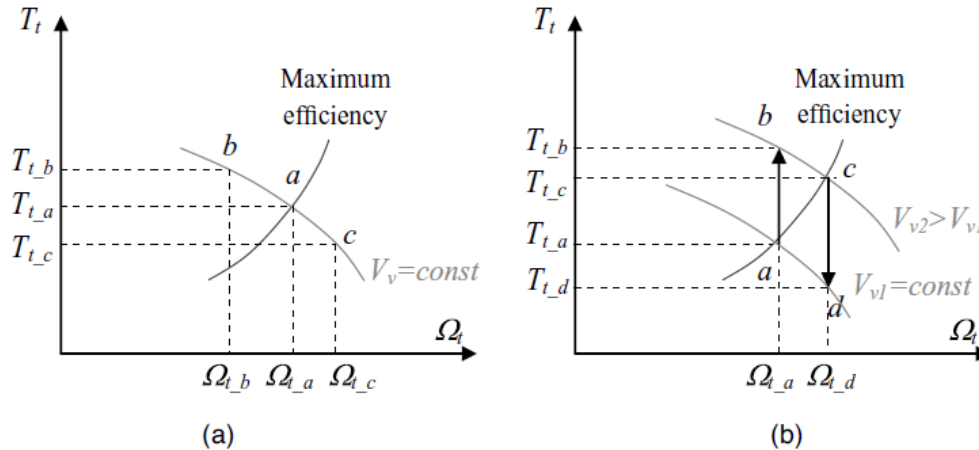


Figure: 3.12. Stability study around a point of the maximum power curve.

When the turbine is working on the maximum power point,

$$\lambda_{opt} = \frac{R\Omega_t}{V_v}, \quad C_p = C_{p_max}, \quad \text{and} \quad C_t = C_{t_opt}$$

The aerodynamic torque extracted by the turbine is then given by

$$T_t = \frac{1}{2} \rho \pi R^3 \frac{R^2 \Omega_t^2}{\lambda_{opt}^2} \frac{C_{p,max}}{\lambda_{opt}} \quad (3.13)$$

That is,

$$T_t = \frac{1}{2} \rho \pi \frac{R^5 \Omega_t^2}{\lambda_{opt}^3} C_{p,max} \Omega_t^2 = k_{opt-t} \Omega_t^2 \quad (3.14)$$

where

$$k_{opt-t} = \frac{1}{2} \rho \pi \frac{R^5 \Omega_t^2}{\lambda_{opt}^3} C_{p,max}$$

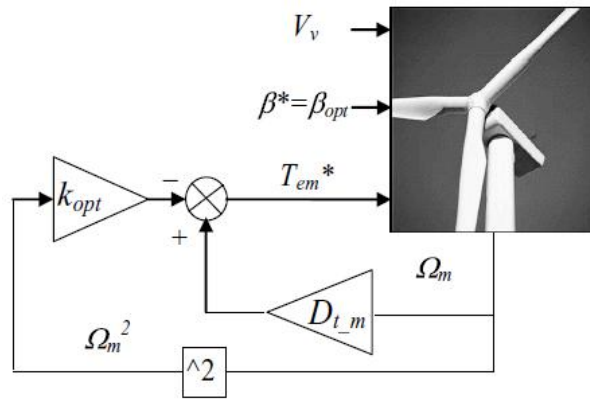


Figure: 3.13. Indirect speed control ($D_{tm}=D_t + D_m$).

It results in an optimal torque evolving as a quadratic function of the wind turbine speed. Moreover, from Equation (3.10) written in steady state,

$$0 = \frac{T_t}{N} - D_t \Omega_t N - K_m (\Omega_{t-ar} - \Omega_m) \quad (3.15)$$

$$0 = T_{em} - D_m \Omega_m - K_m (\Omega_m - \Omega_{t-ar})$$

where $\Omega_m = N \Omega_t$

$$T_{em} = -\frac{T_t}{N} + (D_t + D_m) \Omega_m \quad (3.16)$$

Replacing T_t in Equation (3.16) by the expression (3.14), we have

$$T_{em} = -k_{opt} \Omega_m^2 + (D_t + D_m) \Omega_m \quad (3.17)$$

where

$$k_{opt} = \frac{1}{2} \rho \pi \frac{R^5}{\lambda_{opt}^3 N^3} C_{p_max} \quad (3.18)$$

This last expression leads to the controller illustrated in Figure 3.13.

As seen in Equation (3.17), the behavior of the rotational speed Ω_t depends on the dynamics of the mechanical coupling.

With the ISC method, the behavior of the electromagnetic torque T_{em} and that of Ω_t is the same, since the relation between Ω_t and T_{em} has no dynamics. The electromagnetic torque is not used to increase the Ω_t dynamics as it could be if it were the output of a regulator. Thus, the main disadvantage of the ISC is that the mechanical coupling dynamics is not cancelled out, leading to a fixed soft response of the system.

3.2.1.9 DIRECT SPEED CONTROLLER (DSC)

The DSC tracks the maximum power curve more closely with faster dynamics.

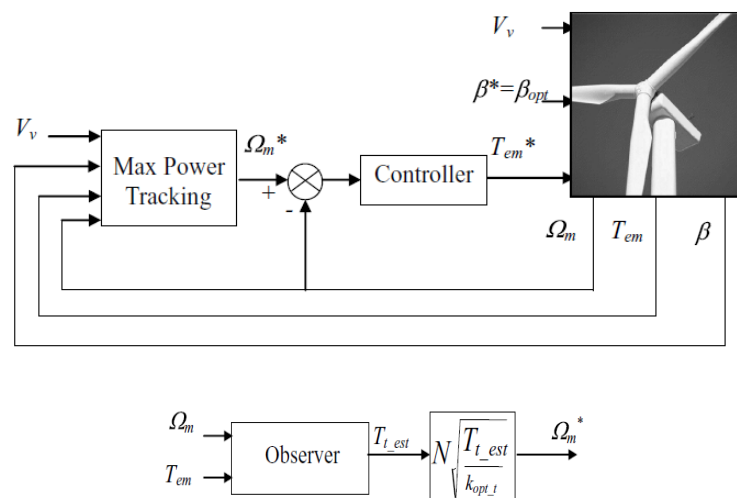


Figure: 3.14. Direct speed control.

Knowing the definition of the tip speed ratio λ , the optimal VSWT rotational speed Ω_{t_opt} could be found from the wind speed (V_v). Unfortunately, V_v cannot be measured because it is a fictitious wind speed; it does not exist.

The rotational speed optimal value can nevertheless be obtained from an estimation of the aerodynamic torque. An observer based on Equation (3.10) and using magnitudes such as the electromagnetic torque T_{em} and the turbine rotational speed Ω_t , directly linked to measured signals, can easily be designed to estimate the turbine aerodynamic torque T_{t_est} .

Thus, from equation (3.14) in the optimal operating point,

$$\Omega_m^* = N \sqrt{\frac{T_{t_est}}{k_{opt_t}}}$$

Once the rotational speed reference is generated, a regulator controls Ω_t using the electromagnetic torque value T_{em} . The diagram of the DSC is illustrated in Figure 3.14.

3.2.1.10 REGION 4: POWER CONTROL

The most common control structure for controlling the wind turbine in this region is illustrated in Figure 3.15. Here the electromagnetic torque is held constant at its nominal value. Most of the electrical power generated is that of the stator, that is, the electro-magnetic torque produced by the electrical stator pulsations; this structure leads to proper regulation of electric power. The flicker emission is therefore low with this configuration. The electromagnetic torque does not, however, contribute to regulation of the speed of rotation. Another disadvantage is that, since T_{em} is constant, the mechanical coupling at low fundamental resonance and flexibility of this coupling cannot be dumped.

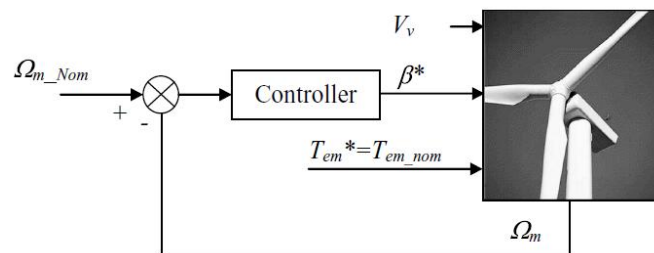


Figure: 3.15. Power control.

3.3 DOUBLY FED INDUCTION GENERATOR (DFIG)

This chapter introduces the operation and control of a Doubly Fed Induction Generator (DFIG) system. The DFIG is currently the system of choice for multi-MW wind turbines. The aerodynamic system must be capable of operating over a wide wind speed range in order to achieve optimum aerodynamic efficiency by tracking the optimum tip speed ratio. Therefore, the generator's rotor must be able to operate at a variable rotational speed. The DFIG system therefore operates in both sub- and super-synchronous modes with a rotor speed range around the synchronous speed.

The stator circuit is directly connected to the grid while the rotor winding is connected via slip-rings to a three-phase converter. For variable-speed systems where the speed range requirements are small, for example $\pm 30\%$ of synchronous speed, the DFIG offers adequate performance and is sufficient for the speed range required to exploit typical wind resources [40-44].

An AC-DC-AC converter is included in the induction generator rotor circuit. The power electronic converters need only be rated to handle a fraction of the total power -the rotor power – typically about 30% nominal generator power. Therefore, the losses in the power electronic converter can be reduced, compared to a system where the converter has to handle the entire power, and the system cost is lower due to the partially-rated power electronics. This chapter will introduce the basic features and normal operation of DFIG systems for wind power applications basing the description on the standard induction generator. Different aspects that will be described include their variable-speed feature, power converters and their associated control systems, and application issues.

3.3.1 POWER FLOW/OPERATING MODES OF DFIG

The DFIG stator is connected to the grid with fixed grid frequency (f_s) at fixed grid voltage (V_s) to generate constant frequency AC Power during all operating conditions and the rotor is connected to the frequency converter/VSC having a variable (slip/rotor) frequency ($f_r = s \cdot f_s$). At constant frequency f_s , the magnetic field produced in the stator rotates at constant angular velocity/speed ($\omega_s = 2 \pi f_s$), which is the synchronous speed of the machine. The stator rotating magnetic field will induce a voltage between the terminals of the rotor. This induced rotor voltage produces a rotor current (I_r), which in turn produces a rotor magnetic field that rotates at variable angular velocity/speed ($\omega_r = 2 \pi f_r$). Usually the stator and rotor have the same number of poles (P) and the convention is that the stator magnetic field rotates clockwise. Therefore, the stator magnetic field rotates clockwise at a fixed constant speed of ω_s (rpm) = $120 f_s / P$. Since the rotor is connected to the variable frequency VSC, the rotor magnetic field also rotates at a speed of ω_r (rpm) = $120 f_r / P$.

3.3.2 SUB-SYNCHRONOUS SPEED MODE

Figure 3.16 illustrates the case where the rotor magnetic field rotates at a slower speed than the stator magnetic field.

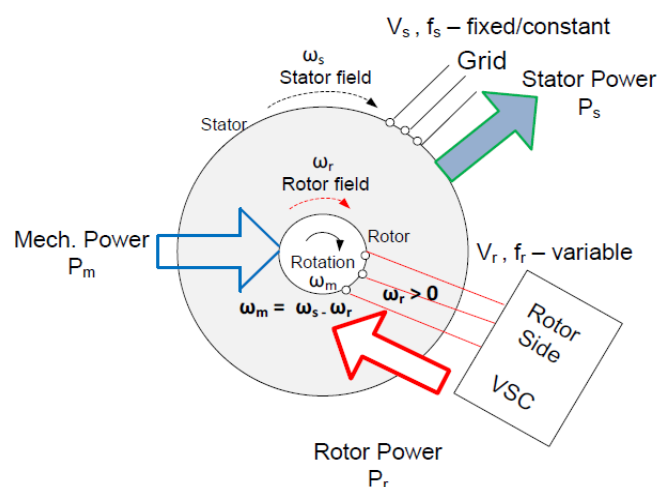


Figure: 3.17. Sub-synchronous operating mode of DFIG.

The machine is operated in the sub-synchronous mode, i.e., $\omega_m < \omega_s$,

- if and only if its speed is exactly $\omega_m = \omega_s - \omega_r > 0$, and
- both the phase sequences of the rotor and stator mmf's are the same and in the positive direction, as referred to as positive phase sequence ($\omega_r > 0$). This condition takes place during slow wind speeds. In order to extract maximum power from the wind turbine, the following conditions should be satisfied:
 - The rotor side VSC shall provide low frequency AC current (negative V_r will apply) for the rotor winding.
 - The rotor power shall be supplied by the DC bus capacitor via the rotor side VSC, which tends to decrease the DC bus voltage. The grid side VSC increases/controls this DC voltage and tends to keep it constant. Power is absorbed from the grid via the grid side VSC and delivered to the rotor via the rotor side VSC. During this operating mode, the grid side VSC operates as a rectifier and rotor side VSC operates as an inverter. Hence power is delivered to the grid by the stator.
 - The rotor power is capacitive .

3.3.3 SUPER-SYNCHRONOUS SPEED MODE

The super-synchronous speed mode is achieved by having the rotor magnetic field rotate counterclockwise. Figure 3.17 represents this scenario. However, in order to represent the counterclockwise rotation of the rotor, which is analytically equivalent to inverting the direction of the rotor magnetic field.

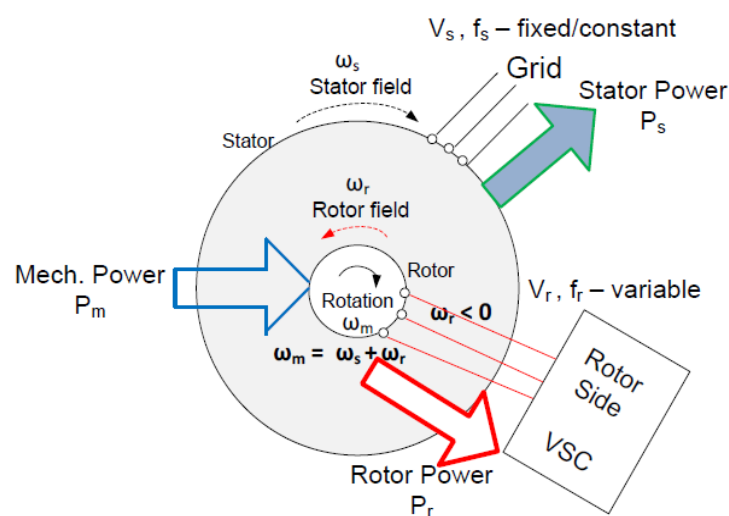


Figure: 3.17. Super-synchronous operating mode of DFIG.

The machine is operated in the super-synchronous mode, i.e., $\omega_m > \omega_s$,

- if and only if its speed is exactly $\omega_m = \omega_s - (-\omega_r) = \omega_s + \omega_r > 0$, and
- the phase sequence in the rotor rotates in opposite direction to that of the stator, i.e., negative phase sequence ($\omega_r < 0$). This condition takes place during the condition of high wind speeds. The following conditions need to be satisfied in order to extract maximum power from the wind turbine and to reduce mechanical stress:
 - The rotor winding delivers AC power to the power grid through the VSCs.
 - The rotor power is transmitted to DC bus capacitor, which tends to raise the DC voltage. The grid side VSC reduces/controls this DC-link voltage and tends to keep it constant. Power is extracted from the rotor side VSC and delivered to the grid. During this operating mode, the rotor side VSC operates as a rectifier and the grid side VSC operates as an inverter. Hence power is delivered to the grid directly by the stator and via the VSCs by the rotor.
 - The rotor power is inductive.

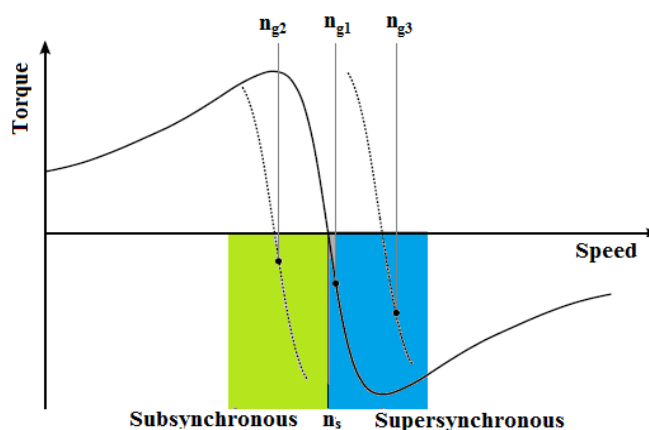


Fig: 3.18. Torque-speed characteristics of induction machine.

The torque speed characteristic of doubly fed induction generator is shown in Figure.3.18.

3.3.4 SYNCHRONOUS SPEED MODE

The synchronous speed mode is represented by figure 3.19.

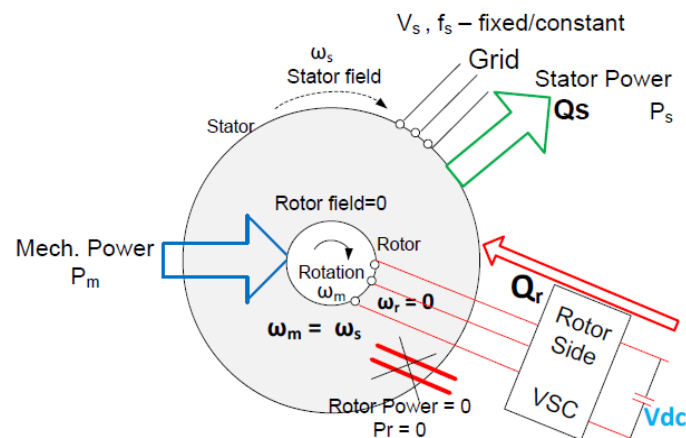


Figure:3.19.Synchronous operating mode of DFIG

The machine is operated in the synchronous speed mode, i.e., $\omega_m = \omega_s$,

- if and only if its speed is exactly $\omega_m = \omega_s - 0 = \omega_s > 0$, and
- the phase sequence in the rotor is the same as that of the stator, but no rotor mmf is produced ($\omega_r = 0$). The following conditions are necessary in order to extract maximum power from the wind turbine under this condition:
 - The rotor side converter shall provide DC excitation for the rotor, so that the generator operates as a synchronous machine. The rotor side VSC will not provide any kind of AC current/power for the rotor winding. Hence the rotor power is zero ($P_r = 0$).
 - A substantial amount of reactive power can still be provided to the grid by the stator. As per the operating modes described above, at any wind speeds a wide range of variable speed operation can be performed to achieve maximum wind power extraction.

3.3.5 MODELLING OF DFIG

The doubly fed induction generator has been used for years for variable speed drives. The stator is connected directly to the grid and the rotor is fed by a bidirectional converter that is also connected to the grid (Figure 3.20). Using vector control techniques, the bidirectional converter assures energy generation at nominal grid frequency and nominal grid voltage independently of the rotor speed. The converter's main aim is to compensate for the difference between the speed of the rotor and the synchronous speed with the slip control [44-45].

The main characteristics may be summarized as follows:

- Limited operating speed range (-30% to + 20%)
- Small scale power electronic converter (reduced power losses and price)
- Complete control of active power and reactive power exchanged with the grid
- Need for slip-rings
- Need for gearbox (normally a three-stage one)

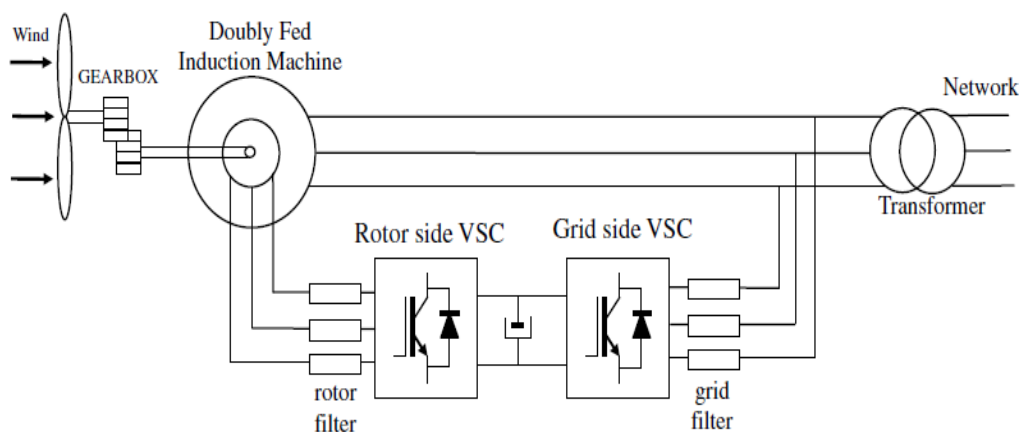


Figure: 3.20. Doubly fed induction machine based wind turbine.

For a DFIG associated with a back-to-back converter on the rotor side and with the stator directly connected to the grid, an SFOC (stator flux oriented control) system is used in order to control separately the active and reactive power on the stator side [45].

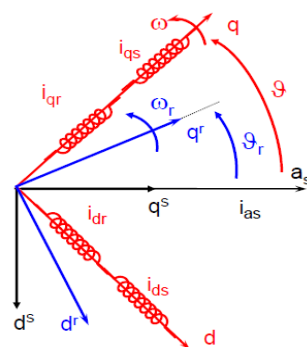


Figure: 3.21. Phasor diagram of DFIG.

In the dq reference frame rotating synchronously with the stator flux, the stator voltages and flux equations for a DFIG can be written as follows

$$V_{ds} = R_s i_{ds} + \frac{d\phi_{ds}}{dt} - \omega \phi_{qs} \quad (3.19)$$

$$V_{qs} = R_s i_{qs} + \frac{d\phi_{qs}}{dt} + \omega \phi_{ds} \quad (3.20)$$

$$V_{dr} = R_r i_{dr} + \frac{d\phi_{dr}}{dt} - (\omega_s - \omega) \phi_{rq} \quad (3.21)$$

$$V_{qr} = R_r i_{qr} + \frac{d\phi_{qr}}{dt} - (\omega_s - \omega) \phi_{rd} \quad (3.22)$$

$$\phi_{ds} = L_s i_{ds} + L_m i_{dr} \quad (3.23)$$

$$\phi_{qs} = L_s i_{qs} + L_m i_{qr} = 0$$

$$\phi_{dr} = L_r i_{dr} + L_m i_{ds} \quad (3.24)$$

$$\phi_{qr} = L_r i_{qr} + L_m i_{qs}$$

where ω_s is the stator flux pulsation, ω is the rotor electrical speed. In steady state conditions, by neglecting the stator phase resistance and by introducing the magnetizing current $i_{dms} = \phi_{ds}/L_m$, the stator voltage and current components become

$$V_{ds} \cong 0 \quad (3.25)$$

$$V_{qs} \cong |V_s| \cong \omega \phi_{ds} \quad (3.26)$$

$$i_{ds} = \frac{L_m}{L_s} (i_{dms} - i_{dr}) \quad (3.27)$$

$$i_{qs} = -\frac{L_m}{L_s} i_{qr} \quad (3.28)$$

The active and reactive powers are as follows

$$P_s = 1.5 (V_{ds} i_{ds} + V_{qs} i_{qs}) \quad (3.29)$$

$$Q_s = 1.5 (V_{qs} i_{ds} - V_{ds} i_{qs}) \quad (3.30)$$

By introducing (3.25)–(3.28) in (3.29) and (3.30), it is possible to rewrite the active and reactive power as function of stator voltage and rotor current components, leading to

$$P_s \cong -1.5|V_s| \cdot \frac{L_m}{L_s} i_{qr} \quad (3.31)$$

$$Q_s \cong 1.5|V_s| \cdot \frac{L_m}{L_s} \left(\frac{|V_s|}{2\pi f L_m} - i_{dr} \right) \quad (3.32)$$

By using (3.31) and (3.32) and assuming constant stator voltage magnitude V_s and frequency f , it is possible to consider the stator active power proportional to the q-axis rotor current component i_{qr} and the stator reactive power related to the d-axis rotor current component.

Electromagnetic torque of DFIG is given by

$$T_e = 1.5 Z_p (\varphi_{ds} i_{qs} - \varphi_{qs} i_{ds}) \quad (3.33)$$

The rotor side control of DFIG control system is shown in Fig. 3.22. This control has two cascaded control loops. The outer loop is dedicated to the stator active and reactive power control, whereas the inner loop is related to the control of the dq components of the rotor current [46]. In both cases PI controllers are used. Since the control system is symmetrical, the parameters of the controllers are the same for the d-axis and the q-axis currents loops and for the active and reactive power loops.

The two PI controllers of the outer loop are used to determine the dq components of the rotor current references on the basis of the active and reactive power errors. The two PI controllers of the inner loop are used to determine the dq components of the rotor modulating signals using the dq rotor current errors as input variables.

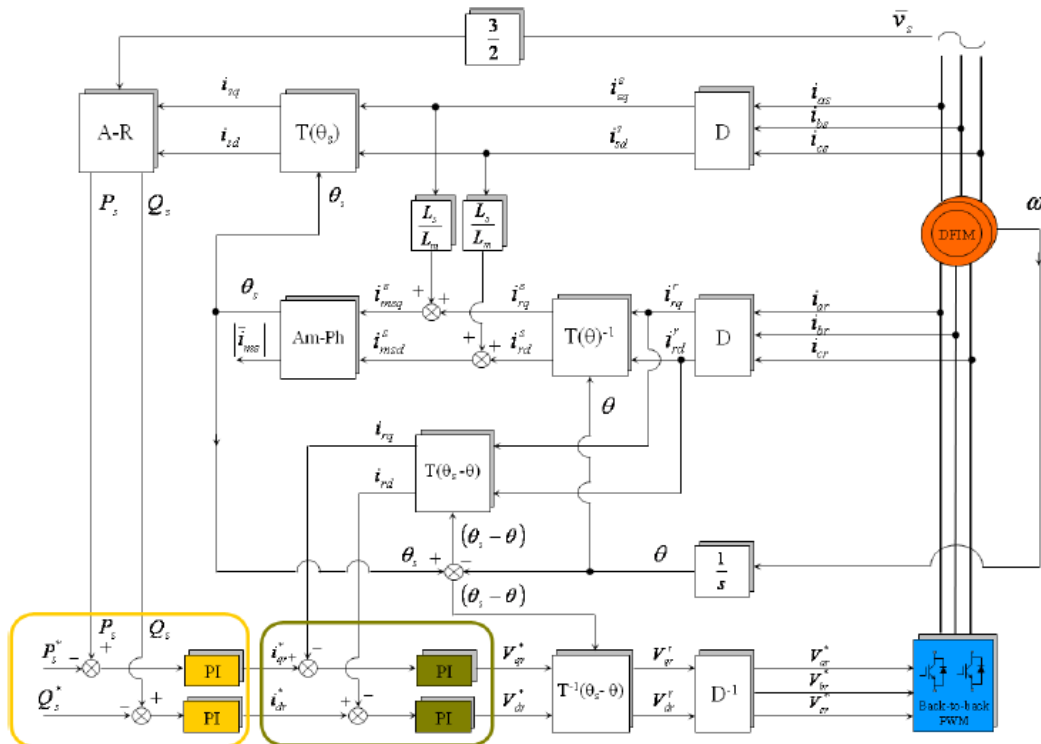


Fig. 3.22 Block-scheme representation of the DFIG control system.

The transformations from three phase quantities to a dq stationary reference frame and the inverse transformations are performed by the blocks D and D^{-1} respectively. Being θ_s and θ the stator flux phase angle and the rotor position angle respectively, the block $T(\theta_s)$ represents the transformation from a stationary reference frame to a synchronous rotating reference frame, as well as the block $T(\theta_s-\theta)$ represents the transformation from a rotor reference frame to a synchronous stator flux oriented reference frame. The blocks $T^T(\theta_s)$ and $T^T(\theta_s-\theta)$ represent the corresponding inverse transformations.

The control algorithm computes the phase angle θ_s of the stator flux vector using the components of the magnetizing current space vector i_{msd}^s and i_{msq}^s in the stator reference frame, according to:

$$\theta_s = \arctan\left(\frac{i_{msq}^s}{i_{msd}^s}\right) \quad (3.34)$$

In order to increase the accuracy in the computation of the phase angle θ_s , a complex digital filter is applied to isolate the fundamental frequency component of the magnetizing current space vector \bar{i}_{ms}^s . An alternative solution would be the utilization of a Phase Locked Loop (PLL) system in order to track the fundamental phase angle. Such a solution will be presented in the next paragraph where the grid side control of the back to back converter is discussed. The complex digital filter was preferred since it allows to extract not only the phase angle but also the magnitude of the magnetizing current space vector that is used for the dynamic emf compensation in the q-axis rotor current loop.

The transfer function of the digital filter in terms of Laplace transform is derived hereafter. In the synchronous reference frame which rotates at a constant angular speed $2\pi f_s$, the filtered magnetizing current vector \bar{i}_{ms}^s is obtained by applying a first order low-pass filter to the magnetizing current vector $ms\ i$ yielding:

$$\bar{i}_{ms(fil)}^s = \frac{1}{1 + \tau_s} \bar{i}_{ms}^s \quad (3.35)$$

where τ is the low-pass filter time constant.

The magnetizing current vector in the synchronous reference frame is related to the magnetizing current vector in the stationary reference frame by the following relationship:

$$\bar{i}_{ms}^s = \bar{i}_{ms}^s e^{-j\theta_s} \quad (3.36)$$

By substituting (3.36) in (3.35), the equation of the filtered magnetizing current vector in the stationary reference frame becomes:

$$\bar{i}_{ms(fil)}^s = \frac{1}{1 + \tau_s - j\omega_s \tau} \bar{i}_{ms}^s \quad (3.37)$$

where ω_s is the stator flux angular frequency, assumed constant and equal to $2\pi fs$ [rad/s], i.e. the grid angular frequency. Then the dq components of the magnetizing current vector can be derived from (3.37), yielding:

$$i_{msd(fil)}^s = \frac{(1 + \tau_s) i_{msd}^s - \omega_s \tau i_{msq}^s}{(1 + \tau_s)^2 + \omega_s^2 \tau^2} \quad (3.38)$$

$$i_{msq(fil)}^s = \frac{(1 + \tau_s) i_{msq}^s - \omega_s \tau i_{msd}^s}{(1 + \tau_s)^2 + \omega_s^2 \tau^2} \quad (3.39)$$

Equations (3.38),(3.39) and (3.34) are implemented in the block named “Am-Ph” in the control scheme of Fig. 3.23. It’s worth underlining that an Euler discretization for (3.38),(3.39) may lead to unstable behavior of the complex digital filter for high value of the time constant τ . To overcome this limitation a discretization based on a second order Taylor series expansion has been adopted to make the filter stable for all the time constant values of interest.

Finally the block “A-R” of Fig. 3.23 calculates the stator active and reactive power by using(3.29) and (3.30).Once the relationship between stator and rotor dq current components in the stator flux oriented reference frame has been found, it’s possible to express rotor fluxes and voltages as a function of solely rotor currents.

In fact by substituting (3.27), (3.28) in (3.24) the following expression for the dq rotor fluxes can be retrieved:

$$\varphi_{rd} = \sigma L_r i_{rd} + \frac{L_m^2}{L_s L_m \omega_s} \left| \overline{v_s} \right| \quad (3.40)$$

$$\varphi_{rq} = \sigma L_r i_{rq} \quad (3.41)$$

where σ is the well known leakage factor expressed as:

$$\sigma = \frac{L_s L_r - L_m^2}{L_s L_r} \quad (3.42)$$

The rotor voltages as a function of the rotor currents can be obtained by substituting (3.27),(3.28), (3.40) and (3.41) in (3.21) and (3.22):

$$v_{rd} = R_r i_{rd} + \sigma L_r \frac{di_{rd}}{dt} - (\omega_s - \omega) \sigma L_r i_{rq} \quad (3.43)$$

$$v_{rq} = R_r i_{rq} + \sigma L_r \frac{di_{rq}}{dt} + (\omega_s - \omega) \sigma L_r i_{rd} + (\omega_s - \omega) \frac{L_m^2}{L_s L_m \omega_s} \left| \overline{v_s} \right| \quad (3.44)$$

These two equations are used for the design of rotor currents PI controllers as will be shown in the next chapter. If steady state operation is assumed and the rotor active power is computed through the following expression:

$$P_r = 1.5(v_{rd} i_{rd} + v_{rq} i_{rq}) \quad (3.45)$$

combining (3.43), (3.44) and (3.45) leads to:

$$P_r = 1.5(R_r i_{rd}^2 + R_r i_{rq}^2) + 1.5(\omega_s - \omega) \frac{L_m^2}{L_s L_m \omega_s} \left| \overline{v_s} \right| i_{rq} \quad (3.46)$$

Finally introducing in the last term at the right end side the relation between the rotor and stator q current components as in (3.28) we find the following expression relating stator and rotor active power under the hypothesis of negligible stator resistances:

$$P_r = 1.5(R_r i_{rd}^2 + R_r i_{rq}^2) - s P_s \quad (3.47)$$

$$s = \frac{\omega_s - \omega}{\omega_s} \quad \text{and} \quad P_s = 1.5 v_{sq} i_{sq} = 1.5 \left| \overline{v_s} \right| i_{sq} \quad (3.48)$$

Equation (3.47) is useful to understand the working principles and the power flows for this DFIG stator flux oriented control drive. It's worth noting that the motoring convention was adopted to write the expressions (3.29) and (3.45) for the stator and rotor active power. For this reason positive active power means power absorbed by the machine, whereas negative active power means power delivered by the machine.

Thus taking into account generating operations, P_s will be always negative and univocally determined by the dq rotor currents components, whereas the sign of P_r will depend on the slip sign s , if joule losses are neglected. More specifically if sub synchronous operations are considered (i.e. positive slip operations), the active power on the rotor side will be positive, i.e. power absorbed by the rotor windings. On the other hand if super synchronous operations are considered (i.e. negative slip operations), the active power on the rotor side will be

negative, i.e. power delivered by the rotor windings towards the back to back converter. Obviously (3.47) holds its validity also in motoring operating conditions. In this case stator active power will keep a positive sign, whereas the rotor active power will be delivered towards the converter if sub synchronous operations are considered and absorbed by rotor windings in case of super synchronous operations.

3.3.6 GRID SIDE CONTROL DESCRIPTION

In order to allow sub synchronous and super synchronous operating modes a back to back converter is commonly used on the rotor side of the DFIM. As shown in Fig. 3.3 this converter consists of a traditional inverter on the machine side and of a three phase PWM boost rectifier on the grid side with a common DC link. This topology allows obviously bidirectional power flow operations, i.e. from the machine to the grid and vice versa. Moreover the three phase PWM boost rectifier has other important features as nearly sinusoidal input currents, regulation of input power factor to unity, low harmonic distortion of line currents, adjustment and stabilization of DC link voltage and reduced capacitor size with respects to traditional passive rectifiers. The decoupling filter in Fig. 3.23 serves two main purposes: it's used as short term energy storage for the boost type converter and keeps the switching noise away from the power grid [46-50].

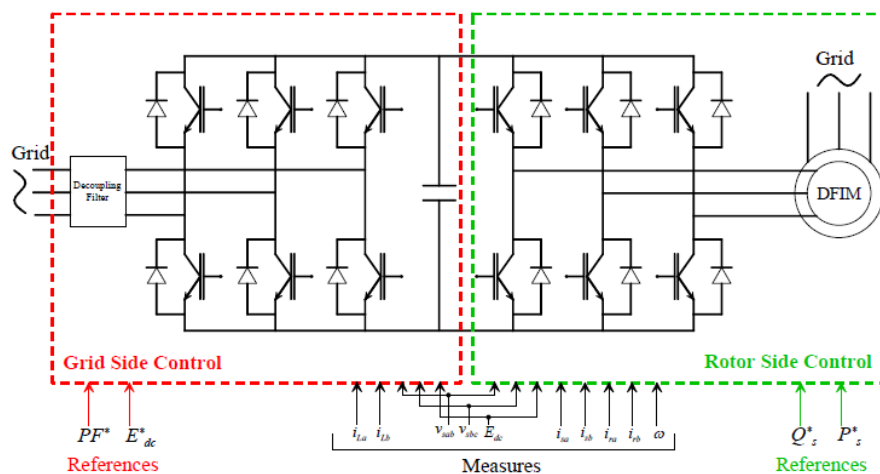


Figure:3.23. Simplified scheme of the back to back converter used to allow bidirectional power flow on the rotor side of the doubly fed induction machine.

In order to fulfill IEEE 519-1992 standards typically an LCL filter is applied between the PWM rectifier and the grid to reduce harmonics around the switching frequency and its multiplications. Anyway the project of such a filter is not a trivial task and is beyond the scope of this thesis. For this reason, in order to ease lab tests and to avoid instability problems linked to the resonant frequency of the LCL filter, three line inductors have been used for this purpose without losing in generality. In literature several strategies can be found for the control of PWM rectifiers such as Voltage Oriented Control (VOC), in which an internal

current loop guarantees high dynamic operations, or Direct Power Control (DPC), that is based on the instantaneous active and reactive power control loops. More recently new methods such as Virtual Flux Direct Power Control (VF-DPC) and Virtual Flux Voltage Oriented Control (VF-VOC) have been developed starting from the interpretation of the grid as a virtual machine in which a virtual flux can be estimated for control purposes.

Both DPC and VOC strategies have been implemented in simulations. Anyway for the experimental tests the VOC algorithm has been preferred since the grid side voltages are accurately measured, thus making the orientation strategy very easy to implement. For this reason only the aspects concerning VOC strategy will be presented in the next. With reference to Fig. 3.24 the set of equations for the PWM rectifier system can be derived as follow:

$$u_{ga} = R_f i_{ga} + L_f \frac{di_{ga}}{dt} + u_{ca} \quad (3.49)$$

$$u_{gb} = R_f i_{gb} + L_f \frac{di_{gb}}{dt} + u_{cb} \quad (3.50)$$

$$u_{gc} = R_f i_{gc} + L_f \frac{di_{gc}}{dt} + u_{cc} \quad (3.51)$$

$$C \frac{dE_{dc}}{dt} = S_a i_{ga} + S_b i_{gb} + S_c i_{gc} - i_{load} \quad (3.52)$$

where R_f and L_f are the resistance and the self inductance coefficient for the line inductors, i_{ga} , i_{gb} , i_{gc} are the line currents S_a , S_b , S_c represents the switching states of the three active rectifier legs (respectively 1 if the high side IGBT is conducting and 0 if the low side IGBT is conducting) and u_{ca} , u_{cb} , u_{cc} are the converter voltages, which can be expressed as:

$$u_{ca} = \frac{(2S_a - S_b - S_c)}{3} E_{dc} \quad (3.53)$$

$$u_{cb} = \frac{(2S_b - S_a - S_c)}{3} E_{dc} \quad (3.54)$$

$$u_{cc} = \frac{(2S_c - S_a - S_b)}{3} E_{dc} \quad (3.55)$$

Equations (3.49)-(3.55) completely describe the dynamic of the grid side back to back converter. By applying the three phase to two phase transformations and working in the grid voltage space vector reference frame (3.49)-(3.51) become:

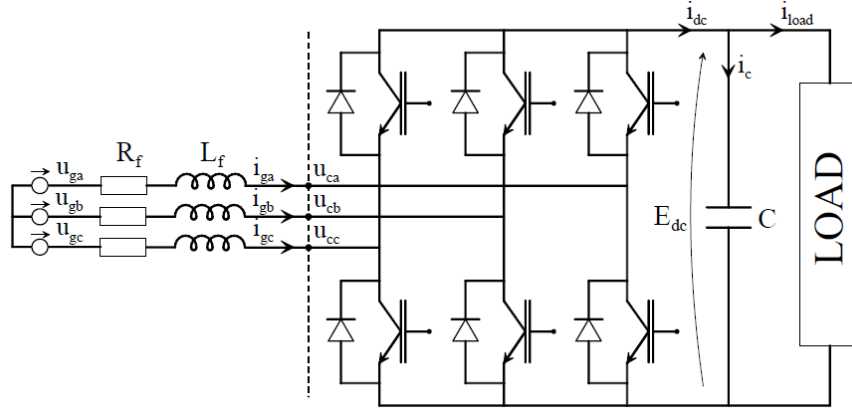


Figure: 3.24. Simplified representation of three phase PWM rectifier for bi-directional power flow.

$$u_{gd} = R_f i_{gd} + L_f \frac{di_{gd}}{dt} - \omega_s L_f i_{gq} + u_{cd} \quad (3.56)$$

$$u_{gq} = R_f i_{gq} + L_f \frac{di_{gq}}{dt} + \omega_s L_f i_{gd} + u_{cq} \quad (3.57)$$

where ω_s is the grid pulsation. Focusing the attention on the active and reactive power equations it is possible to notice that considering the d-axis of the synchronous reference frame aligned with the grid voltage space vector ($u_{gq}=0$) the active power is proportional to the i_{gd} current, whereas the reactive power is in inverse proportion to the i_{gq} current.

$$P_g = \frac{3}{2} (u_{gd} i_{gd} + u_{gq} i_{gq}) = \frac{3}{2} u_{gd} i_{gd} \quad (3.58)$$

$$Q_s = \frac{3}{2} (u_{gq} i_{gd} - u_{gd} i_{gq}) = -\frac{3}{2} u_{gd} i_{gq} \quad (3.59)$$

Thus a decoupled control of the active and reactive power can be achieved by imposing the proper value of the dq grid current components through the grid side converter. More in detail, neglecting the filter and converter losses, the active power balance of the line side and DC side gives:

$$i_{dc} = \frac{3}{2} \frac{u_{gd} i_{gd}}{E_{dc}} \quad (3.60)$$

Finally, the DC link voltage dynamic can be written as.

$$C \frac{dE_{dc}}{dt} = \frac{3}{2} \frac{u_{gd} i_{gd}}{E_{dc}} - i_{load} \quad (3.61)$$

From (3.61) it becomes clear that the DC link voltage can be controlled by the d component of the line current. On the other hand controlling the q component, we are able to control the reactive power and therefore the line power factor. For this reason, in order to have a unity power factor, the reference value for the q current component is always kept to zero.

Equations (3.56) and (3.57) shows that, if a perfect compensation of the cross coupling terms is achieved, two PI regulators can be designed considering the system as a first order system if delays due to the processing time of the algorithm, sampling of feedback variables and dead times of the converter are neglected. The direct and quadrature components of the inverter voltages for current regulation can be then computed as:

$$u_{cd}^* = u_{gd} + \omega_s L_f i_{gq} + \Delta u_{cd} \quad (3.62)$$

$$u_{cq}^* = -\omega_s L_f i_{gd} + \Delta u_{cq} \quad (3.63)$$

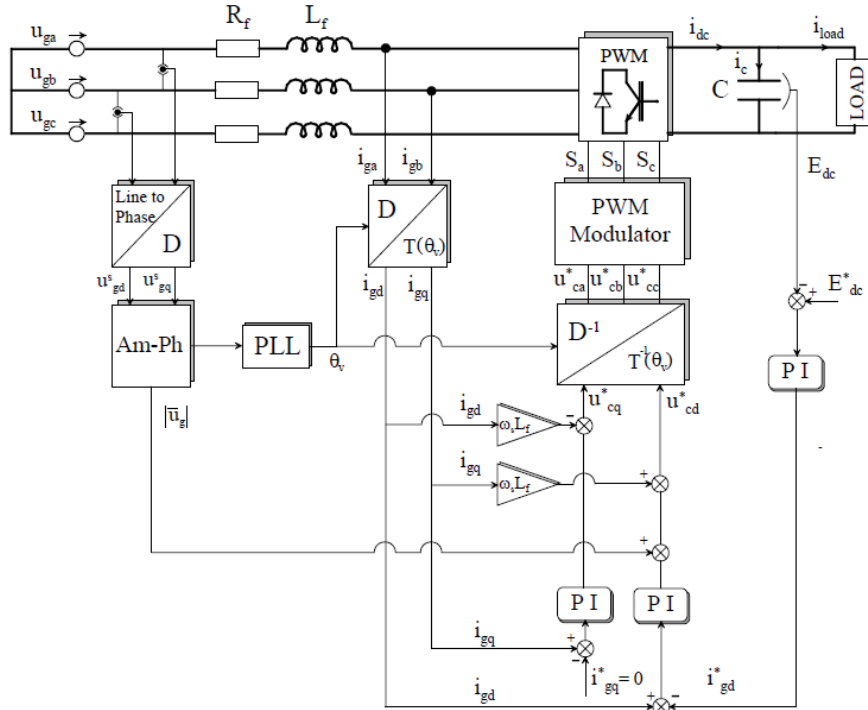


Figure: 3.25. Control scheme block diagram for the three phase PWM rectifier for bi-directional power flow.

where u_{gd} is the amplitude of the grid side voltage in the chosen reference frame and Δu_{cd} and Δu_{cq} are the output of the two current PI regulators with proportional gain K_p and integral gain K_i .

$$\Delta u_{cd} = K_p (i_{gd} - i_{gd}^*) + K_i \int (i_{gd} - i_{gd}^*) dt \quad (3.64)$$

$$\Delta u_{cq} = K_p (i_{gq} - i_{gq}^*) + K_i \int (i_{gq} - i_{gq}^*) dt \quad (3.65)$$

Finally an outer DC link voltage control loop is considered. The PI regulator is designed to furnish the proper d reference current component i_{gd}^* to the inner current loop in order to take the error on the DC link voltage to zero. The whole control scheme for the grid side converter of the back to back is depicted in Fig. 3.25, where the amplitude of the grid voltage space vector used as a feed-forward signal on the d axis loop is computed as:

$$\left| \overline{u_g} \right| = u_{gd} = \sqrt{u_{gd}^{s^2} + u_{gq}^{s^2}} \quad (3.66)$$

The matrixes D and $T(\theta_v)$ represent the three phase to two phase transformation and the stationary to synchronous reference frame transformation respectively; similarly the D^{-1} and $T^{-1}(\theta_v)$ are used for the inverse transformation from the synchronous to the stationary reference frame and from two to three phase system.

For a correct tracking of the phase angle of the grid voltage space vector a Phase Locked Loop (PLL) system has been used. This system allows to extract only the phase angle related to the fundamental positive sequence component of the grid voltage space vector. In such a way we are able to keep the voltage orientation even in presence of a strong harmonic distortion on the grid side due both to low pre existing harmonic components and to higher harmonics introduced by inverter commutations.

A block scheme of the employed PLL system is presented in Fig. 3.26. The aim of this closed loop system consists in bringing to zero the error between the actual phase angle of the fundamental positive sequence component of the grid voltage space vector γ and the synchronous reference frame phase angle θ_v employed in reference frame transformations.

If we consider a three phase sinusoidal and symmetric voltage system, the two components of the fundamental grid voltage space phasor can be computed as:

$$\cos \gamma = \frac{u_{gd}^s}{\sqrt{u_{gd}^{s^2} + u_{gq}^{s^2}}} \quad (3.67)$$

$$\sin \gamma = \frac{u_{gq}^s}{\sqrt{u_{gd}^{s^2} + u_{gq}^{s^2}}} \quad (3.68)$$

Subsequently (3.67) and (3.68) are multiplied by the two components of the space phasor used for reference frame transformations as follow:

$$\sin \gamma \cos \theta_v - \sin \theta_v \cos \gamma = \sin(\gamma - \theta_v) \quad (3.69)$$

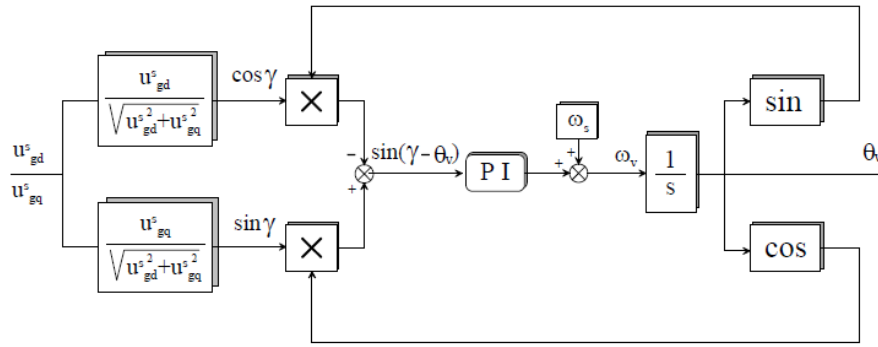


Figure: 3.26. Phase Locked Loop (PLL) block diagram for the simulated and implemented three phase PWM rectifier.

Thus the input of the PI regulator is the sine of the error between the two phase angles, whereas its output is the pulsation of $\theta_v(t)$, whose variation allows to bring the error to zero. For this purpose such a pulsation ω_v is integrated and its sine and cosine trigonometric functions are used as feedback signals.

During the initial locking phase the input of the PI regulator (3.69) will obviously assume both positive and negative values. Assuming that $\theta_v(t)$ is lagging behind the fundamental voltage phase angle γ , there will be a time interval in which the PI regulator will increase the pulsation ω_v (for positive values of the sine of the error) making it closer to the pulsation of the input grid voltage space phasor. Then, for negative values of the sine of the error, there will be a shorter time interval in which the PI regulator will decrease the pulsation ω_v , thus increasing the difference between such a pulsation and the fundamental pulsation of the grid voltage space phasor. This asymmetry in time between the positive and negative half wave of the sine of the error produces a positive mean value in the input signal of the PI regulator and therefore a periodic increase of the pulsation ω_v until the output angle $\theta_v(t)$ perfectly tracks the fundamental grid voltage phase angle γ with zero steady state error.

In operating conditions close to synchronization the error between the two phase angles γ and θ_v is small and close to zero so that the input of the PI regulator can be approximated to:

$$\sin(\gamma - \theta_v) \cong \delta \quad \text{with } \delta = \gamma - \theta_v \quad (3.70)$$

With such approximation the PLL system can be considered to have a linear phase detector, i.e. an input signal to the PI regulator proportional to the difference between the fundamental component phase angle of the grid voltage and the synchronous reference frame phase angle employed in reference frame transformations.

Typically the design of the PI regulator parameters is performed making reference to the linear approximated system presented in Fig. 3.27. The feed forward open loop transfer function has two poles at the origin. Consequently the steady state error to a ramp input will be zero as requested to a PLL system.

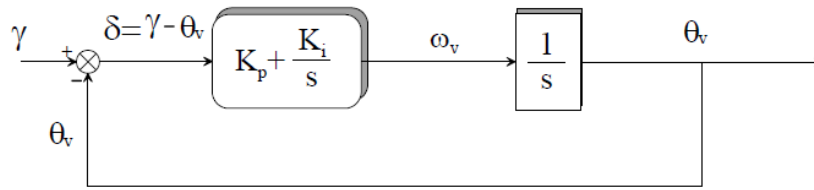


Figure: 3.27. Linearized PLL block diagram for the design of PI regulator parameters.

On the other hand, the closed loop system is a simple second order system with one zero and two poles. The choice of the proportional and integral gains (K_p and K_i respectively) has to be a compromise between a fast dynamic response during the locking phase and a limited bandwidth of the system in order to filter higher order harmonics present in the grid voltage space vector.

Such a bandwidth has been chosen in order to damp the effect of an inverse sequence on the grid voltage consisting in a disturbance on the input signal at a pulsation of $2\omega s$. Once the system is designed to damp the effect of an inverse sequence, it is consequently able to filter all the higher order harmonics usually present on the grid voltage.

3.3.7 GRID MODEL IN DFIG SYSTEM

Grid was defined as a controllable three-phase voltage source [51-54]. The phase voltages defined as:

$$V_a = V_m \sin \omega t \quad (3.71)$$

$$V_b = V_m \sin(\omega t - \frac{2\pi}{3}) \quad (3.72)$$

$$V_c = V_m \sin(\omega t - \frac{4\pi}{3}) \quad (3.73)$$

In the above equations ω represents the angular frequency and V_m represents the phase voltage amplitude.

The three-phase voltage source line-to-line voltages are defined as:

$$V_{ab} = V_a - V_b$$

$$V_{bc} = V_b - V_c$$

$$V_{ca} = V_c - V_a$$

Figure A.12 presents the vector representation of the grid voltage and current.

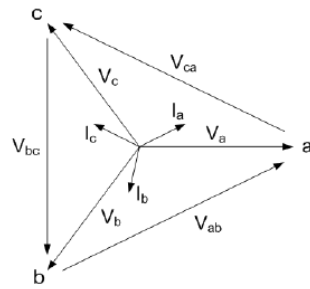


Figure: 3.28.Phasor diagram for balanced 3 phase voltage.

Figure 3.28 represent vector representation of the symmetrical three-phase grid.

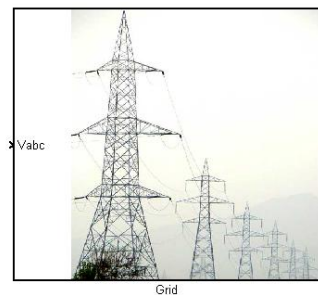


Figure: 3.29. Implemented grid model.

Above model was implemented in MATLAB Simulink software and it is presented in Figure 3.29.

3.4 REFERENCES

- [1] Bjørn Andresen, Eckardt Siebenthaler, and Lorenz Feddersen, “Variable speed wind turbine having a passive grid side rectifier with scalar power control and dependent pitch control,” Canadian Patent Application CA2003/418561, November 2003.
- [2] L.N. Arruda, B.J. Cardoso Filho, S. M. Silva, S.R. Silva, and A.S.A.C. Diniz, “Wide bandwidth single and three-phase PLL structures for grid-tied PV systems”, Photovoltaic Specialist Conference, Vol. 1:pp. 1660–1663, Sept 2000.
- [3] D. Arsudis and W. Vollstedt, “ Sensor-less power control of a double-fed AC-machine with nearly sinusoidal line currents. EPE 3rd European Conference on Power Electronics and Application”, Vol. 2:pp. 899–904, 9.-12. October 1989.
- [4] D. Arsudis and W. Vollstedt, “Sensorlose regelung einer doppeltgespeisten asynchrony maschine mit geringen netz'uckwirkungen”, Archiv f'ur Elektrotechnik, Vol.74:pp. 89–97, 1990.
- [5] Michael M. Bech, “Analysis of random pulse-width modulation techniques for power electronic converters”, PhD thesis, Aalborg University, 9220 Aalborg East, November 2000. ISBN: 87-89179-32-3.
- [6] M.H. Bierhoff and F.W. Fuchs, “Semiconductor losses in Voltage Source and Current Source IGBT Converters Based on Analytical Derivation”, IEEE Power Electronics Specialists Conference, Vol. 4:pp. 2836–2842, June 2004.
- [7] Frede Blaabjerg, Ulrik Jaeger, Stig Munk-Nielsen, and John K. Pedersen, “Power losses in PWM-VSI inverter using NPT or PT devices”, IEEE Transactions on Power Electronics, Vol. 10 No. 3:pp. 358–367, May 1995.
- [8] E. Bogalecka, “Power control of a doubly fed induction generator without speed or position sensor”, EPE 5th European Conference on Power Electronics and Application, Vol. 8:pp. 224–228, 13.-16. September 1993.
- [9] Heinz Willi Van Der Broeck, Hans-Christoph Skudelny, and Georg Viktor Stanke, “ Analysis and realization of a pulse width modulator based on voltage space vectors”, IEEE Transactions on Industry Applications, Vol. 24 No. 1:pp. 142–150, January/February 1988.
- [10] S.-K. Chung, “Phased-locked loop for grid-connected three-phase power conversion systems”, IEE Proc.-Electr. Power Appl., Vol. 147 No. 3:pp. 213–219, May 2000.
- [11] M. Depenbrock, “Pulse width control of a 3-phase inverter with non-sinusoidal phase voltages”, IEEE Industrial Application Society Annual Meeting, pages 399– 403, 1977.
- [12] B. Eggert, “1.5 MW wind power station with low ac-line distortion using a standard doubly fed generator system with field orientated control”, EPE 7th European Conference on Power Electronics and Application, Vol. 2:pp. 739–742, 8.-10. September 1997.
- [13] Adel A. Ghandakly and Ziad H. Sbeiti, “A digital optimal controller for VSCF wind generators”, IEEE Industrial Application Society Annual Meeting, Vol. 2:p.1787–1792, 7.-12. October 1990.
- [14] Anders Grauers, “Efficiency of three wind energy generator systems”, IEEE Transactions on Energy Conversion, Vol. 11 No. 3:pp. 650–657, September 1996.

- [15] Ahmet M. Hava, Russel J. Kerkman, and Thomas A. Lipo, "A high performance generalized discontinuous PWM algorithm", IEEE Applied Power Electronics Conference and Exposition, Vol. 2:pp. 886–894, 23.-27. February 1997.
- [16] N. Mohan, T. M. Undeland, and W. P. Robbins, "Power Electronics: Converters, Applications, and Design", 3rd Ed., John Wiley & Sons Inc., October 2002.
- [17] J. I. Jang, Y. S. Kim, and D. C. Lee, "Active and reactive power control of DFIG for wind energy conversion under unbalanced grid voltage", IPEMC Shanghai, vol. 3, pp. 1487-1491, Aug. 2006.
- [18] R. Pena, J. Clare, and G. Asher, "Doubly fed induction generator using back-to-back PWM converters and its application to variable-speed wind-energy generation," IEE Proceedings Electric Power Applications, vol. 143, pp. 231–241, May 1996.
- [19] J.G. Slootweg, H. Polinder, and W. L. Kling, "Dynamic modeling of a wind turbine with doubly fed induction generator", in Proceeding of IEEE, Power Engineering Society Summer Meeting, vol.1, pp. 644-649, Vancouver, Canada, Jul., 2001.
- [20] R. Datta and V.T. Ranganathan, "A method of tracking the peak power points for a variable speed wind energy conversion system", IEEE Trans. on Energy Conversion, vol.18, No.1, pp. 163- 168, 2003.
- [21] S. Muller, M. Deicke, and R. D. Doncker, "Doubly fed induction generator systems for wind turbines," IEEE Industry Applications Magazine, vol. 8, pp. 26–33, June 2002.
- [22] R. Pena, J. C. Clare, and G. M. Asher, "Double fed induction generator using back-to-back PWM converter and its application to variable-speed wind-energy generation," Proc. Inst. Elect. Eng. B, vol. 143, no. 3, pp. 231–241, 1996.
- [23] A. Lubosny, "Wind Turbine Operation in Electric Power Systems -Advanced Modeling", Springer Verlag, 2003.
- [24] Ahmet M. Hava, Russel J. Kerkman, and Thomas A. Lipo, "Simple analytical and graphical methods for carrier-based PWM-VSI drives", IEEE Transactions on Power Electronics, Vol. 14 No. 1:pp. 49–61, January 1999.
- [25] Joachim Holtz, Wolfgang Lotzkat, and Ashwin M. Khambadkone "On continuous control of PWM inverters in the over modulation range including the six-step mode", IEEE Transactions on Power Electronics, Vol. 8 No. 4:pp. 546–553, October 1993.
- [26] K. G. King, "A three-phase transistor class-B inverter with sine-wave output and high efficiency", IEE International Conference on Power Electronics - Power Semiconductors and Their Applications, No. 123:pp. 204–209, 1974.
- [27] Johan W. Kolar, Thomas M. Wolbank, and Manfred Schrödl, "Analytical calculations of the RMS current stress on the DC link capacitor of voltage DC link PWM converter systems", IEE Conference on Electrical Machines and Drives, pages pp. 81–89, 1999.
- [28] Johann W. Kolar, Hans Ertl, and Franz C. Zach, "Calculation of the passive and active component stress of three phase PWM converter systems with high pulse rate", EPE 3rd European Conference on Power Electronics and Application, Vol. 3:pp. 1303–1311, 9.-12. October 1989.
- [29] Johann W. Kolar, Hans Ertl, and Franz C. Zach, "Influence of the modulation method on the conduction and switching losses of a PWM converter system", IEEE Industrial Application Society Annual Meeting, Vol. 1:pp. 502–512, 1990.

- [30] P. K. Kovács, “Transient phenomena in electrical machines”, Studies in Electrical and Electronic Engineering, Vol. 9, Elsevier scientific publishers, Amsterdam, 1984, (English translation and expansion of P. K. Kovács and I. Rácz, *Transiente Vorgänge in Wechselstrommaschinen*, Akadémiai Kiadó, Budapest, Hungary, 1959).
- [31] P. C. Krause, O. Wasynczuk, and M. S. Hildebrandt, “Reference frame analysis of a slip energy recovery system”, IEEE Transactions on Power Conversion, Vol. 3 No. 2:pp. 404–408, June 1988.
- [32] Morten Lindholm, “Doubly Fed Drives for Variable Speed Wind Turbines - A 40kW laboratory setup”, PhD thesis, DTU, September 2003.
- [33] Fuji Electric Device Technology Co. Ltd. “Fuji IGBT Modules application manual”, Technical report, Fuji Electric, February 2004.
- [34] Peter R. W. Martin, Ulrich Nicolai, Jürgen Petzoldt, and Josef Lutz. Semikron innovation + service - Application manual power modules. ISLE, ISBN : 3-932633-46-6, April 2000.
- [35] L. K. Mestha and P. D. Evans, “Analysis of on-state losses in PWM inverters”, IEE Proceeding on Electric Power Applications, Vol. 136 No. 4:pp. 189–195, July 1989.
- [36] Satoshi Ogasawara, Hirofumi Akagi, and Akira Nabae, “A novel PWM scheme of voltage source inverters based on space vector theory”, EPE 3rd European Conference on Power Electronics and Application, Vol. 3:pp. 1197–1202, 9.-12. October 1989.
- [37] M. P. Papadopoulos and S. A. Papathanassiou, “Dynamic characteristics of variable speed wind turbine configurations. International Conference on Electrical Machines”, Vol. 3:pp. 1723–1728, 2.-4. September 1998.
- [38] J. L. Rodríguez, M. Chinchilla, S. Arnalte, and J. C. Burgos, “Comparison of two variable speed wind energy generators and their control: Direct driven PM synchronous generator and doubly fed induction generator”, Universities Power Engineering Conference, Vol. 2:pp. 667–670, 8.-10. September 1998.
- [39] L. Sack, “AC current of the DC link capacitor in bidirectional power converters”, Conference on Power Conversion and Intelligent Motion, Vol. 1:pp. 293–300, June 1997.
- [40] L. Sack, “DC-link currents in bidirectional power converters with coordinated pulse patterns”, EPE 7th European Conference on Power Electronics and Application, Vol. 4:pp. 239–244, 1997.
- [41] N.Y.A. Shamma, M.P. Rodriguez, A.T. Plumpton, and D. Newcombe, “Finite element modelling of thermal fatigue effects in IGBT modules”, IEE Proc.-Circuit Devices Syst., Vol. 148 No. 2:pp. 95–100, April 2001.
- [42] Eckardt Siebenthaler, Bjørn Andresen, and Lorenz Feddersen, “Variable speed wind turbine having a passive grid side rectifier with scalar power control and dependent pitch control”, US2004222642, November 2004.
- [43] Yifan Tang and Longya Xu, “A flexible active and reactive power control for a variable speed constant frequency generating system”, IEEE Transaction on Power Electronics, Vol. 10 No. 4:pp. 472–478, July 1995.
- [44] Kjeld Thorborg. Power electronics. Chartwell-Bratt Ltd, ISBN : 0-86238-341-2, 1993.
- [45] Domenico Casadei, “Dinamica degli azionamenti elettrici”, University of Bologna – Dept. of Electrical Engineering.

- [46] Andrea Stefani “Induction Motor Diagnosis in Variable Speed Drives”, PhD thesis, Dept. of Electrical Engineering ,University of Bologna.
- [47] C. Rossi, D. Casadei, F. Filippetti, A. Stefani, A. Yazidi, G.A. Capolino, “Doubly-Fed Induction Machines Diagnosis Based on Signature Analysis of Rotor Modulating Signals”, IEEE Transactions on Industry Applications, Volume: 44, Issue 6, November/December 2008, pp. 1711-1721.
- [48] R. Abari, T. Chen, O. Malik, J. Anderson, T. G. Croda, S. Nahavandi, S. Basu, S. Farshchi, M. S. Newman, A. Chatterjee, B. M. Hammerli, W. Reeve “Doubly Fed Induction Machine” IEEE Press, 445 Hoes Lane, Piscataway, NJ 08854.
- [49] Robert C. Thurston and Stanislaw F. Legowski. A simple and accurate method of computing average and RMS currents in a three-phase PWM inverter . IEEE Transaction on Power Electronics, Vol. 8 No. 2:pp. 192–199, April 1993.
- [50] Rohit Tirumala and Ned Mohan. Dynamic simulation and comparison of slip ring induction generators used for wind energy generation. International Power Electronics Conference, Vol. 3:pp. 1597–1602, 3.-7. April 2000.
- [51] M. T. Wishart and J. K. Steinke. Vector control of a high power induction machine. AFRICON, pages 132–135, 22.-24. September 1993.
- [52] Longya Xu and Wei Cheng. Torque and power control of a doubly fed induction machine by position sensorless scheme. IEEE Transactions on Industry Applications, Vol. 31 No. 3:pp. 636–642, May/June 1995.
- [53] Mitsutoshi Yamamoto and Osamu Motoyoshi. Active and reactive power control for doubly-fed wound rotor induction generator. IEEE Transactions on Power Electronics, Vol. 6 No. 4:pp. 624–629, October 1991.
- [54] N. Miller, W. Price, and J. Sanchez Gasca, “Dynamic modeling of GE 1.5 and 3.6MW wind turbine generators,” tech. rep., GE Power Systems Energy Consulting, 2003.

CHAPTER 4

POWER FLOW ANALYSIS OF DFIG WIND TURBINE SYSTEM

4.1 INTRODUCTION

This chapter deals with a power flow analysis of grid connected Doubly Fed Induction generator (DFIG) driven by the wind turbine to estimate the performance of DFIG. Recent advancements in size and technology of wind turbines require sophisticated control systems to effectively optimize energy conversion and enhance grid integration. The wind energy conversion system (WECS) is equipped with a DFIG and a back-to-back converter in the rotor circuit. A control technique is presented for extracting the maximum power from the wind turbine. The proposed control technique is based on using the grid-side converter to regulate the dc link voltage as constant [1-10]. The task of the rotor side converter is to track the maximum power point for the wind turbine. Simulation results for different operating conditions are presented.

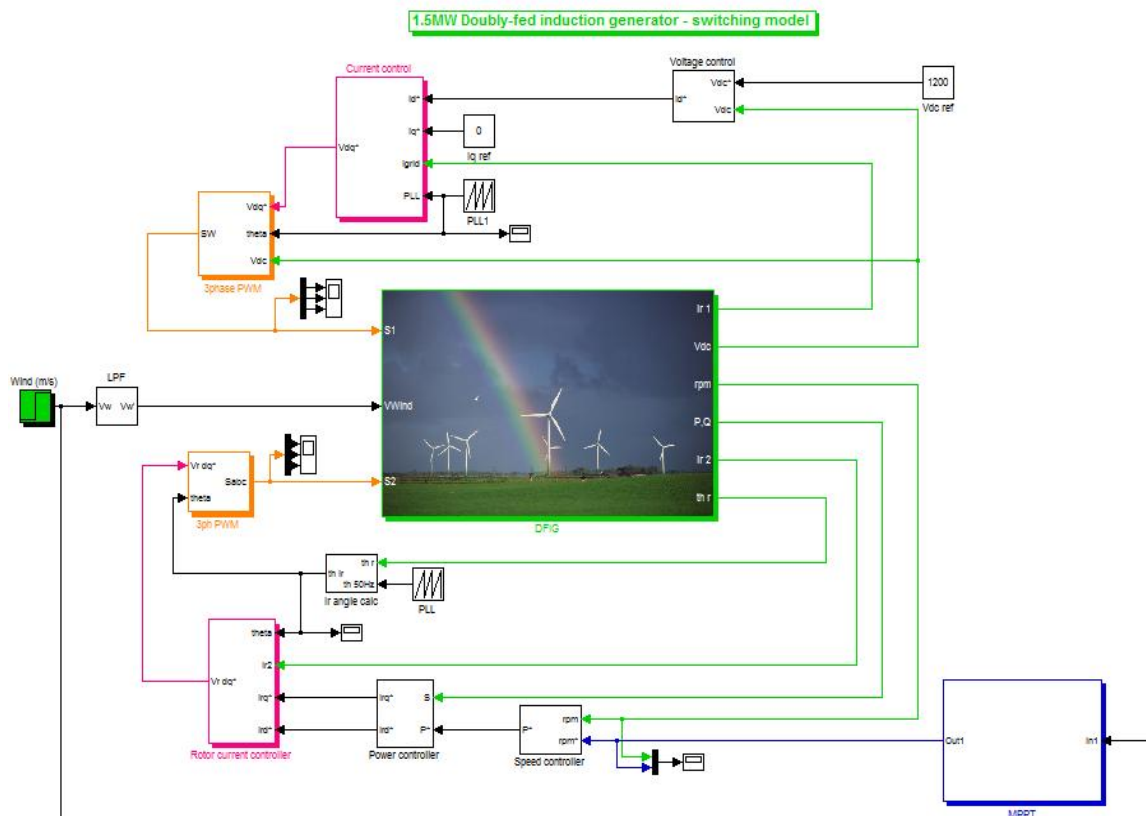


Figure: 4.1. Simulink model of DFIG Wind Turbine system.

4.2 SYSTEM PERFORMANCE UNDER RATED WIND SPEED

The power flow performance of DFIG wind turbine can be used to study the behavior and control of the system for the rated wind speed and it is implemented in Simpower system tool Matlab/Simulink and PLECS. The simulink model of DFIG system is shown in Fig 4.1. Based on the analysis, the controller parameter can be designed and optimized. As specified in [11-43], this approach serves to verify the dynamic model under rated wind conditions. In this simulation study, the rated power of DFIG wind turbine is 1.5MW and its parameters are enclosed in Annexure II.

The simulated steady state wave form of stator voltage, stator current, rotor voltage, rotor current, generator speed and torque of DFIG system with rated wind speed of 12m/s are shown in Fig 4.2.

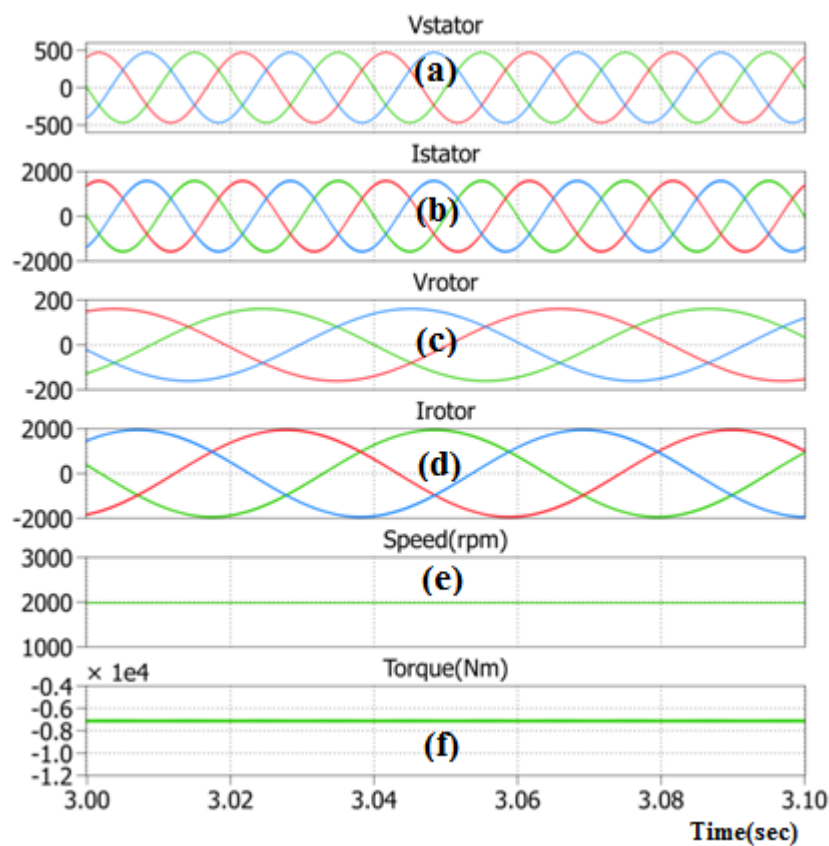


Figure 4.2: Simulation results of DFIG for rated wind speed 12 m/s: (a) stator voltage, (b) stator current, (c) rotor voltage, (d) rotor current, (e) speed, (f) electrical torque.

From the simulated waveform, we could see the rated electric speed of 200rpm in DFIG wind turbine system and the rated stator current and rotor current of 1800A (line peak), 1998A (line-peak) are noted. Figure 4.3 shows the DC bus performance during rated wind speed of 12m/s and the grid side converter does the DC link voltage as constant of 1200V as shown in Figure 4.3. The DC bus current and DC bus power are also shown in Figure 4.3(b) - 4.3(c). Figure 4.4 shows the stator and rotor flux of DFIG system at the rated wind speed. Figure 4.5 shows the grid angle that has calculated from the Phase Locked Loop (PLL).

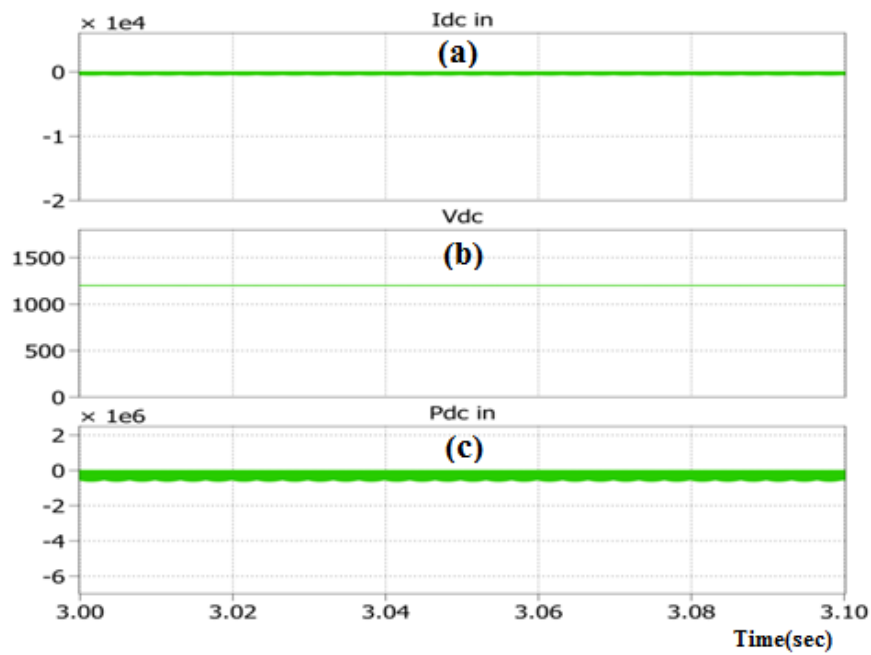


Figure 4.3: Simulation results of DFIG for rated wind speed 12 m/s: (a) DC current, (b) DC Voltage, (c) DC Power.

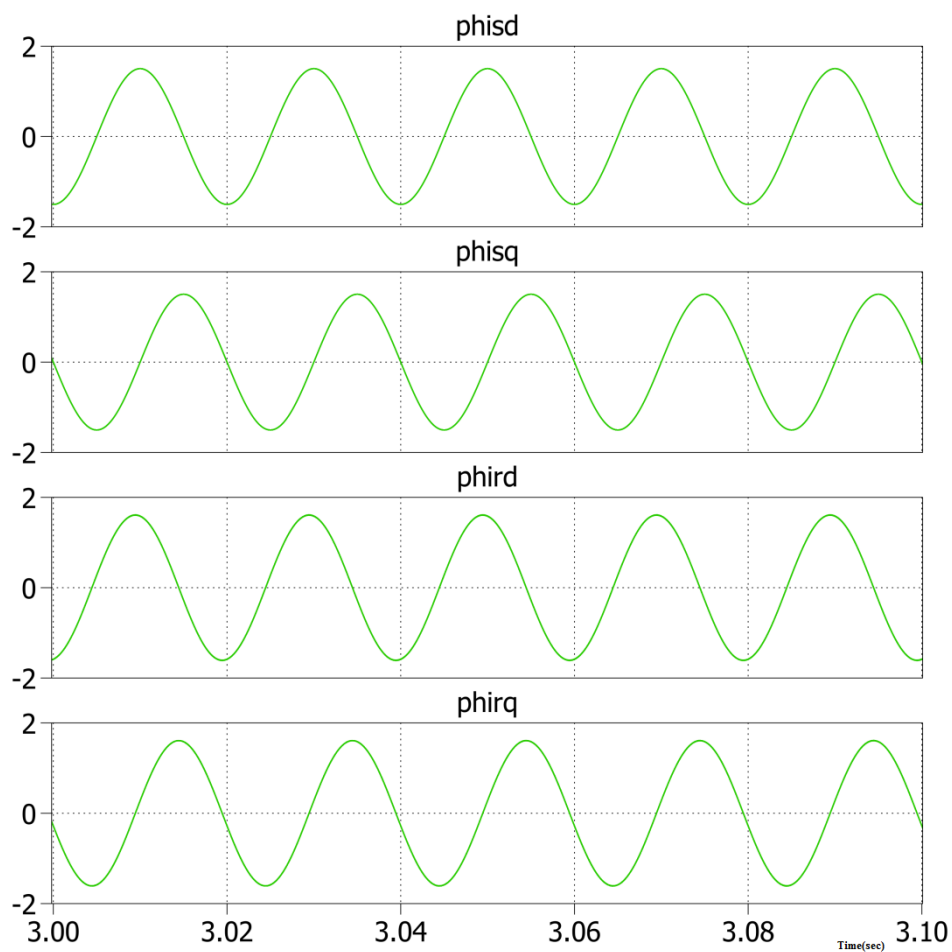


Figure 4.4: Simulation results of DFIG for rated wind speed 12 m/s: stator and rotor flux.

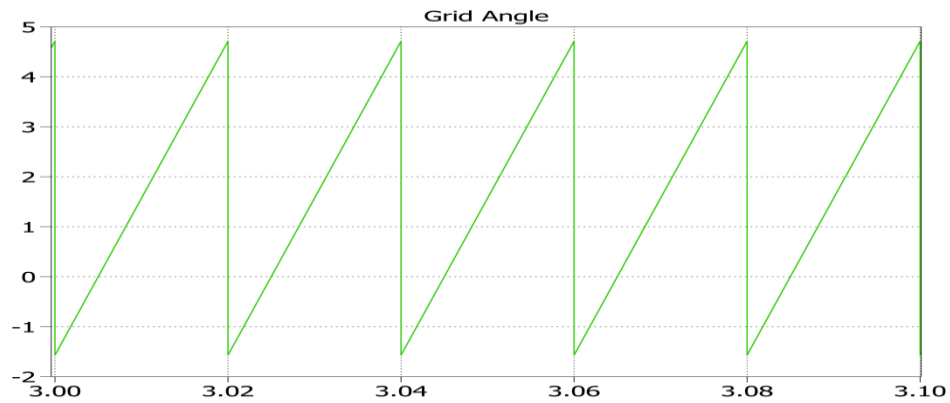


Figure 4.5: Simulation results of DFIG for rated wind speed 12 m/s: Grid angle.

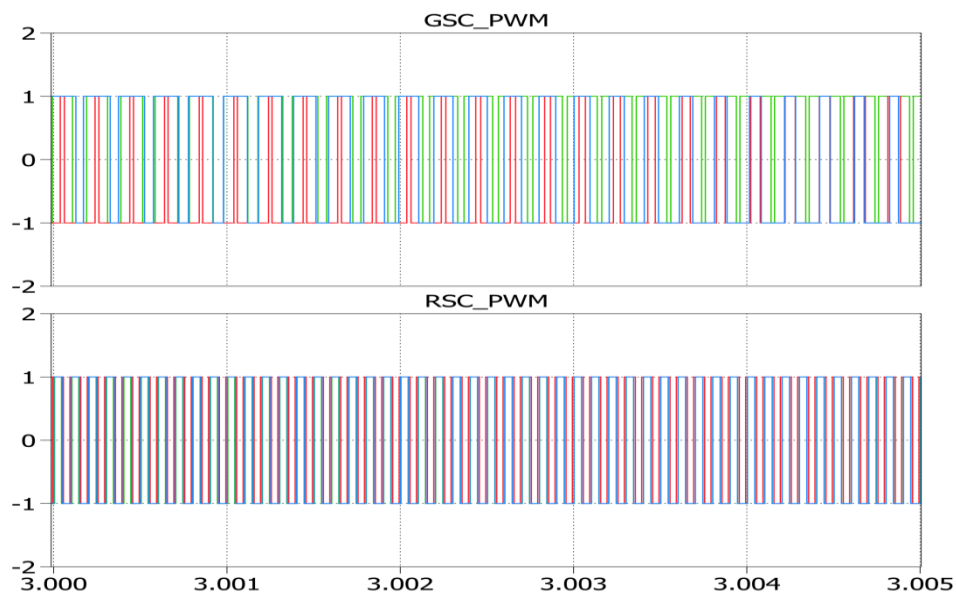


Figure 4.6: Simulation results of DFIG for rated wind speed 12 m/s: (a) GSC_PWM, (b) RSC_PWM.

Figure 4.6 shows the waveform for Pulse Width Modulation (PWM) signal for Grid side converter and Rotor Side Converter at the steady state operating condition of DFIG system with rated wind speed of 12m/s. The stator active and Stator reactive power are shown in Figure 4.7. From the wave form, we could see that the DFIG system able to generate the stator active power of 1.1MW and the reactive power kept zero during steady state operating condition.

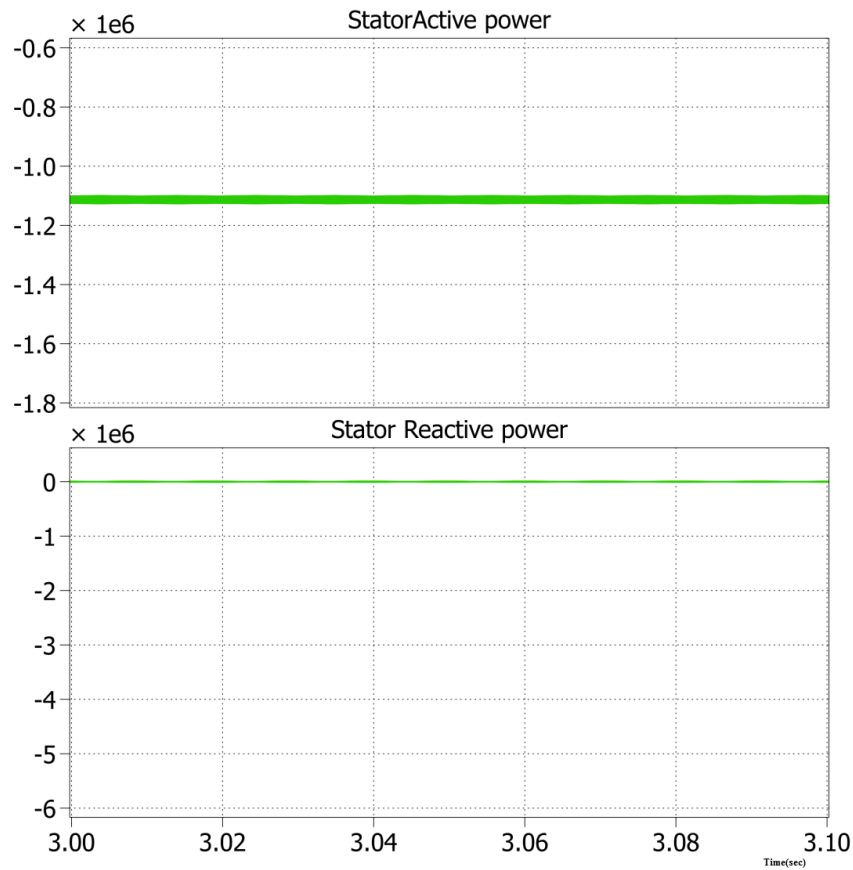


Figure 4.7: Simulation results of DFIG for rated wind speed 12 m/s: (a) active Power, (b)Reactive Power.

4.3 MAXIMUM POWER POINT TRACKING

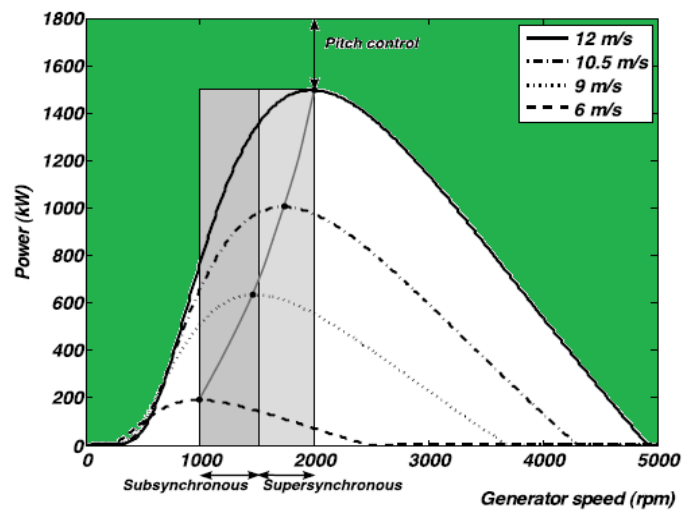


Figure 4.8: The maximum power point tracking (MPPT) for different wind speeds.

In DFIG Wind turbine ,maximum power tracking is implemented using a simple technique that infers the optimal rotational speed of the generator, n_g^* ,from the wind speed measurement V [44-46] .The relationship between optimal generator rotational speed in rpm and wind speed is given by

$$n_g^* = \frac{60\lambda_{opt}n}{2\pi R} \times V$$

The system rated power of 1.5MW could attain at the rated wind speed of 12m/s with rated electric speed of 2000rpm and its shown in Figure 4.2(e) and also the same set of waveform are generated for different power with different wind speed condition and it is shown in Figure 4.8.

4.4 SYSTEM PERFORMANCE UNDER VARIABLE WIND SPEED

CASE 1: WIND SPEED FROM 12m/s To 8m/s

The power flow performance of DFIG wind turbine can be used to study the behavior and control of the system for variable wind speed and it is implemented in Simpower system tool Matlab/Simulink and PLECS. Based on the analysis, the controller parameter can be designed and optimized. As specified in [11-43], this approach serves to verify the model under steady state and different operating wind conditions.

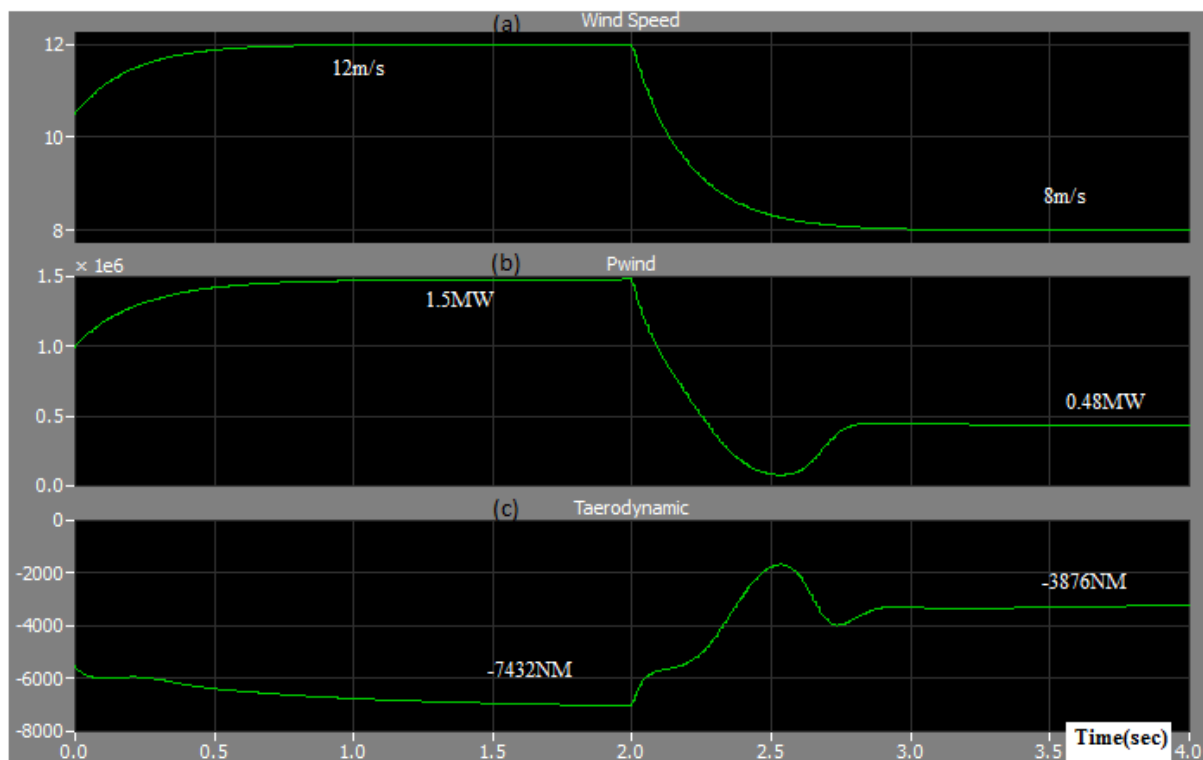


Figure: 4.9.(a) Wind Speed,(b)Wind Power,(c)Turbine Speed,(d)Aerodynamic torque.

Figure: 4.9 shows the performance of the DFIG wind turbine with different wind speed from 12m/s to 8m/s. Figure: 4.9(a) represents the wind speed profile of 12m/s and 8m/s. From time $t=0s$ to $t=2s$, the wind speed is 12m/s (rated wind speed) and the time $t=2s$ to $t=4s$, the wind speed reduced to 8m/s. The corresponding power available in the wind with appropriate wind speed and the aero dynamic torque are also shown in Figure 4.9

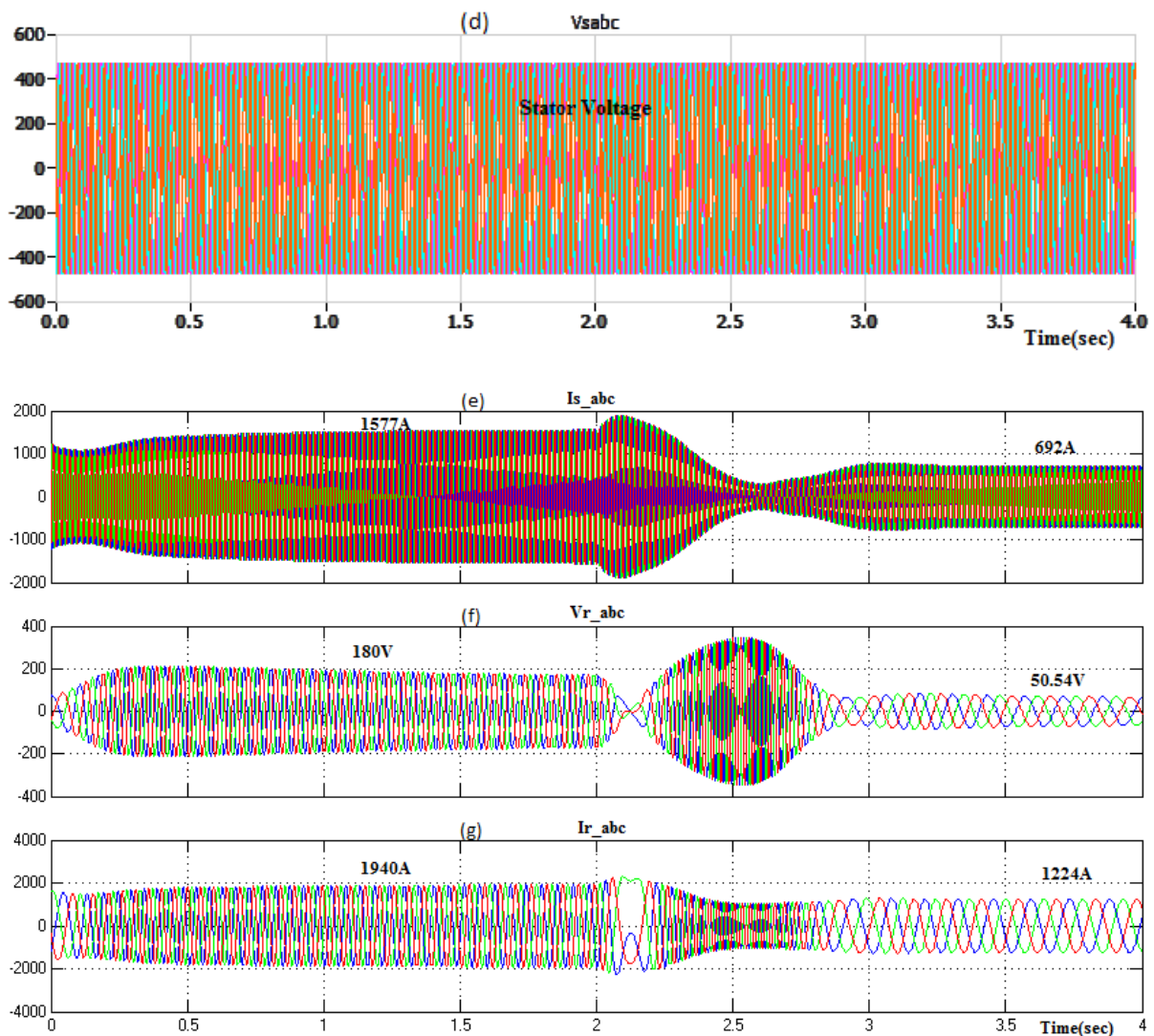


Figure: 4.10.Simulation results of DFIG for wind speed changing from 12 m/s to 8 m/s: (d) stator voltage, (e) stator current, (f) rotor voltage, (g) rotor current.

Figure 4.10 shows the simulation results of DFIG for wind speed changing from 12m/s to 8 m/s and the corresponding stator voltage, stator current, rotor voltage and rotor current are also shown.

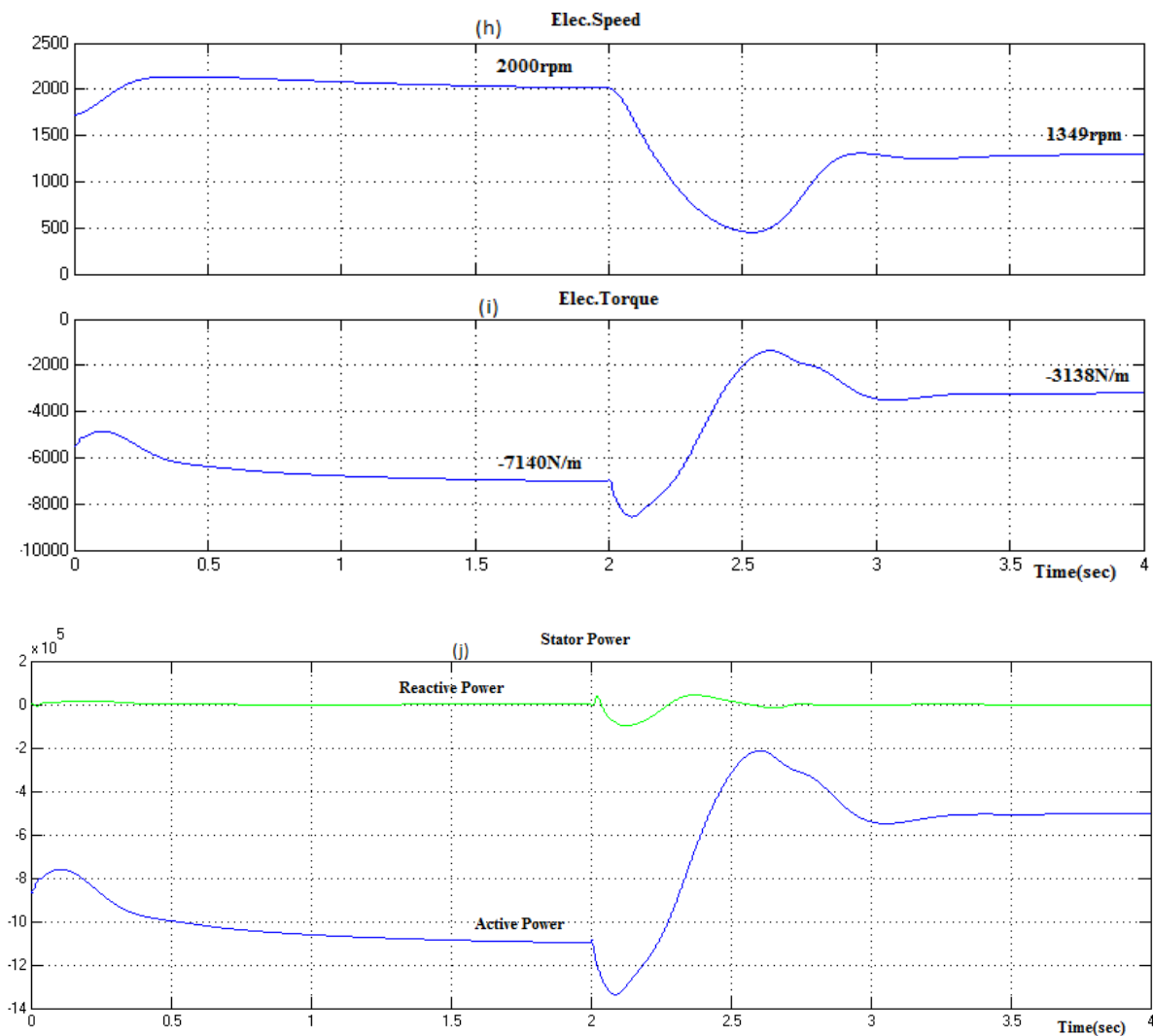


Figure 4.11: (h) generator speed, (i) electromagnetic torque, (j) stator reactive and active power.

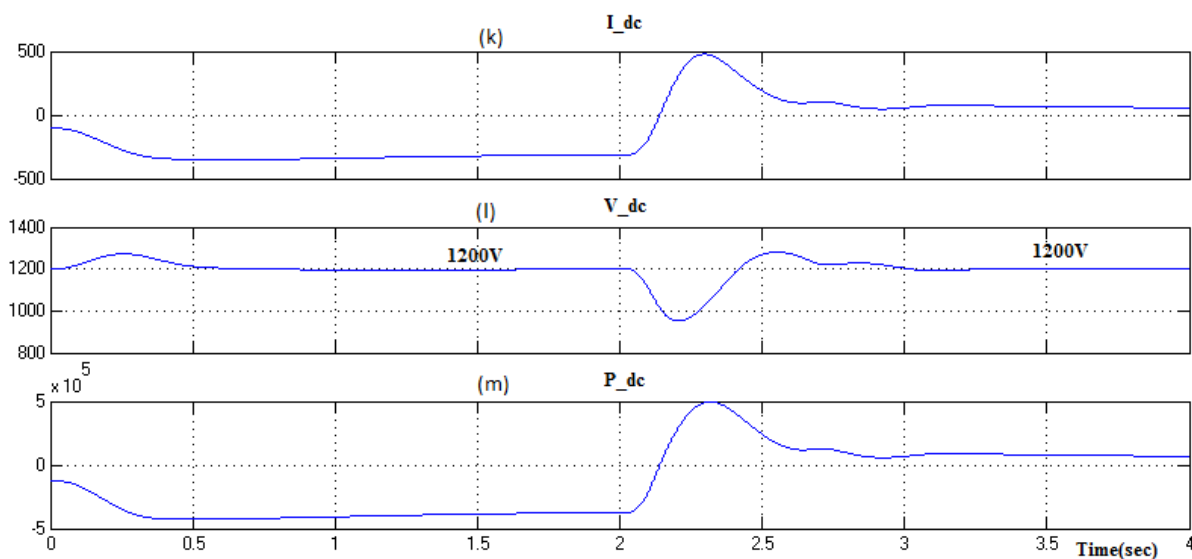


Figure 4.12: (k) DC bus current, (l) DC bus voltage, (m) P_{dc}

The waveforms in Fig. 4.9 describes the wind speed, the power extracted from the wind and mechanical torque with the wind speed changing from 12 m/s to 8m/s. From $t=0.6$ s to $t= 2$ s the machine operates at the wind speed of 12 m/s. From $t=2$ s to $t=4$ s the machine is subjected to operate with a wind speed changing from 12 m/s to 8 m/s. The corresponding stator current, rotor voltage and rotor current, electrical speed, torque, and stator power are presented from top to bottom in Fig.4.10-Fig.4.11. The DC bus current, DC bus voltage and DC bus power are shown in Fig. 4.12.

CASE 2: WIND SPEED FROM 8m/s To 10.5m/s

The power flow performance of DFIG wind turbine can be used to study the behavior and control of the system for variable wind speed and it is implemented in Simpower system tool Matlab/Simulink and PLECS. Based on the analysis, the controller parameter can be designed and optimized. As specified in [11-43], this approach serves to verify the model under steady state and different operating wind conditions (from 8m/s to 10.5m/s).

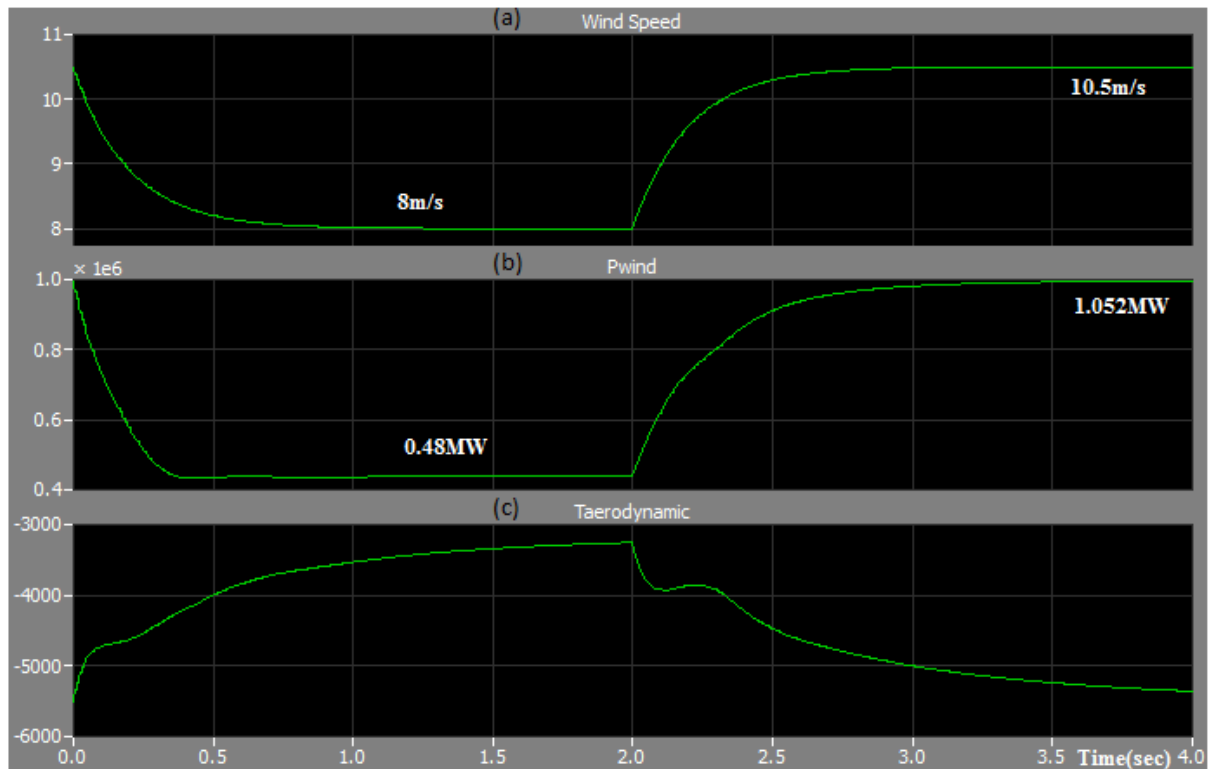


Figure 4.13: (a) Wind Speed,(b)Wind Power,(c)Turbine Speed,(d)Aerodynamic torque

Figure 4.13 shows the performance of the DFIG wind turbine with different wind speed from 8m/s to 10.5 m/s. Figure 4.13(a) represents the wind speed profile of 8m/s and 10.5m/s. From time $t=0$ s to $t=2$ s, the wind speed is 8m/s and the time $t=2$ s to $t=4$ s, the wind speed increased to 10.5m/s. The corresponding power available in the wind with appropriate wind speed and the aero dynamic torque are also shown in Figure 4.13.

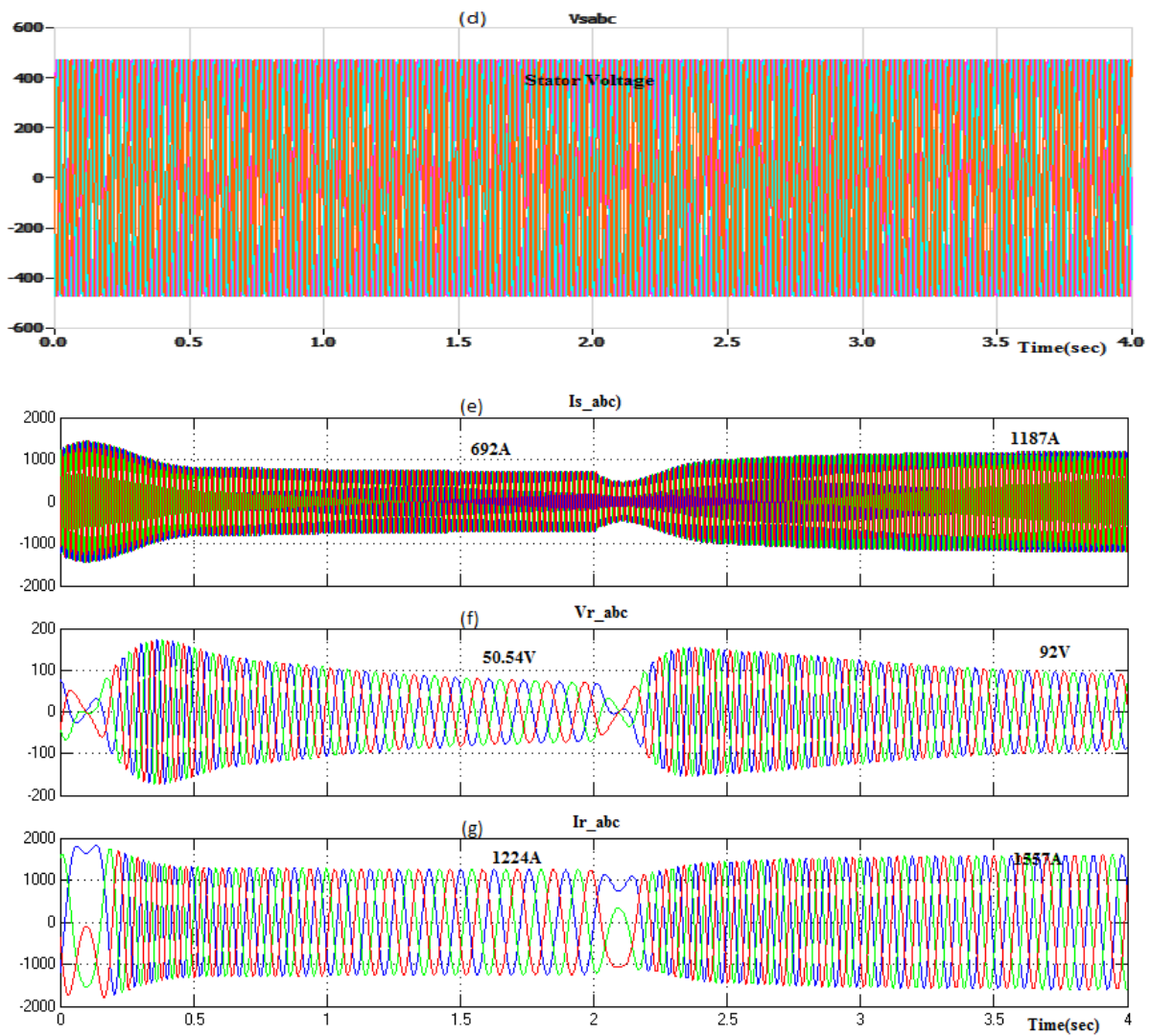


Figure: 4.14.Simulation results of WECS for wind speed changing from 8 m/s to 10.5 m/s: (d) stator voltage (e) stator current, (f) rotor voltage, (g) rotor current.

Figure 4.14 shows the simulation results of DFIG for wind speed changing from 8m/s to 10.5 m/s and the corresponding stator voltage, stator current, rotor voltage and rotor current are also shown.

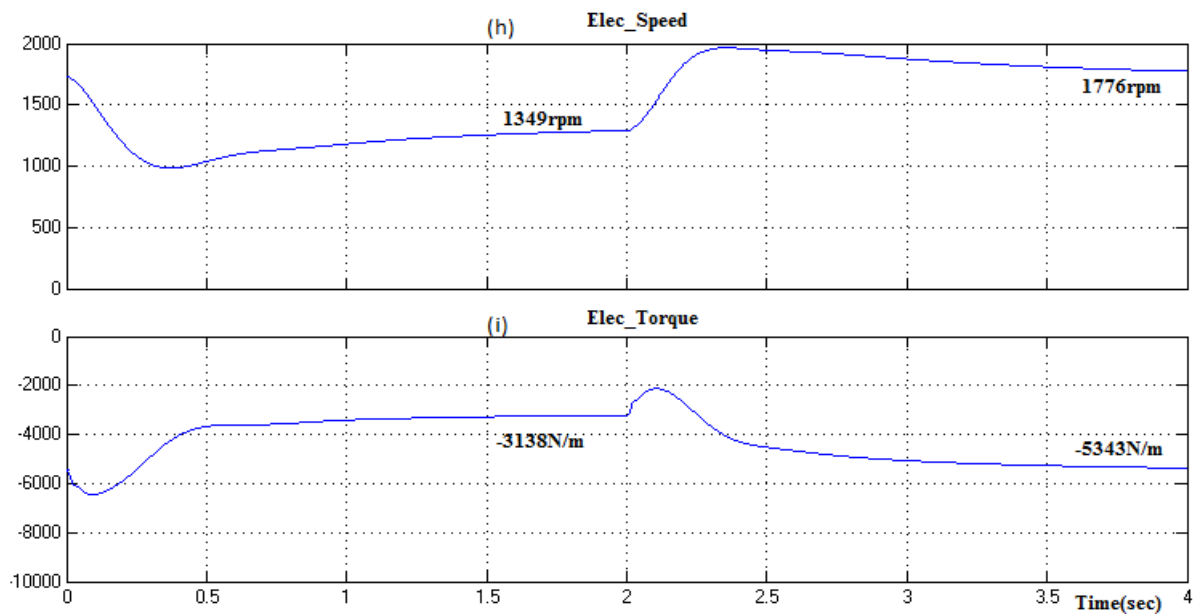


Figure 4.15: Simulation results of WECS for wind speed changing from 8 m/s to 10.5 m/s: (h) generator speed, (i) electromagnetic torque.

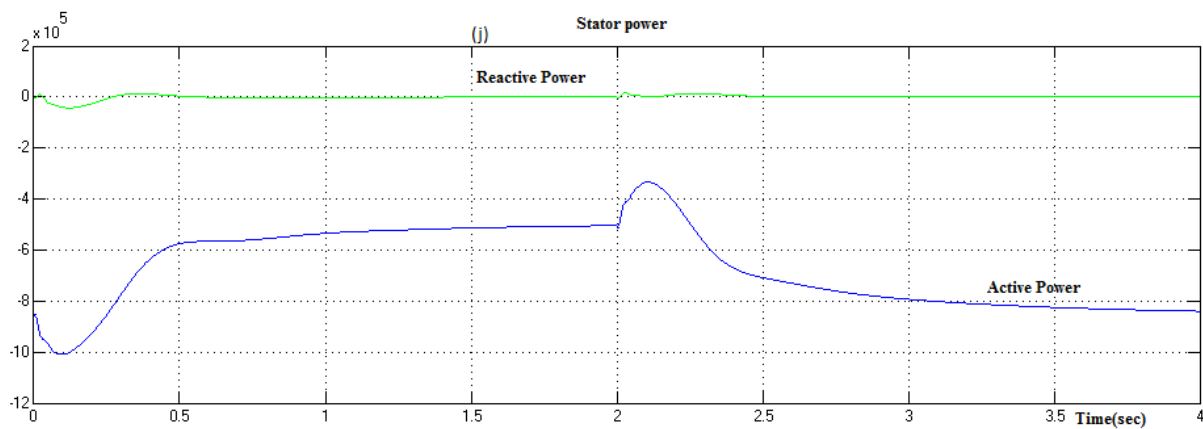


Figure 4.16: (j) stator reactive and active power

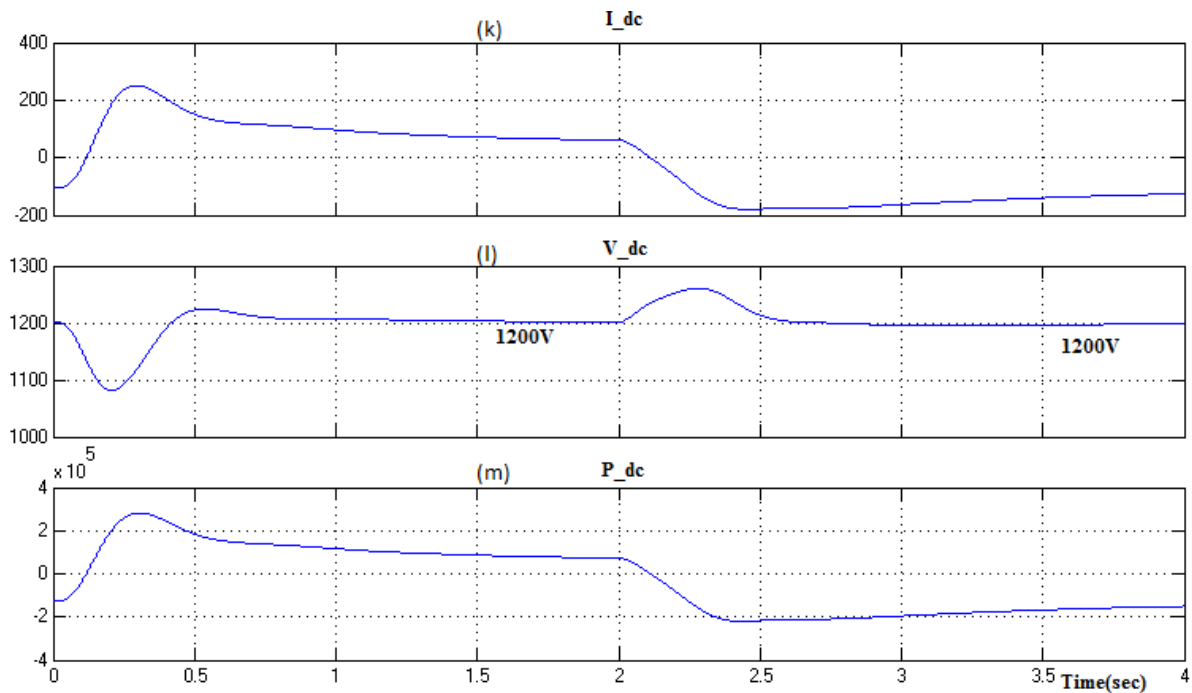


Figure 4.17 :(k) DC bus current, (l) DC bus voltage, (m) P_{dc}

The waveforms in Fig. 4.13 describes the wind speed, the power extracted from the wind and mechanical torque with the wind speed changing from 8 m/s to 10.5 m/s. From $t=0.6$ s to $t=2$ s the machine operates at the wind speed of 8m/s. From $t=2$ s to $t=4$ s the machine is subjected to operate with a wind speed varying from 8 m/s to 10.5 m/s. The corresponding stator current, rotor voltage and rotor current, electrical speed, torque, and stator power are presented from top to bottom in Fig.4.14-Fig.4.16. The DC bus current, DC bus voltage and DC bus power are shown in Fig. 4.17. From the simulation results we have seen that there is small transients occur at the change of wind speed this could be mitigated using averaged PWM converter.

4.5 SUMMARY

This chapter has presented an analysis and simulation study of DFIG based wind energy generation system operating under rated and varying wind speed condition. The average PWM converter model is adopted in order to get faster dynamic response and longer simulation for the varying wind speed. Also the maximum power point tracking operations are studied and presented. The developed model is particularly suitable for analyzing the transient phenomena that occur during faults or perturbations in the grid. As a consequence, using this model it will be possible to investigate the Low Voltage Ride Trough capability of WECS based on the use of DFIG and it is discussed in chapter 6.

4.6 REFERENCES

- [1] Hansen M.H., Hansen A.D., Larsen T. J., Øye S., Sørensen P., Fuglsang P., “Control design for a pitch regulated, variable speed wind turbine”, Risø report R-1500, Risø National Laboratory, Denmark, 2005.
- [2] P. Vas, “Sensorless vector and direct torque control”, Oxford University Press, New York, 1998.
- [3] R. Pena, J. C. Clare, G. M. Asher, “Doubly fed induction generator using back-to-back PWM converters and its application to variable-speed wind-energy generation,” IEE Proc. Electr. Power Appl., vol. 143, no. 3, pp. 231-241, May 1996.
- [4] B. Hopfensperger, D. J. Atkinson, R. A. Lakin, “Stator-flux-oriented control of a doubly-fed induction machine with and without position encoder,” IEE Proc. Electr. Power Appl., vol. 147, no. 4, pp. 241-250, July 2000.
- [5] Y. Tang, L. Xu, “A flexible active and reactive power control strategy for a variable speed constant frequency generating system,” IEEE Trans. on Power Electronics, vol. 10, no. 4, pp. 472–478, July 1995.
- [6] J. G. Ziegler, N. B. Nichols, “Optimum settings for automatic controllers,” Transactions of the ASME, vol. 64, pp. 759-768, 1942.
- [7] S. E. Lyshevski, “Control systems theory with engineering applications”, Birkhäuser, Boston, 2001.
- [8] R. S. Burns, “Advanced control engineering”, Butterworth-Heinemann, Oxford, 2001.
- [9] R. N. Bateson, “Introduction to control system technology”, Prentice Hall, New Jersey, 1996.
- [10] P. H. Lewis, C. Yang, “Basic control system engineering”, Prentice Hall, New Jersey, 1997.
- [11] W. S. Levine, “Control system fundamentals”, CRC Press, Boca Raton, 2000.
- [12] L. Harnefors, H. P. Nee, “Model-based current control of AC machines using the internal model control method,” IEEE Trans. on Industry Applications, vol. 34, no. 1, pp. 133-141, Jan./Feb. 1998.
- [13] J. G. Zhang, Z. M. Chen, Z. C. Zhao, “A new antiwindup speed controller for induction motor drive system,” Proc. of the Fifth International Conference on Electrical Machines and Systems, vol. 2, pp. 1240-1243, Aug. 2001.
- [14] L. Harnefors, H. P. Nee, “Robust current control of AC machines using the internal model control method,” Proc. of the 1995 IEEE Industry Applications conference, vol. 1, pp. 303-309, Oct. 1995.
- [15] K. Hentabli, M. E. H. Benbouzid, D. Pinchon, “CGPC with internal model structure: Application to induction motor control,” Proc. of the 1997 IEEE International Conference on Control Applications, pp. 235-237, Oct. 1997.
- [16] A. Petersson, “Analysis, modeling and control of doubly-fed induction generators for wind turbines, Ph.D thesis”, Department of Electric Power Engineering, Chalmers University of Technology, 2003.

- [17] J. F. Manwell, J. G. McGowan, A. L. Rogers, “Wind energy: theory, design and application”, John Wiley & Sons Ltd, Chichester, 2002.
- [18] J. H. S. Hansen, M. Lau, P. F. Sørensen, “Sensorless control of a double fed induction generator”, Institute of Energy Technology, Aalborg University, 1999.
- [19] Domenico Casadei: “Dinamica degli azionamenti elettrici”, University of Bologna – Dept. of Electrical Engineering.
- [20] Andrea Stefani “Induction Motor Diagnosis in Variable Speed Drives”, PhD thesis, Dept. of Electrical Engineering, University of Bologna.
- [21] C. Rossi, D. Casadei, F. Filippetti, A. Stefani, A. Yazidi, G.A. Capolino, “Doubly-Fed Induction Machines Diagnosis Based on Signature Analysis of Rotor Modulating Signals”, IEEE Transactions on Industry Applications, Volume: 44, Issue 6, November/December 2008, pp. 1711-1721.
- [22] Bjørn Andresen, Eckardt Siebenthaler, and Lorenz Feddersen, “Variable speed wind turbine having a passive grid side rectifier with scalar power control and dependent pitch control”, Canadian Patent Application CA2003/418561, November 2003.
- [23] L.N. Arruda, B.J. Cardoso Filho, S. M. Silva, S.R. Silva, and A.S.A.C. Diniz. “Wide bandwidth single and three-phase PLL structures for grid-tied PV systems”. Photovoltaic Specialist Conference, Vol. 1:pp. 1660–1663, Sept 2000.
- [24] D. Arsudis and W. Vollstedt. “Sensor-less power control of a double-fed AC-machine with nearly sinusoidal line currents”. EPE 3rd European Conference on Power Electronics and Application, Vol. 2:pp. 899–904, 9.-12. October 1989.
- [25] D. Arsudis and W. Vollstedt. “Sensorlose regelung einer doppeltgespeisten asynchrony maschine mit geringen netz'uckwirkungen”. Archiv f'ur Elektrotechnik, Vol.74:pp. 89–97, 1990.
- [26] Michael M. Bech, “Analysis of random pulse-width modulation techniques for power electronic converters. PhD thesis”, Aalborg University, 9220 Aalborg East, November 2000. ISBN: 87-89179-32-3.
- [27] M.H. Bierhoff and F.W. Fuchs, “Semiconductor losses in Voltage Source and Current Source IGBT Converters Based on Analytical Derivation”, IEEE Power Electronics Specialists Conference, Vol. 4:pp. 2836–2842, June 2004.
- [28] Frede Blaabjerg, Ulrik Jaeger, Stig Munk-Nielsen, and John K. Pedersen, “Power losses in PWM-VSI inverter using NPT or PT devices”, IEEE Transactions on Power Electronics, Vol. 10 No. 3:pp. 358–367, May 1995.
- [29] E. Bogalecka. “Power control of a doubly fed induction generator without speed or position sensor”, EPE 5th European Conference on Power Electronics and Application, Vol. 8:pp. 224–228, 13.-16. September 1993.
- [30] Heinz Willi Van Der Broeck, Hans-Christoph Skudelny, and Georg Viktor Stanke, “Analysis and realization of a pulse width modulator based on voltage space vectors”. IEEE Transactions on Industry Applications, Vol. 24 No. 1:pp. 142–150, January/February 1988.
- [31] S.-K. Chung. “Phased-locked loop for grid-connected three-phase power conversion systems”, IEE Proc.Electr. Power Appl., Vol. 147 No. 3:pp. 213–219, May 2000.
- [32] M. Depenbrock. “Pulse width control of a 3-phase inverter with non-sinusoidal phase voltages”, IEEE Industrial Application Society Annual Meeting, pages 399– 403, 1977.

- [33] B. Eggert, "1.5 MW wind power station with low ac-line distortion using a standard doubly fed generator system with field orientated control", EPE 7th European Conference on Power Electronics and Application, Vol. 2:pp. 739–742, 8.-10. September 1997.
- [34] Adel A. Ghandakly and Ziad H. Sbeiti, "A digital optimal controller for VSCF wind generators", IEEE Industrial Application Society Annual Meeting, Vol. 2:p.1787–1792, 7.-12. October 1990.
- [35] Anders Grauers, "Efficiency of three wind energy generator systems", IEEE Transactions on Energy Conversion, Vol. 11 No. 3:pp. 650–657, September 1996.
- [36] Ahmet M. Hava, Russel J. Kerkman, and Thomas A. Lipo, "A high performance generalized discontinuous PWM algorithm", IEEE Applied Power Electronics Conference and Exposition, Vol. 2:pp. 886–894, 23.-27. February 1997.
- [37] N. Mohan, T. M. Undeland, and W. P. Robbins, "Power Electronics: Converters, Applications, and Design", 3rd Ed., John Wiley & Sons Inc., October 2002.
- [38] J. I. Jang, Y. S. Kim, and D. C. Lee, "Active and reactive power control of DFIG for wind energy conversion under unbalanced grid voltage", IPEMC Shanghai, vol. 3, pp. 1487-1491, Aug. 2006.
- [39] R. Datta and V.T. Ranganathan, "A method of tracking the peak power points for a variable speed wind energy conversion system", IEEE Trans. on Energy Conversion, vol.18, No.1, pp. 163- 168, 2003.
- [40] S. Muller, M. Deicke, and R. D. Doncker, "Doubly fed induction generator systems for wind turbines," IEEE Industry Applications Magazine, vol. 8, pp. 26–33, June 2002.
- [41] R. Pena, J. C. Clare, and G. M. Asher, "Double fed induction generator using back-to-back PWM converter and its application to variable-speed wind-energy generation," Proc. Inst. Elect. Eng. B, vol. 143, no. 3, pp. 231–241, 1996.
- [42] A. Lubosny, Wind Turbine Operation in Electric Power Systems -Advanced Modelling, Springe Verlag, 2003.
- [43] Ahmet M. Hava, Russel J. Kerkman, and Thomas A. Lipo. "Simple analytical and graphical methods for carrier-based PWM-VSI drive", IEEE Transactions on Power Electronics, Vol. 14 No. 1:pp. 49–61, January 1999.
- [44] Joachim Holtz, Wolfgang Lotzkat, and Ashwin M. Khambadkone, "On continuous control of PWM inverters in the over modulation range including the six-step mode", IEEE Transactions on Power Electronics, Vol. 8 No. 4:pp. 546–553, October 1993.
- [45] R. Pena, J. Clare, and G. Asher, "Doubly fed induction generator using back-to-back PWM converters and its application to variable-speed wind-energy generation," IEE Proceedings Electric Power Applications, vol. 143, pp. 231–241, May 1996.
- [46]J.G. Slootweg , H. Polinder, and W. L. Kling, "Dynamic modeling of a wind turbine with doubly fed induction generator," in Proceeding of IEEE, Power Engineering Society Summer Meeting, vol.1, pp. 644-649, Vancouver, Canada, Jul., 2001.

CHAPTER 5

GRID CODE REQUIREMENTS

INTRODUCTION

This chapter describes the necessary grid code requirements of grid connected wind turbine in the various countries. The grid codes of most countries generally aim to achieve the same thing. Electricity networks are constructed and operated to serve a huge and diverse customer demographic.

Electricity transmission and distribution systems serve, by way of example, the following types of user:

- Large high-consumption industrial factories
- High-sensitivity loads requiring high quality and reliable uninterrupted supplies
- Communications systems (e.g., national)
- Farms
- Shops and offices
- Domestic dwellings
- Large power stations

In simple terms, it is vital that electricity supplies remain “on.” To do this, the system operator not only balances the system with suitable levels of generation to meet demand, but also requires larger capacity users of the system, including both generation and load, to actively participate in ensuring system security.

To achieve this, the following technical requirements are possibly the most crucial and appear common across most European countries:

- Frequency and voltage tolerance
- Fault ride through
- Reactive power and voltage control capability
- Operating margin and frequency regulation
- Power ramping

And future technical requirements may include:

- Inertial response
- Power system stabilizer
- Wind farm control

5.1 FREQUENCY AND VOLTAGE OPERATING RANGE

The electrical behavior of the network, in terms of frequency and voltage, due to its dynamic nature is continuously changing. Generally, these changes occur in very small quantities. It is a requirement that users of the transmission system are able to continue operating in a normal manner over a specified range of frequency and voltage conditions. With respect to frequency and for a 50Hz system, this would be in the range of 49 to 51Hz. With respect to voltage, this range could be +or -10% of the nominal voltage. However, at times the ranges could be wider, although it would normally be expected that the user would continue operating under an extreme condition for a defined period of time, for example, 47 Hz for 15 seconds or $\pm 20\%$ of the nominal voltage for 1 hour. Beyond these extremes, the user would normally be required to disconnect from the system [1-4]. Table 5.1 shows a common range of conditions within which a user would be required to operate.

TABLE: 5.1 Examples of Possible Frequency and Voltage Tolerance Requirement;

	Normal Continuous Operation	Required	Very Short Term
Frequency	49–51 Hz	47.5–49 Hz and 51–52 Hz	47–47.5 Hz
Voltage	$\pm 5\%$	$\pm 10\%$	

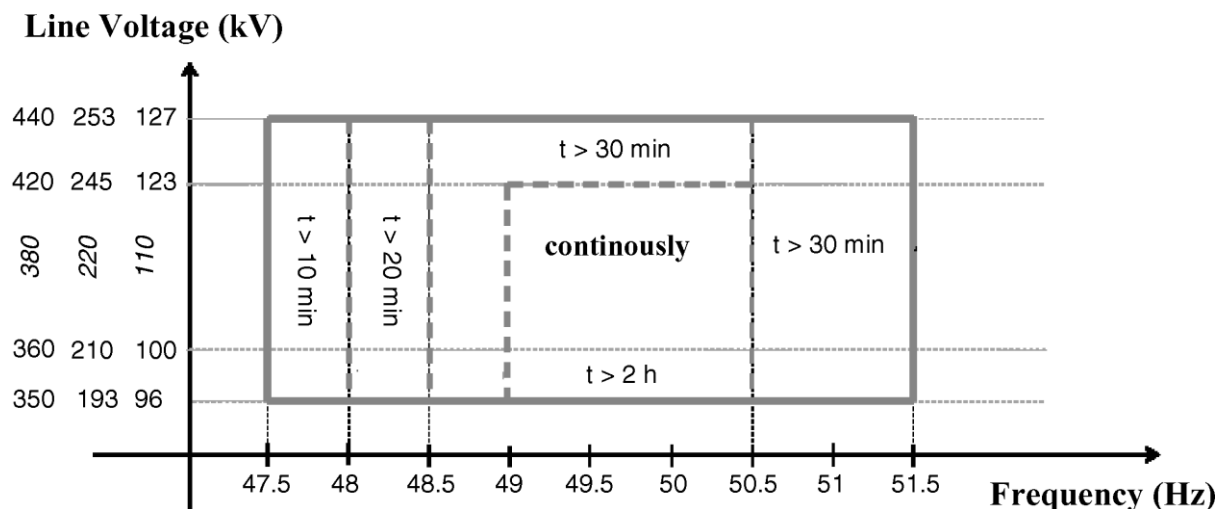


Figure:5.1. EON Netz GMBH grid code related to frequency.

As an example, the EON grid code related to the operating times as a function of frequency is illustrated in Figure.5.1.

5.2 REACTIVE POWER AND VOLTAGE CONTROL CAPABILITY

To minimize losses and thus maintain high levels of efficiency, it is preferable that networks operate with voltage and current in phase - that is, the power factor is unity.

However, users of electrical systems often tend to have inductive loads or generation facilities that operate such that voltage and current are out-of-phase. In addition, power system components including lines and transformers, for example, produce or consume large levels of reactive power. From the network user's perspective (looking from the installation toward the network) an inductive load/ generation facility is said to have a leading power factor because the current leads the voltage. Put another way, the user is consuming reactive power [5-8].

As the behavior of the network is continuously changing, users are required to have the ability to adjust their reactive power production or consumption, in order that reactive power production and consumption are balanced over the entire network. In most cases, it is the generators who provide this control ability. The range, for example, could be from 0.95 leading to 0.95 lagging.

An example is the proposed curve of power factor as a function of grid voltage in the EON grid code (see Figure.5.2).

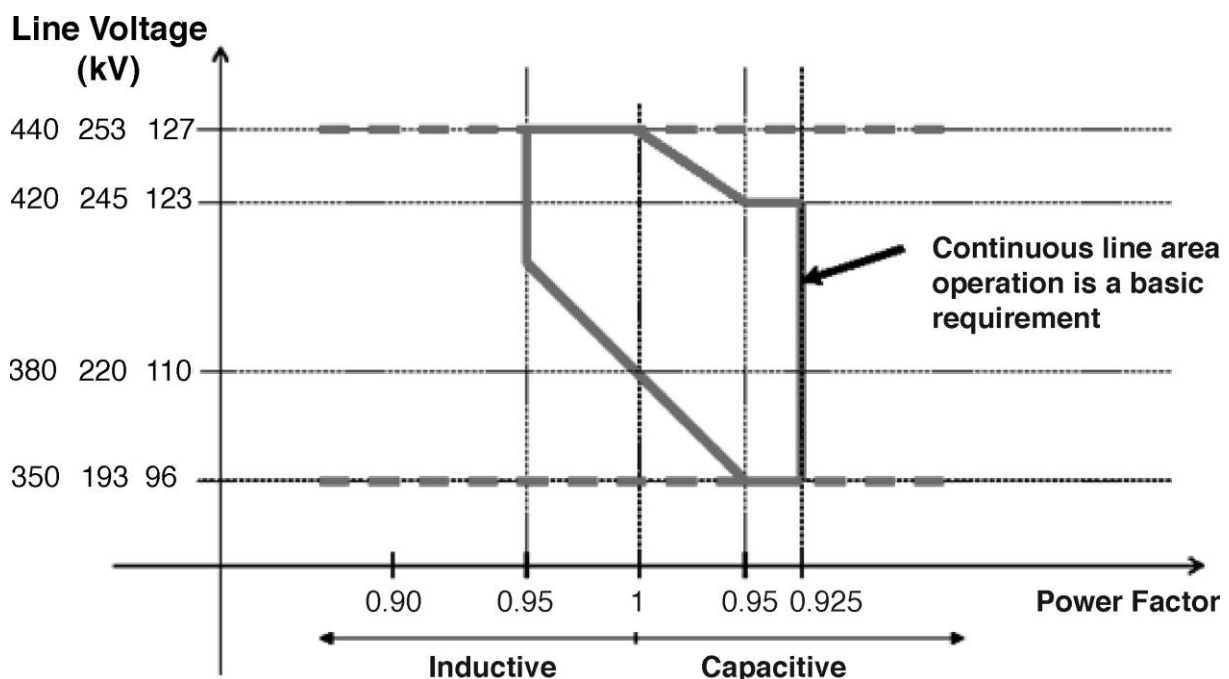


Figure: 5.2. Reactive power control as a function of grid voltage (EON Netz GmbH).

5.3 VOLTAGE SUPPORT

A generating station may be required to operate over a range of power factors to provide or consume reactive power as discussed and shown above. Alternatively, the installation may be required to operate in voltage control mode, that is, to adjust its reactive power production or consumption in order to control voltage on the local network.

If the network voltage decreases to a level below a predefined range, an installation may be required to supply reactive power to the network to raise the voltage. Conversely, if the network voltage increases to a level above a predefined upper limit, then the installation would be required to consume reactive power to bring the voltage back within acceptable limits [8], [9-12].

5.4 REACTIVE POWER WIND TURBINE OPERATION MODES

In order to accomplish the functionalities mentioned, the following operation modes (Figure 5.3) for the reactive power control of the wind turbine are typically defined:

- Reactive power control—the wind turbine is required to produce or absorb a constant specific amount of reactive power.
- Automatic voltage control—the voltage in the wind turbine point of common coupling (PCC) is controlled. This implies that the wind farm can be ordered to produce or absorb an amount of reactive power.

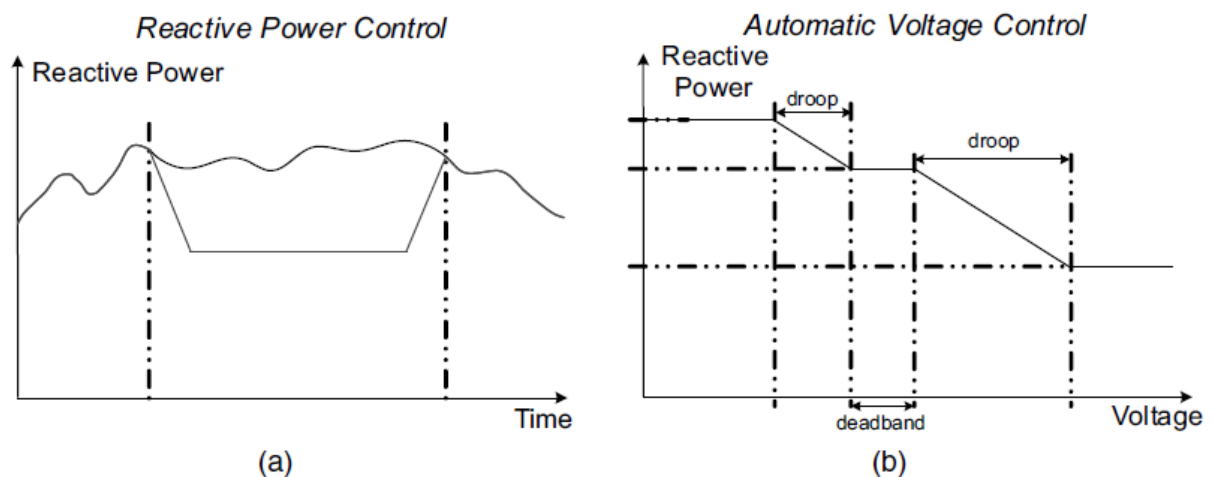


Figure: 5.3. Reactive power operation modes: (a) reactive power Control and (b) automatic voltage control.

5.5 POWER CONTROL

Some network operators impose limits on power output. This could be during normal continuous operation and/or during ramping up to an increased output or ramping down to a decreased output. This requirement might be necessary in the first case to limit output because of limitations in the capabilities of other generators or the transmission or distribution networks. In the latter case, this might be necessary so that network control systems and other generators have time to respond to a new operating state. When a generator comes on-line it is providing the network with an increased amount of power which not only affects frequency, but also requires existing operating installations to adjust their operational characteristics to adapt to the “new” operating state.

With respect to wind power, for decreasing wind speed conditions there are limitations in the capabilities of wind turbines. If the wind speed is falling, a wind turbine may not be able to maintain its output or fully control the rate of decrease of output. However, wind speed profiles can be predicted and so if a controlled ramp down or clearly defined power reduction rate is required, a wind turbine's output can be reduced early, thus reducing the maximum rate of change of output power [13-18]. An example is the proposed curve of power (as a percentage of the momentary possible power production) as a function of grid frequency in the Electricity Supply Board (ESB) National Grid code (see Figure 5.4).

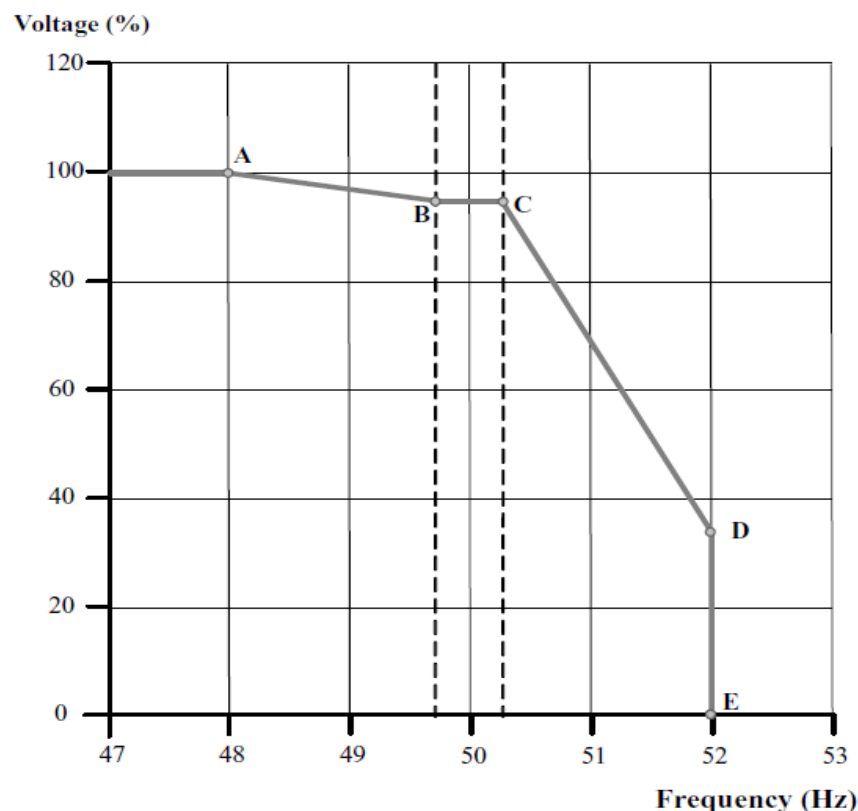


Figure: 5.4. Power versus frequency in ESB National Grid.

5.6 ACTIVE POWER WIND TURBINE OPERATION MODES

In order to accomplish the functionalities mentioned, the following operation modes (Figure.5.5) for the power control of the wind turbine are typically defined [14-18]:

- Balance control—whereby wind turbine production can be adjusted downward or upward, in steps, at constant levels.
- Delta control—whereby the wind turbine is ordered to operate with a certain constant reserve capacity in relation to its momentary possible power production capacity. This operation mode allows an installation to operate at a margin below its rated power output—maximum power extraction so that it may respond to significant changes in frequency by increasing or decreasing its output.
- Power gradient limiter—which sets how fast the wind turbine power production can be adjusted upward and downward. Such a limiter helps to keep production balance between wind farms and conventional power plants.
- Automatic frequency control—the frequency measured in the wind farm point of common coupling (PCC) is controlled. The wind turbine must be able to produce more or less active power in order to compensate for a deviant behavior in the frequency.

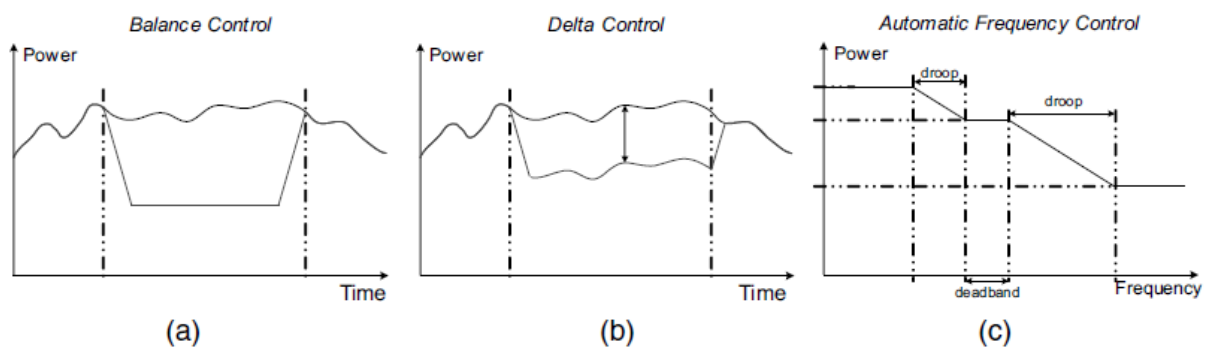


Figure: 5.5. Active power operation modes: (a) balance control, (b) delta control, and (c) automatic frequency control.

5.7 INERTIAL RESPONSE

Most wind turbine concepts utilize variable rotor speed, as this has major advantages for reduction of drive train and structural loads. All conventional generators are fixed speed; that is, the entire drive train rotates at synchronous speed and therefore provides a substantial synchronously rotating inertia. Rotating loads also provide such inertia, although the generators dominate. This inertia provides substantial short-term energy storage, so that small deviations in system frequency result in all the spinning inertias accelerating or decelerating slightly and thereby absorbing excess energy from the system or providing additional energy as required.

This happens without any control system, effectively instantaneously. Without this, modern power systems could not operate. In addition to this “smoothing” effect in normal operation, the spinning inertia also provides large amounts of energy in the event of a sudden loss of generation: the rate of decrease of system frequency in the first second or so after such an event is entirely governed by the amount of spinning inertia in the system [19-20].

Variable speed wind turbines have less synchronously connected inertia, and in the case of the FC concept, none at all. As wind turbines displace conventional generation, there will be less spinning inertia, and therefore the system will become harder to control and more vulnerable to sudden loss of generation. It is feasible that future grid codes will require all or some generators to provide an inertia effect. This can in principle be provided by variable speed wind turbines, but this requires a control function and cannot occur without intervention. The control function will sense frequency changes and use this to adjust generator torque demand, in order to increase or decrease output power.

The effect is similar to the frequency-regulation function discussed earlier, but is implemented by generator torque control rather than pitch control. A more complex implementation could also include pitch control. It is possible that wind turbines would not need to provide this function for small scale frequency deviations, as conventional generation capacity may still be sufficient. Instead, the requirement could be limited to responses to large-scale deviations associated with a sudden loss of generation.

Initial studies show that, in principle, variable speed wind turbines can provide a greater inertia effect than conventional synchronous machines, because generator torque can be increased at will, extracting relatively large amounts of energy from the spinning wind turbine rotor. This decelerates the wind turbine rotor rapidly, and so may not be sustained for very long before aerodynamic torque is reduced. High generator torque also results in high loads on the drive train, which may add significant cost [21-24]. It is concluded that an inertia effect is available, in principle, but may have implications for wind turbine design and cost. It is not clear if some of the FSWT concepts may provide the necessary control.

5.8 POWER SYSTEM STABILIZER FUNCTION

Power system stabilizer (PSS) functions can be provided by conventional generators. In essence, the output power of the generator is modulated in response to frequency deviations, in order to damp out resonances between generators. These resonances are most likely to occur between two groups of large generators separated by a relatively weak interconnection. Again, because of the tight control of generator torque provided by the DFIG concept, and possibly also FSWT, this function should also be able to be provided if required [25].

However, it should be pointed out that because variable speed wind turbines have very little synchronously connected inertia, the risk of such resonances actually reduces as wind penetration increases. Thus, there is an argument that PSS functions should be provided only by conventional generation.

5.9 LOW VOLTAGE RIDE THROUGH (LVRT)

The LVRT fulfillment for wind turbines has become a major requirement from the TSO-DSOs all around the world. The first wind turbines based on squirrel cage asynchronous generators were very sensitive to grid outages. The protections were tuned in such a way that the wind turbine disconnected with even minor disturbances [10-30].

This caused two major problems for the TSO-DSO:

1. The protections were unable to detect faults in lines near wind farms, due to loss of short-circuit current from the wind farms.
2. The loss of wind power generation (reconnection of a fixed speed wind farm takes several minutes) necessitates fast response generation plants (such as hydro) or an increase in the fast reserve power.

So, as mentioned earlier, the first requirement of the TSO is to “keep connected.” But wind turbine behavior during a grid fault is very different depending on the technology (fixed speed or variable speed, and full converter technologies or doubly fed) and also different from conventional power plants based on synchronous generators.

Thus, the TSOs decided to standardize the pattern of current versus voltage during faults, that is, the current that the generator consumes during the fault.

In Chapter 6, the crowbar control strategy and design will be studied in detail. The control strategy must allow the wind turbine:

- To remain connected to the power system and not consume active power during the fault.
- To return to normal operation conditions after the fault.

Voltage recovery is a complementary requirement; wind generators try to minimize the impact of wind parks in the power system during a short circuit and fault clearing. Voltage recovery is performed by reactive current injection of the wind generator.

5.9.1 VOLTAGE DIPS AND LVRT

If a defined fault occurs on the transmission system, it is a normal requirement of the transmission system operator that a generating station remain in operation and connected to the system—thus, it “rides through” the fault.

The definition of the fault is derived from the response time of the network protection systems to clear the fault. A normal duration to clear a fault is in the range of hundreds of milliseconds; hence, the requirement of the user will be to ride through a fault that has a significant drop in voltage of some hundreds of milliseconds in duration.

Because this issue is very important for the grid integration of wind energy systems, the following subsections will be oriented to describe the basic concepts:

- The electric power system (EPS) and the origin of the dips in the EPS
- The definition, classification, and transmission in the EPS of dips
- The procedure to validate the simulated LVRT requirements for wind turbines in Europe.

5.9.2 ELECTRIC POWER SYSTEM

The electric power system (EPS) is the set of infrastructures responsible for the generation, transport, and distribution of electrical energy and can be considered as some of the biggest infrastructures in the world. Electric power transmission is the bulk transfer of electrical energy from generating power plants to substations located near population centers. This is distinct from the local wiring between high voltage substations and customers, which is typically referred to as electricity distribution. Transmission lines, when interconnected with each other, become high voltage transmission networks [20-31].

Figure.5.6 shows a schematic diagram of an EPS, with traditional distribution from generation to a residential user. Historically, transmission and distribution lines were owned by the same company, but over the last decade or so many countries have introduced market reforms that have led to the separation of the electricity transmission business from the distribution business. Thus, in many countries, there are one or two transmission system operators (TSOs), several distribution system operators (DSOs), and trading companies.

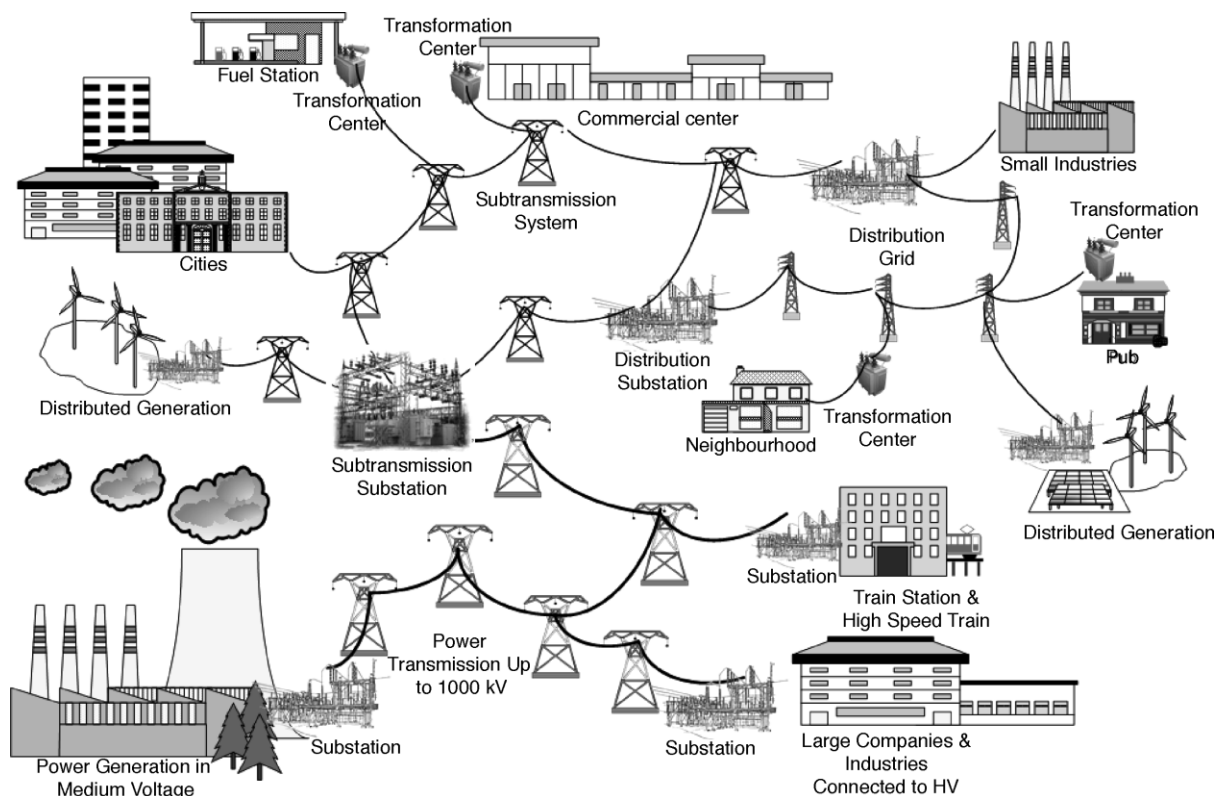


Figure: 5.6.Schematic diagram of an EPS.

Wind power generators are commonly connected at all the voltage levels of the EPS, from the most powerful wind farms (from 25 to 250MW) that are connected to transmission or sub

transmission lines (from 66 to 745 kV) to the lower power wind turbines (50 to 500 kW) connected directly to the low voltage (380, 400, 440V) distribution lines.

Therefore, the connection rules (grid codes) for each voltage level are elaborated by the different companies that operate the networks. Another important point is the connection of different transformers and ground (related to the protective systems for lines) at different levels; for example, Figure 5.7 shows a diagram of the European transmission and distribution network. The transmission system operator is responsible for operating the high voltage transmission system. In Europe the TSO operates the 220 and 400 kV transmission system. The 220 and 400 kV systems are connected by means of autotransformers. Big power generation plants such as nuclear, coal, and hydro are connected at this level.

The distribution system operators are responsible for operating the distribution lines and also the sub transmission system necessary to connect the consumer centers to the transmission system. Typical voltages in this sub transmission system are 69 and 132 kV in Europe. The sub transmission system and the transmission system are connected by means of star–star transformers with neutral connected to earth. Once the lines arrive at the consumer centers, it's necessary to step down the voltage to the proper level for domestic customers. This is done in two steps:

- A high voltage line arrives at the distribution substations where the DSO decreases the voltage levels to 10, 20, 30 kilovolts and distributes the power in different feeders. These transformers have a Delta-Star connection with neutral to ground.
- From each feeder several transformation centers reduce the voltage from medium voltage to low voltage (400 V) and distribute the single-phase lines to domestic customers. These transformers have a Delta connection.

5.9.3 ORIGIN OF VOLTAGE DIPS

Voltage dips are primarily caused by short duration over currents flowing through the power system. The principal contributions to over currents are power system faults, motor starting, and transformer energizing. Power system faults are the most frequent cause of voltage dips, particularly single-phase short circuits. In the event of a short circuit, for a large area of the adjacent network, the voltage in the faulted phase drops to a value between 0 and 1 p.u., depending on the impedance between the point of fault and the point of measurement[15-20].

Voltage dips are caused by faults on the utility network or within the wind farm. A network fault indicates either a short-circuit condition or an abnormal open-circuit condition. The nature of voltage dips can be influenced by the symmetry of a network fault.

Two types of voltage dips are depicted: asymmetrical dip and symmetrical dip.

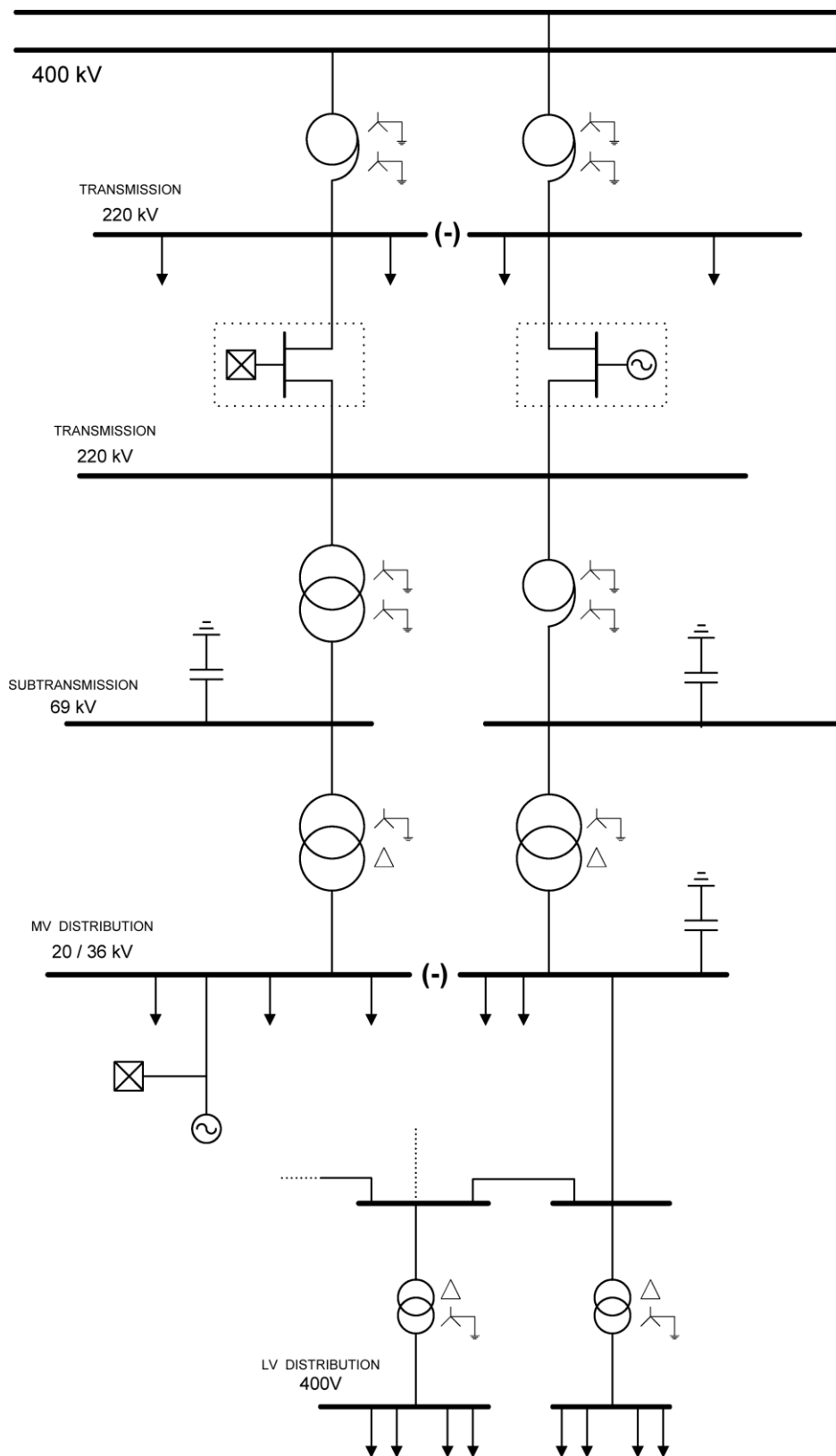


Figure: 5.7. Typical transmission and distribution network.

The supply network is very complex. The extent of a voltage dip at one site due to a fault in another part of the network depends on the topology of the network and the relative source impedances of the fault, load, and generators at their common point of coupling.

The drop in voltage is a function of the characteristics of fault current and the position of the fault in relation to the point of measurement. The duration of the dip event is a function of the characteristics of system protection and recovery time of the connected loads.

5.9.4 VOLTAGE DIPS

Voltage dips—or sags, which are the same thing—are brief reductions in voltage, typically lasting from a cycle to a second or so, or tens of milliseconds to hundreds of milliseconds. (Longer periods of low or high voltage are referred to as “under voltage” or overvoltage.”) Voltage dips are the most common power disturbance. At a typical industrial site, it is not unusual to see several dips per year at the service entrance, and far more at equipment terminals. The frequency is even higher in the interior of the site or in developing countries that have not achieved the same levels of power quality as more developed nations [2-31].

Dips do not generally disturb incandescent or fluorescent lighting, motors, or heaters. However, some electronic equipment lacks sufficient internal energy storage and therefore cannot ride through dips in the supply voltage. Equipment may be able to ride through very brief, deep dips, or it may be able to ride through longer but shallower dips.

Normally, the grid voltage fluctuates around its nominal value with variations within a maximum range of 10% of that value. A dip is the sudden drop in voltage from one or more phases followed by a rapid restoration to its nominal value after a short space of time between half a period (10 ms at 50 Hz) and 1 minute. For the voltage fall to be considered a dip, the voltage value must be between 1% and 90% of its nominal value (IEC 61000-2-1, EN50160). A drop below 1% is usually called a short interruption. Above 90% it is considered that the voltage is within the normal range of operation.

The voltage dips are normally characterized by the depth and duration, as can be seen in Figure 5.8.

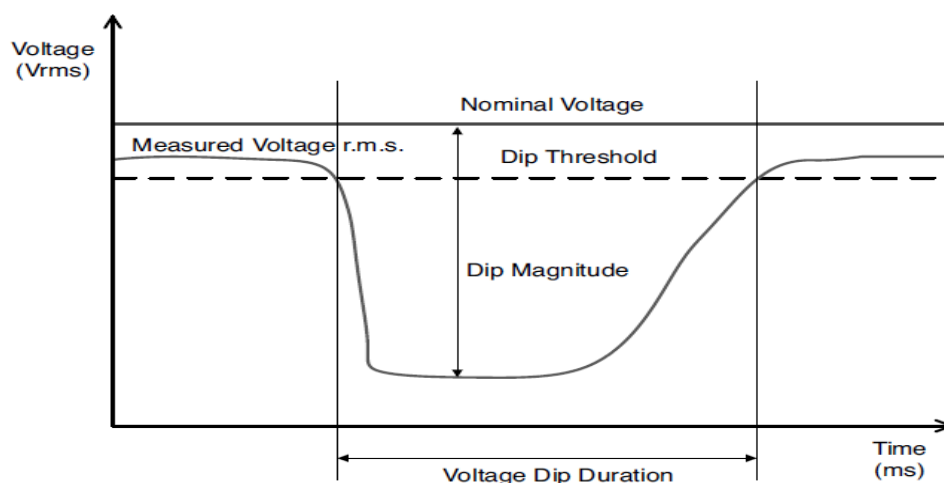


Figure: 5.8. Parameters of a dip.

In three-phase grids, dips can be divided into two broad categories:

- Three-phase dips, when the voltages of the three phases fall into the same proportion.
- Asymmetric dips, where all three phase drops are not equal and the voltage is unbalanced: for example,
 - Single-phase dips that affect only one phase.
 - Biphasic dips that involve two phases.

The depth measures the voltage drop in relative terms. It is measured at the deepest point of the valley. The voltage is usually measured by the rms value calculated for each half-period; hence, the minimum duration for a voltage dip is set for half a period. The duration is defined as the length of time that voltage is less than 90% of the nominal value.

5.9.5 CLASSIFICATION

Bollen and co-workers propose a more intuitive approach to the characterization of three-phase voltage dips. The ABC classification method distinguishes between seven dip types (A to G) by analyzing the possible types of short circuits and the dip propagation through transformers. Table 5.2 summarizes these dip classes as a function of fault type, location and connection of measuring instruments in the AC grid. Figure.5.9 shows voltage phasors for different dip classes, in which the positive sequence, negative-sequence, and zero-sequence impedances are considered to be equal. If the amplitude depth is defined with the variable p , the fault voltages are defined in the equations for each fault type [15-25].

TABLE: 5.2 Dip Classes of Several Faults Measured at Different Locations.

Fault Type	Dip Class (measured between phase and neutral)	Dip Class (measured between phase and neutral after a Δy or $Y\Delta$ transformer)	Dip Class (measured between phases)	Dip Class (measured between phases after a Δy or $Y\Delta$ transformer)
Three-phase	A	A	A	A
Single-phase	B	C	D	C
Phase-to-phase	C	D	C	D
Two-phase-to-ground	E	F	F	G

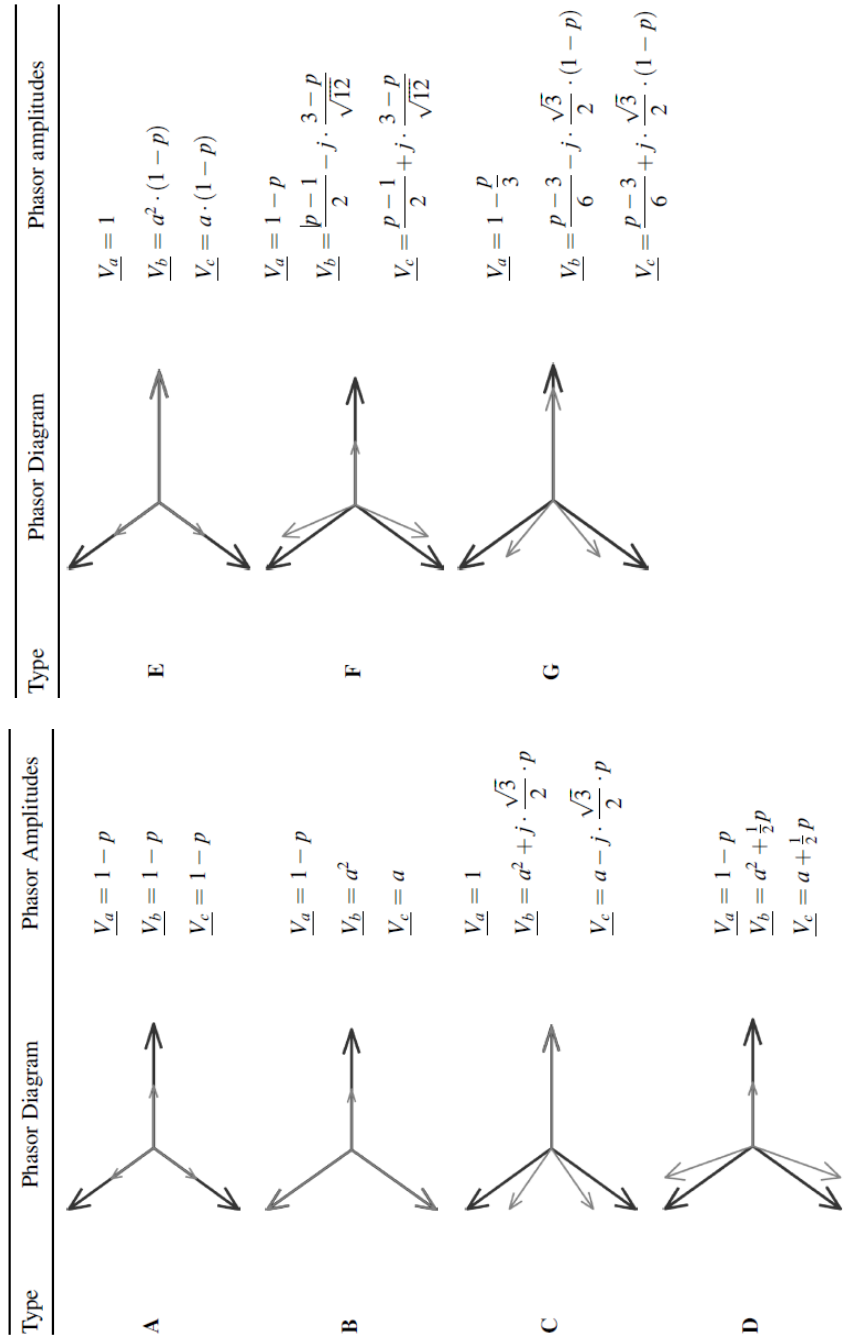


Figure: 5.9. Different types of voltage dip

5.9.6 TRANSFORMER EFFECT

The ABC classification method was introduced to describe the propagation of voltage dips through transformers. This method of voltage dip classification is the oldest and the most commonly used, possibly due to its simplicity.

Three groups of transformer connections must be analyzed:

- Wye–wye with neutral point connected
- Delta–delta and wye–wye without connecting neutral point
- Wye–delta and delta–wye

The first group of transformers allows circulating common mode currents. The second groups of transformers do not allow circulating common mode currents. This means that the common mode component is eliminated.

The third group of transformers, apart from common mode component elimination, introduces a phase angle between primary and secondary voltages. Note that positive and negative sequences are phase shifted by the opposite signed angle. Due to these reasons, the type of voltage dip in the primary side can be changed in the secondary side. A Type A voltage dip does not change with a transformer because it only has a positive sequence. Figure 5.9 represents the transformation of different types of voltage dip according to the ABC classification method [18-25].

5.6.1 TRANSFORMER EFFECT IN A WIND FARM

The wind turbine can suffer grid outages at the point where it's connected to the high, medium, or low voltage network. In low voltage networks the turbine is directly connected to the low voltage distribution grid without a transformer. In medium voltage grids (distribution), the turbine is connected by means of the turbine step-up transformer.

Turbines connected to high voltage grids (transmission and sub transmission) are usually found in wind farms with the electrical layout explained in Figure.5.12. In this case a typical example of the electrical circuit between the point of common coupling of the wind farm to the wind turbine is represented in Figure.5.10.

In order to study the effect of transmission network short circuits on the wind turbine, the following elements are modeled:

- The high voltage equivalent grid, represented by the equivalent Thevenin circuit
- The substation transformer with a short-circuit impedance
- The impedance of the feeder from the substation to the wind turbine
- The coupling transformer with a short-circuit impedance
- The internal electrical circuit of the turbine

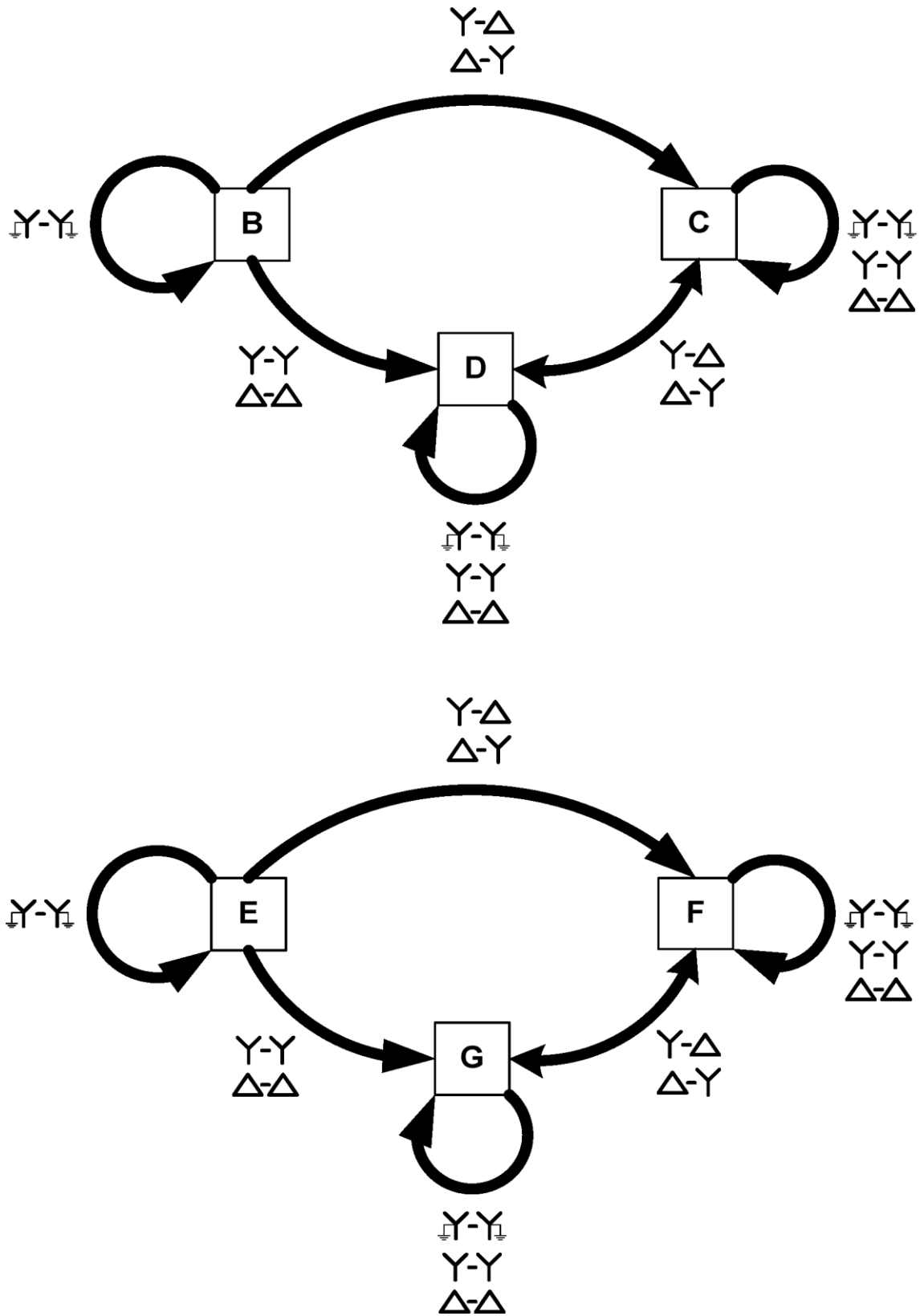


Figure: 5.10 Transformer effect in the type of voltage dip.

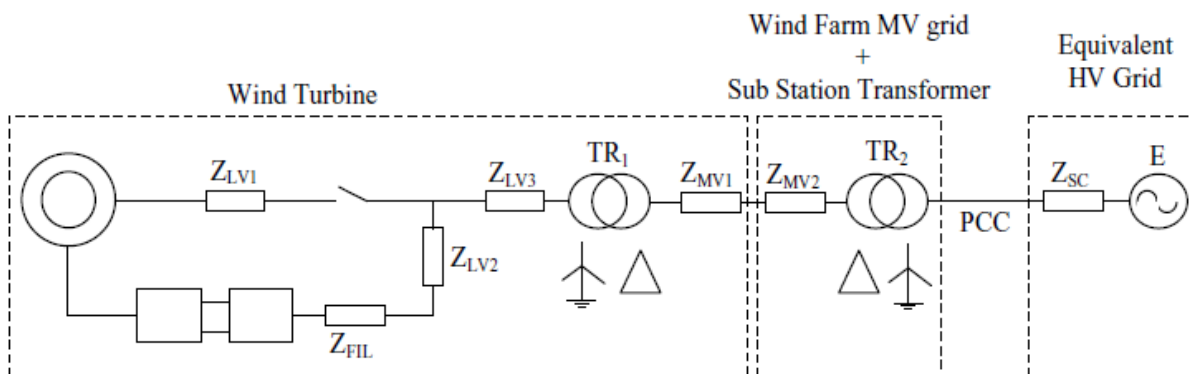


Figure: 5.11. Transformer effects in the type of voltage dip for high voltage grid.

The short circuits can be located in high voltage (HV) or medium voltage (MV) grids and will affect the wind turbine in different ways but due to the transformer configuration only three-phase and two-phase voltage dips will occur at the low voltage connection point of the turbine. The electrical configuration of wind farms is different in each country and the same goes for how the transmission and distribution systems are operated; each example must be considered separately.

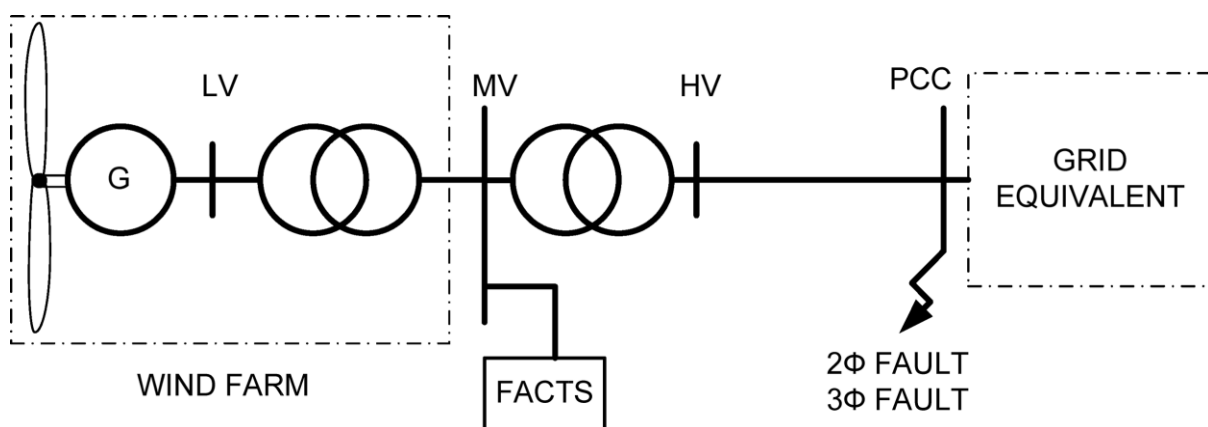


Figure: 5.12 Single-line schematic of the electrical system layout.

5.7 REFERENCES

[1] W. Qiao and R. G. Harley, "Grid connection requirements and solutions for DFIG wind turbines," in Proc. IEEE Energy 2030 Conf., Atlanta, GA, Nov. 17–18, 2008, pp. 1–8.

[2] Federal Energy Regulatory Commission. (2005, Jun. 2). Regulatory Order No. 661: Interconnection for Wind Energy [Online]. Available:

<http://www.ferc.gov/industries/electric/indus-act/gi/wind.asp>

- [3] Federal Energy Regulatory Commission. (2005, Dec. 12). Regulatory Order No. 661-A: Interconnection for Wind Energy [Online]. Available: <http://www.ferc.gov/industries/electric/indus-act/gi/wind.asp>
- [4] J. Lopez, P. Sanchis, X. Roboam, and L. Marroyo, "Dynamic behavior of the doubly fed induction generator during three-phase voltage dips," *IEEE Trans. Energy Convers.*, vol. 22, no. 3, pp. 709–717, Sep. 2007.
- [5] J. Morren and S. W. H. de Hann, "Ride through of wind turbines with doubly-fed induction generator during a voltage dip," *IEEE Trans. Energy Convers.*, vol. 20, no. 2, pp. 435–441, Jun. 2005.
- [6] I. Erlich, H. Wrede, and C. Feltes, "Dynamic behavior of DFIG-based wind turbines during grid faults," in *Proc. Power Convers. Conf. (PCC 2007)*, Nagoya, Japan, Apr. 2–5, pp. 1195–1200.
- [7] W. Qiao, G. K. Venayagamoorthy, and R. G. Harley, "Real-time implementation of a STATCOM on a wind farm equipped with doubly fed induction generators," *IEEE Trans. Ind. Appl.*, vol. 45, no. 1, pp. 98–107, Jan./Feb. 2009.
- [8] W. Qiao, R. G. Harley, and G. K. Venayagamoorthy, "Coordinated reactive power control of a large wind farm and a STATCOM using heuristic dynamic programming," *IEEE Trans. Energy Convers.*, vol. 24, no. 2, pp. 493–503, Jun. 2009.
- [9] C. Abbey and G. Joos, "Supercapacitor energy storage for wind energy applications," *IEEE Trans. Ind. Appl.*, vol. 43, no. 3, pp. 769–776, May/Jun. 2007.
- [10] P. Flannery and G. Venkataramanan, "A fault tolerant doubly fed induction generator wind turbine using a parallel grid side rectifier and series grid side converter," *IEEE Trans. Power Electron.*, vol. 23, no. 3, pp. 1126–1135, May 2008.
- [11] O. Abdel-Baqi and A. Nasiri, "A dynamic LVRT solution for doubly fed induction generators," *IEEE Trans. Power Electron.*, vol. 25, no. 1, pp. 193–196, Jan. 2010.
- [12] D. Xiang, L. Ran, P. J. Tavner, and S. Yang, "Control of a doubly fed induction generator in a wind turbine during grid fault ride-through," *IEEE Trans. Energy Convers.*, vol. 21, no. 3, pp. 652–662, Sep. 2006.
- [13] J. Liang, W. Qiao, and R. G. Harley, "Direct transient control of wind turbine driven DFIG for low voltage ride-through," presented at the *IEEE Symp. Power Electronics and Machines In Wind Applications (PEMWA 2009)*, Lincoln, NE, Jun. 24–25.
- [14] D. W. Novotny and T. A. Lipo, *Vector Control and Dynamics of AC Drives*. London, U.K.: Oxford University Press, 2000, ISBN-10: 0198564392/ISBN-13: 978-0198564393.
- [15] W. Qiao, W. Zhou, J. M. Aller, and R. G. Harley, "Wind speed estimation based sensorless output maximization control for a wind turbine driving a DFIG," *IEEE Trans. Power Electron.*, vol. 23, no. 3, pp. 1156–1169, May 2008.
- [16] R. Lorenz and D. Lawson, "Performance of feed forward current regulators for field-oriented induction machine controllers," *IEEE Trans. Ind. Appl.*, vol. IA-23, no. 4, pp. 597–602, Jul./Aug. 1987.
- [17] N. Miller, J. Sanchez-Gasca, W. Price, and R. Delmerico, "Dynamic modeling of GE 1.5 and 3.6 MW wind turbine-generators for stability simulations," in *Proc. IEEE PES Gen. Meeting*, Toronto, ON, Canada, Jul. 13–17, 2003, pp. 1977–1983.

- [18] S. Seman, J. Niiranen, and A. Arkkio, "Ride-through analysis of doubly fed induction wind-power generator under unsymmetrical network disturbance," *IEEE Trans. Power Syst.*, vol. 21, no. 4, pp. 1782–1789, Nov. 2006.
- [19] J. Niiranen, "Simulation of doubly fed induction generator wind turbine with an active crowbar," presented at the 11th Int. Conf. Power Electronics and Motion Control (EPE-PEMC 2004), Riga, Latvia, Sep. 2–4.
- [20] A. Hansen and G. Michalke, "Fault ride-through capability of DFIG wind turbines," *Renewable Energy*, vol. 32, no. 9, pp. 1594–1610, Jul. 2007.
- [21] Lopez j., Sanchis p., Roboam x., Marroyo l.: 'Dynamic Behavior of the doubly fed induction generator during three-phase voltage dips', *IEEE trans. energy convers.*, 2007, 22, (3), pp. 709–717.
- [22] Chondrogiannis S., Barnes M.: 'Stability of doubly-fed induction generator under stator voltage oriented vector control', *IET Renew. Power Generation*, 2008, 2, (3), pp. 170–180.
- [23] Muyseen S.M., Takahashi R., Murata T, "Low voltage ride-through capability enhancement of wind turbine generator system during network disturbance", *IET Renew. Power Generation*, 2009, 3, (1), pp. 65–74.
- [24] Kasem A.H., EI-Saadany E.F., EI-Tamaly H.H., Wahab M.A.A, "An improved fault ride-through strategy for doubly fed induction generator-based wind turbines", *IET Renew. Power Generation*, 2008, 2, (4), pp. 201–214.
- [25] Chondrogiannis S., Barnes M, "Specification of rotor side voltage source inverter of a doubly-fed induction generator for achieving ride-through capability", *IET Renew. Power Generation*, 2008, 2, (3), pp. 139–150.
- [26] Morren J., DE Hann S, "Ride-through of wind turbines with doubly-fed induction generator during a voltage dip", *IEEE Trans. Energy Conversion.*, 2005, 20, (2), pp. 435–441.
- [27] J. Morren, S. W. H. de Haan, "Ride through of wind turbines with doubly-fed induction generator during a voltage dip". *IEEE Transaction Energy Conversion*, vol. 20, no. 2, pp. 435–441, June. 2005.
- [28]. ENEL – DK 5400 - Criteri di allacciamento di clienti alla rete AT della distribuzione, October 2004.
- [29]. ENEL - – DK 5740 - Criteri di allacciamento di impianti di produzione alla rete MT di ENEL distribuzione, February 2005.
- [30]. TERNA - Codice di trasmissione, dispacciamento, sviluppo e sicurezza della rete, 2006.
- [31] A. Lubosny, *Wind Turbine Operation in Electric Power Systems -Advanced Modeling*, Springe Verlag, 2003.

CHAPTER 6

LOW VOLTAGE RIDE THROUGH (LVRT) CAPABILITY OF DFIG WIND TURBINE

INTRODUCTION

In the past, most national grid codes and standards did not require wind turbines to support the power system during a disturbance. For example during a grid fault or sudden drop in frequency wind turbines were tripped off the system. However, as the wind power penetration continues to increase, the interaction between the wind turbines and the power system has become more important. This is because, when all wind turbines would be disconnected in case of a grid failure, these renewable generators will, unlike conventional power plants, not be able to support the voltage and the frequency of the grid during and immediately following the grid failure. This would cause major problems for the systems stability [1-13].

Therefore, wind farms will have to continue to operate during system disturbances and support the network voltage and frequency. Network design codes are now being revised to reflect this new requirement. A special focus in this requirement is drawn to both the fault ride-through capability and the grid support capability [1-10]. Fault ride-through capability addresses mainly the design of the wind turbine controller in such a way that the wind turbine is able to remain connected to the network during grid faults (e.g. short circuit faults). While grid support capability represents the wind turbine capability to assist the power system by supplying ancillary services, i.e. such as supplying reactive power, in order to help the grid voltage recovery during and just after the clearance of grid faults. Due to the partial-scale power converter, wind turbines based on the DFIG are very sensitive to grid disturbances, especially to voltage dips during grid faults.

Faults in the power system, even far away from the location of the turbine, can cause a voltage dip at the connection point of the wind turbine. The abrupt drop of the grid voltage will cause over-current in the rotor windings and over-voltage in the DC bus of the power converters [11-18]. Without any protection, this will certainly lead to the destruction of the converters. In addition, it will also cause over-speeding of the wind turbine, which will threaten the safe operation of the turbine [19-25]. Thus a lot of research works have been carried out on the LVRT ability of DFIG wind turbines under the grid fault. These LVRT strategies can be divided into two main types: the active method by improving control strategies, the passive scheme with additional hardware protective devices.

6.1 IMPROVED CONTROL STRATEGIES IMPLEMENTATION

In the operational control of the DFIG, traditional vector control based on stator flux orientation or stator voltage orientation has been widely used. With this kind of control strategy, the PI controller is usually used in order to regulate independently the active and reactive power. But when there is a sharply voltage dip on the grid side, the PI controller will get saturation easily, and it is hard to get back to the effective regulate state. The command ability of the DFIG is then lost. In order to overcome the shortcoming of the traditional vector control, the researchers around the world have proposed many improved strategies to achieve LVRT.

The simulation results of [12-13] show that through the appropriately increasing of the proportional factor of the PI regulator in the current loop of the traditional DFIG vector controller, the generator can remain in a continuous operation within a certain range when a grid fault appears. However, a dynamic response of two important state variables such as rotor current and rotor voltage cannot be obtained. The proposed method can only keep the DFIG operating under a symmetrical three-phase fault, which causes a slight drop in the bus voltage. When the fault causes a serious dip in the bus voltage, over-current and over-voltage are in the exciting converter.

An improved vector control strategy has been proposed in [11] to explain that the dc and negative sequence components are caused in the machine by flux linkages, resulting in a large Electro Motive Force (EMF) induction in the rotor circuit. A new method is proposed to control the rotor-side converter so that the rotor current contains components in order to oppose the undesired components in the stator-flux linkage. A fast observation of the stator-flux linkage components is essential to the control. This constrains the rotor current given by the voltage capability of the converter. An increased machine leakage inductance is useful to the proposed ride-through control method. The advantage of this method is that it can be applied to all types of symmetric and asymmetric grid failures and the disadvantages is that the rotor side converter is used to generate the rotor current, which is opposite to the transient component of the stator flux so that the control effect is limited to the converter capacity.

The dynamic changes of the exciting current are taken into account when designing the controller in [25], which is also based on the traditional vector control method. The improved controller can be obtained by considering the dynamic changes of the exciting current as feed-forward compensation in the rotor current regulator. This method can effectively reduce the rotor over-current under grid voltage drops, but it is achieved by increasing the rotor-side converter output voltage. As the maximum output voltage of the rotor side inverter is limited, this method can be applied to the situation when grid faults caused a slight drop in the generator terminal voltage. But for a serious drop in the generator stator voltage (caused by serious grid faults), the rotor side converter cannot provide a sufficient high exciting voltage. So the rotor currents will still be out of control. In addition, because the method cannot reduce the power fed into the rotor side converter, the stability of the DC voltage is not improved.

The above control strategies are all based on the traditional vector control strategy, because the vector control strategy has a high precision, constant switching frequency and good steady-state performances. But at the same time, in order to achieve a decoupling control of the active power and reactive power, the control structure of the vector control is usually

complicated. Therefore, there are some researchers who have proposed other control strategies. In order to avoid the impact of the cross-coupling compensation, a doubly-fed generator rotor Flux Magnitude and Phase Angle control (FMAC) is proposed in [14]. Unlike the vector control, which uses the rotor current to achieve control objectives, it uses the rotor flux amplitude to control the generator terminal voltage, and the rotor flux phase angle to control the output active power. Compared with the traditional vector control methods in [18], simulation results show that the new controller has better decoupling control performance on terminal voltage and output power, and when a slight drop happens in the grid voltage, the terminal voltage recovery capability and the power oscillation damping effect under grid faults are better than vector control.

6.2 LVRT STRATEGIES WITH HARDWARE IMPLEMENTATION

Since in doubly fed wind power generation systems, the capacity of rotor side converter is relatively small compared with the rated capacity of generator, the rotor side converter can provide partial control of the generator. Therefore when power system faults occur and a deep drop of generator terminal voltage occurs, the rotor side converter will still lose the control of rotor currents. That is why an additional hardware protection circuit is necessary. The hardware implementation can be in the rotor side, the dc side or the stator side. Currently, the most commonly used protecting scheme is short circuiting the rotor winding through the crowbar protection circuit when rotor currents of the doubly fed generator or DC bus voltage exceed their rated value during the grid fault. Hence a path for the rotor over current is provided, so that the rotor side converter can be well protected [20]. Since the traditional crowbar circuits cannot be turned off shortly after the grid fault because of the thyristors, which does not meet the new grid codes.

Therefore, new active crowbars, using active switches such as IGBT and GTO, are proposed to protect the system [26-30]. The rotor-side converter with this kind of circuit can be still connected to the rotor when a grid fault occurs. And after the fault, the power system can be more flexible, taking less time to return to a normal operating mode. In order to decrease the rotor transient faster, the active crowbar circuit usually has a resistor on the DC side. In [28], the pitch control is used to restrain the over-speeding of the turbine while a crowbar is implemented to protect the system. But there are many time delays to control the pitch angle, so that a damping controller is proposed to reduce the torsional oscillations in the drive train during grid faults before the crowbar is triggered [29]. Then a voltage controller from the rotor-side and a reactive power boosting controller from the grid-side are proposed to support the grid voltage during the fault [30]. With the cooperation of the above three controllers and the crowbar protection, the LVRT capability of the DFIG system can be greatly enhanced.

It should be mentioned that the timing sequence for the crowbar removal affects the variations of currents and the electromagnetic torque after the fault clearance. A PWM control strategy of the active crowbar is proposed in [31-32]. The DC bus is controlled by a PI regulator. Compared to the traditional ON-OFF control method, the new PWM control can effectively reduce the electromagnetic torque ripple and thus a more stable output DC bus voltage is obtained in fault condition. However, rapid switching under this PWM control mode may exacerbate the transient progress of the DFIG, resulting in a higher transient current and a longer recovery time.

6.3 PERFORMANCE OF THE DFIG DURING VOLTAGE DIPS WITH AN ACTIVE CROWBAR

Although the modified vector control strategy can provide adequate control of the DFIG during grid voltage dips, its ride-through capability is limited by the relative small rating of the rotor side converter compared to the generator rating. If the depth of the dip is small and the required voltage does not exceed the maximum voltage that the rotor side converter can generate, the current remains controlled. But for larger dips, an increased rotor voltage will be needed to control the rotor currents. When this required voltage exceeds the voltage limit of the converter, it is not possible any longer to control the current as desired. It is confirmed that if the stator voltage decreases to zero, the required rotor voltage is close to the stator rated voltage instead of the small percentage induced in normal operation. So, a converter with a rated power similar to that of the generator is required therefore the advantages of this wind energy conversion structure are lost.

Therefore, an additional protection device is always needed in the case of large voltage dips. Protection devices such as crowbar circuits [33-46], energy storage system, stator switches and auxiliary parallel grid-side rectifier have already been used to protect DFIG during grid faults. In this chapter, an active crowbar protection system will be modeled. And then an improved control strategy for the crowbar protection coordinated with a demagnetization method of the DFIG and voltage support by both the generator and the grid-side converter will be proposed to enhance the ride-through capability.

6.3.1 CROWBAR PROTECTION CIRCUIT

Crowbar protection systems are commonly used to protect the power converters during voltage dips. The key of this solution is to limit the high current in the rotor and the high voltage across the DC bus. With a crowbar protection circuit, it is possible to ride-through grid faults without disconnection of the turbine from the grid.

6.3.2 DEVELOPMENT OF THE CROWBAR CIRCUIT

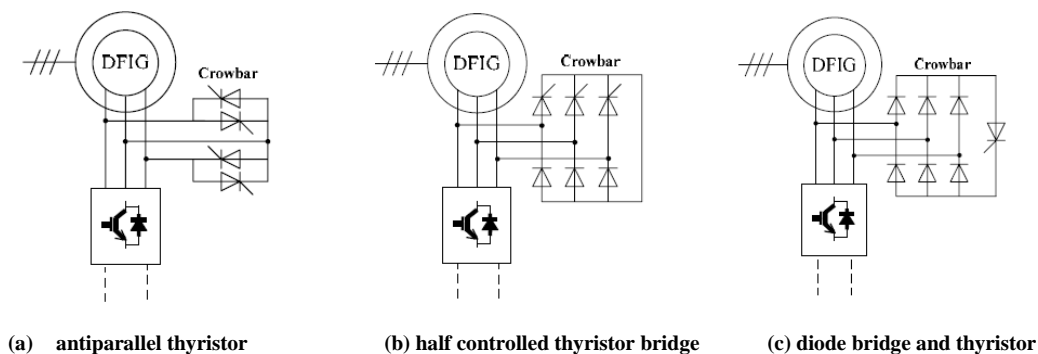


Figure: 6.1. Conventional crowbars.

The crowbar circuit is usually implemented between the rotor circuit and rotor-side converter to provide a bypass for the high transient rotor current, which is induced by voltage dips. Initially, the industrial solution implemented was just to short circuit the rotor windings with the crowbar circuit. This conventional crowbar circuit can be constructed in many ways, as illustrated in Figure 6.1 [46].

In Figure 6.1(a), the rotor can be short-circuited by two pairs of anti parallel thyristors connected between the phases. Another alternative is to use a half-controlled thyristor bridge, as it is shown in Figure 6.1(b). The third possibility as in Figure 6.1(c) is to rectify the phase currents with diode bridge and to use a single thyristor to trigger the crowbar. The main drawback of this solution is that the wind turbines are not able to resume in normal operation cooperating with the grid because of its turn-off problem. For crowbars of Figure 6.1(a) and (b), because the rotor currents may have a significant DC component, the phase current reversals that would turn the thyristors off do not exist when they would be needed. And for the crowbar of Figure 6.1(c), as the current through the thyristor is continuous, it does not allow the thyristor to turn off. Moreover, the snubber design for the thyristors of the crowbar may be problematic.

In order to fulfill the newest grid codes, the crowbar circuit should be tripped off after the clearance of the grid faults. Thus fully controllable semiconductor switches are needed to construct an active crowbar [36-46]. From the conventional crowbars, the anti parallel thyristor one is difficult to convert into active crowbar because of the large number of the controlled components. The same problem is faced by the half-controlled bridge one. However, the crowbar circuit with a diode bridge has only one controlled component, thus it is optimal in this transformation. Either a GTO or an IGBT can be used as the fully controllable switch for the active crowbar circuit, as it is shown in Figure 6.2 (a) and (b). As an improvement on the active crowbar, resistances are added to the crowbar to restrict the high rotor current. This solution is most widely used by the manufacturers nowadays. Another kind of improved active crowbar can be constructed by three-phase AC switches and resistors, as illustrated in Figure 6.2 (c).

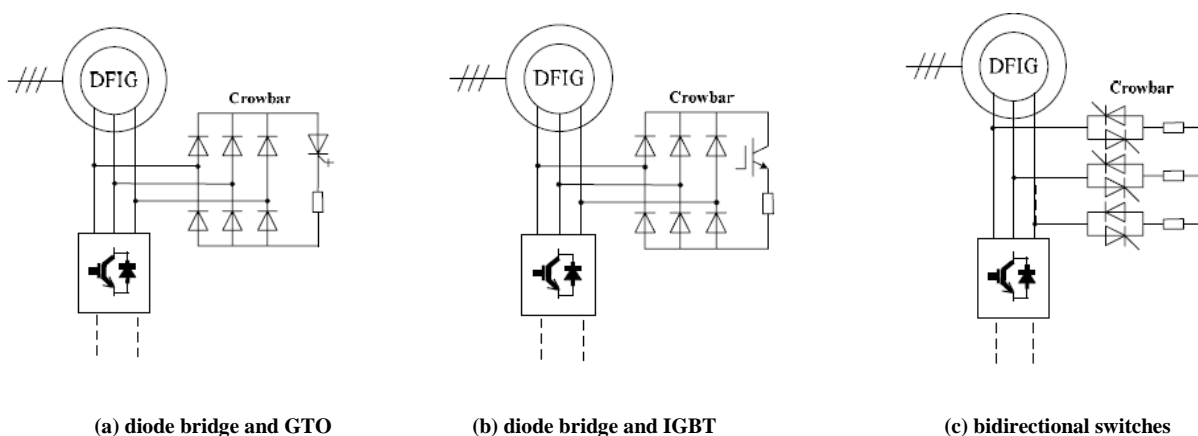


Figure: 6.2. Improved active crowbars.

With this improved crowbar, the wind turbine can remain connected to the grid during the dips. Because of the generator and converter can stay connected during the grid fault, they can resume in normal operation immediately after the fault has been cleared. Recently, there

are some papers that discuss the protection scheme of the DFIG with active crowbars during grid disturbances. However, most papers give little information of the protection scheme that is implemented [33-46].

DC side crowbar consists of a chopper and a resistor that are added across to the DC bus of the converter. It can limit the DC voltage from exceeding safe range, as shown in Figure 6.3. The chopper module is not essential for fault ride-through operation but it increases the normal range of DFIG operation by smoothing the dc-link voltage during heavy imbalances of active power on the rotor side and grid side converters. The rotor side converter has to be dimensioned to handle the high current transients in addition to the normal load. Thus oversized components have to be used and make this scheme unattractive [35-46].

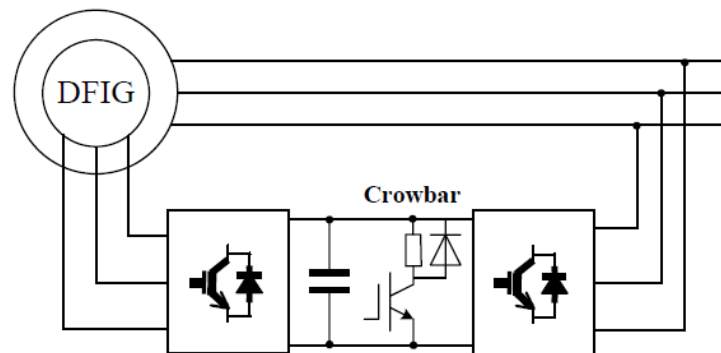


Figure: 6.3.DC side crowbar.

6.3.3 MODELING OF THE ACTIVE CROWBAR

As we can see in Figure 6.4, the crowbar protection circuit is connected between the rotor of DFIG and the rotor-side converter. The crowbar protection circuit is composed of three phase bidirectional switches and bypass resistors.

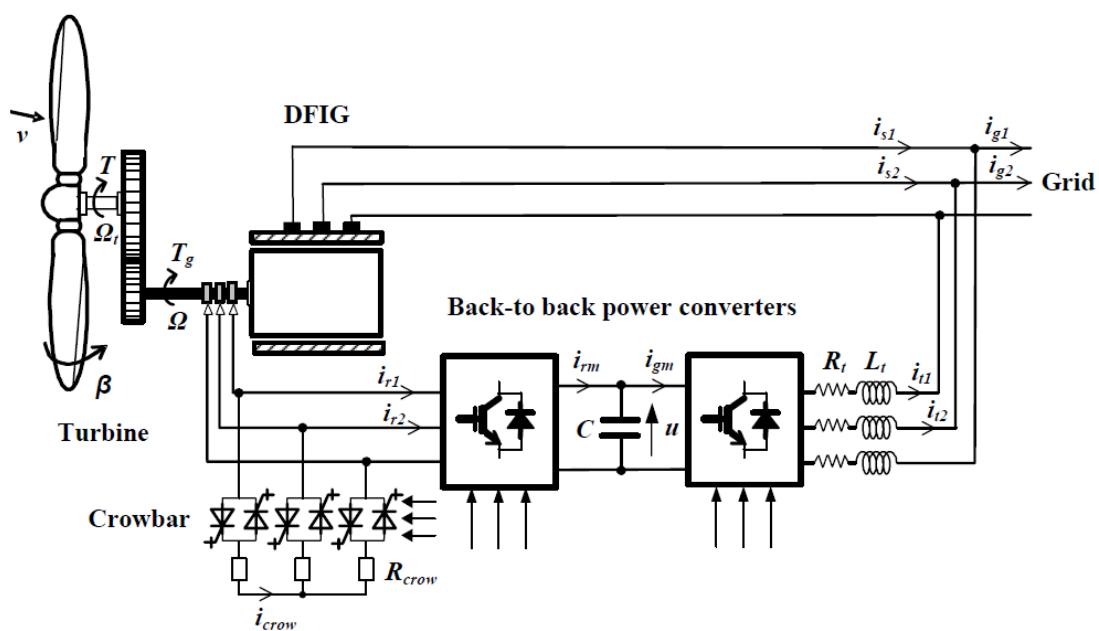


Figure: 6.4.DFIG based wind turbine with crowbar protection.

The semiconductors are considered to be ideal and a switching function S_c is defined for the switches, which takes the values 1 when the switch is closed and 0 when it is open. Then Crowbar protection component can be modeled by a simple equation as:

$$V_{\text{crow}} = S_c R_{\text{crow}} i_{\text{crow}} \quad (6.1)$$

The behavior of such systems during grid faults is greatly affected by the resistor value of crowbar. It has been shown by simulation in [45] that a low crowbar resistance leads to a higher electrical torque, over currents and low rotor voltages. High values for the crowbar resistor will result in a lower electrical torque and rotor currents but also higher rotor voltages. Therefore, the crowbar resistors should be sufficiently low to avoid large voltages on the converter terminals. On the other hand, they should be high enough to limit the rotor current. In our study, this resistance value is chosen to be equal to $30 R_r$ and R_r is rotor resistance of DFIG.

6.4 SYNTHETIC CONTROL AND PROTECTION STRATEGY

Although there are many papers, which discuss the control and protection strategy of the DFIG under grid faults, the most of them gives little information of the protection scheme that is implemented. In this chapter, a hysteresis control strategy of crowbar circuit is designed to protect the system in serious grid faults. And a demagnetization method of the DFIG is adopted to decrease the oscillations of the transient current. Moreover, the grid voltage can be supported by both the generator and the grid-side converter.

6.4.1 HYSTERESIS CONTROL OF THE CROWBAR

Commonly the crowbar is triggered in case of over voltage across the DC bus or over current in rotor windings. When the crowbar is triggered, the rotor side converter will be disconnected from the rotor circuit at the same time. As a result, the controllability of the DFIG is lost during the voltage dip, which is the main drawback of the crowbar protection. Moreover, the DFIG then behaves as a classical squirrel cage induction generator with a variable rotor resistance until the crowbar is cut off and the rotor side converter resumes normal operation. In this situation, the DFIG absorbs reactive power from the grid for magnetization, which will even deteriorate the stability of the weak grid. Therefore it is better to reduce the activation time of crowbar.

In order to reduce the operation time of the crowbar, an improved hysteresis control strategy is adopted, as it is shown in Figure 6.5. The maximum absolute value of rotor current $|i_r|_{\text{max}}$ is compared with a threshold value i_{th} and a safety value i_{sa} . If $|i_r|_{\text{max}}$ is greater than i_{th} , the crowbar is activated for protecting the power converters. And when $|i_r|_{\text{max}}$ decreases to be less than i_{sa} , the crowbar will be cut off and the rotor side converter is restarted to control the DFIG.

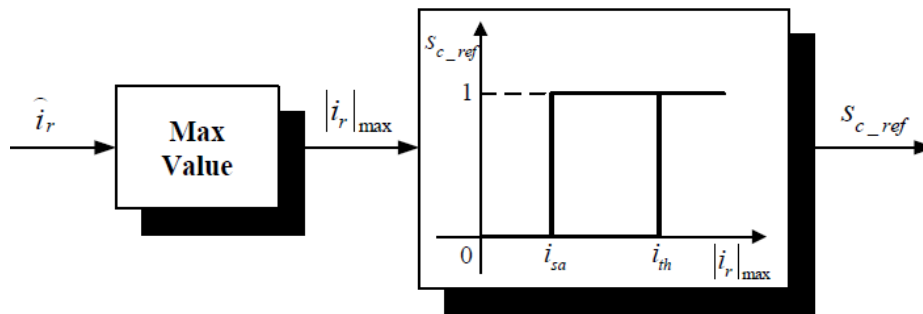


Figure: 6.5.Hysteresis control of the active crowbar.

6.4.2 DEMAGNETIZATION OF DFIG UNDER GRID VOLTAGE DIPS

During a symmetrical grid fault, there will be high oscillations of the stator and rotor currents due to the dc component of the stator flux. In [43-58] the authors suggest to control the rotor current in order to compensate for this dc component of the stator flux. Normally, a very large rotor current is needed to count this flux. But due to the limited capacity of the power converter, its capability is greatly restricted. When the stator flux vector is oriented along the d -axis of the synchronously rotating frame, it can then be expressed as:

$$\varphi_{ds} = \frac{L_s}{R_s} V_{sd} + L_m i_{dr} \quad (6.2)$$

Therefore if the direct component of the rotor current is reduced, the stator flux can be reduced and then the oscillations of the currents will be attenuated. A simple demagnetization method can be obtained by setting the reference of i_{dr} to zero. Moreover, from the flux equations of the DFIG, if the rotor current is reduced, the stator flux will be reduced. So that the reference value of i_{qr} is also set to zero. This method is used as soon as a voltage dip is detected and a few hundred milliseconds after the clearance of the fault in order to avoid large transients. The control block diagram is shown in Figure 6.6.

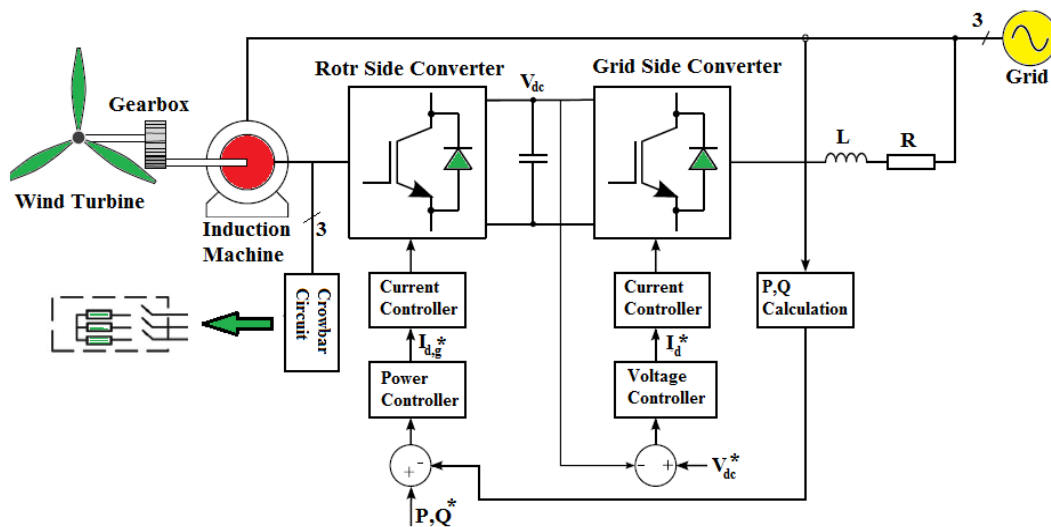


Figure: 6.6. Control block diagram of DFIG.

6.4.3 REQUIREMENTS AND STRATEGIES

Wind turbine capacity scale increases and when large scale wind turbine generators break from power grid, they would lose the support of voltage, lead to serious effect and cause serious impact on the stable operation of power grids. In response, many foreign power grid operators proposed a mandatory requirement LVVRT. The general rules for connecting to the transmission system in Italy are given in [47-50]. The voltage profile for the fault ride-through capability of the wind turbines is given in Figure 6.7.

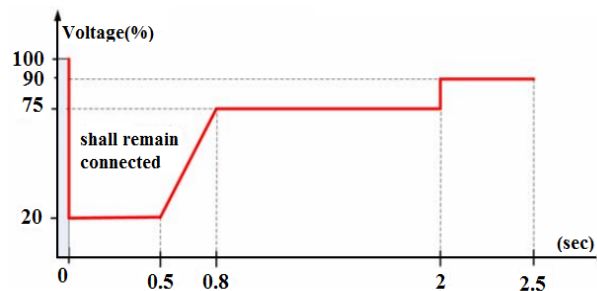


Figure: 6.7. Voltage profile for fault ride-through capability.

6.5 SIMULATION RESULTS

The parameters of the turbine and induction machine are given in Annexure II. The parameters have been adapted from a GE (General Electric) 1.5MW turbine [54]. In order to examine the effect of the proposed control strategies, such as demagnetization method and hysteresis control scheme, against three phase voltage dips, simulations for a practical 1.5MW DFIG wind turbine have been carried out using PLECS and Matlab Simulink™.

CASE 1

The system performance of the DFIG is shown in Figure 6.8.

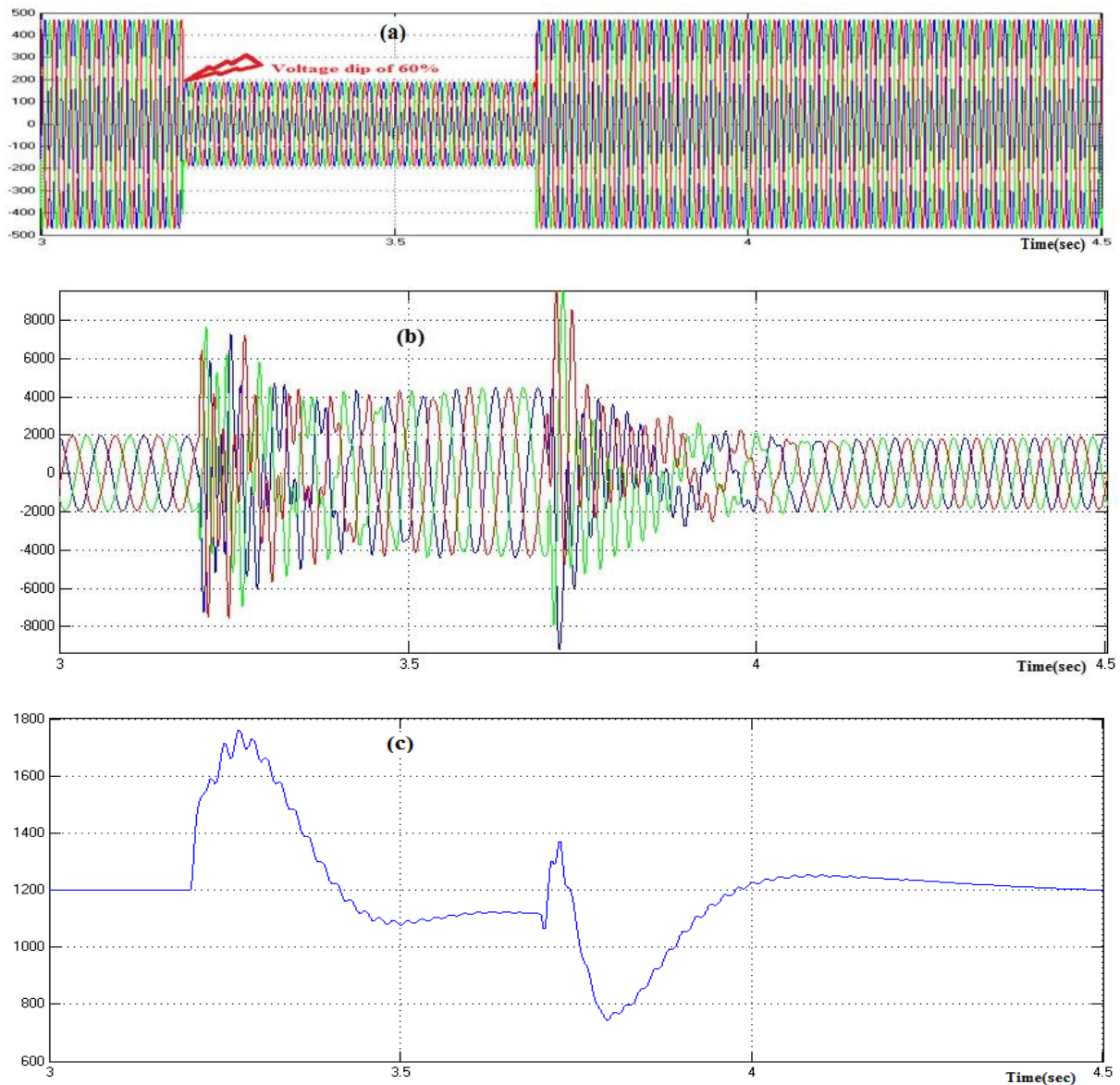


Figure: 6.8.(a)Grid voltage, (b)Rotor current, (c)DC bus voltage.

In this case 1, we have not provided any protection circuit during voltage dip of 60% for 500ms. Once the fault occur at $t=3.2s$ there is tremendous amount of rotor current which is almost four times of the rated current, this current will leads to damage the power converter in the rotor and also there is more ripple voltage in the DC bus. Thus, our aim is to reduce the peak initial current of the rotor during fault and that was implemented in the case 2.

CASE 2

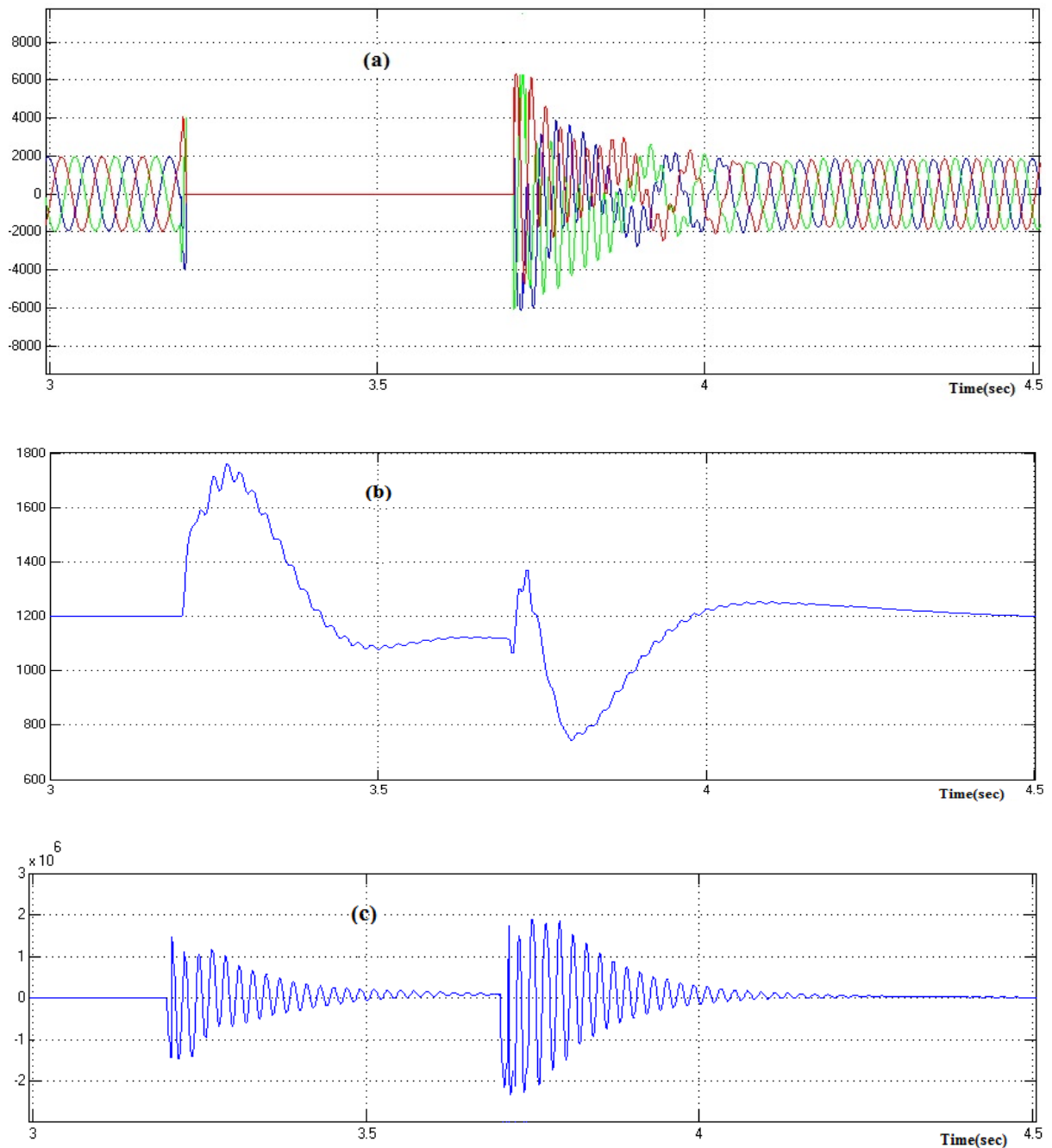
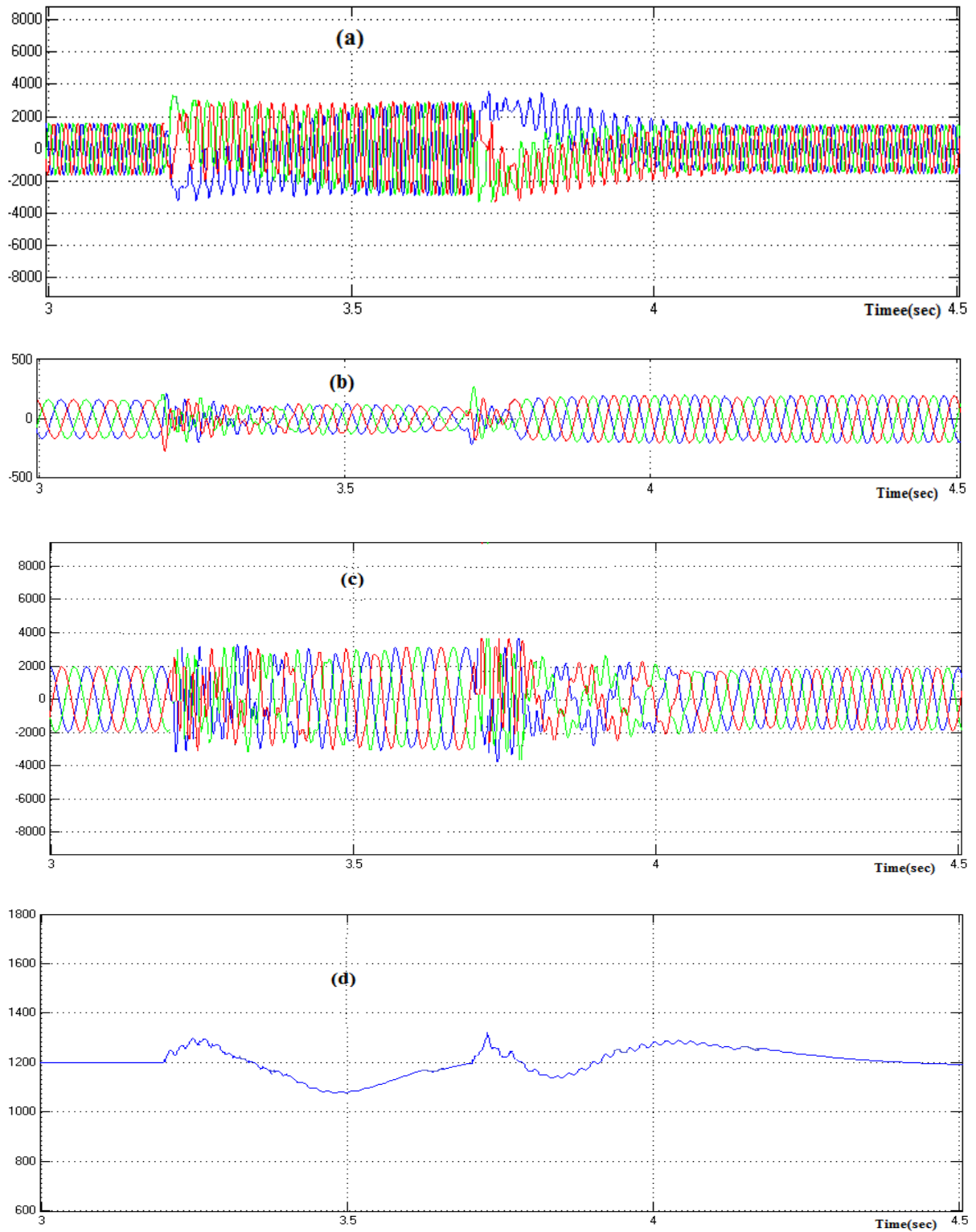


Figure: 6.9.(a)Rotor current, (b) DC bus voltage, (c)Stator Reactive Power.

In case 2, when the fault occur at $t=3.2s$, set the new reference values of i_{dr} and i_{qr} is equal to zero. Once the controller changed to new reference value, the rotor current decreases to zero for the whole period of fault as shown in Figure 6.9. This way we could reduce the high rotor current but it has disadvantage of absorbing reactive power from the network which deteriorate the stability of the weak grid. Also there will be ripple in DC bus voltage. Thus we have implemented a new control strategy which could overcome the entire disadvantage in case 1 and 2 and it would meet the grid codes requirement and it is discussed in case 3.

CASE 3

Figure 6.10 shows the simulated results of the LVRT operation of the DFIG with the proposed protection strategy. A grid voltage dip of 60% which has duration of 500ms is considered.



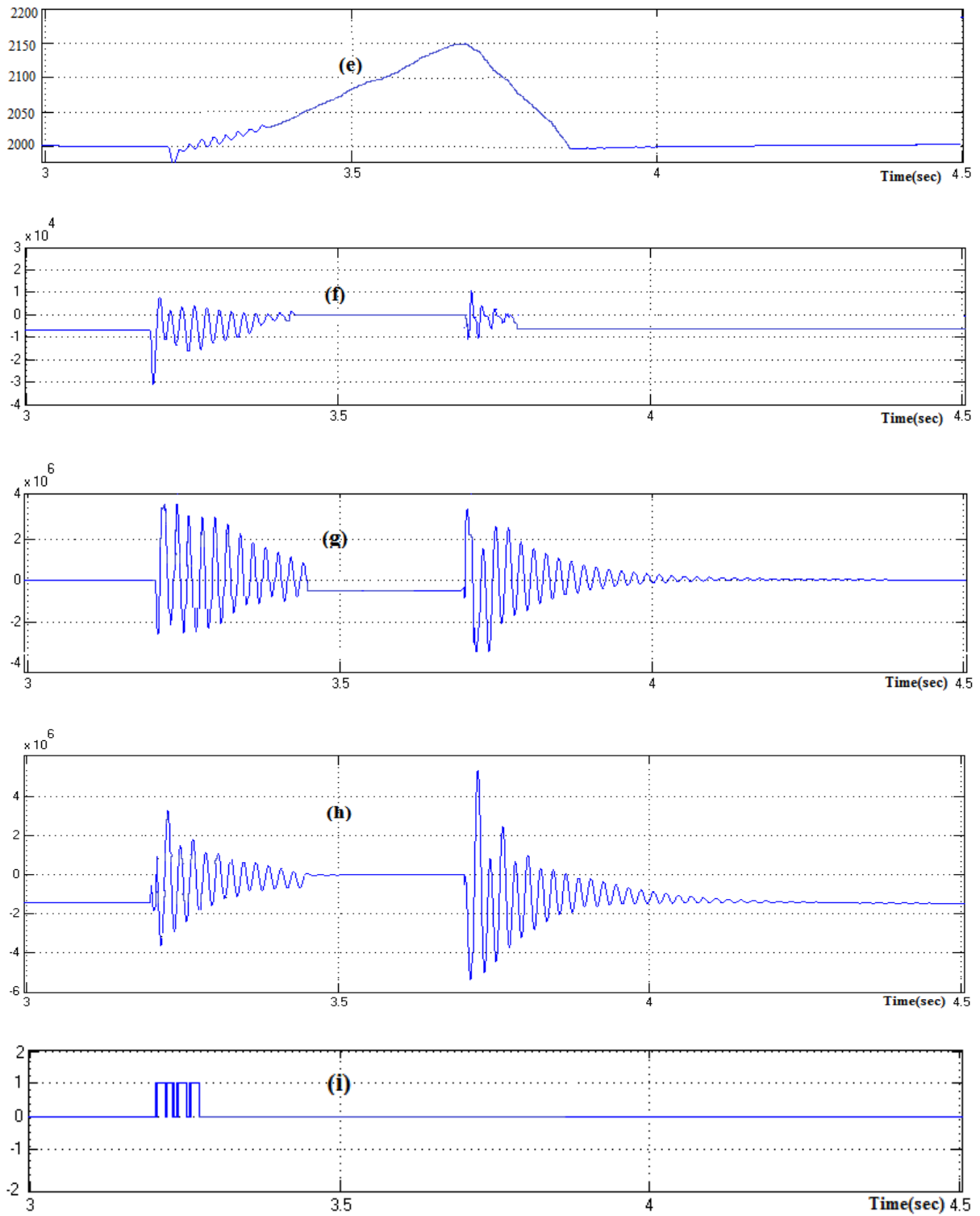


Figure:6.10.(a)Stator current, (b) Rotor voltage, (c)Rotor current, (d)DC bus voltage, (e)Electric speed, (f)Electric Torque, (g)Stator Reactive power, (h)Stator active power, (i) Crowbar signal.

As soon as the voltage at the wind turbine terminal drops at 3.2s, the demagnetization method is adopted, but the rotor current still exceeds the threshold value because of the limited capability of the power converter. Thanks to the crowbar protection, the rotor current decreases to the secure region rapidly. From Figure. 6.10(i), it is clear that crowbar only works for a few milliseconds, which means the DFIG is controllable for most of the time during the voltage dip.

Moreover, with the help of the demagnetization method, the crowbar does not need to be activated after the clearance of the fault, which means that the rotor side converter can control the DFIG to resume normal operation in less time. As we can see in Figure 6.10, about 0.2s after the grid voltage recovers, the DFIG can supply maximum active power captured from the wind again. When the voltage dips remains for a longer time, the generator is required to supply reactive power to help the grid voltage recovery. The proposed protection scheme can also offer the capability to supply reactive power during a voltage dip of 60% which has duration of 500ms.

From the Figure 6.10(c), we can see that immediately after the rotor current decreases to the secure region, the reactive power reference is changed to 0.5MVAR. The supplied reactive power is not as large as in normal grid condition due to the reduced grid voltage. As a result, in most time of the voltage dip, the DFIG can supply reactive power to the weak grid as shown in Figure 6.10(g), which will increase the grid voltage and help the grid recovery.

6.6 SUMMARY

This section is focused on the control strategy of a DFIG wind turbine system which equips with an active crowbar against severe grid faults. In order to reduce the activated time of the crowbar as much as possible, an improved hysteresis control strategy is proposed. Moreover, a simple demagnetization method is adopted to decrease the oscillations of the transient current both during the voltage dips and after the clearance of the faults. With the help of both control schemes, the DFIG is controllable for most of the time during voltage dips while the crowbar provides sufficient protection. As the crowbar is not required to provide a bypass for the potential high rotor current, the wind turbine can resume normal operation in a few hundred milliseconds after the fault is cleared. For longer time voltage dips, the DFIG can even supply reactive power to the weak grid during voltage dips to assist the voltage recovery. Simulation results show the enhanced low voltage ride through capability of the generator with the proposed technique. Future work will be done to improve the power quality of the WECS as well as supplying reactive power during grid faults.

To compensate the faulty line voltage, we have proposed a Dynamic Voltage Restorer (DVR) controller in existing DFIG wind turbine and the detailed working principle and control scheme are explained in the next section.

6.7 DYNAMIC VOLTAGE RESTORER (DVR)

The application of a dynamic voltage restorer (DVR) connected to a wind-turbine-driven doubly fed induction generator (DFIG) is investigated. The setup allows the wind turbine system an uninterrupted fault ride-through of voltage dips. The DVR can compensate the faulty line voltage, while the DFIG wind turbine can continue its nominal operation as demanded in actual grid codes. If an external power electronic device is used to compensate the faulty grid voltage, any protection method in the DFIG system can be left out. Such a system is introduced in [59-90] and is called a dynamic voltage restorer (DVR) that is a voltage source converter connected in series to the grid to correct faulty line voltages. The advantages of such an external protection device are thus the reduced complexity in the DFIG system. The disadvantages are the cost and complexity of the DVR. Note that a DVR can be used to protect already installed wind turbines that do not provide sufficient fault ride-through behavior or to protect any distributed load in a micro grid.

Different DVR topologies are compared with respect to rating in power and voltage in [77]. A medium-voltage DVR is described in [78]. Control structures based on resonant controllers to compensate unsymmetrical voltages are presented in [79] and [80]. A DVR is used to provide fault ride-through capability for a squirrel cage induction generator. A DVR to protect a DFIG wind turbine has been presented in [81], but only symmetrical voltage dips have been investigated in [82], but the reactive power is not considered and measurement results do not cover transient grid faults.

A DVR is a voltage source converter equipped with a line filter (usually LC type). Usually, a coupling transformer is used in series to the grid in order to correct deteriorated line voltages to reduce possible problems on a sensitive load or generator. Different transformer-based topologies are compared with respect to the number of hardware components, switching harmonics, dc-link control, and the ability to inject zero sequence voltages in [85]. Different system topologies are investigated in regard to the connection of the dc link and the rating in power and voltage in [77]. The rating of the DVR system depends mainly on the depth of the voltage fault that should be compensated.

For voltage sags or swells with zero-phase angle jump, the requirement of active power of the DVR is simply given by

$$P_{\text{DVR}} = \left(\frac{V_1 - V_2}{V_1} \right) P_{\text{load}} \quad (6.3)$$

6.7.1 CONTROL METHODS

The schematic diagram of DFIG wind turbine system with DVR as shown in Fig 6.11. The basic functions of a controller in a DVR are the detection of voltage sag/swell events in the system; computation of the correcting voltage, generation of trigger pulses to the sinusoidal PWM based DC-AC inverter, correction of any anomalies in the series voltage injection and termination of the trigger pulses when the event has passed. The controller may also be used to shift the DC-AC inverter into rectifier mode to charge the capacitors in the DC energy link in the absence of voltage sags/swells.

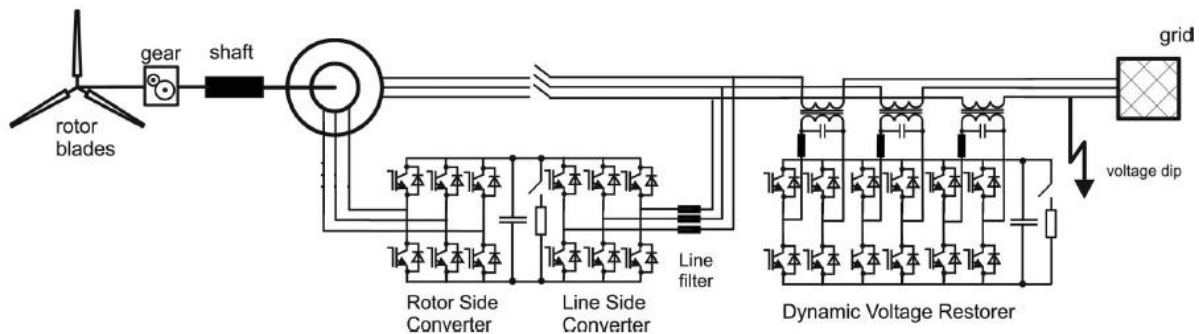


Figure: 6.11. Schematic diagram of DFIG wind turbine system with DVR.

The dqo transformation or Park's transformation is used to control of DVR. The dqo method gives the sag depth and phase shift information with start and end times. The quantities are expressed as the instantaneous space vectors. Firstly convert the voltage from a-b-c reference frame to d-q-o reference. For simplicity zero phase sequence components is ignored.

Figure 6.12 illustrates a flow chart of the feed forward dqo transformation for voltage sags/swells detection. The detection is carried out in each of the three phases. The control is based on the comparison of a voltage reference and the measured terminal voltage (V_a, V_b, V_c). The voltage sags is detected when the supply drops below 90% of the reference value whereas voltage swells is detected when supply voltage increases up to 25% of the reference value. The error signal is used as a modulation signal that allows generating a commutation pattern for the power switches (IGBT's) constituting the voltage source converter. The commutation pattern is generated by means of the sinusoidal pulse width modulation technique (SPWM); voltages are controlled through the modulation.

Flow chart of technique for DVR is illustrated in Figure 6.12. The Phase Locked Loop (PLL) circuit is used to generate a unit sinusoidal wave in phase with mains voltage.

$$\begin{bmatrix} V_d \\ V_q \\ V_o \end{bmatrix} = \begin{bmatrix} \cos(\theta) & \cos(\theta - \frac{2\pi}{3}) & 1 \\ -\sin(\theta) & -\sin(\theta - \frac{2\pi}{3}) & 1 \\ \frac{1}{2} & \frac{1}{2} & \frac{1}{2} \end{bmatrix} \begin{bmatrix} V_a \\ V_b \\ V_c \end{bmatrix} \quad (6.4)$$

Equation (6.4) defines the transformation from three phase system a, b, c to dqo stationary frame. In this transformation, phase A is aligned to the d-axis that is in quadrature with the q-axis. The theta (θ) is defined by the angle between phase A to the d-axis.

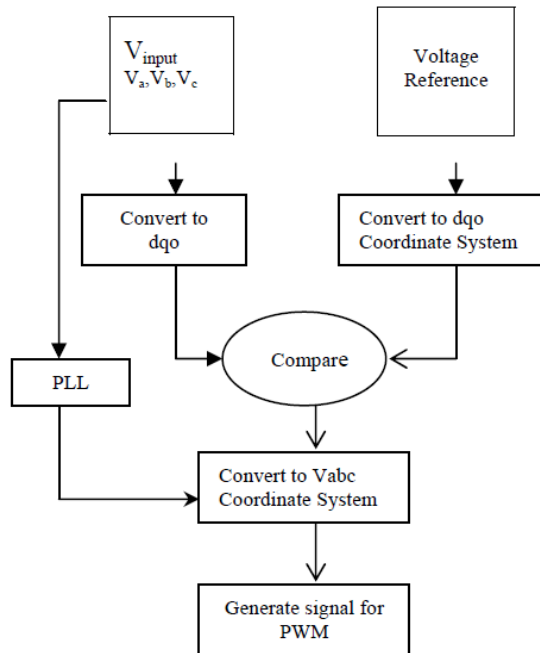


Figure 6.12. Flow chart of technique for DVR based on dqo transformation.

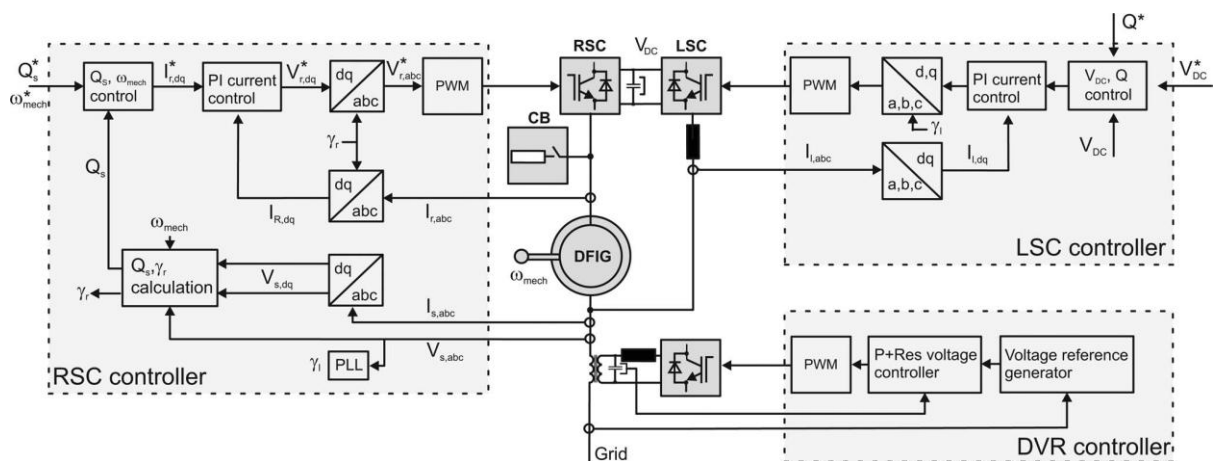


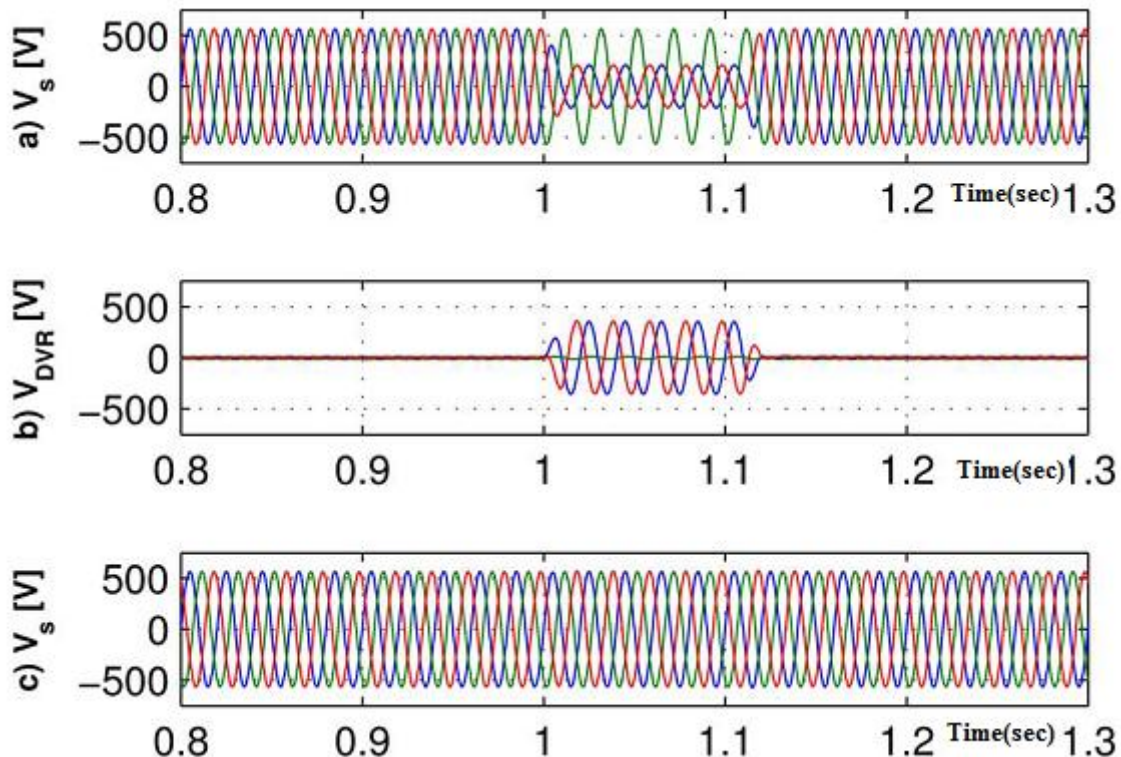
Figure 6.13. Schematic diagram of DFIG wind turbine and DVR control structure.

6.7.2 SIMULATION RESULTS

To show the effectiveness of the proposed technique, simulations have been performed using MATLAB /Simulink and PLECS for a 1.5MW DFIG wind turbine system and a DVR, as shown in Figure 6.11. The DVR simulation parameters are given in Annexure II. The control structure, as shown in Figure 6.13, is implemented in Simulink, while all power electronic components are modeled in PLECS.

The system performance of the DFIG protected by DVR during a two-phase 37 % voltage dip of 100 ms duration is shown in Figure 6.14 [see (a)]. The DFIG reacts with high stator currents I_s , and thus, high rotor currents are induced in the rotor circuit. When the wind turbine system is protected by the DVR, as shown in Figure 6.14, the voltage dip can almost be compensated [see Fig. 6.14(c)].

The DFIG response is much less critical, which means that lower stator over currents and rotor over currents are produced. Note that although the stator voltage dip is fairly well-compensated, a slight distortion in the stator currents (dc components), and thus, disturbed rotor currents can be observed. Anyway, the RSC remains in operation and can control stator active and reactive power independently. Thus, the speed is kept constant and a reactive power production ($Q_s = 0.5\text{Mvar}$) during grid fault as demanded in grid codes is performed. Note that a communication between DVR and DFIG is necessary. In Figure 6.14(h), the DVR power to compensate the voltage dip is shown. It becomes clear that the active and reactive power that cannot be fed into the faulty grid during grid fault must be consumed by the DVR.



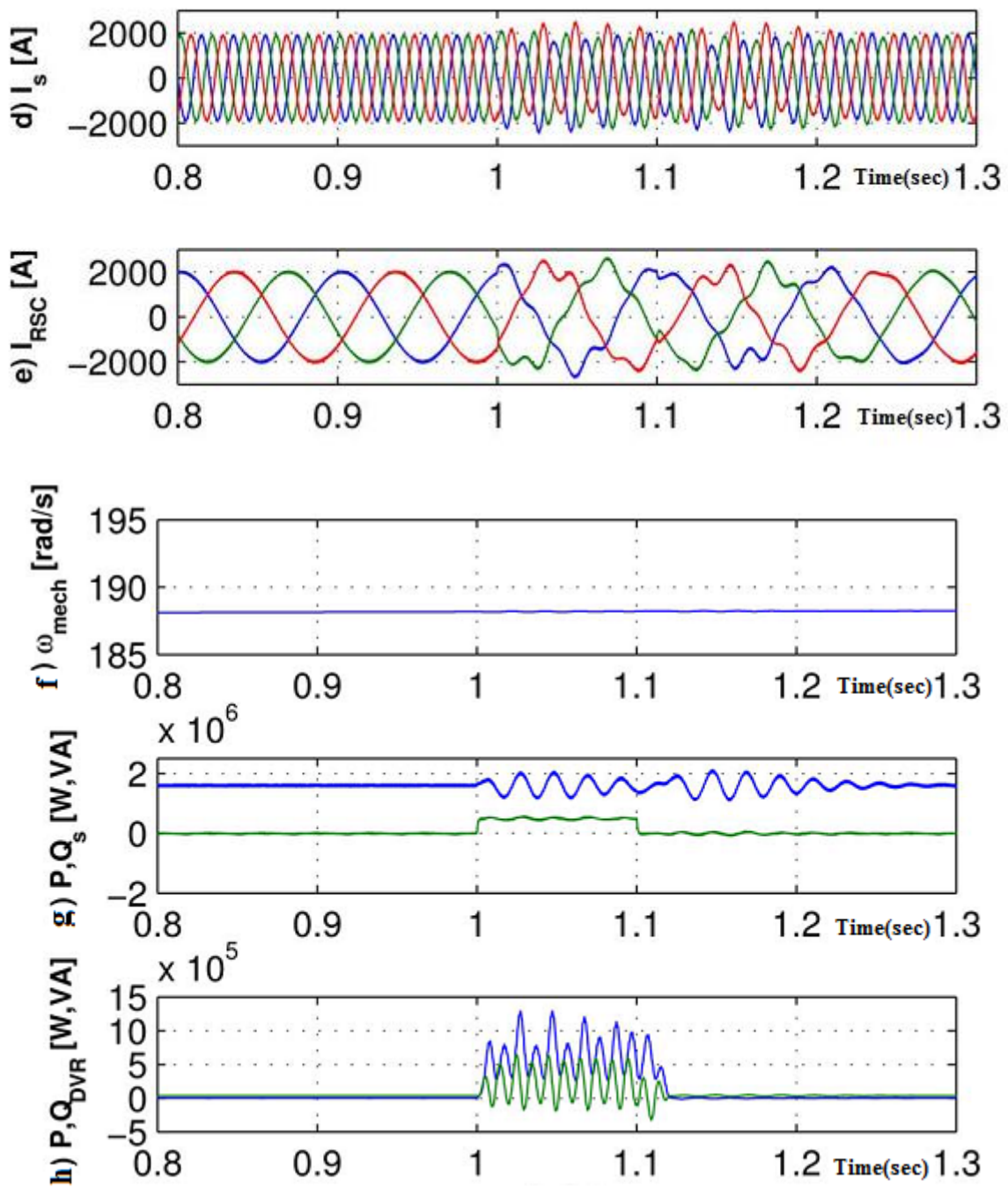


Figure:6.14.(a)Stator voltage, (b) DVR voltage, (c)Stator voltage, (d).Stator current, (e)Rotor current, (f)Mechanic speed, (g) Stator Reactive power, Stator active power, (h)DVR power.

6.7.3 MEASUREMENT RESULTS

Measurement results are taken at a 22 kW test bench and a 30 kVA DVR connected in series to the grid. The schematic diagram of the laboratory setup is similar to the one shown in Figure 6.12. The DVR converter is based on three single-phase full bridge voltage source converters using a common DC link. The DC link is charged with a passive six-pulse diode bridge and protected by a dc chopper. The DFIG is driven by an industrial 18.5 kW induction machine drive to emulate the Fig. 6.15 Measurement results for DFIG with DVR protection: (a) line voltages, (b) DVR voltages, (c) stator voltages, (d) stator currents, and (e) rotor currents. The two-phase 37 % grid voltage dip (from 330 to 125 V) of 100 ms duration is generated by a transformer-based voltage sag generator, as described in [84-87].

In all laboratory tests, the grid voltage level has been lowered to 330 V (line to line) by a separate transformer to avoid saturation problems in the series-connected transformers of the DVR. The results have been recorded with a Dewetron data acquisition device. For DFIG with DVR test, the DFIG is operated super synchronous with a slip of $s = -0.2$ (mechanical speed of 1800 r/min), feeding an active stator power of $P_s = 10\text{kW}$ to the grid.

Thus, the DVR must be designed to handle these currents and the LSC control should be designed to create no transients, which is not focused here. At nominal operation, the DVR does not compensate the line voltage. The DVR voltages are only slightly distorted by the grid voltage harmonics of the laboratory grid. When the voltage dip occurs, the DVR compensates the missing voltage in the two phases [see Figure 6.15(b)] so that the stator voltage [see Figure 6.15(c)] is only slightly affected by the voltage dip. No mentionary over currents are generated in the stator or rotor currents and the DFIG can continue directly its nominal operation feeding active power. The laboratory test setup is shown in Figure 6.16(b) and the implementation is existing in the real time application and it is shown in figure 6.16(a). Note that in the laboratory, the generator is always operated at unity power factor. For a reactive power production, according to the grid codes, a communication between DVR and DFIG would be necessary. The simulation and measurement results show a very similar behavior. The results of this investigation show that the DVR can fully protect the DFIG system from asymmetrical grid voltage faults to allow uninterruptible low-voltage ride-through. One can conclude that the DVR can compensate voltage dips and swells of symmetrical and asymmetrical nature to allow a low- or high voltage ride-through for any distributed load.

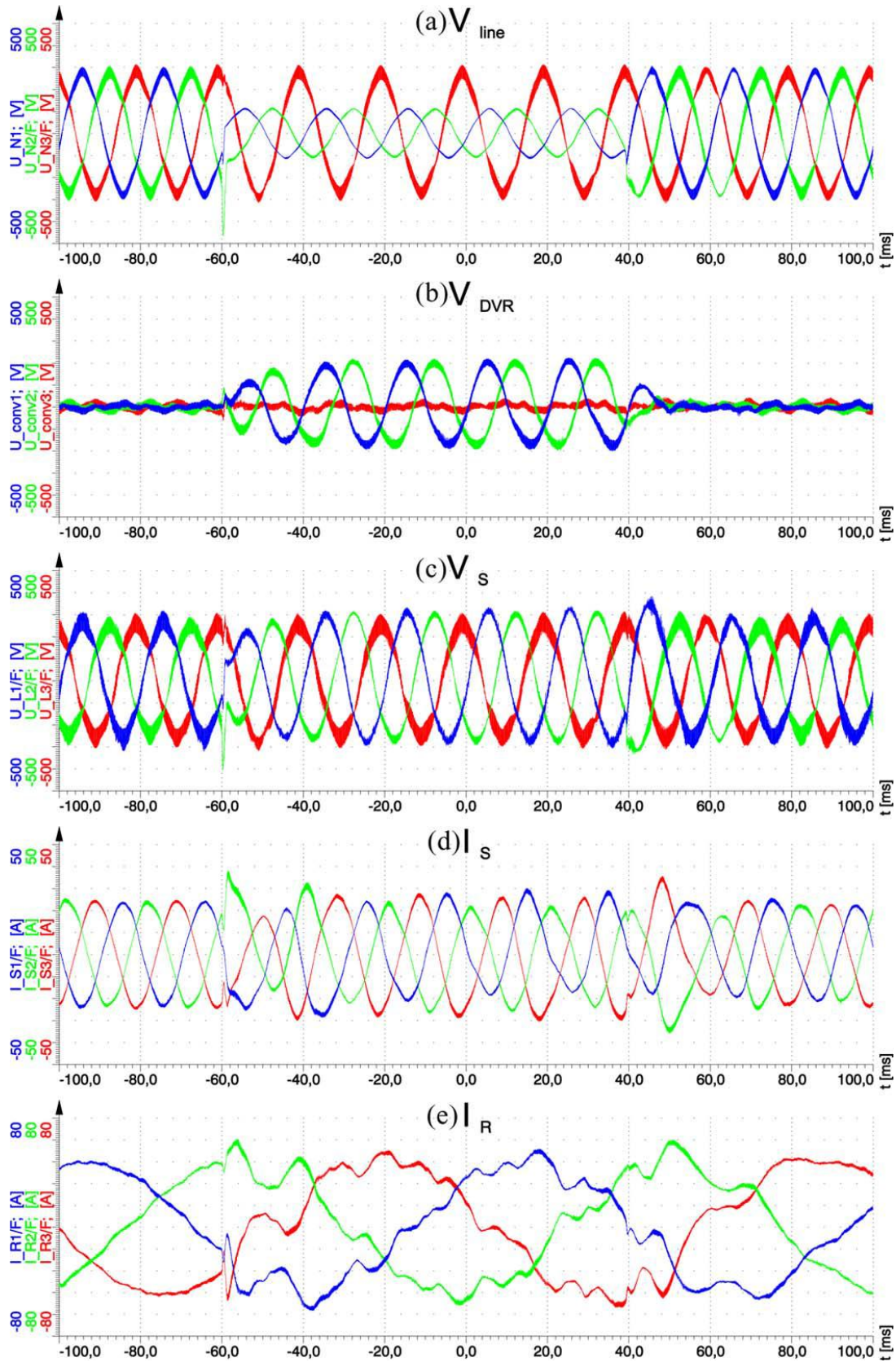


Figure: 6.15. Measurement results for DFIG with DVR protection: (a) line voltages, (b) DVR voltages, (c) stator voltages, (d) stator currents, and (e) rotor currents.

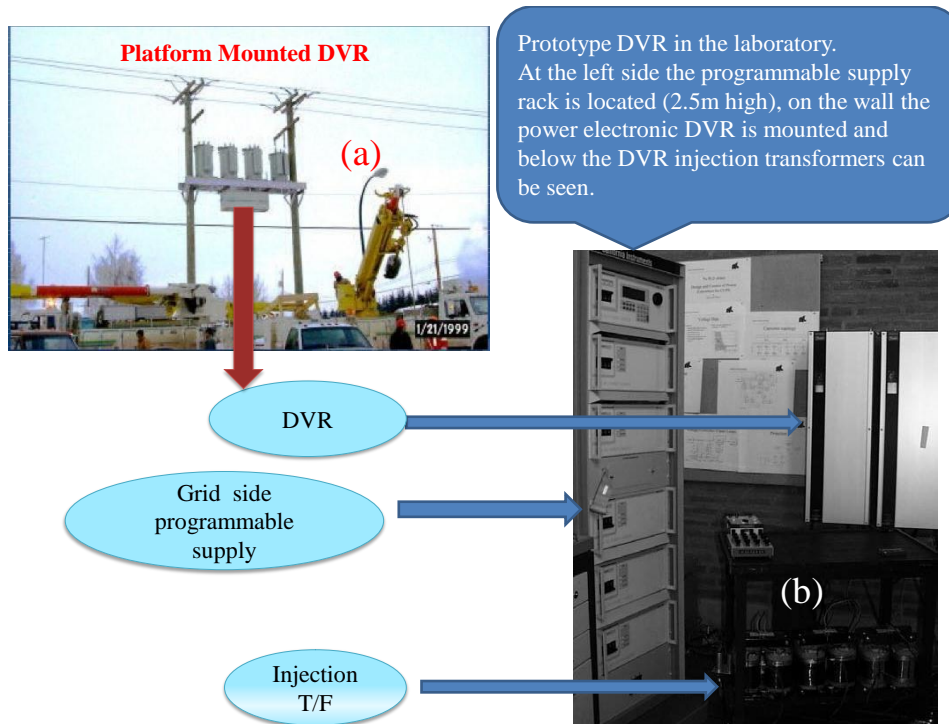


Figure: 6.15. (a) real time application exist in the transmission line. (b) Measurement setup for DFIG with DVR protection.

6.7.4 SUMMARY

The application of a DVR connected to a wind-turbine-driven DFIG to allow uninterrupted fault ride-through of grid voltage faults is investigated. The DVR can compensate the faulty line voltage, while the DFIG wind turbine can continue its nominal operation and fulfill any grid code requirement without the need for additional protection methods. The DVR can be used to protect already installed wind turbines that do not provide sufficient fault ride-through behavior or to protect any distributed load in a micro grid. Simulation results for a 1.5 MW wind turbine under an asymmetrical two-phase grid fault show the effectiveness of the proposed technique in comparison to the low-voltage ride through of the DFIG using a crowbar where continuous reactive power production is problematic. Measurement results under transient grid voltage dips on a 22 kW laboratory setup are presented to verify the results.

To improve the DFIG wind turbine performance during unbalanced grid condition, we have proposed Vector Proportional Integral (VPI) controller and it is briefly discussed with simulation results in the next section.

6.8 VECTOR PROPORTIONAL INTEGRAL (VPI) CONTROLLER

Vector Proportional Integral controller improves the dynamic performance of doubly fed induction generator-based wind turbine with the current increase in wind power penetration into the energy market, control and operation of wind turbine generators becomes a major research topic. Wind turbine based on doubly fed induction generator (DFIG), which is sensitive to grid disturbances, is widely used. Under an unbalanced grid voltage condition, oscillations of the DFIG's electromagnetic torque and instantaneous stator powers strongly affect the dynamic performance of the DFIG.

In this study, a new configuration based on vector proportional–integral (VPI) controller is proposed to eliminate such oscillations. This new configuration is employed in the rotor side converter (RSC) of the DFIG. With the proposed VPI control strategy, decomposition of sequential components and mathematical complexity are reduced. Compared with the conventional field oriented control based on the standard single PI controller, the VPI controller can successfully eliminate torque and stator power oscillations. The effectiveness of the proposed control strategy is validated through simulation results obtained on a 1.5 MW DFIG-based wind turbine system model built in MATLAB/Simulink.

6.8.1 DYNAMIC BEHAVIOUR OF THE DFIG SYSTEM

Various configurations have been used to model the DFIG's equivalent circuit. For the purpose of this work, a synchronously rotating reference frame with stator voltage fixed to the d-axis is adopted. Figure 6.16 shows the schematic diagram of the DFIG wind turbine system, whereas Figure 6.17 represents its equivalent circuit diagram in the synchronous dq frame.

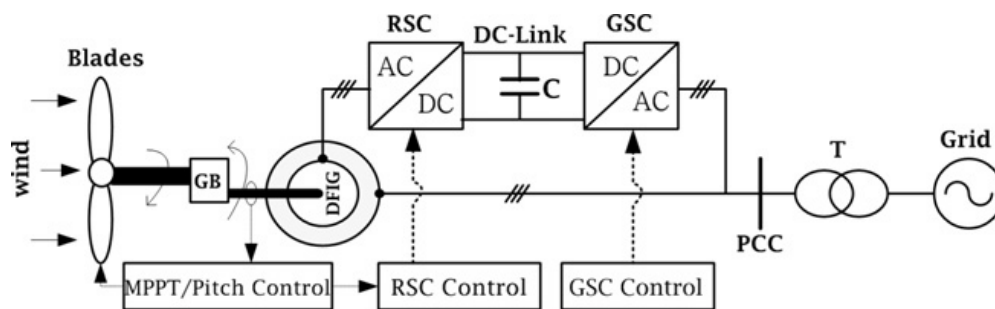


Figure: 6.16. Schematic diagram of the DFIG wind turbine system.

With reference to Figure 6.17, the stator and rotor voltages as well as the flux vector quantities are given below.

$$\begin{aligned}
 V_{sdq} &= R_s I_{sdq} + \frac{d\psi_{sdq}}{dt} + j\omega_s \psi_{sdq} \\
 V_{rdq} &= R_r I_{rdq} + \frac{d\psi_{rdq}}{dt} + j(\omega_s - \omega_r) \psi_{rdq}
 \end{aligned}
 \tag{6.5}$$

$$\begin{aligned}\Psi_{sdq} &= L_s I_{sdq} + L_m I_{rdq} \\ \Psi_{rdq} &= L_r I_{rdq} + L_m I_{sdq}\end{aligned}\quad (6.6)$$

where $L_s = L_{\sigma s} + L_m$ and $L_r = L_{\sigma r} + L_m$. The subscripts 's', 'r' and 'm' stand for the stator, rotor and magnetising, respectively. V , I and ψ represent the voltage, current and flux space vector quantities, respectively. R and L are resistance and inductance, respectively, whereas ω_s and ω_r stand for the synchronous and rotor speed, respectively. Leakage inductances are represented by L_{σ} .

During normal operation, only the positive sequence quantities are applicable and all the negative sequence variables are zero. However, under an unbalanced condition the negative sequence component exists in the flux, voltage and current vectors. As a result, these quantities contain the positive and negative sequence components. The study of the DFIG under unbalanced voltage condition has been presented in [91-102].

Consider a DFIG model based on stator voltage orientation in positive dq frame with positive d -axis aligned with stator voltage V_s . Figure 6.18 illustrates the spatial relationship between the stationary ($\alpha\beta$) and the rotating dq frames under an unbalanced condition. The positive $(dq)^+$ and negative $(dq)^-$ synchronous frames rotate at ω_s and $-\omega_s$, respectively. On the other hand, the vector V represents the DFIG's voltage vector quantity. Flux and current vectors can also be defined in the same fashion as V . The transformation between positive and negative dq frames for vector V is given below.

$$\begin{aligned}V_{sdq}^+ &= V_{sdq}^- e^{-j2\omega_s t}, V_{sdq}^- = V_{sdq}^+ e^{j2\omega_s t} \\ V_{sdq}^+ &= V_{sdq+}^+ + V_{sdq-}^+ = V_{sdq+}^+ + V_{sdq-}^- e^{-j2\omega_s t}\end{aligned}\quad (6.7)$$

where the subscripts + and - represent positive and negative sequence components, respectively. Similarly, the superscripts + and - correspond to positive and negative reference frames.

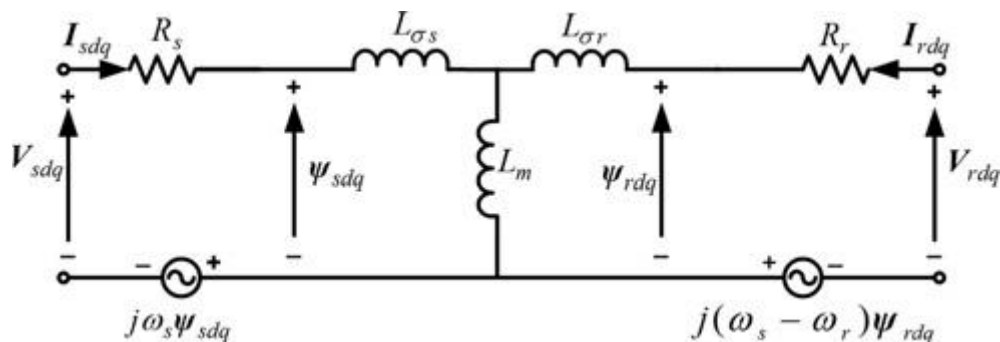


Figure: 6.17. Equivalent circuit diagram of the DFIG in dq synchronous frame.

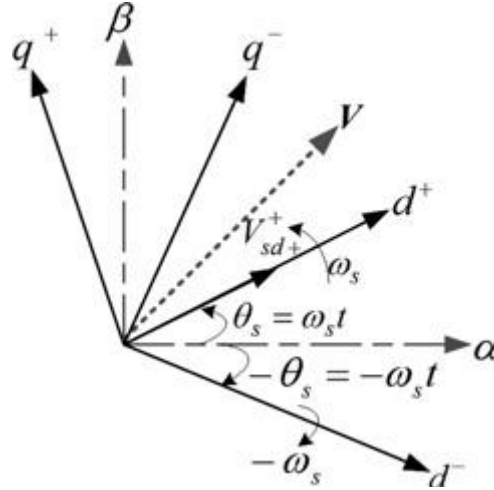


Figure: 6.18. Vector diagram representing the stationary (ab), positive (dq)⁺ and negative (dq)⁻ synchronous rotating reference frames.

As described in (6.7) above, the negative components oscillate at twice the grid frequency ($2\omega_s$) in synchronous dq frame while the positive components are realised as dc quantities. A negative sequence component causes fluctuations in the instantaneous stator powers. At this point, stator voltage and current are formed as addition of two space vectors that rotate in the opposite sense at grid frequency. Hence, the stator active and reactive powers can be expressed as follows.

$$\begin{aligned}
 P_s &= \frac{3}{2} \text{Re}[V_{sdq}^+ \times I_{sdq}^{\wedge+}] \\
 P_s &= \frac{3}{2} \text{Re}[(V_{sdq+}^+ e^{j\omega_s t} + V_{sdq-}^- e^{-j\omega_s t}) \times (I_{sdq+}^+ e^{j\omega_s t} + I_{sdq-}^- e^{-j\omega_s t})^{\wedge}] \\
 Q_s &= \frac{3}{2} \text{Im}[V_{sdq}^+ \times I_{sdq}^{\wedge+}] \\
 Q_s &= \frac{3}{2} \text{Im}[(V_{sdq+}^+ e^{j\omega_s t} + V_{sdq-}^- e^{-j\omega_s t}) \times (I_{sdq+}^+ e^{j\omega_s t} + I_{sdq-}^- e^{-j\omega_s t})^{\wedge}]
 \end{aligned} \tag{6.8}$$

where the superscript \wedge represents a conjugate of a given complex number.

By proper manipulation of (6.8), the following expression can be obtained.

$$\begin{aligned}
 P_s &= \frac{3}{2} \text{Re}[(V_{sdq+}^+ \times I_{sdq+}^{\wedge+}) + (V_{sdq-}^- \times I_{sdq-}^{\wedge-}) + (V_{sdq+}^+ \times I_{sdq-}^{\wedge-} e^{j2\omega_s t}) + (V_{sdq-}^- \times I_{sdq+}^{\wedge+} e^{-j2\omega_s t})] \\
 Q_s &= \frac{3}{2} \text{Im}[(V_{sdq+}^+ \times I_{sdq+}^{\wedge+}) + (V_{sdq-}^- \times I_{sdq-}^{\wedge-}) + (V_{sdq+}^+ \times I_{sdq-}^{\wedge-} e^{j2\omega_s t}) + (V_{sdq-}^- \times I_{sdq+}^{\wedge+} e^{-j2\omega_s t})]
 \end{aligned} \tag{6.9}$$

It can be seen that the first two terms of (6.9) give steady-state active and reactive stator powers, whereas the last two terms introduce pulsation of twice the grid frequency ($2\omega_s$). Similarly, the same fluctuations are manifested in the electromagnetic torque. If the shaft of the DFIG wind turbine has any resonance near twice the grid frequency, these oscillations

can cause vibrations and mechanical stresses in the rotor assembly. The torque expression can be given as

$$T_{em} = \frac{3}{2} \rho \text{Im}[\psi_{sdq}^{\wedge+} \times I_{sdq}^+] \quad (6.10)$$

Actually, these pulsating terms are the major problems for the DFIG's performance. In order to have a smooth operation these terms must be eliminated. With this purpose at hand, a dual current control of the DFIG using a standard PI controller has been presented to regulate the four current components of GSC [96] and RSC [97]. However, the negative and positive sequence extraction involved in the vector control scheme not only deteriorates the dynamic performance of the DFIG but also introduces mathematical complexity, making the control design cumbersome.

6.8.2 VPI CONTROLLER SYNTHESIS

The standard PI regulator is mostly used in control of ac machines. When a linear PI is used in the synchronous frame, it undesirably introduces significant amplitude droop and phase lag, that is to say, the actual signal produced does not precisely track its reference. This is due to the fact that it gives infinite gain only at dc level (i.e. 0 Hz) with relatively low gain realised at the commanded frequency. To increase the tracking capability of the PI controller, a control philosophy often used for a three-phase system is to transform the control variables to the synchronous rotating dq frame at the desired synchronous frequency ω_s . Consequently, the frame transformation shifts the control variables and their references towards the left of the frequency spectrum by the same synchronous frequency. In this case, the PI controller can provide zero steady-state error between the tracking and reference signals. Nevertheless, as the synchronous frequency increases, the PI regulator performance is degraded. Definitely, regulating the stator powers and torque pulsations characterised by higher frequency compared with the synchronous frequency requires a precise controller together with reduced computational burdens. Hence, a new VPI controller is proposed to outweigh the capability of the standard PI controller.

The VPI can be derived from the conventional PI controller and the basic open-loop transfer function is given by (6.11) [100-102]. As stated earlier under an unbalanced condition, the electro-magnetic torque and stator powers oscillate at twice the grid frequency (100 Hz) and therefore the controller is tuned at $2\omega_s$ to give infinite gain at this frequency.

$$G_{PI} = \frac{K_P s + (K_i + j2\omega_s K_P)}{s} \quad (6.11)$$

For regulating both positive and negative sequence, GPI in (6.11) can be transformed to the stationary reference frame by taking appropriate frequency shift and becomes G_{PI}^+ for positive sequence components and G_{PI}^- for negative sequence components.

$$G_{PI+} = \frac{K_p s + K_i}{s - j2\omega_s} \quad (6.12)$$

$$G_{PI-} = \frac{K_p s + K_i}{s + j2\omega_s}$$

In order to simultaneously control both negative and positive sequence components, G_{PI+} and G_{PI-} are superposed to give, $G_{VPI}(s)$ which is given in (6.13)

$$G_{VPI}(s) = G_{PI+} + G_{PI-} = 2 \frac{K_p s^2 + K_i s}{s^2 + (2\omega_s)^2} \quad (6.13)$$

where K_i and K_p are $G_{VPI}(s)$ controller gains.

Remark: This remark describes how to determine the values of controller gains (K_p and K_i). These controller gains are selected based on the pole-zero cancellation and second order band-pass filter design techniques [93]. To this end, the controller ‘zero’ is designed to cancel the plant ‘pole’. A closed-loop transfer function using Vector PI $G_{VPI}(s)$ can be expressed as follows

$$H(s) = \frac{G_{VPI}(s)F(s)}{1 + G_{VPI}(s)F(s)} \quad (6.14)$$

where $F(s)$ is the DFIG plant model, derived from (1) and (2) in the positive dq synchronous frame.

$$F(s) = \frac{1}{s\sigma L_r + R_r} \quad (6.15)$$

where σ is the leakage factor, $\sigma=1-L_m^2/L_s L_r$.

Based on (6.15) the closed-loop $H(s)$ may now be expanded to (6.16)

$$H(s) = \frac{K_p s^2 + K_i s}{(\sigma L_r) s^3 + (R_r + 2K_p) s^2 + ((2\omega_s)^2 \sigma L_r + 2K_i) s + ((2\omega_s)^2 R_r)} \quad (6.16)$$

When the DFIG plant ‘pole’ depicted in (6.15) is cancelled by the controller ‘zero’ in (6.13), the resulting closed-loop transfer function $H_c(s)$ resembles that of a standard second-order band pass filter whose centre frequency is $2\omega_s$. In this case, the controller time constant can be obtained as $K_p/K_i = \sigma L_r / R_r$, and all the symbols retain their original definition.

$$H_c(s) = \frac{2K_p s}{(\sigma L_r) s^2 + 2K_p s + (2\omega_s)^2 \sigma L_r} \quad (6.17)$$

From (6.17) the band-pass filter parameters, quality factor (Q) or band-width (BW) can be used to determine the values of the controller gains. With this purpose at hand, the quality factor Q is used to decide the K_p values which control controller selectivity. Smaller the values selected for K_p , more selective controller response.

$$K_p = \frac{(2\omega_s)\sigma L_r}{2Q}, K_i = K_p \frac{R_r}{\sigma L_r} \tag{6.18}$$

K_p is favoured by selecting $Q > 1/2$ and $K_p > 0$ to maintain a good response and stability margin. A frequency response of the closed-loop $H(s)$ was realised with $K_p = 0.18$ and $K_i = 50$. The overall control methodology is presented in Figure 6.19 below.

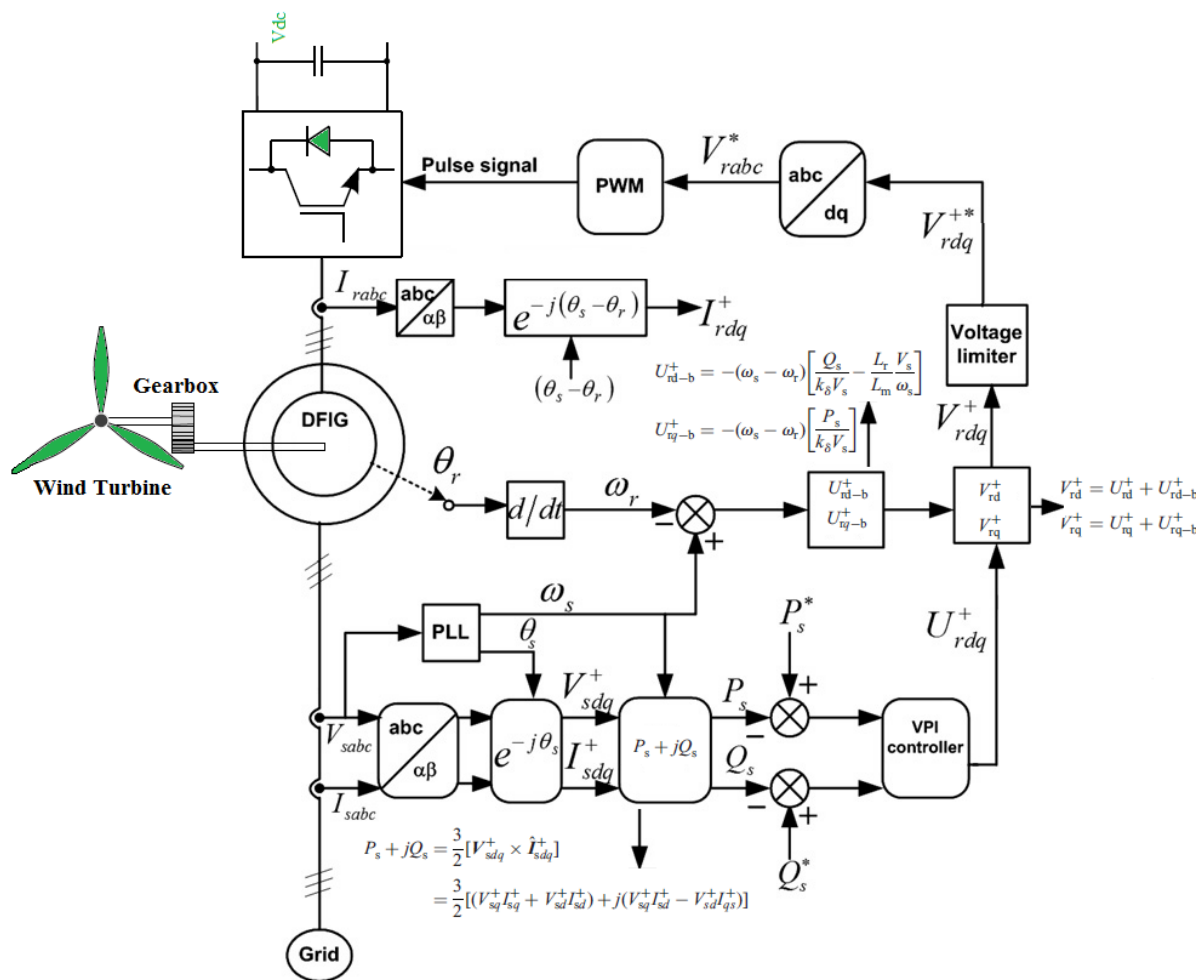


Figure: 6.19. Schematic diagram of the proposed VPI control scheme.

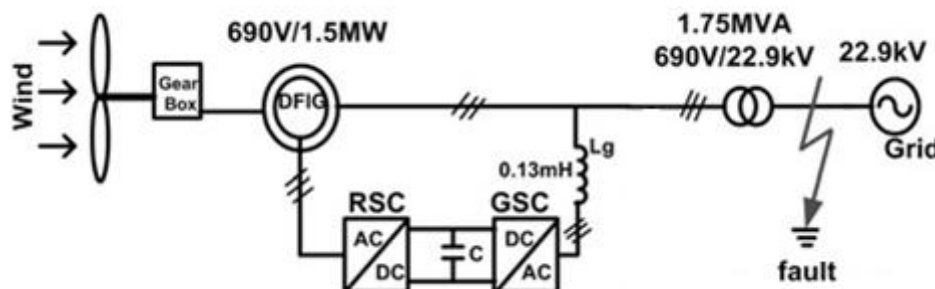


Figure: 6.20. Schematic diagram of the tested system.

6.8.3 SIMULATION RESULTS

Simulations of the proposed control scheme for the DFIG based wind turbine system were performed using a MATLAB/Simulink platform. The schematic diagram of the tested system is shown in Figure 6.20. A single line to ground fault applied on phase ‘a’ was used to create a voltage unbalanced condition in the network at 3.4 s. The voltage unbalance factor during simulation was 20%.

CASE 1

Single phase fault with conventional controller(20% of 1phase unbalanced grid condition)

In Figure 6.21, shows that there are severe oscillations on both electromagnetic torque and stator active/reactive powers. Similarly, the stator voltage and current are highly unbalanced. In this case, the conventional field-oriented control for the DFIG using a standard single PI controller was employed to control the DFIG under an unbalanced grid voltage condition. Nevertheless, the control strategy failed to regulate or eliminate the electromagnetic or stator power pulsations.

This is due to the fact that a negative component introduced by unbalanced stator voltage in the stator flux and current vectors was not controlled to zero. In that context, interaction of these components in the machine creates motoring and generating behaviour resulting in serious oscillation.

At this point, a constant torque and power operation is not achieved. This proves that the standard PI controller has no features, which can make it capable of controlling the torque and stator power oscillations.

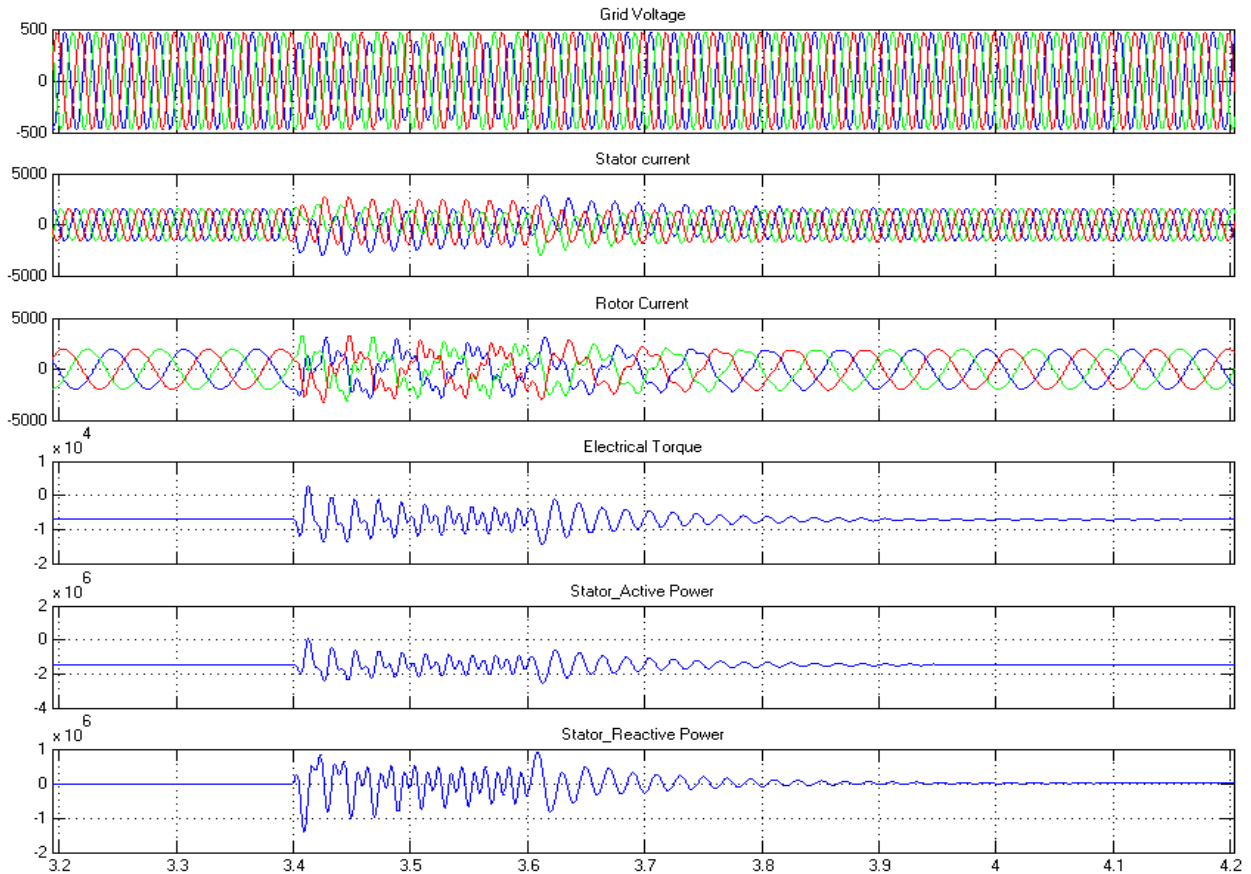


Fig: 6.21.Single phase fault with conventional controller (20% of 1phase unbalanced grid condition).

Figure 6.22 unveil the simulation results when a new controller is applied with two cases, based on power reference generation as detailed in Section 6.8.2. It is observed in Figure 6.22 that, when the proposed scheme is applied with the stator active power P_s and reactive power Q_s selected as illustrated in (6.8) and (6.9), the stator active and reactive powers pulsations are simultaneously eliminated; thanks to the new VPI controller which instantly controlled both positive and negative sequence components generated during network unbalance. In this case, the electromagnetic torque oscillations are still not yet controlled to zero although there are some improvements compared. Rotor current harmonics have also been reduced. This is due to the fact that generated power reference is not precise for torque oscillations cancellation. To be more precise, the torque and stator power oscillations cannot simultaneously be eliminated under this scheme.

Improved DFIG Performance by Single phase fault with VPI controller

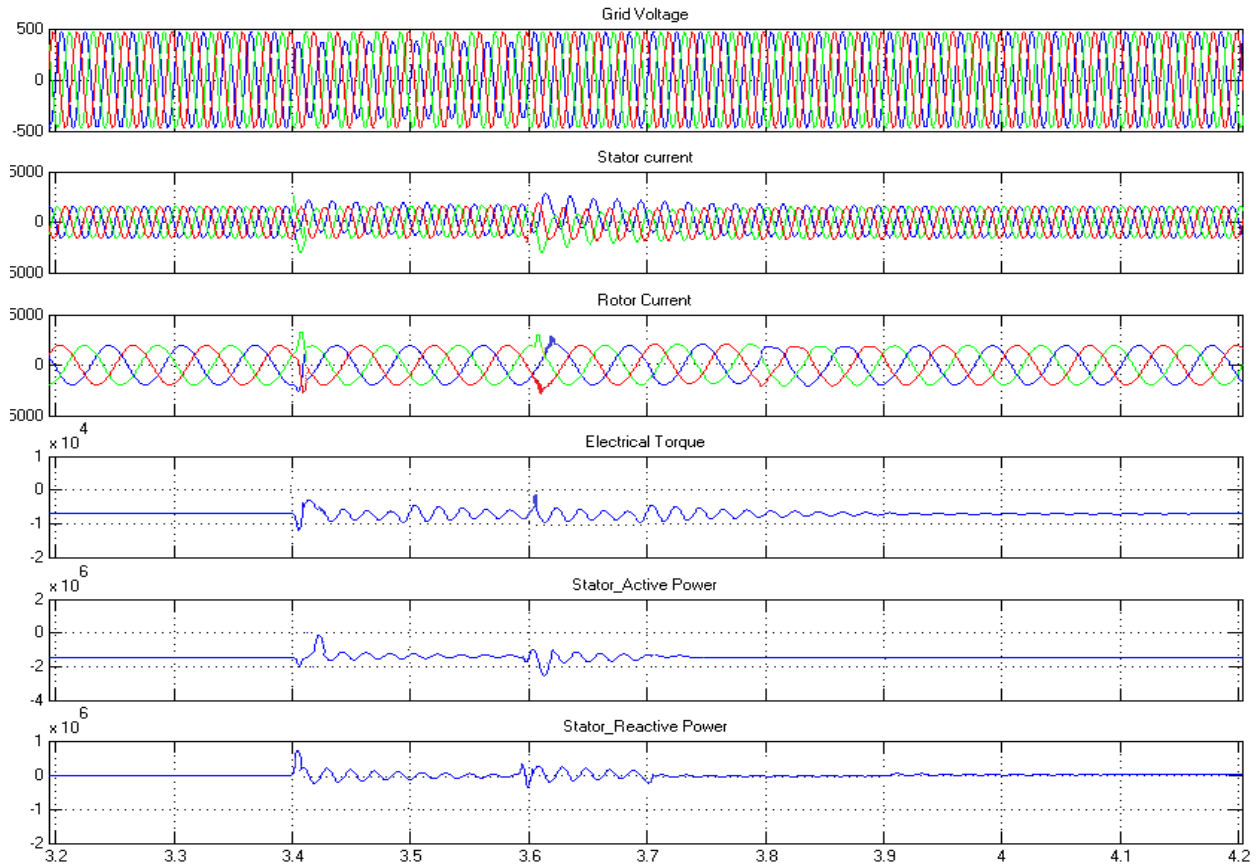


Figure: 6.22.Improved DFIG Performance by Single phase fault with VPI controller.

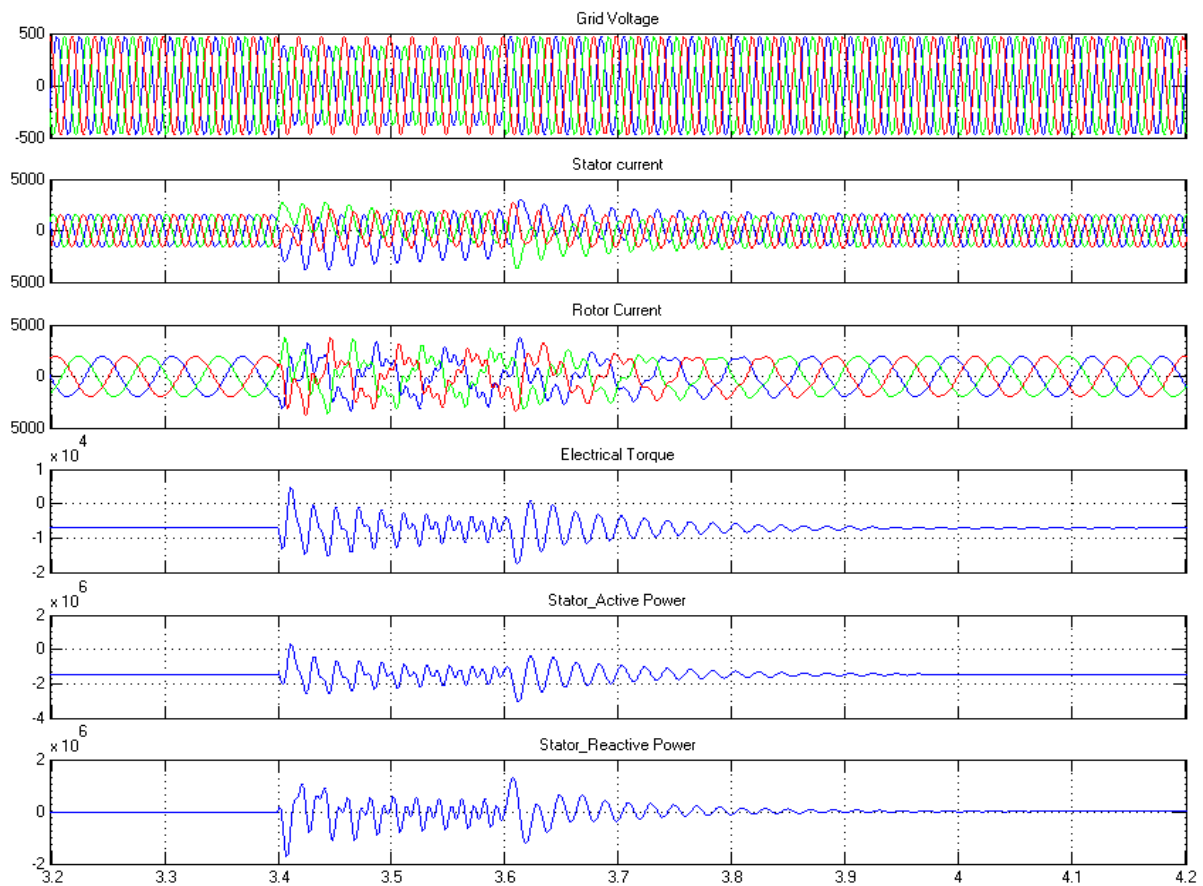
CASE 2

Single phase fault with conventional controller(20% of 2 phase unbalanced grid condition)

In Figure 6.23, shows that there are severe oscillations on both electromagnetic torque and stator active/reactive powers. Similarly, the stator voltage and current are highly unbalanced. In this case, the conventional field-oriented control for the DFIG using a standard single PI controller was employed to control the DFIG under an unbalanced grid voltage condition. Nevertheless, the control strategy failed to regulate or eliminate the electromagnetic or stator power pulsations.

This is due to the fact that a negative component introduced by unbalanced stator voltage in the stator flux and current vectors was not controlled to zero. In that context, interaction of these components in the machine creates motoring and generating behaviour resulting in serious oscillation.

At this point, a constant torque and power operation is not achieved. This proves that the standard PI controller has no features, which can make it capable of controlling the torque and stator power oscillations.



Figur: 6.23.Single phase fault with conventional controller (20% of 2phase unbalanced grid condition).

Figure 6.24 unveil the simulation results when a new controller is applied with two cases, based on power reference generation as detailed in Section 6.8.2. It is observed in Figure 6.24 that, when the proposed scheme is applied with the stator active power P_s and reactive power Q_s selected as illustrated in (6.8) and (6.9), the stator active and reactive powers pulsations are simultaneously eliminated; thanks to the new VPI controller which instantly controlled both positive and negative sequence components generated during network unbalance.

In this case, the electromagnetic torque oscillations are still not yet controlled to zero although there are some improvements compared. Rotor current harmonics have also been reduced. This is due to the fact that generated power reference is not precise for torque oscillations cancellation. To be more precise, the torque and stator power oscillations cannot simultaneously be eliminated under this scheme.

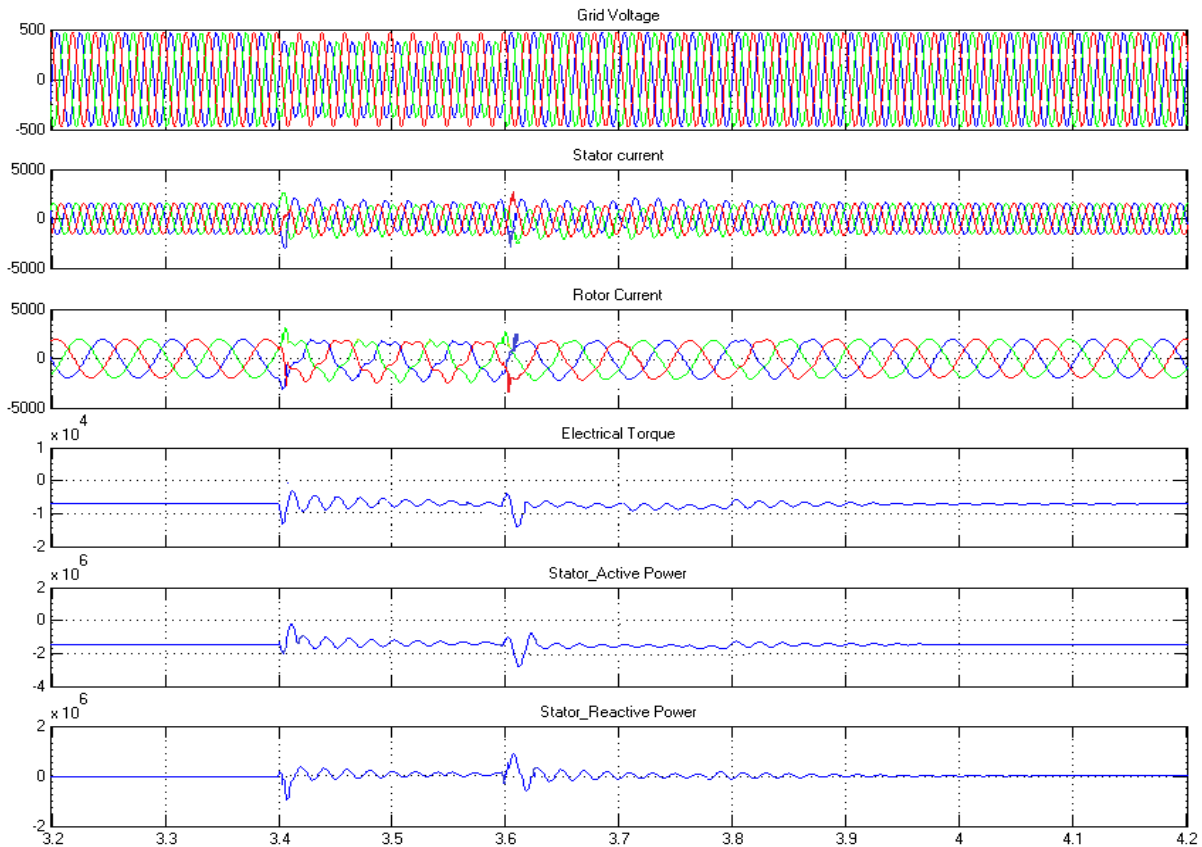


Figure: 6.24.Improved DFIG Performance by Single phase fault with VPI controller.

6.8.4 SUMMARY

This section has proposed a new control strategy of DFIG based wind turbine system to enhance its operation under an unbalanced grid voltage condition. Dynamic behaviour of the DFIG under an unbalanced condition was also investigated in this work. RSC of the DFIG system was controlled to eliminate the electromagnetic torque and stator power oscillations. A new VPI controller in positive synchronous rotating frame was proposed for controlling the RSC of the DFIG under an unbalanced network condition.

The experimental test of DFIG wind turbine under unbalanced grid condition has described in the next section.

6.9 HARDWARE IMPLEMENTATION AND EXPERIMENTAL RESULTS

The control block diagram of DFIG wind turbine is shown in Figure 6.25. The experimental test bench has setup as like in the Figure 6.25 shown. In our test bench, the Doubly fed Induction generator of about 7.5kW is coupled with prime mover of about 7.5kW as a wind turbine emulator. The danfoss PWM converter used as a back to back converter. The parameter for experimental setup has attached in Annexure II.

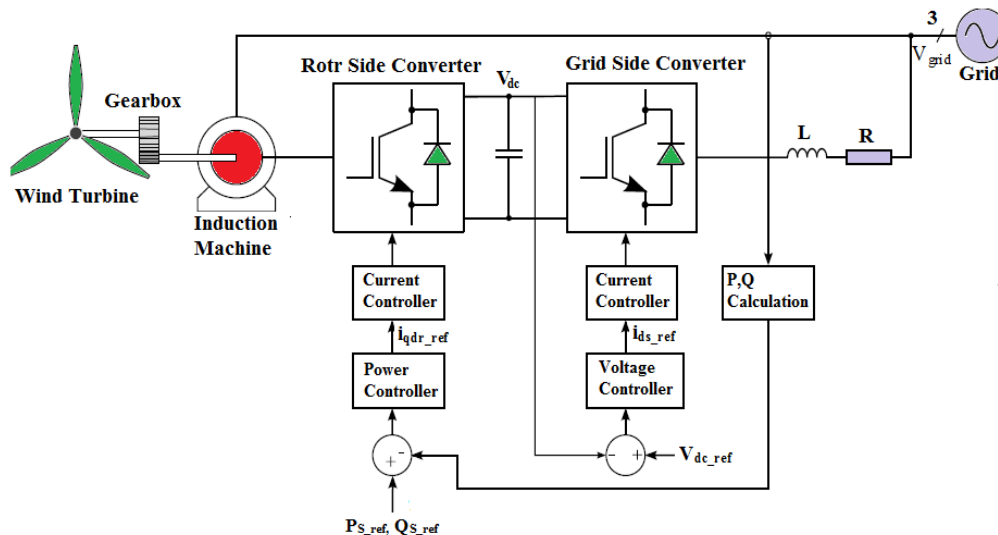


Figure: 6.25. Control block diagram of DFIG.

The experimental test bench of DFIG is shown in Fig. 6.26. The user control front panel is developed in dSPACE with Simulink.

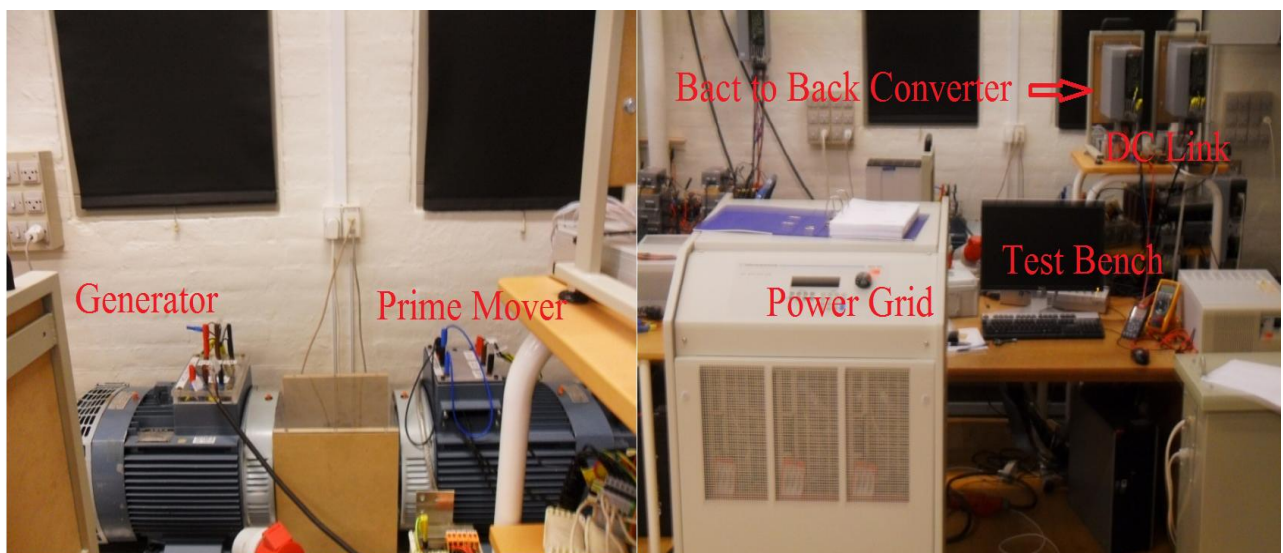
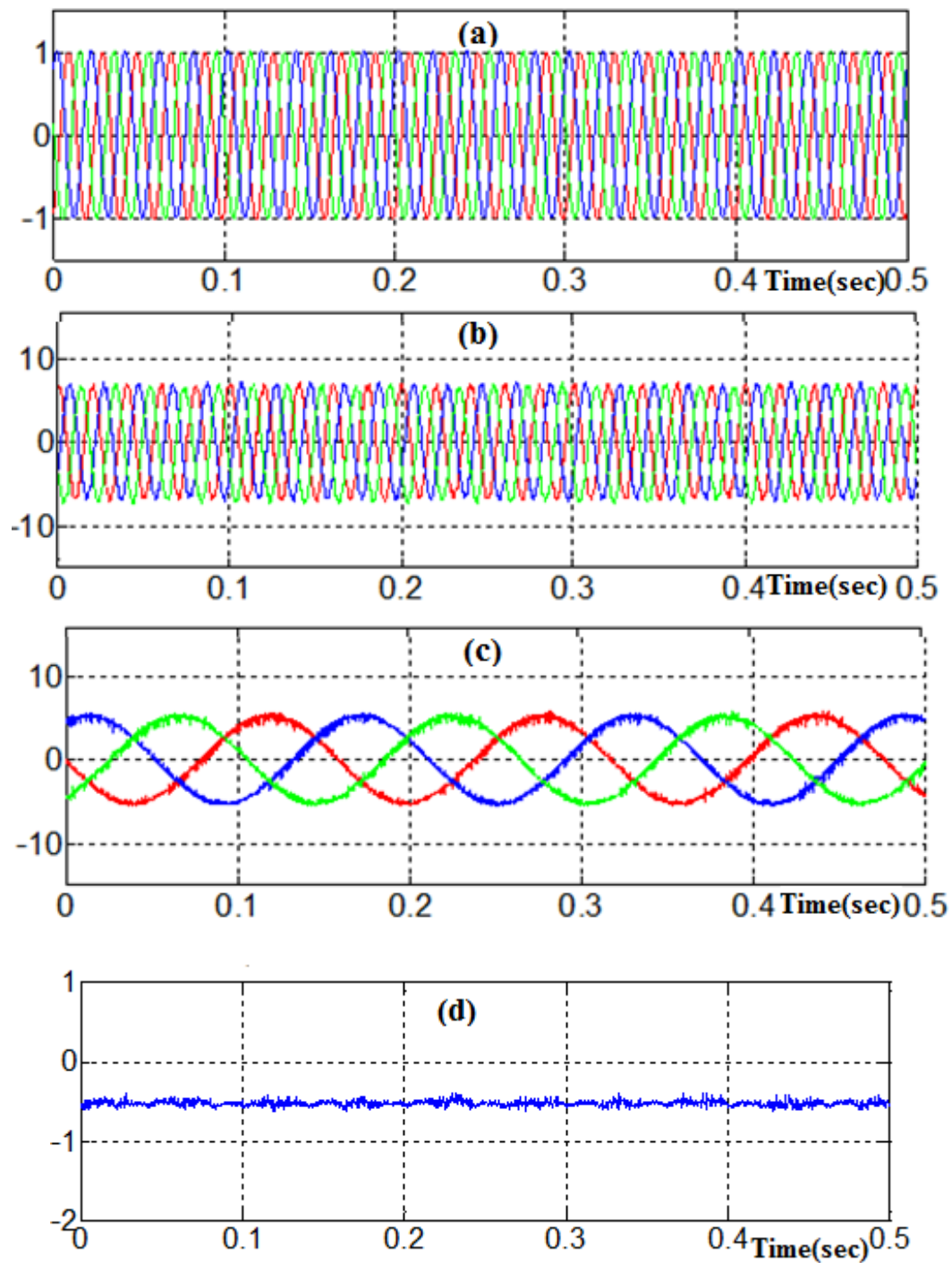


Figure: 6.26. Experimental test bench of DFIG System.

6.9.1 CASE 1(STEADY STATE CONDITION)

The power flow performance of DFIG wind Turbine 7.5kW has done with experimental test and it is verified and the results were shown in Figure 6.27.



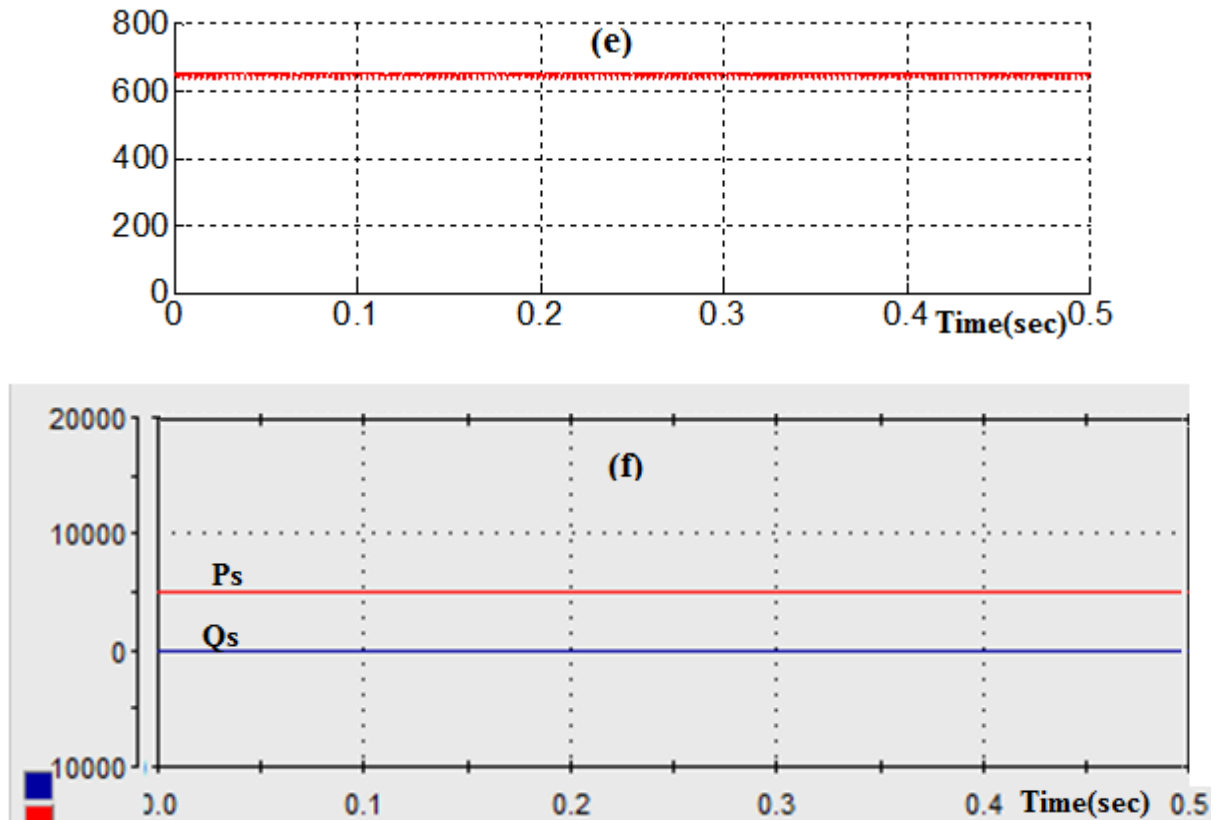


Figure:6.27 .(a)Stator Voltage, (b) Stator current, (c) Rotor current, (d) Torque, (e)DC Voltage, (f)Stator active and reactive power.

6.9.2 CASE 2(Unbalanced Grid Supply)

For protecting the converters, a common used solution is to connect the rotor circuit with a crowbar, which limits the high current in the rotor windings and provides a safe path for the high magnitude transient current [104-105]. Besides to crowbar protection methods there are several control schemes able to limit the over currents and to control the reactive power as discussed in [112] and [114]. In this section different control strategies are compared in order to determine the maximum reactive power that is possible to inject into the grid during the fault, without exceeding the safe converter current.

In case 2, we have done an experiment on low voltage ride through test for DFIG wind turbine. In this test we have considered a unbalanced grid condition (most fault in power system) to check all the possible way for the control strategies which we proposed [92-114] our experimental test.

6.9.3 DERIVATION OF CURRENT REFERENCES FOR DFIG WIND TURBINE

The control block diagram of the DFIG system presented in the paper is shown in Figure 6.25. The rotor supply circuit comprises a grid side inverter and rotor side inverter that are linked through a dc bus. The dc bus capacitor decouples the two inverters, allowing them to be independently controlled. In this paper, we proposed different current control loop in the rotor side to get the reference currents and it is described below [103]-[116].

6.9.3.1 INSTANTANEOUS ACTIVE AND REACTIVE POWER CONTROL (IARC)

The control strategy of instantaneous active and reactive power control is shown in Figure 6.28. In this control, the reference current components are derived from active and reactive power reference and grid voltage in [107]-[112].

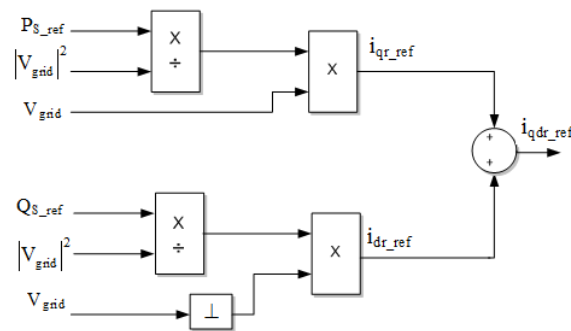


Fig: 6.28. Instantaneous active and reactive power control.

6.9.3.2 POSITIVE AND NEGATIVE SEQUENCE COMPENSATION (PNSC)

In positive and negative sequence compensation (PNSC) scheme, the reference current is derived from the positive and negative sequence of the grid voltage [107]-[112] as shown in figure 6.29.

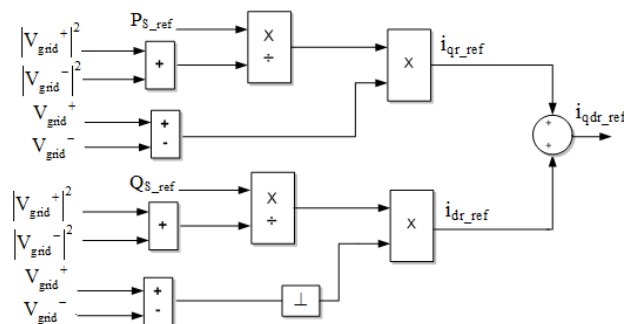


Figure: 6.29 Positive and negative sequence compensation.

6.9.3.3 AVERAGE ACTIVE AND REACTIVE POWER CONTROL (AARC)

In this scheme, the reference current for DFIG system is derived from the active and reactive power reference and average grid voltage [107]-[112] as shown in Figure 6.30.

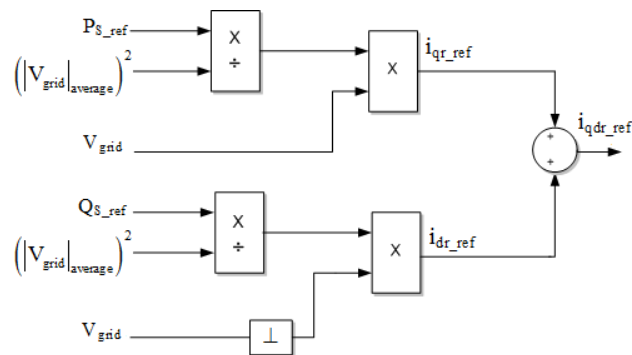


Figure: 6.30. Average active and reactive control.

6.9.3.4 BALANCED POSITIVE SEQUENCE (BPS)

In balanced positive sequence scheme, the reference current is derived from active and reactive power reference and positive grid voltage as shown in Figure 6.31 [107]-[112].

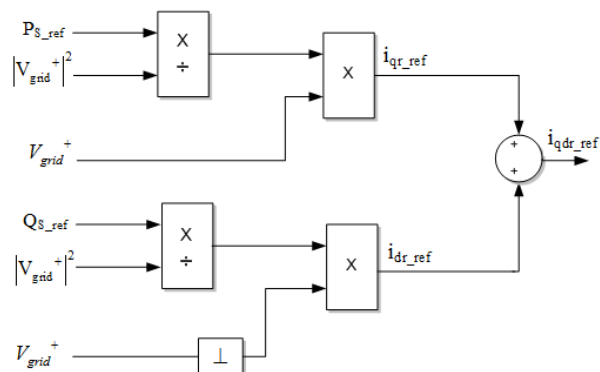


Figure: 6.31. Balanced positive sequence.

In this section we have considered two different kind of faults in the grid voltage and the proposed different control schemes are applied during these two faults which are discussed in Case 1 and Case 2. Under steady state conditions the active and reactive power references are 5 kW and 0 VAR respectively, for all control schemes. As the fault is detected the reference value of active power is set to zero and the reactive power reference is increased by different trial tests in order to achieve the maximum allowed safe value.

6.9.4 CASE 1

In this case we considered a fault characterized by a grid voltage reduction of 90% for line A and 60% for line B and line C. The results obtained using the four control schemes are shown in Figures 6.32-6.35. In instantaneous active and reactive power control method, when the unbalanced fault occurs in the grid voltage there will be initial peak current in the rotor, then it is limited to the normal value as per TSO standard. During this fault, the active power tends to 0 kW and the reactive power injection into the grid is 800 VAR to support the grid network as shown in Figure 6.32.

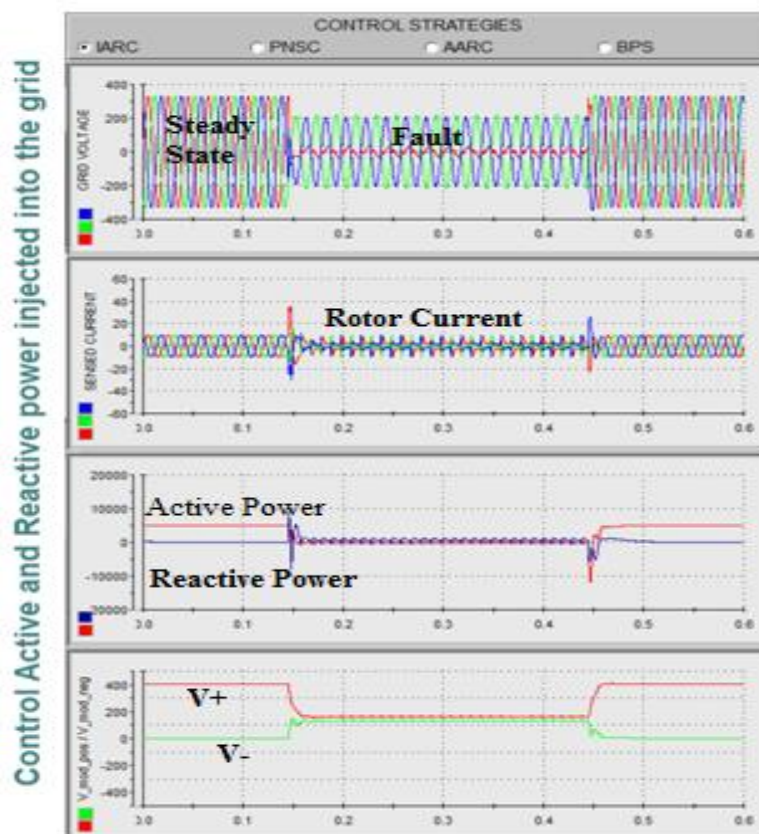


Figure: 6.32. Instantaneous active and reactive power control for DFIG (case 1).

In positive and negative sequence compensation method, when the unbalanced fault occurs in the grid voltage there will be initial peak current in the rotor then it is limited to the normal value as per TSO standard, as in the previous control scheme. During this fault the active power tends to 0 kW and the reactive power injection into the grid is 450 VAR to support the grid as shown in Figure 6.33.

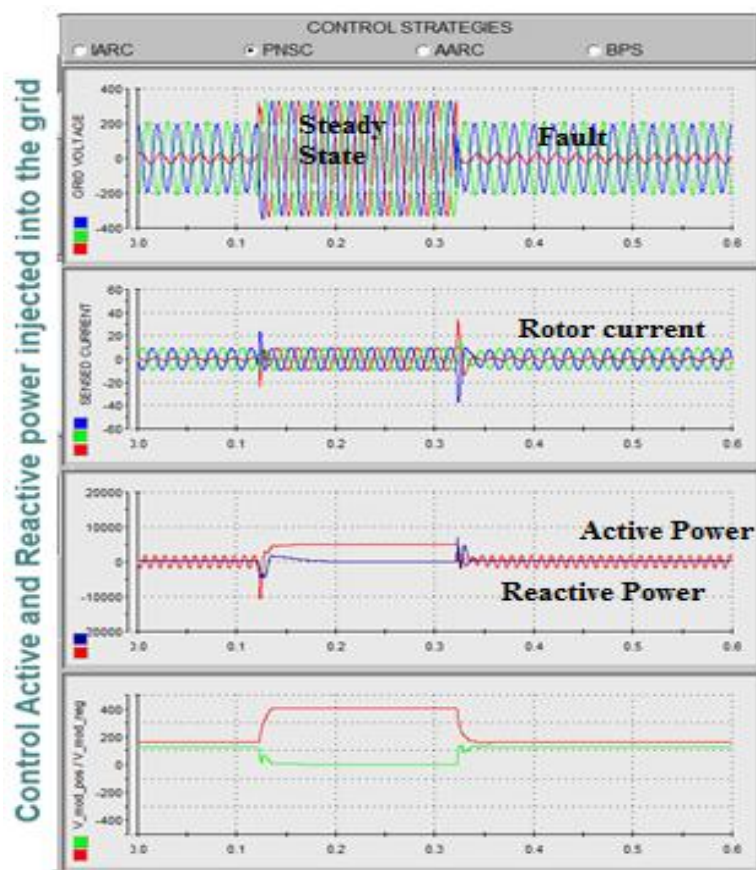


Fig: 6.33. Positive and negative sequence compensation control for DFIG(case 1).

In average active and reactive power control method, when the fault occurs in the grid voltage the rotor current shows a transient behavior similar to that of previous control schemes. During this fault, the active power tends to 0 kW and the reactive power injection into the grid is 2000 VAR to support the grid as shown in Figure 6.34.

In balanced positive sequence control method, when the fault occurs in the grid voltage the rotor current shows a transient behavior similar to that of previous control schemes. During this fault, the active power tends to 0 kW and the reactive power injection into the grid is 1200 VAR to support the grid as shown in Figure 6.35.

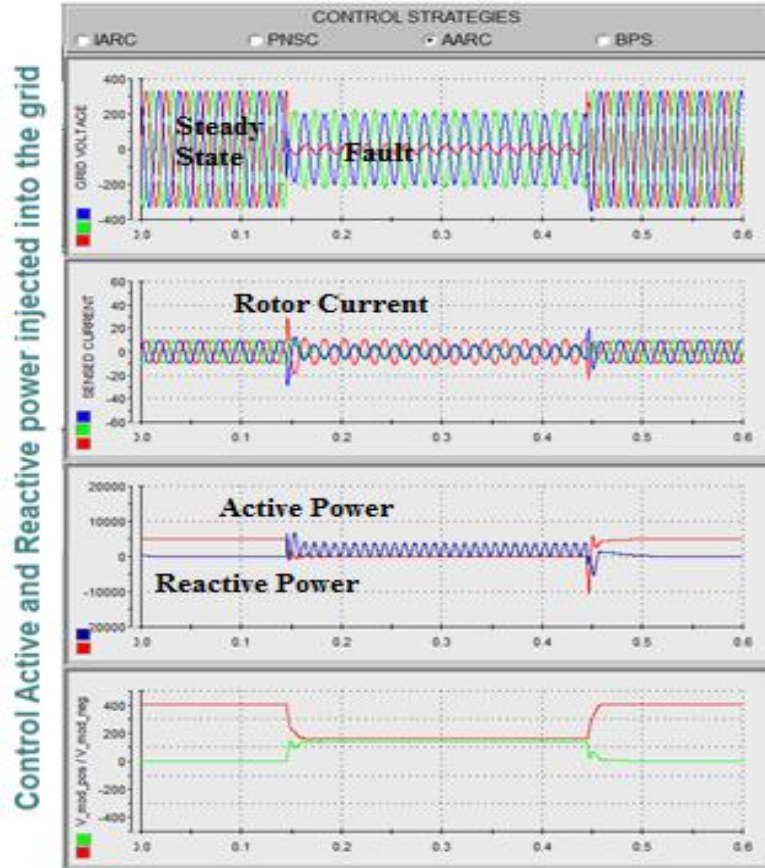


Fig: 6.34. Average active and reactive power control for DFIG (case 1).

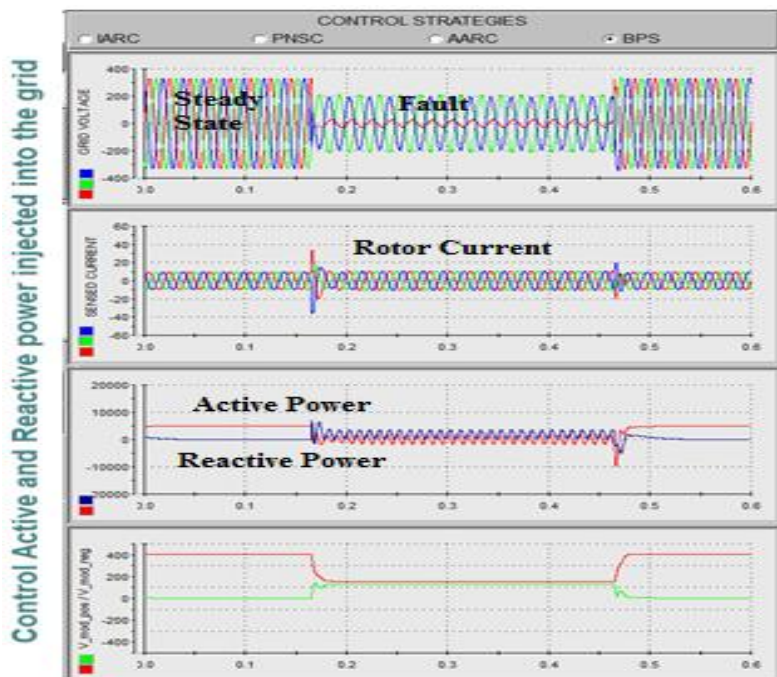


Fig: 6.35. Balanced positive sequence control for DFIG (case 1).

6.9.5 CASE 2

In this case we considered a fault characterized by a grid voltage reduction of 30% for line A and 50% for line B and line C. The results obtained for the four control schemes are shown in Figure (6.36)-(6.39).

In instantaneous active and reactive power control method, when the fault occurs in the grid voltage there will be initial peak current in the rotor then it is limited to the normal value as per TSO standard. During this fault the active power tends to 0 kW and the reactive power injection into the grid is 800 VAR to support the grid as shown in Figure 6.36.

In positive and negative sequence compensation method, when the fault occurs in the grid voltage the rotor current shows a transient behavior similar to that of previous control schemes. During this fault the active power tends to 0 kW and the reactive power injection into the grid is 400 VAR to support the grid as shown in Figure 6.37.

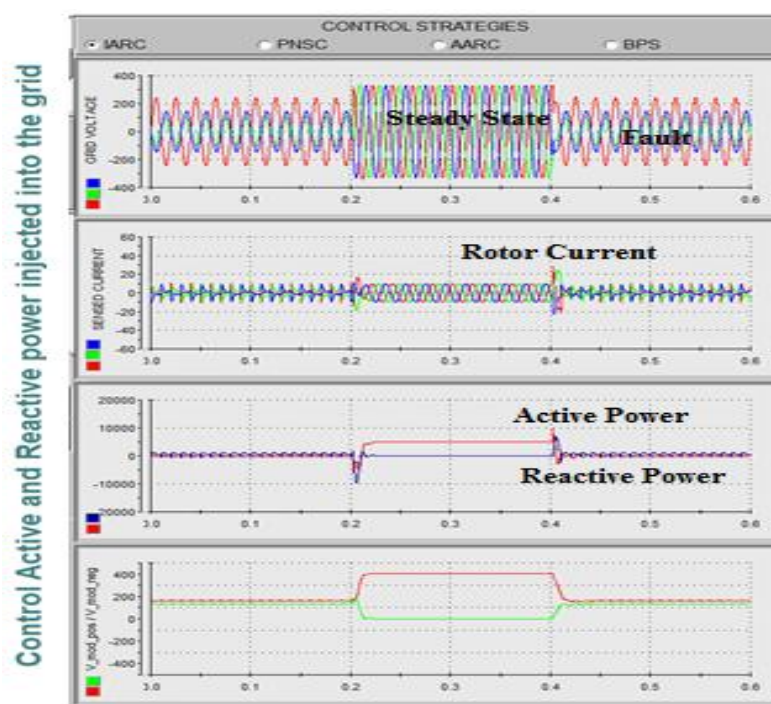


Fig: 6.36. Instantaneous active and reactive power control for DFIG (case 2).

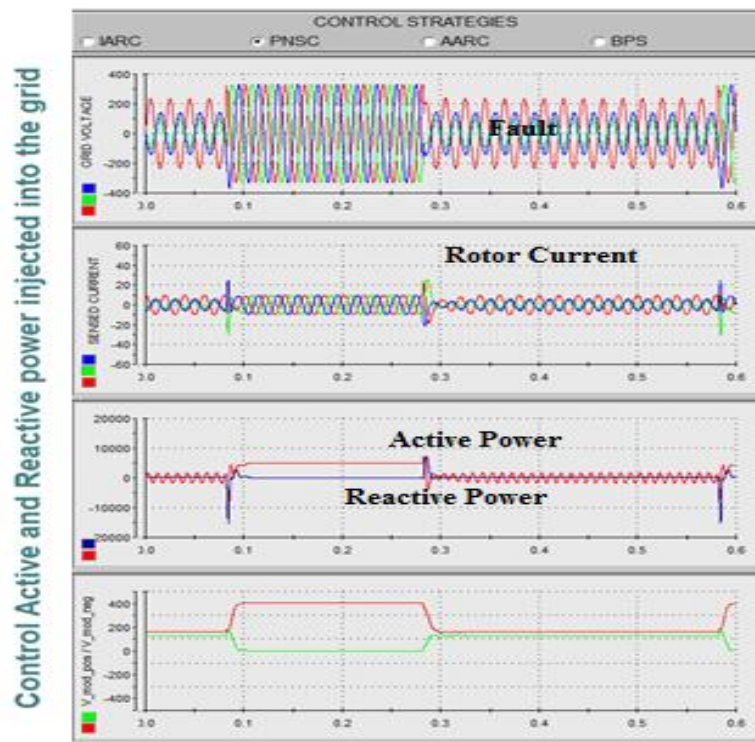


Figure: 6.37. Positive and negative sequence compensation control for DFIG (case 2).

In average active and reactive power control method, when the fault occurs in the grid voltage the rotor current shows a transient behavior similar to that of previous control schemes. During this fault the active tends to 0 kW and the reactive power injection into the grid is 2000 VAR to support the grid as shown in Figure 6.38.

In balanced positive sequence control method, when the fault occurs in the grid voltage the rotor current shows a transient behavior similar to that of previous control schemes. During this fault the active tends to 0 kW and the reactive power injection into the grid is 1400 VAR to support the grid as shown in Figure 6.39.

The results obtained for the reactive power injection into the network during fault using the different control strategies are summarized in Table. 6.1.

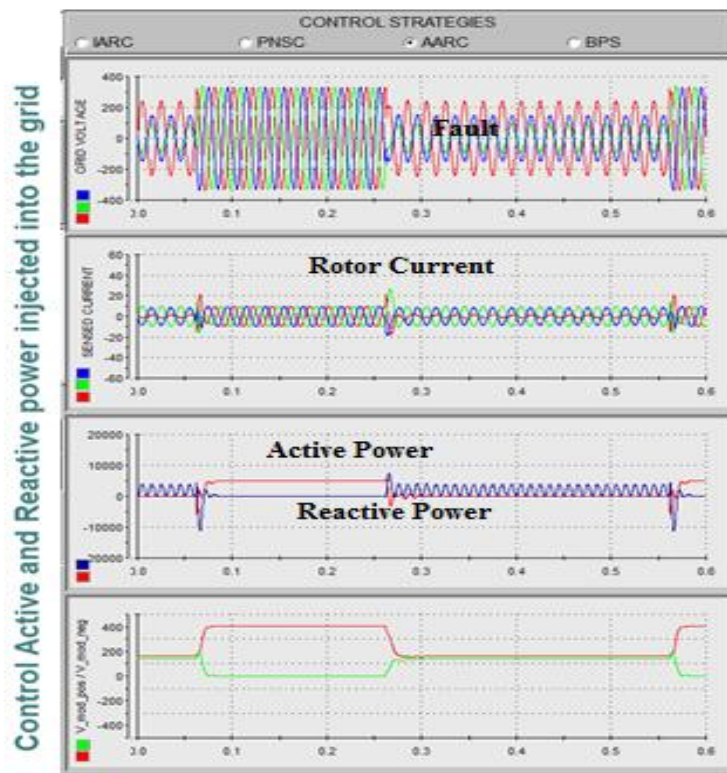


Figure: 6.38. Average active and reactive power control for DFIG (case 2).

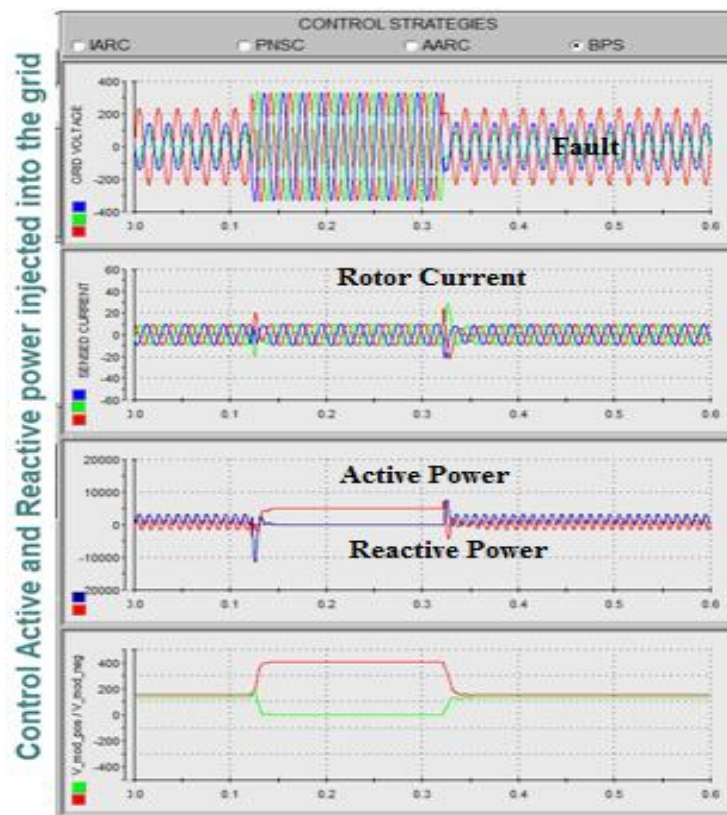


Figure: 6.39. Balanced positive sequence control for DFIG (case 2).

Table 6.1: Comparison of control strategies

Reactive Power(VAR) Injection into Grid		
Control Scheme	Case 1	Case 2
IARC	800	800
PNSC	450	400
AARC	2000	2000
BPS	1200	1400

6.9.6 SUMMARY

In this section we have analyzed different control strategies for the active and reactive power control of DFIG system under grid fault. From the experimental results it is verified that average active and reactive power control (AARPC) is the most suitable reference current control strategy to be applied during unbalanced grid supply to meet the transmission system operator requirements.

6.10 REFERENCES

- [1] J. Morren, S.W.H. de Haan, "Ridethrough of wind turbines with doubly-fed induction generator during a voltage dip", *IEEE Transaction on Energy Conversion*, vol. 20, no. 2, pp. 435 – 441, June 2005.
- [2] A. Petersson, S. Lundberg, T. Thiringer, "A DFIG Wind Turbine Ride-through System", *Wind Energy*, vol. 8, pp. 251–263, 2005.
- [3] I. Erlich, J. Kretschmann, J. Fortmann, S. Mueller-Engelhardt, H. Wrede, "Modeling of Wind Turbines Based on Doubly-Fed Induction Generators for Power System Stability Studies", *IEEE Transactions on Power Systems*, vol. 22, no. 3, pp. 909 – 919, August 2007.
- [4] J. Lopez, P. Sanchis, X. Roboam, L. Marroyo, "Dynamic Behavior of the Doubly Fed Induction Generator During Three-Phase Voltage Dips", *IEEE Transaction on Energy Conversion*, vol. 22, no. 3, pp. 709 – 717, Sept. 2007.
- [5] S.Seman, J. Niiranen, S. Kanerva, A. Arkkio, J. Saitz, "Performance Study of a Doubly Fed Wind-Power Induction Generator Under Network Disturbances", *IEEE Transaction on Energy Conversion*, vol. 21, no. 4, pp. 883 – 890, December 2006.
- [6] J.B. Ekanayake, L. Holdsworth, Xue Guang Wu; N. Jenkins, "Dynamic modeling of doubly fed induction generator wind turbines", *IEEE Transactions on Power Systems*, vol. 18, no. 2, pp. 803 – 809, May 2003.
- [7] E. Muljadi, C.P. Butterfield, B. Parsons, A. Ellis, "Effect of Variable Speed Wind Turbine Generator on Stability of a Weak Grid", *IEEE Transaction on Energy Conversion*, vol. 22, no. 1, pp. 29 – 36, March 2007.
- [8] P.S. Flannery, G. Venkataramanan, "A Fault Tolerant Doubly Fed Induction Generator Wind Turbine Using a Parallel Grid Side Rectifier and Series Grid Side Converter", *IEEE Transactions on Power Electronics*, vol. 23, no. 3, pp. 1126 – 1135, May 2008.
- [9] A.D. Hansen, G. Michalke, "Fault ride-through capability of DFIG wind turbines", *Renewable Energy*, vol 32, 2007, pp 1594-1610.
- [10] A.D. Hansen, G. Michalke, P. Sørensen, T. Lund, F. Iov, "Coordinated voltage control of DFIG wind turbines in uninterrupted operation during grid faults", *Wind Energy*, No. 10, 2007, pp. 51-68.
- [11] R. Datta, V. Ranganathan, "Variable-Speed Wind Power Generation Using a Doubly Fed Wound Rotor Induction Machine", *IEEE Transaction on Energy Conversion*, 2002, 17(3):414-421.
- [12] F. Blaabjerg, Z. Chen, S. Kjaer, "Power electronics as efficient interface in dispersed power generation systems," *IEEE Transaction on Power Electronics*, 2004, 19(5):1184-1194.
- [13] J. Carrasco, L. Franquelo, J. Bialasiewicz, "Power Electronic Systems for the Grid Integration of Renewable Energy Sources", *IEEE Transaction on Industrial Electronics*, 2006, 53(4):1002-1016.
- [14] L. Hansan, L. Helle, F. Blaabjerg, "Conceptual survey of generators and power electronics for wind turbines", *Riso National Laboratory Technical Report Riso-R-1205(EN)* Roskilde, Denmark, December 2001.

- [15] H. Polinder, J. Morren, “Developments in wind turbine generator systems”, Electrimacs 2005, Hammamet, Tunisia.
- [16] A. Hansan, L. Hansan, “Wind turbine concept market penetration over 10 years (1995-2004)”, *Wind Energy*, 2007, 10, (1):81-97.
- [17] S. Muller, M. Deicke, R. De Doncker, “Doubly fed induction generator systems for wind turbines”, *IEEE Industry Applications Magazine*, 2002, 8(3):26-33.
- [18] H. Li, Z. Chen, “Overview of different wind generator systems and their comparisons” *IET Renewable Power Generation*, 2008, 2(2):123-138.
- [19] M. Dubois, H. Polinder, J. Ferreira, “Comparison of generator topologies for direct-drive wind turbines”, *Proceeding of Nordic Countries Power and Industrial Electronics Conference*, Aalborg, Denmark, June 2000:22-26.
- [20] J. Baroudi, V. Dinavahi, A. Knight, “A review of power converter topologies for wind generators”, *Renewable Energy* 2007, 32:2369-2385.
- [21] F. Blaabjerg, R. Teodorescu, M. Liserre, “Overview of Control and Grid Synchronization for Distributed Power Generation Systems”, *IEEE Transaction on Industrial Electronics*, 2006, 53(5):1398-1409.
- [22] R. Pena, J. Clare, G. Asher, “Double fed induction generator using back-to-back PWM converter and its application to variable-speed wind-energy generation”, *Proc. IEE Electr. Power Appl.*, vol. 143, no. 3, pp. 231–241, May 1996.
- [23] Seman S, Niiranen J, Arkkio A “ Ride-Through Analysis of Doubly Fed Induction Wind-Power Generator Under Unsymmetrical Network Disturbance” , *IEEE Transaction on Power Systems*, 2006, 21(4):1782-1789.
- [24] Anaya-Lara O, Hughes F, Jenkins N, “Rotor flux magnitude and angle control strategy for doubly fed induction generators” , *Wind Energy*, 2006, 9:479-495.
- [25] Almeida R, Lopes J, Barreiros J., “ Improving power system dynamic behavior through doubly fed induction machines controlled by static converter using fuzzy control”, *IEEE Transactions on Power Systems*, 2004, 19(4):1942-1950.
- [26] Rathi M, Mohan N. , “A novel robust low voltage and fault ride through for wind turbine application operating in weak grids”, *IECON 2005*, 2005.
- [27] Quang N, Dittrich A, Lan P, “Doubly-fed induction machine as generator in wind power plant nonlinear control algorithms with direct decoupling”, *EPE'05*, 2005.
- [28] Bollen M, Styvaktakis S., “Characterization of three-phase unbalanced sags, as easy as one, two, three”, *IEEE PES Summer Meeting*, 2000.
- [29] Bollen M., “Characterization of voltage sags experienced by three phase adjustable-speed drives”, *IEEE Transactions on Power Delivery*, 1997, 12: 1666- 1671.
- [30] Bollen M, Graaff R., “ Behavior of AC and DC drives during voltage sags with phase-angle jump and three-phase unbalance”, *IEEE Power Engineering Society Winter Meeting*, 1999.
- [31] Bollen M, Olguin G, Martins M., “Voltage dips at the terminals of wind power installations”, *Wind Energy*, 2005, 8:307-318.

- [32]Lopez J, Sanchis P, Roboam X, “Dynamic behavior of the Doubly Fed Induction Generator during three-phase voltage dips”, IEEE Transaction on Energy Conversion, 2007, 22(3):709-717.
- [33] Niiranen J. “Voltage dip ride through of a doubly-fed generator equipped with an active Crowbar”, Nordic Wind Power Conference, 2004.
- [34]Morren J, Haan S. ,“Ride through of wind turbines with doubly-fed induction generator during a voltage dip”, IEEE Transaction on Energy Conversion, 2005, 20(2):435-441.
- [35]Erlich I, Kretschmann J, Fortmann J, “Modeling of wind turbines based on doubly-fed induction generators for power system stability studies”, IEEE Transactions on Power Systems, 2007, 22(3):909-919.
- [36]Abbey C, Joos G, “Super capacitor energy storage for wind energy applications”, IEEE Transactions on Industry Applications, 2007, 43(3):769-776.
- [37]Petersson A, Lundberg S, Thiringer T, “A DFIG wind turbine ride-through system influence on the energy production”, Wind Energy, 2005, 8:251-263.
- [38]Flannery P, Venkataramanan, “ G. A fault tolerant doubly fed induction generator wind turbine using a parallel grid side rectifier and series grid side converter”, IEEE Transactions on Power Electronics, 2008, 23(3):1126-1135.
- [39]Hansen A, Michalke G., “ Fault ride-through capability of DFIG wind turbines ” Renewable Energy, 2007, 32:1594-1610.
- [40]Hansen A, Michalke G, Sorensen P, “ Coordinated voltage control of DFIG wind turbines in uninterrupted operation during grid faults”, Wind Energy, 2007, 10:51-68.
- [41]Seman S, Niiranen J, “ Ride-Through Analysis of Doubly Fed Induction Wind-Power Generator Under Unsymmetrical Network Disturbance ”, IEEE Transactions on Power Systems, 2006, 21(4):1782-1789.
- [42]Tsourakis G, Vournas C, “Simulation of low voltage ride through capability of wind turbines with Doubly fed induction generator”, EWEC 2006, Athens, Greece.
- [43]Rodriquez M, Abad G, “Crowbar control algorithms for doubly fed induction generator during voltage dips”, EPE 2005, Dresden, Germany.
- [44]Dittrich A, Stoev A., “Comparison of fault ride-through strategies for wind turbines with DFIM generators”, EPE 2005, Dresden, Germany.
- [45]Lohde R, Jensen S, Knop A, “ Analysis of three phase grid failure on doubly fed induction generator ride-through using Crowbars”, EPE 2007, Aalborg, Denmark.
- [46]J.K. Niiranen , “Simulation of Doubly Fed Induction Generator wind turbine with an active crowbar”, EPE-PEMC 2004, Latvia, CD-ROM.
- [47]. ENEL – DK 5400 - Criteri di allacciamento di clienti alla rete AT della distribuzione, October 2004.
- [48]. ENEL – DK 5740 - Criteri di allacciamento di impianti di produzione alla rete MT di ENEL distribuzione, February 2005.
- [49]. TERNA - Codice di trasmissione, dispacciamento, sviluppo e sicurezza della rete, 2006.

- [50] A. Lubosny, "Wind Turbine Operation in Electric Power Systems -Advanced Modeling", Springer Verlag, 2003.
- [51] C. Rossi, D. Casadei, F. Filippetti, A. Stefani, A. Yazidi, G.A. Capolino, "Doubly-Fed Induction Machines Diagnosis Based on Signature Analysis of Rotor Modulating Signals", IEEE Transactions on Industry Applications, Volume: 44, Issue 6, November/December 2008, pp. 1711-1721.
- [52] S.Chandrasekaran, C.Rossi, D.Casadei, "Modeling and Simulation of Grid Connected Wind Energy Conversion System (WECS) Based on a Doubly Fed Induction Generator (DFIG)", the Third International Renewable Energy Congress, December 20-22, 2011 – Hammamet, Tunisia.
- [53] R. Lohde, S. Jensen, A. Knop, F.W. Fuchs, "Analysis of three phase grid failure on doubly fed induction generator ride-through using Crowbars", Proceedings of EPE 2007, Aalborg, Denmark, September, 2007.
- [54] N. Miller, W. Price, and J. Sanchez-Gasca, "Dynamic modeling of ge 1.5 and 3.6 wind turbine generators," tech. rep., GE Power Systems Energy Consulting, 2003.
- [55] Zhao Dongli, Guo Jingdong, Xu Honghua, "The study and realization on the decoupling control of active and reactive power of a variable speed constant frequency doubly fed induction generator", ACTA ENERGIAE SOLARIS SINICA, vol. 27(2), pp. 174–179, Feb. 2006.
- [56] J. I. Jang, Y. S. Kim, and D. C. Lee, "Active and reactive power control of DFIG for wind energy conversion under unbalanced grid voltage," IPEMC Shanghai, vol. 3, pp. 1487-1491, Aug. 2006.
- [57] Dawei Xiang, Li Ran, Tavner, P.J. and Yang, S., "Control of a doubly fed induction generator in a wind turbine during grid fault ride-through," IEEE Trans. Energy Convers., vol. 21, no. 3, pp. 652-662, Sep. 2006.
- [58] S.Muller, M.Deicke, and R.DeDoncker, "Doubly fed induction generator systems for wind turbines," IEEE Ind. Appl.Mag., vol. 8, no. 3, pp. 26–33, May/Jun. 2002.
- [59] J. Lopez, E. Gubia, P. Sanchis, X. Roboam, and L. Marroyo, "Wind turbines based on doubly fed induction generator under asymmetrical voltage dips," IEEE Trans. Energy Convers., vol. 23, no. 1, pp. 321–330, Mar. 2008.
- [60] M. Mohseni, S. Islam, and M. Masoum, "Impacts of symmetrical and asymmetrical voltage sags on dfig-based wind turbines considering phase angle jump, voltage recovery, and sag parameters," IEEE Trans. Power Electron., to be published.
- [61] S. Seman, J. Niiranen, and A. Arkkio, "Ride-through analysis of doubly fed induction wind-power generator under unsymmetrical network disturbance," IEEE Trans. Power Syst., vol. 21, no. 4, pp. 1782–1789, Nov. 2006.
- [62] W. Zhang, P. Zhou, and Y. He, "Analysis of the by-pass resistance of an active crowbar for doubly-fed induction generator based wind turbines under grid faults," in Proc. Int. Conf. Electr. Mach. Syst. (ICEMS), Oct., 2008, pp. 2316–2321.
- [63] G. Pannell, D. Atkinson, and B. Zahawi, "Minimum-threshold crowbar for a fault-ride-through grid-code-compliant dfig wind turbine," IEEE Trans. Energy Convers., vol. 25, no. 3, pp. 750–759, Sep. 2010.

- [64] J. Morren and S. de Haan, "Short-circuit current of wind turbines with doubly fed induction generator," *IEEE Trans. Energy Convers.*, vol. 22, no. 1, pp. 174–180, Mar. 2007.
- [65] J. Yang, J. Fletcher, and J. O'Reilly, "A series-dynamic-resistor-based converter protection scheme for doubly-fed induction generator during various fault conditions," *IEEE Trans. Energy Convers.*, vol. 25, no. 2, pp. 422–432, Jun. 2010.
- [66] A. Causebrook, D. Atkinson, and A. Jack, "Fault ride-through of large wind farms using series dynamic braking resistors (march 2007)," *IEEE Trans. Power Syst.*, vol. 22, no. 3, pp. 966–975, Aug. 2007.
- [67] P. Flannery and G. Venkataramanan, "Unbalanced voltage sag ride through of a doubly fed induction generator wind turbine with series grid-side converter," *IEEE Trans. Ind. Appl.*, vol. 45, no. 5, pp. 1879–1887, Sep./Oct. 2009.
- [68] J. Liang, W. Qiao, and R. Harley, "Direct transient control of wind turbine driven dfig for low voltage ride-through," in *Proc. IEEE Power Electron. Mach. Wind Appl. (PEMWA)*, Jun. 2009, pp. 1–7.
- [69] D. Xiang, L. Ran, P. Tavner, and S. Yang, "Control of a doubly fed induction generator in a wind turbine during grid fault ride-through," *IEEE Trans. Energy Convers.*, vol. 21, no. 3, pp. 652–662, Sep. 2006.
- [70] F. Lima, A. Luna, P. Rodriguez, E. Watanabe, and F. Blaabjerg, "Rotor voltage dynamics in the doubly fed induction generator during grid faults," *IEEE Trans. Power Electron.*, vol. 25, no. 1, pp. 118–130, Jan. 2010.
- [71] P. Zhou, Y. He, and D. Sun, "Improved direct power control of a dfig-based wind turbine during network unbalance," *IEEE Trans. Power Electron.*, vol. 24, no. 11, pp. 2465–2474, Nov. 2009.
- [72] G. Abad, M. Rodriguez, G. Iwanski, and J. Poza, "Direct power control of doubly-fed-induction-generator-based wind turbines under unbalanced grid voltage," *IEEE Trans. Power Electron.*, vol. 25, no. 2, pp. 442–452, Feb. 2010.
- [73] L. Xu, "Coordinated control of dfig's rotor and grid side converters during network unbalance," *IEEE Trans. Power Electron.*, vol. 23, no. 3, pp. 1041–1049, May 2008.
- [74] D. Santos-Martin, J. Rodriguez-Amenedo, and S. Arnaltes, "Providing ride-through capability to a doubly fed induction generator under unbalanced voltage dips," *IEEE Trans. Power Electron.*, vol. 24, no. 7, pp. 1747–1757, Jul. 2009.
- [75] J. Lopez, E. Gubia, E. Olea, J. Ruiz, and L. Marroyo, "Ride through of wind turbines with doubly fed induction generator under symmetrical voltage dips," *IEEE Trans. Ind. Electron.*, vol. 56, no. 10, pp. 4246–4254, Oct. 2009.
- [76] M. H. J. Bollen, *Understanding Power Quality Problems Voltage Sags and Interruptions*. New York: Wiley, 2000.
- [77] J. Nielsen and F. Blaabjerg, "A detailed comparison of system topologies for dynamic voltage restorers," *IEEE Trans. Ind. Appl.*, vol. 41, no. 5, pp. 1272–1280, Sep./Oct. 2005.
- [78] C. Meyer, R. De Doncker, Y. W. Li, and F. Blaabjerg, "Optimized control strategy for a medium-voltage dvr ; theoretical investigations and experimental results," *IEEE Trans. Power Electron.*, vol. 23, no. 6, pp. 2746–2754, Nov. 2008.

- [79] Y. W. Li, F. Blaabjerg, D. Vilathgamuwa, and P. C. Loh, "Design and comparison of high performance stationary-frame controllers for dvr implementation," *IEEE Trans. Power Electron.*, vol. 22, no. 2, pp. 602–612, Mar. 2007.
- [80] F. Marafao, D. Colon, J. Jardini, W. Komatsu, L. Matakas, M. Galassi, S. Ahn, E. Bormio, J. Camargo, T. Monteiro, and M. Oliveira, "Multiloop controller and reference generator for a dynamic voltage restorer implementation," in *Proc. 13th Int. Conf. Harmon. Quality Power (ICHQP)*, Oct. 2008, pp. 1–6.
- [81] C. Wessels and F. Fuchs, "High voltage ride through with facts for dfig based wind turbines," in *Proc. 13th Eur. Conf. Power Electron. Appl.(EPE)*, Sep. 2009, pp. 1–10.
- [82] A. O. Ibrahim, T. H. Nguyen, D.C. Lee, and S.C. Kim, "Ride-through strategy for dfig wind turbine systems using dynamic voltage restorers," in *Proc. IEEE Energy Convers. Congr. Expo. (ECCE)*, Sep. 2009, pp. 1611–1618.
- [83] C. Wessels, F. Gebhardt, and F. W. Fuchs, "Dynamic voltage restorer to allow LVRT for a dfig wind turbine," in *Proc. IEEE Int. Symp. Ind. Electron. (ISIE)*, Jul. 2010, pp. 803–808.
- [84] M. P. Kazmierkowski, R. Krishnan, F. Blaabjerg, and D. Irwin, *Control in Power Electronics: Selected Problem (Series in Engineering)*. New York: Academic, 2002.
- [85] J. G. Nielsen, "Design and control of a dynamic voltage restorer," Ph.D. dissertation, Inst. Energy Technol., Aalborg Univ., Aalborg, Denmark, Mar. 2002.
- [86] S. Mahesh, M. Mishra, B. Kumar, and V. Jayashankar, "Rating and design issues of dvr injection transformer," in *Proc. 23rd Annu. IEEE Appl. Power Electron. Conf. Expo. (APEC)*, Feb. 2008, pp. 449–455.
- [87] C. Wessels, R. Lohde, and F. W. Fuchs, "Transformer based voltage sag generator to perform lvrt and hvrt tests in the laboratory," in *Proc. 14th Int. Power Electron. Motion Control Conf. (EPE/PEMC)*, Sep. 2010, pp. T11- 8–T11-13.
- [88] Byeon, G., Park, I.K., Jang, G.: 'Modeling and control of a doubly-fed induction generator (DFIG) wind power generation system for real-time simulations', *J. Electr. Eng. Technol.*, 2010, 5, (1), pp. 61–69.
- [89] Lee, J.H., Jeong, J.K., Han, B.M., Choi, N.S., Cha, H.J.: "DFIG wind power system with a DDPWM controlled matrix converter", *J. Electr. Eng. Technol.*, 2010, 5, (2), pp. 299–306.
- [90] Brekken, T., Mohan, N.: "Control of a doubly fed induction generator under unbalanced grid voltage conditions", *IEEE Trans. Energy Convers.*, 2007, 22, (1), pp. 129–135.
- [91] Zhou, Y., Bauer, P., Ferreira, J.A., Pierik, J.: "Operation of grid connected DFIG under unbalanced grid voltage condition", *IEEE Trans. Energy Convers.*, 2009, 24, (1), pp. 240–246.
- [92] Hu, J., Nian, H., Xu, H., He, Y.: "Dynamic modeling and improved control of DFIG under distorted grid voltage conditions", *IEEE Trans. Energy Convers.*, 2011, 26, (1), pp. 163–175.
- [93] Hu, J., He, Y.: "Reinforced control and operation of DFIG based wind power generation system under unbalanced grid voltage conditions", *IEEE Trans. Energy Convers.*, 2009, 24, (4), pp. 905–915.

- [94] Tsili, M., Papathanassiou, S, "A review of grid code technical requirements for wind farms", *IET Renew. Power Gener.*, 2009, 3, (1), pp. 308–332.
- [95] Wang, Y., Xu, L., Williams, B.W, "Compensation of network voltage unbalance using doubly fed induction generator-based wind farms", *IET Renew. Power Gener.*, 2009, 3, (1), pp. 12–22.
- [96] Xu, L, "Coordinated control of DFIG's rotor and grid side converters during network unbalance", *IEEE Trans. Power Electron.*, 2008, 23,(3), pp. 1041–1049.
- [97] Xu, L., Wang, Y, "Dynamic modeling and control of DFIG-based wind turbine under unbalanced network conditions", *IEEE Trans. Power Syst.*, 2007, 22, (1), pp. 314–323.
- [98] Lee, S.B., Lee, K.B., Lee, D.C., Kim, J.M, "An improved control method for DFIG in a wind turbine under an unbalanced grid voltage condition", *J. Electr. Eng. Technol.*, 2010, 5, (4), pp. 614–622.
- [99] Hu, J., He, Y., Xu, L., Williams, B.W, "Improved control of DFIG systems during network unbalance using PI-R current regulators", *IEEE Trans. Ind. Appl.*, 2009, 56, (2), pp. 439–451.
- [100] Gomis Bellmunt, O., Junyent Ferre, A., Sumper, A., Bergas-Jane, J, "Ride-through control of a doubly fed induction generator under unbalanced voltage sags", *IEEE Trans. Energy Convers.*, 2008, 23,(4), pp. 1036–1045.
- [101] Phan , V.T., Lee, H.H, "Performance enhancement of stand-alone DFIG systems with control of rotor and load side converters using resonant controllers", *IEEE Trans. Ind. Appl.*, 2012, 48, (1), pp. 199–2010.
- [102] Phan, V.T., Lee, H.H, "Enhanced proportional-resonant current controller for unbalanced stand-alone DFIG-based wind turbines", *J. Electr. Eng. Technol.*, 2010, 5, (3), pp. 443–450.
- [103] Hu, J., He, Y, "Modeling and enhanced control of DFIG under unbalanced grid voltage conditions", *Electr. Power Syst. Res.*, 2009, 79, (2), pp. 273–281.
- [104] Abad, G., Rodriguez, M., Iwanski, G., Poza, J, "Direct power control of doubly-fed-induction-generator based wind turbines under unbalanced grid voltage", *IEEE Trans. Power Electron.*, 2010, 25, (2), pp. 442–452.
- [105] Hu, J.B., He, Y.K, "Dynamic modeling and direct power control of wind turbine driven DFIG under unbalanced network voltage condition", *J. Zhejiang Univ. Sci. A*, 2008, 9, (12), pp. 1731–1740.
- [106] Lascu, C., Asiminoaei, L., Boldea, I., Blaabjerg, F, "High performance current controller for selective harmonic compensation in active power filters", *IEEE Trans. Power Electron.*, 2007, 22, (5), pp. 1826–1835.
- [107] Zhi, D., Xu, L, "Direct power control of DFIG with constant switching frequency and improved transient performance", *IEEE Trans. Energy Convers.*, 2007, 22, (1), pp. 110–118.
- [108] Hailiang Xu, Jiabing Hu, Yikang He: "Integrated Modeling and Enhanced Control of DFIG Under Unbalanced and Distorted Grid Voltage Conditions", *IEEE transactions on energy conversion*, vol. 27, no. 3, September 2012.

- [109] Jiabing Hu, Hailiang Xu, Yikang He: "Coordinated Control of DFIG's RSC and GSC Under Generalized Unbalanced and Distorted Grid Voltage Conditions", IEEE transactions on industrial electronics, vol. 60, no. 7, July 2013.
- [110] R. Lohde, S. Jensen, A. Knop, F.W. Fuchs, "Analysis of three phase grid failure on doubly fed induction generator ride-through using Crowbars", Proceedings of EPE 2007, Aalborg, Denmark, September, 2007.
- [111] Francisco K. A. Lima, Alvaro Luna, Pedro Rodriguez, Edson H. Watanabe, and Frede Blaabjerg, "Rotor Voltage Dynamics in the Doubly Fed Induction Generator During Grid Faults," IEEE Transactions on Power Electronics, vol. 25, no. 1, January 2010.
- [112] K. Lima, A. Luna, P. Rodriguez, E.Watanabe, R. Teodorescu, and Frede Blaabjerg, "Doubly-Fed Induction Generator Control Under Voltage Sags," IEEE Energy 2030 Atlanta, GA USA 17-18 November, 2008.
- [113] T. Sun, Z. Chen, and Frede Blaabjerg, "Voltage Recovery of Grid-Connected Wind Turbines with DFIG After a Short-circuit Fault," 2004 35th Annual IEEE Power Electronics Specialists Conference.
- [114] Zhao Dongli, Guo Jingdong, Xu Honghua, "The study and realization on the decoupling control of active and reactive power of a variable speed constant frequency doubly fed induction generator", ACTA ENERGIAE SOLARIS SINICA, vol. 27(2), pp. 174-179, Feb. 2006.
- [115] J. I. Jang, Y. S. Kim, and D. C. Lee, "Active and reactive power control of DFIG for wind energy conversion under unbalanced grid voltage," IPEMC Shanghai, vol. 3, pp. 1487-1491, Aug. 2006.
- [116] Dawei Xiang, Li Ran, Tavner, P.J. and Yang, S., "Control of a doubly fed induction generator in a wind turbine during grid fault ride-through," IEEE Trans. Energy Conversion., vol. 21, no. 3, pp. 652-662, Sep. 2006.

CHAPTER 7

ELECTRICAL SIMULATION MODELS-IEC 61400-27-1: DFIG WIND TURBINE (TYPE-3)

INTRODUCTION

The IEC 61400-27 series specify standard dynamic electrical simulation models [1-8] for wind power generation. IEC 61400-27-1 specifies wind turbine models and model validation procedure. IEC 61400-27-2 will specify wind power plant models and model validation procedure.

The increasing penetration of wind energy in power systems implies that Transmission System Operators (TSOs) and Distribution System Operators (DSOs) need to use dynamic models of wind power generation for power system stability studies. The models developed by the wind turbine manufacturers reproduce the behaviour of their machines with a high level of detail. Such level of detail is not suitable for stability studies of large power systems with a huge number of wind power plants. Firstly because the use of these models requires a substantial amount of input data to represent the individual wind turbine types. Secondly, due to the large number of state variables in the models, the simulation computer time and complexity are hugely increased.

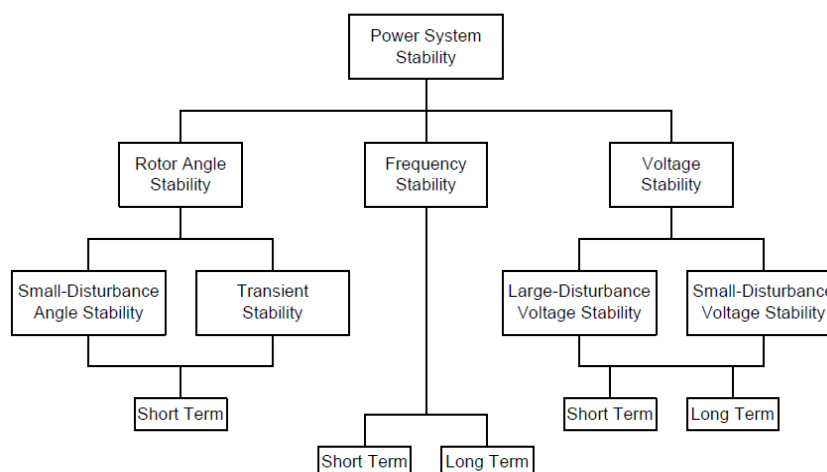


Figure: 7.1. Classification of power system stability according to IEEE/CIGRE Joint Task Force on Stability Terms and Definitions. (© IEEE 2004)

The purpose of this standard is to specify generic dynamic models, which can be applied in power system stability studies. IEEE/CIGRE Joint Task Force on Stability Terms and Definitions classified power system stability in categories according to Figure 7.1.

Referring to these categories, the models are developed to represent wind power generation in studies of large-disturbance short term voltage stability phenomena, but they will also be applicable to study other dynamic short term phenomena such as rotor angle stability, frequency stability and small-disturbance voltage stability. Thus, the models are applicable for dynamic simulations of power system events such as short circuits (low voltage ride through), loss of generation or loads, and system separation of one synchronous area into more synchronous areas as specified in the scope.

The complexity of the models has on the one hand to be exact enough with respect to the dynamic behaviour of the turbines terminals, but on the other hand be suitable for large-scale grid studies. Therefore simplified wind turbine models are specified to perform the typical response of known wind turbine technologies.

The wind turbine models specified in this standard are for fundamental frequency positive sequence response.

The models have the following limitations:

- The models are not intended for long term stability analysis.
- The models are not intended for investigation of sub-synchronous interaction phenomena.
- The models are not intended for investigation of the fluctuations originating from wind speed variability in time and space. This implies that the models are not including phenomena such as turbulence, tower shadow, wind shear and wakes.
- The models do not cover phenomena such as harmonics, flicker or any other EMC emissions included in the IEC 61000 series.
- The models have not been developed explicitly with eigen value calculation (for small signal stability) in mind.
- The models specified here apply only to wind turbines, and therefore do not include wind power plant level controls and additional equipment such as SVCs, STATCOMs and other devices which will be covered by IEC 61400-27-2.
- This standard does not address the specifics of short circuit calculations
- The models are not applicable to studies of extremely weak systems including situations where wind turbines are islanded without other synchronous generation.

The validation procedure specified in this standard shall be applied to standard models and other fundamental frequency wind turbine models.

The validation procedure has the following limitations:

- ❖ The validation procedure is not specifying any requirements to model accuracy. It only specifies measures to quantify the accuracy of the model.
- ❖ The validation procedure is not specifying test and measurement procedures, as it is based on tests specified in IEC 61400-21.

- ❖ The simulation model validation is not intended to justify compliance to any grid code requirement, power quality requirements or national legislation.
- ❖ The test and measurement procedures introduce errors which limit the possible accuracy as specified in the validation procedure.
- ❖ The validation procedure does not include steady state validation, but focuses on validation of the dynamic performance of the model.

The following stakeholders are potential users of the models specified in this standard:

- TSOs and DSOs are end users of the models, performing power system stability studies as part of the planning as well as the operation of the power systems,
- wind plant owners are typically responsible to provide the wind power plant models to TSO and/or DSO prior to plant commissioning,
- wind turbine manufacturers will typically provide the wind turbine models to the owner, developers of modern software for power system simulation tools will use the standard to implement standard wind power models as part of the software library, and
- education and research communities, who can also benefit from the generic models, as the manufacturer specific models, are typically confidential.

7.1 WIND TURBINES

PART 27-1: ELECTRICAL SIMULATION MODELS – WIND TURBINES

7.1.1 SCOPE

IEC 61400-27 shall define standard electrical simulation models for wind turbines and wind power plants. The specified models will be time domain positive sequence simulation models, intended to be used in power system and grid stability analyses. The models should be applicable for dynamic simulations of short term stability in power systems. IEC 61400-27 shall include procedures for validation of the specified electrical simulation models. The validation procedure for IEC 61400-27 shall be based on tests specified in IEC 61400-21.

IEC 61400-27 SHALL CONSIST OF TWO PARTS WITH THE FOLLOWING SCOPE:

– IEC 61400-27-1 shall specify dynamic simulation models for generic wind turbine topologies/ concepts / configurations on the market. IEC 61400-27-1 shall define the generic terms and parameters with the purpose of specifying the electrical characteristics of a wind turbine at the connection terminals. In addition IEC 61400-27-1 shall specify a method to create models for future wind turbine concepts. The dynamic simulation models shall refer to the wind turbine terminals (WTT). The validation procedure specified in IEC 61400-27-1 shall focus on the IEC 61400-21 tests for response to voltage dips and set245 point changes.

– IEC 61400-27-2 shall specify dynamic simulation models for the generic wind power plant topologies / configurations on the market including wind power plant control and auxiliary equipment. In addition IEC 61400-27-2 shall specify a method to create models for future wind power plant configurations. The wind power plant models shall be based on the wind turbine models specified in IEC 61400-27-1. The electrical simulation models specified in IEC 61400-27 shall be independent of any software simulation tool.

7.1.2 WIND TURBINE MODEL INTERFACE

The purpose of this clause is to specify the interface of the wind turbine models. The wind turbine model interfaces to the grid model in the power system simulation tool and to the wind power plant model specified in IEC 61400-27-2. The General dynamic simulation interface between wind turbine model and grid model is illustrated in Figure 7.2.

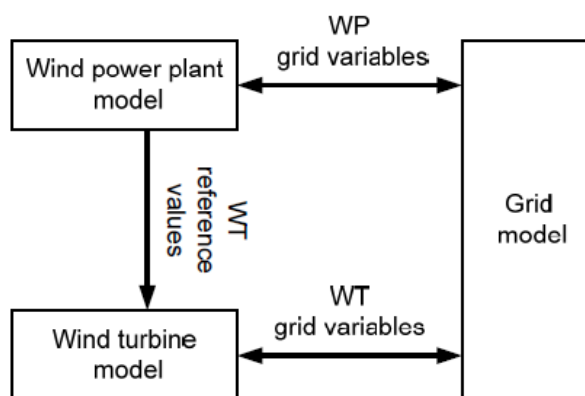


Figure: 7.2. General interface between wind turbine model, grid model and plant control model.

The model can either be excited by an event in the grid model such as a short-circuit, or by a change in a wind turbine reference value from the plant controller. The wind turbine model takes the grid voltages as input from the grid model and gives the grid currents as output. These inputs and outputs refer to the wind turbine terminals (WTT). Wind turbines can receive online reference values, typically via the wind power plant SCADA system from a wind power plant controller or from a remote control. The available set of reference values is different, depending on the wind turbine type, the wind turbine manufacturer and operation mode. The following reference values are considered in the generic wind turbine models:

- Active power reference value.
- Reactive power reference value.
- Voltage reference value.

Note that the wind turbine models can also simulate power factor control mode, but in that case, it is assumed that the power factor reference value of the wind turbine is constant throughout the simulation.

7.2. GENERIC MODULAR STRUCTURE

This standard uses the generic modular structure of the wind turbine model shown in Figure 7.3. The structure is consistent with the interface of the wind turbine model defined in Figure 7.2. The horizontal sequence of blocks in the middle reflects the physical power flow, while protection and control is shown above and below respectively.

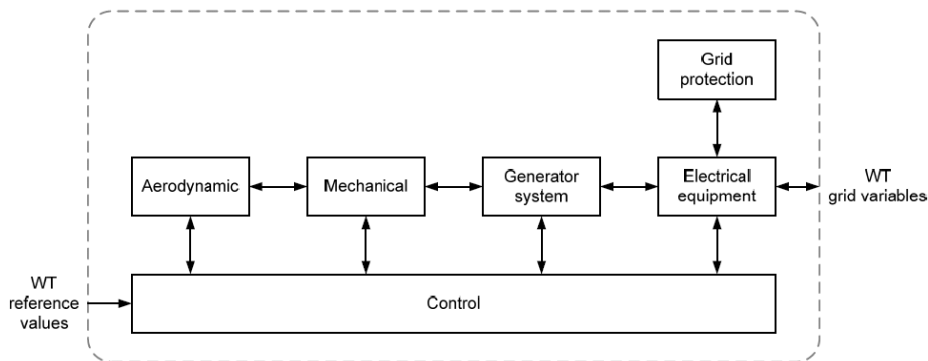


Figure 7.3: Generic modular structure of wind turbine models.

7.3 TYPE 3

7.3.1 DEFINITION OF TYPE 3(DFIG)

A type 3 wind turbines uses a doubly fed induction generator (DFIG), where the stator is directly connected to the grid and the rotor is connected through a back-to-back power converter. Figure 7.4 shows the main electrical and mechanical components which are considered in the type 3 wind turbine models in this standard. The power converter consists of the generator side converter (GSC), the line side converter (LSC) and the DC link (DCL). Besides the DCL capacitor (C), it may use a crowbar (CB) to protect the GSC during grid faults, and / or a chopper (CH) to prevent overvoltage in the DCL during the grid fault.

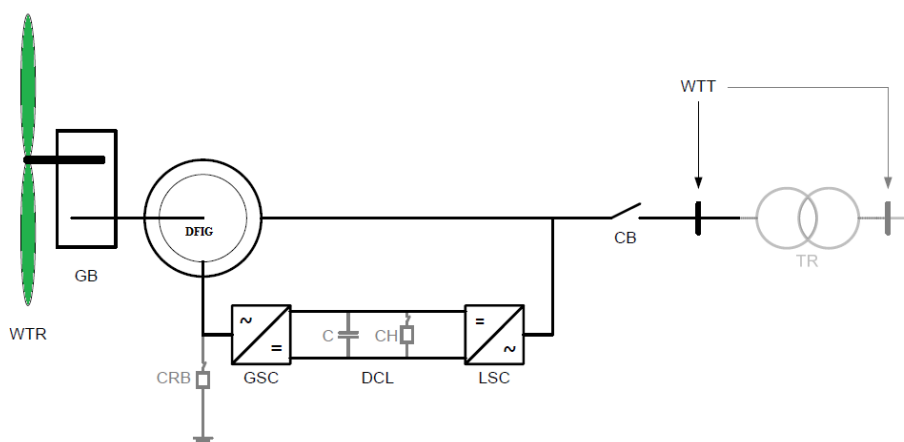


Figure 7.4. Main electrical and mechanical components of type 3 wind turbine.

7.3.2 MODEL SPECIFICATION OF TYPE 3

The generic type 3 model specified in this clause includes modules for the mechanical system as well as the aerodynamics. This level of detail is not always needed. In some cases, one of the generic type 4 models will be sufficient to simulate the behaviour at the wind turbine terminals.

The modular structure for the type 3 wind turbine model is shown in Figure 7.5. The losses in the generator system is neglected setting the wind turbine terminal power p_{WTT} equal to the generator air gap power p_{ag} . Type 3 models can have a converter sufficiently dimensioned for voltage ride-through without bypassing or disconnecting the converter. However, others type 3 wind turbines include a crowbar device which short circuits the rotor during electromagnetic transients and convert the wind turbine generator during this time into an induction machine.

Therefore, two type 3 models are specified below:

- Type 3A: a model with over dimension of the converter
- Type 3B: a model with crowbar

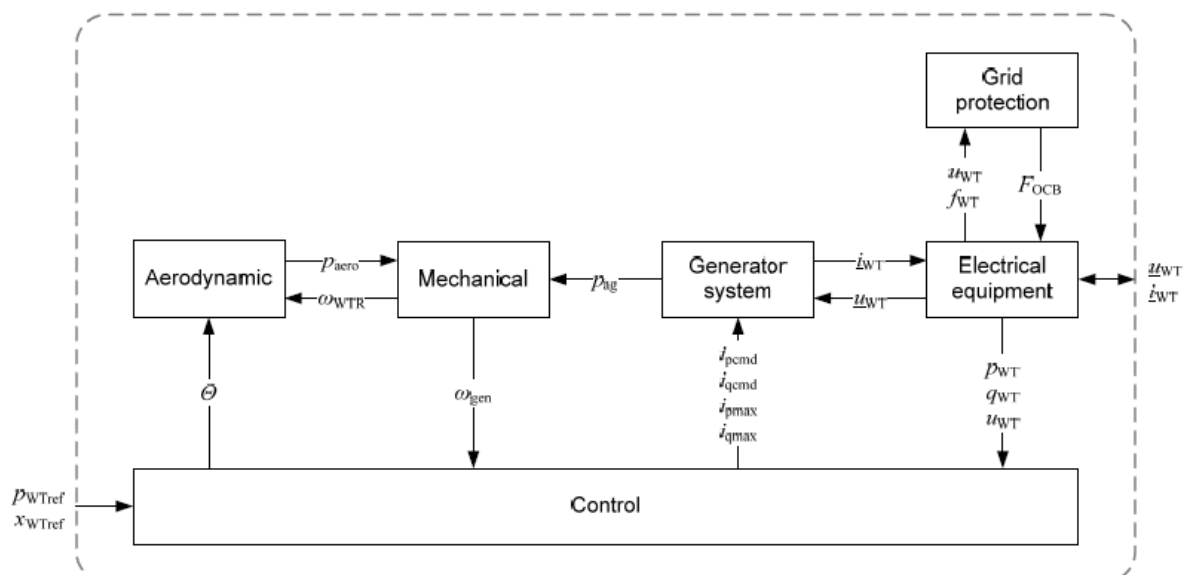


Figure: 7.5. Modular structure for the type 3 wind turbine model.

Figure 7.6 shows the modular structure for the type 3 control models.

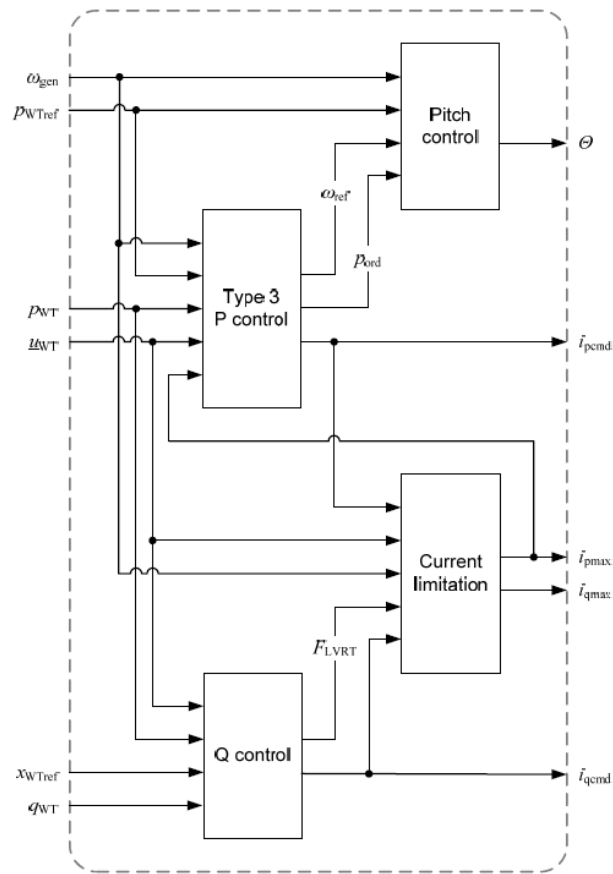


Figure: 7.6. Modular structure for the type 3 control models.

The details for each block are given in the Modules referred to in Table 7.1 and Table 7.2.

Table: 7.1. Modules used in type 3A model.

Block	Module Name
Aerodynamic	Linearised aerodynamic model
Mechanical	Two mass model
Generator system	Type 3A generator set model
Electrical equipment	Circuit breaker model (Transformer model)
Control	P control model type 3 Q control model Current limitation model Pitch angle control model
Grid protection	Grid Protection model

Table: 7.2. Modules used in type 3B model.

Block	Module Name
Aerodynamic	Linearised aerodynamic model
Mechanical	Two mass model
Generator system	Type 3B generator set model
Electrical equipment	Circuit breaker model (Transformer model)
Control	P control model Type 3 Q control model Current limitation model Pitch angle control model
Grid protection	Grid Protection model

7.3.3 LINEARISED AERODYNAMIC MODEL

The linearised aerodynamic model parameters are given in Table 7.3, and the block diagram is given in Figure 7.7.

Table: 7.3. Parameter list for linearised aerodynamic model.

Symbol	Base unit	Description
p_{avail}	P_N	Available aerodynamic power
Θ_0	deg	Pitch angle if the wind turbine is not derated
ω_0	Ω_{base}	Rotor speed if the wind turbine is not derated
$d_{p\Theta}$	P_N / deg	Partial derivative of aerodynamic power with respect to changes in pitch angle
$d_{p\omega}$	P_N / Ω_{base}	Partial derivative of aerodynamic power with respect to changes in WTR speed

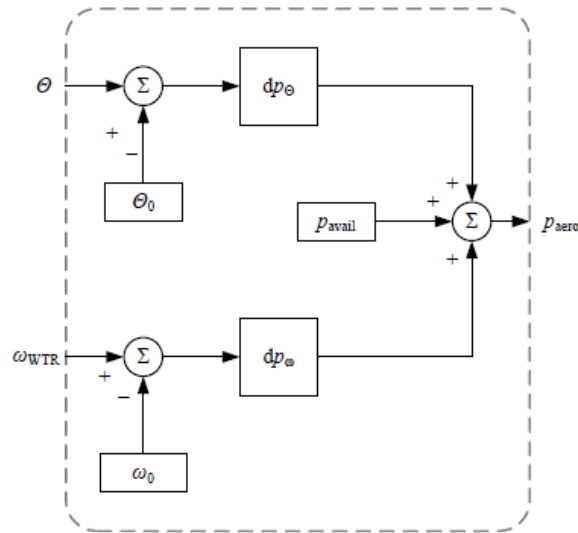


Figure: 7.7. Block diagram for linearised aerodynamic model.

7.3.4 MECHANICAL MODELS

TWO MASS MODEL

The module parameters are given in Table 7.4, and the block diagram is given in Figure 7.8.

Table: 7.4. Parameter list for two-mass model.

Symbol	Base Unit	Description
H_{WTR}	s	Inertia constant of wind turbine rotor
H_{gen}	s	Inertia constant of generator
k_{drt}	T_{base}	Drive train stiffness Type
c_{drt}	T_{base}/ω_{base}	Drive train damping Type

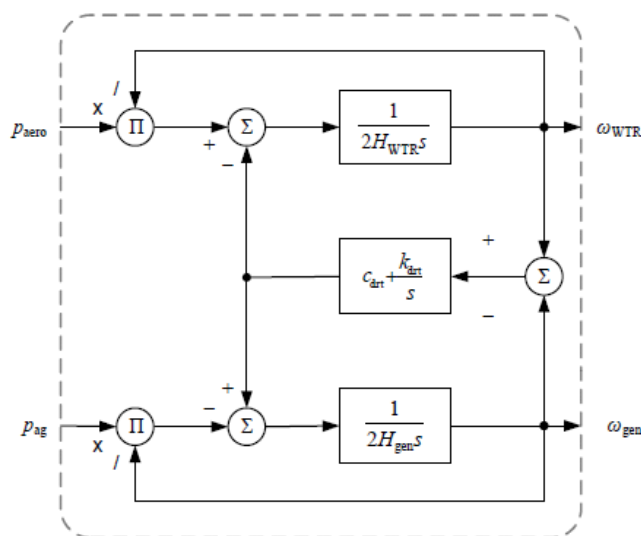


Figure: 7.8. Block diagram for two mass model.

7.3.5 ASYNCHRONOUS GENERATOR MODEL

This standard does not specify a model for the asynchronous generator. The standard asynchronous generator model in the simulation tool should be used. Normal practice for stability studies is to include the rotor flux transients and neglect the stator flux transients.

TYPE 3A GENERATOR SET MODEL

The module parameters are given in Table 7.5, and the block diagram is given in Figure 7.9.

Table: 7.5. Parameter list for type 3A generator set model.

Symbol	Base Unit	Description
K_{PC}	-	Current PI controller proportional gain
T_{ic}	s	Current PI controller integration time constant
x_s	Z_{base}	Electromagnetic transient reactance
di_{pmax}	I_{base}/s	Maximum active current ramp rate
di_{qmax}	I_{base}/s	Maximum reactive current ramp rate

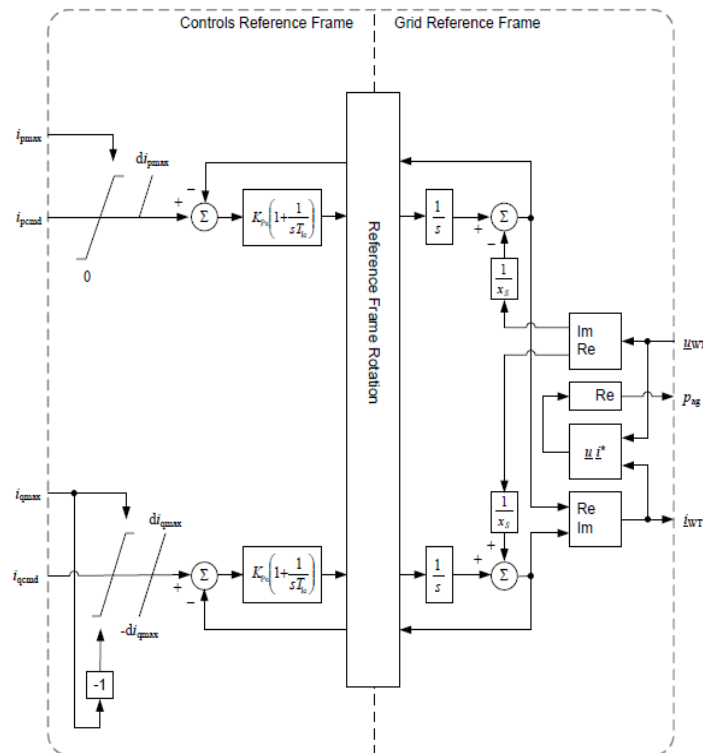


Figure: 7.9. Block diagram for type 3A generator set model.

TYPE 3B GENERATOR SET MODEL

The module parameters are given in Table 7.6, and the block diagram is given in Figure 7.10.

Table: 7.6. Parameter list for type 3B generator set model.

Symbol	Base Unit	Description
T_g	-	Current PI controller proportional gain
di_{pmax}	I_{base}/s	Maximum active current ramp rate
di_{qmax}	I_{base}/s	Maximum reactive current ramp rate
x_s	Z_{base}	Electromagnetic transient reactance
$F_{duCW()}$	s vs U_n	Crowbar duration versus voltage variation look-up table
T_{wo}	s	Time constant for crowbar washout filter
M_{WTcp}	-	Crowbar control mode

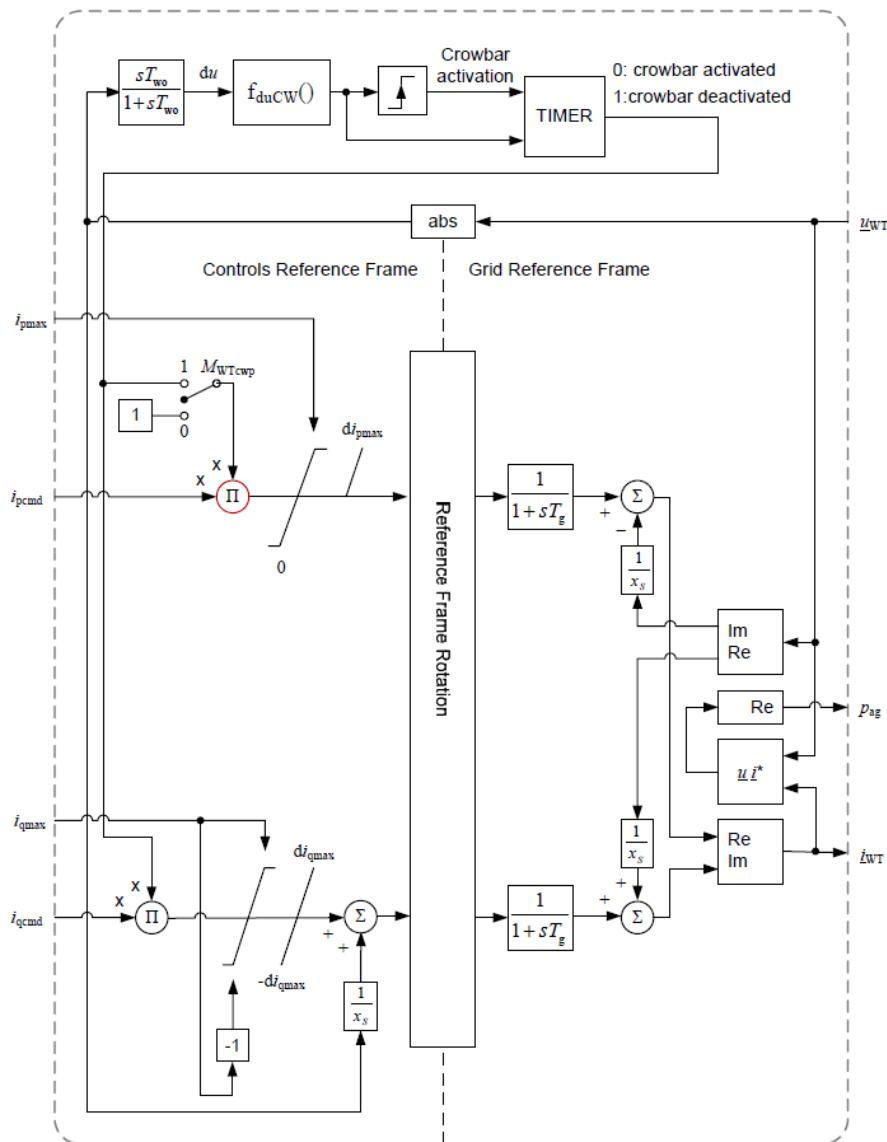


Figure: 7.10. Block diagram for type 3B generator set model.

7.3.6 ELECTRICAL EQUIPMENT

SHUNT CAPACITOR MODEL

This standard does not specify a model for shunt capacitors. For fixed capacitor banks (FC), the standard fundamental frequency capacitor model in the simulation tool should be used. For variable capacitor banks (VC), a standard SVC model can be used. Normally, the turbine compensations do not include the reactor, which is standard in SVCs.

CIRCUIT BREAKER MODEL

The standard circuit breaker model in the simulation tool should be used. The circuit breaker model must open the circuit breaker when it receives the F_{OCB} flag.

TRANSFORMER MODEL

This standard does not specify a model for the transformer. The standard transformer model in the simulation tool should be used.

7.4 CONTROL MODELS

7.4.1 PITCH CONTROL EMULATOR MODEL

The module parameters are given in Table 7.7, and the block diagram is given in Figure 7.11.

Table: 7.7. Parameter list.

Symbol	Base Unit	Description
T_{Pe}	s	Time constant in generator air gap power lag
$K_{\omega aero}$	P_N/ω_{base}	Aerodynamic power change vs. ω WTR change
K_{droop}	-	Power error gain
$K_{P,pce}$	-	Pitch control emulator proportional constant
$K_{I,pce}$	s^{-1}	Pitch control emulator integral constant
p_{imax}	P_N	Maximum steady state power
p_{imin}	P_N	Minimum steady state power
T_1	s	First time constant in pitch control lag
T_2	s	Second time constant in pitch control lag
ω_{ref}	ω_{base}	Rotor speed in initial steady state

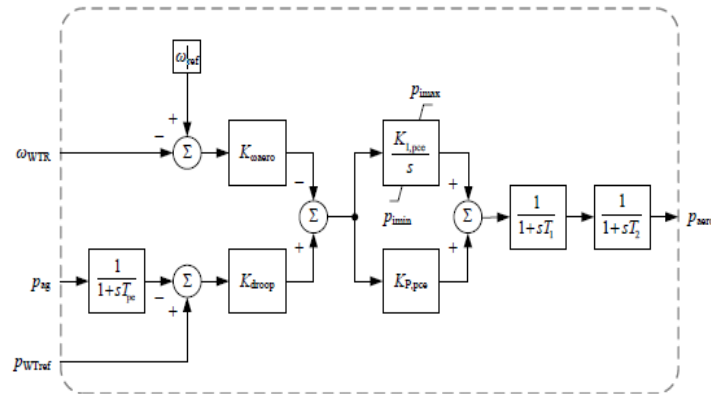


Figure: 7.11. Block diagram for pitch control emulator model.

7.4.2 P CONTROL MODEL TYPE 3

The module parameters are given in Table 7.8, and the block diagram is given in Figure 7.12 (a).

Table: 7.8. Parameter list.

Symbol	Base Unit	Description
ω_{offset}	ω_{base}	Offset to reference value that limits controller action during rotor speed changes
$f_{p\omega}()$	P_N vs. Ω_{base}	Power vs. speed lookup table
K_{Pp}	$T_{\text{base}}/\Omega_{\text{base}}$	PI controller proportional gain
K_{Ip}	$T_{\text{base}}/\Omega_{\text{base}}/s$	PI controller integration parameter
$T_{p\text{filt}}$	s	Filter time constant for power measurement
$T_{u\text{filt}}$	s	Filter time constant for voltage measurement
$T_{\omega\text{ref}}$	s	Time constant in speed reference filter
$T_{\omega\text{filt}}$	s	Filter time constant for generator speed measurement
K_{DTD}	P_N/Ω_{base}	Gain for active drive train damping
$p_{DTD\text{max}}$	P_N	Maximum active drive train damping power
ζ	-	Coefficient for active drive train damping
ω_{DTD}	Ω_{base}	Active drive train damping frequency, can be calculated from two mass model parameters in Table 7.4. $\omega_{DTD} = \sqrt{k_{drt} \left(\frac{1}{2H_{WTR}} + \frac{1}{2H_{gen}} \right)}$
T_{pord}	s	Time constant in power order lag
$d_{p\text{max}}$	P_N/s	Maximum wind turbine power ramp rate
u_{pdip}	U_n	Voltage dip threshold for P-control. Part of turbine control, often different (e.g 0.8) from converter thresholds
R_{ramp}	T_{base}/s	Ramp limitation of torque, required in some grid codes
T_{emin}	T_{base}	Minimum electrical generator torque
T_{uscale}	T_{base}/U_n	Voltage scaling factor of reset-torque

7.4.3 Q CONTROL MODEL

The Q-control model supports the 4 different general Q control modes M_{qG} listed in Table 7.9.

Table: 7.9. General wind turbine Q control modes M_{qG} .

M_{qG}	Description
$M_{G,u}$	Voltage control
$M_{G,q}$	Reactive power control
$M_{G,qol}$	Open loop reactive power control (only used with closed loop at plant level)
$M_{G,pf}$	Power factor control

The Q-control model supports the 3 different LVRT Q control modes M_{qLVRT} listed in Table 7.10. The control modes specify the reactive current injection during the voltage dip, and in an optional post-fault period.

Table: 7.10. LVRT Q control modes M_{qLVRT} .

M_{qLVRT}	Description
$M_{LVRT,1}$	Voltage dependent reactive current injection
$M_{LVRT,2}$	Reactive current injection controlled as the pre-fault value plus an additional voltage dependent reactive current injection
$M_{LVRT,3}$	Reactive current injection controlled as the pre-fault value plus an additional voltage dependent reactive current injection during fault, and as the pre-fault value plus an additional constant reactive current injection post fault

The module parameters for the Q-control module are given in Table 7.11, and the block diagram is given in Figure 7.12(b). Warning: Extreme care should be taken in coordinating the parameters u_{dbd1} , u_{dbd2} and u_{dip} , u_{up} so as not to have an unintentional response from the reactive power injection control loop.

Table: 7.11. Parameter list.

Symbol	Base Unit	Description
M_{qG}	-	General Q control mode (see Table 18 and Table 21)
M_{qLVRT}	-	LVRT Q control modes (see Table 19 and Table 23)
T_{ufilt}	s	Voltage measurement filter time constant
T_{pfilt}	s	Power measurement filter time constant
K_{Pq}	U_n/P_N	Reactive power PI controller proportional gain
K_{Iq}	$U_n/P_N/s$	Reactive power PI controller integration gain
K_{Pu}	I_{base}/U_n	Voltage PI controller proportional gain
K_{Iu}	$I_{base}/U_n/s$	Voltage PI controller integration gain
u_{db1}	U_n	Voltage dead band lower limit
u_{db2}	U_n	Voltage dead band upper limit
K_{qv}	I_{base}/U_n	Voltage scaling factor for LVRT current
u_{max}	U_n	Maximum voltage in voltage PI controller integral term
u_{min}	U_n	Minimum voltage in voltage PI controller integral term
u_{ref0}	U_n	User defined bias in voltage reference $uWTref = u_{ref0} + \Delta uWTref$ (used when $MqG = MG,u$).
u_{qdip}	U_n	Voltage threshold for LVRT detection in q control
T_{qord}	s	Time constant in reactive power order lag
T_{iq}	s	Time constant in reactive current lag
T_{post}	s	Length of time period where post fault reactive power is injected
q_{max}	P_N	Maximum reactive power
q_{min}	P_N	Minimum reactive power
i_{qmax}	I_{base}	Maximum reactive current injection
i_{qmin}	I_{base}	Minimum reactive current injection
i_{qh1}	I_{base}	Maximum reactive current injection during dip
i_{qpost}	I_{base}	Post fault reactive current injection
r_{droop}	Z_{base}	Resistive component of voltage drop impedance
x_{droop}	Z_{base}	Inductive component of voltage drop impedance

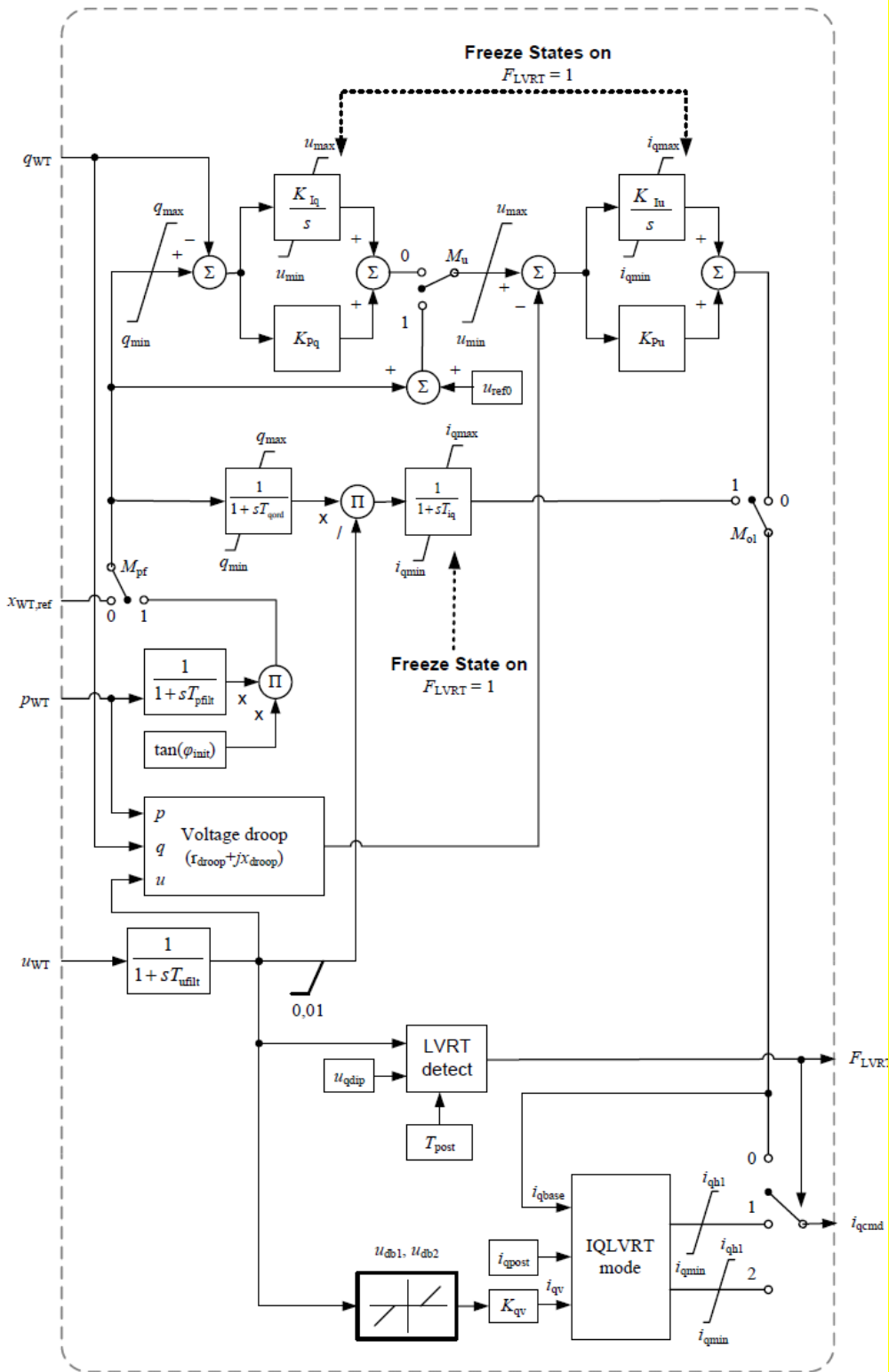


Figure: 7.12(b). Block diagram for Q control model.

The external reference x_{WTref} can either be a reactive power or delta voltage command from the park controller, depending on the Q control mode. If no park controller model is applied, this signal is initialized as a constant input. The general Q control mode is selected by the combination of the mode switches M_u , M_{ol} and M_{pf} specified in Table 7.12.

Table: 7.12. General Q control mode selection.

General Q control mode	M_u	M_{ol}	M_{pf}
$M_{G,u}$	1	0	0
$M_{G,q}$	0	0	0
$M_{G,qol}$	-	1	0
$M_{G,pf}$	0	0	1

The “LVRT detect” block outputs the $FLVRT$ flag in 1 of 3 stages described in Table 7.13.

Table: 7.13. Description of FLVRT flag values.

F_{LVRT}	Description
0	Normal operation ($u_{WT} > u_{dip}$)
1	During fault ($u_{WT} \leq u_{dip}$)
2	Post fault stays in stage 2 with ($u_{WT} > u_{dip}$) for $t = T_{post}$

The “IQLVRT mode” block selects the reactive current during ($F_{LVRT} = 1$) and post ($F_{LVRT} = 2$) fault as a sum of contributions from the voltage dependent current i_{qv} , the frozen current i_{qbase} and the constant post fault current i_{qpost} . Table 7.14 specifies 3 the reactive current injection for the 3 options defined in Table 19. It should be noted that i_{qv} will be zero in some configurations by setting $K_{qv} = 0$.

Table: 7.14. IQLVRT block.

LVRT Q control mode	$F_{LVRT} = 1$	$F_{LVRT} = 2$
$M_{LVRT,1}$	i_{qv}	i_{qv}
$M_{LVRT,2}$	$i_{qbase} + i_{qv}$	$i_{qbase} + i_{qv}$
$M_{LVRT,3}$	$i_{qbase} + i_{qv}$	$i_{qbase} + i_{qpost}$

The “Voltage droop” block shall calculate the voltage in a point which is located with the serial impedance distance $r+jx$ from WTT (typically a transformer), i.e.

$$u = \sqrt{\left(u_{WT} - r_{droop} \frac{P_{WT}}{u_{WT}} - x_{droop} \frac{Q_{WT}}{u_{WT}}\right)^2 + \left(x_{droop} \frac{P_{WT}}{u_{WT}} - r_{droop} \frac{Q_{WT}}{u_{WT}}\right)^2} \quad (7.1)$$

T_{iq} filter represent fast current dynamics which are fast enough not to consider in this model but the filter is kept because a state is required for freezing on $F_{LVRT} = 1$.

7.4.4 CURRENT LIMITATION MODEL

The current limitation model combines the physical limits. The module parameters are given in Table 7.15, and the block diagram is given in Figure 7.13.

Table: 7.15. Parameter list.

Symbol	Base Unit	Description
i_{max}	I_{base}	Maximum continuous current at the wind turbine terminals
$i_{max,dip}$	I_{base}	Maximum current during voltage dip at the wind turbine terminals
M_{DFSLim}	-	Limitation of type 3 stator current (0: total current limitation, 1: stator current limitation)
M_{qpri}	-	Prioritisation of q control during LVRT (0: active power priority –1: reactive power priority)
$i_{pVDL}()$	I_{base} vs. U_n	Lookup table for voltage dependency of active current limits
$i_{qVDL}()$	I_{base} vs. U_n	Lookup table for voltage dependency of reactive current limits
T_{ufilt}	s	Voltage measurement filter time constant

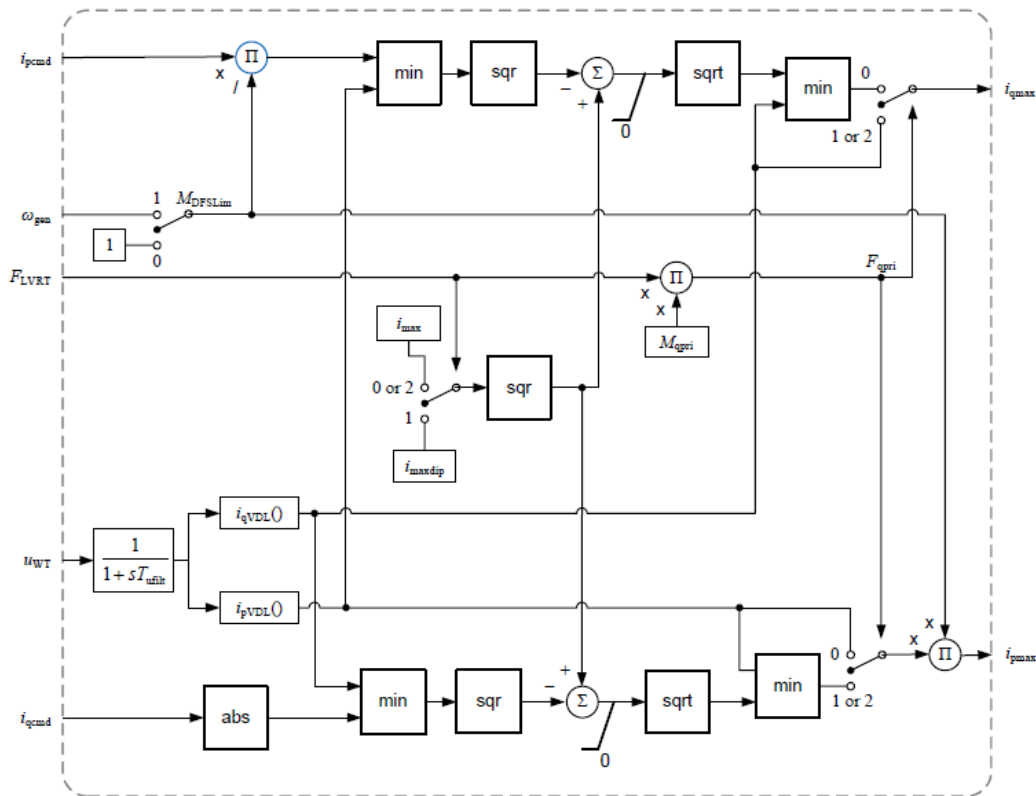


Figure: 7.13 Block diagram for current limiter.

7.4.5 PITCH ANGLE CONTROL MODEL

The module parameters are given in Table 7.15, and the block diagram is given in Figure 7.14.

Table: 7.15. Parameter list.

Symbol	Base Unit	Description
$K_{P\omega}$	deg/ Ω_{base}	Speed PI controller proportional gain
$K_{I\omega}$	deg/ Ω_{base}/s	Speed PI controller integration gain
K_{Pc}	deg/ P_N	PN Power PI controller proportional gain
K_{Ic}	deg/ P_N/s	Power PI controller integration gain
K_{PX}	Ω_{base}/P_N	Pitch cross coupling gain
θ_{max}	deg	Maximum pitch angle
θ_{min}	deg	Minimum pitch angle
$d\theta_{max}$	deg/s	Maximum pitch positive ramp rate
$d\theta_{min}$	deg/s	Maximum pitch negative ramp rate
T_{θ}	s	Pitch time constant

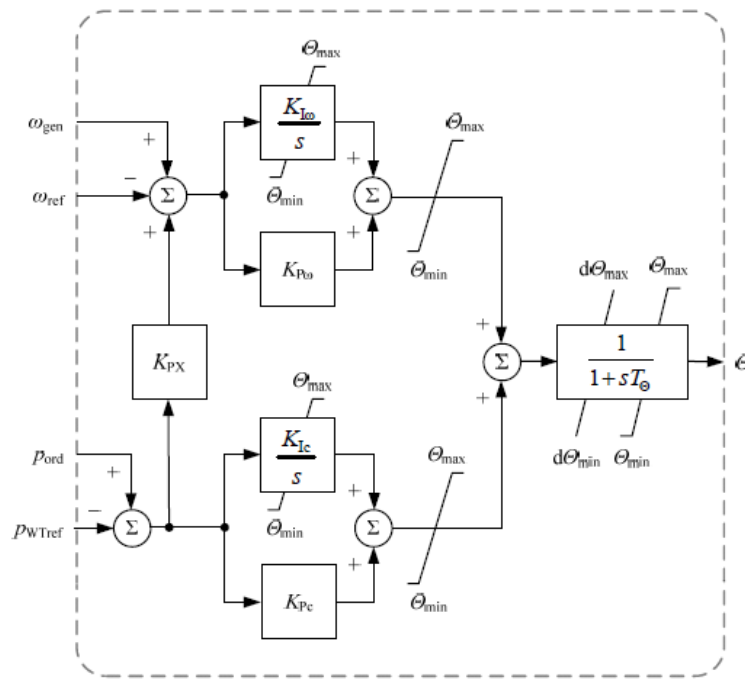


Figure: 7.14. Block diagram for pitch angle control model.

7.4.6 GRID PROTECTION MODEL

The grid protection model includes protection against over and under voltage, and against over and under frequency. The grid protection is characterized by a set of protection levels and a corresponding set of disconnection times as defined and tested in IEC 61400-2115. The module parameters are given in Table 7.16.

Table: 7.16. Parameter list.

Symbol	Base Unit	Description
u_{over}	U_n	Set of wind turbine over voltage protection levels
T_{uover}	s	Set of corresponding wind turbine over voltage protection disconnection times
u_{under}	U_n	Set of wind turbine under voltage protection levels
T_{uunder}	s	Set of corresponding wind turbine under voltage protection disconnection times
f_{over}	f_n	Set of wind turbine over frequency protection levels
T_{fover}	s	Set of corresponding wind turbine over frequency protection disconnection times
f_{under}	f_n	Set of wind turbine under frequency protection levels
T_{funder}	s	Set of corresponding wind turbine under frequency protection disconnection times

7.5 SIMULATION RESULTS

7.5.1 STEADY STATE ANALYSIS

Figure 7.15 shows the steady state waveform for the Type- 3A generator with constant wind speed. From the waveform, we can see that there will be maximum generated power for $i_pcmd=1pu$ with grid voltage of u_WT 1pu.

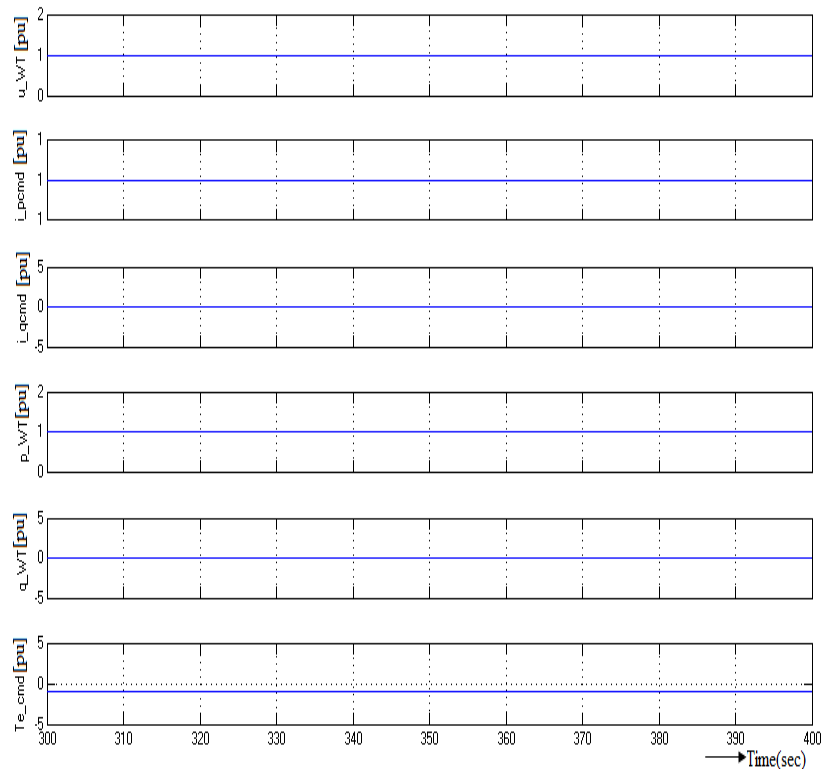


Figure: 7.15. Steady State waveform for the constant wind speed.

7.5.2 LVRT ANALYSIS

The simulations in this section have been carried out using the test system described in [9-21], see also Fig. 7.17. The test system includes a Thevenin equivalent model for the external grid, step-up transformers, the collection cable, a circuit breaker, and the wind turbine generator.

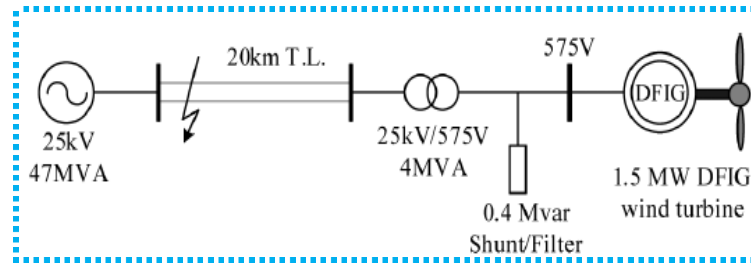


Figure: 7.16. Single line diagram of the test system.

The parameters of the electrical components of the test system can be found in [21]. A typical 3-phase short circuit of 400 ms duration has been simulated at the MV bus, as illustrated in Figure 7.16. The result shows that the priority of the reactive current component is applied in the current limitation block during the LVRT period. This feature provides with the capability to represent a Type-3A WEG response during voltage dips for different grid codes' requirements regarding the active/reactive current injection during the low voltage instant. In this set of results reactive power current is prioritized during the voltage dip. Figure (7.17)-(7.19) illustrate the voltage, the reactive current components as well as the LVRT and F_{postFRT} detection signals. As soon as the short circuit is cleared the F_{postFRT} signal remains equal to one for $T_{\text{post}}=1\text{sec}$.

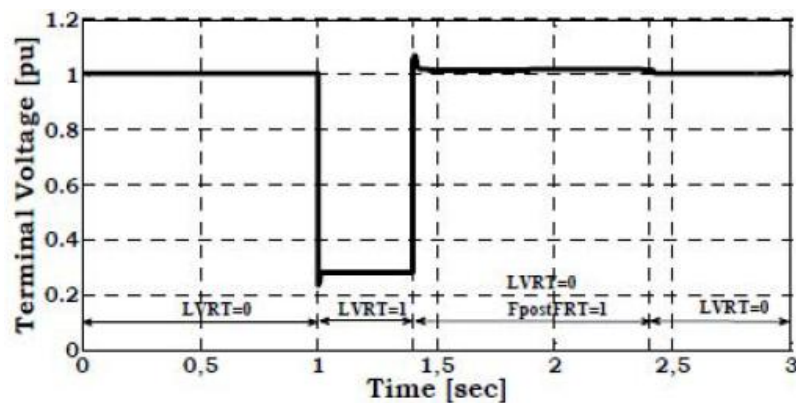


Figure: 7.17. Voltage at the WT terminals during and short after the short Circuit

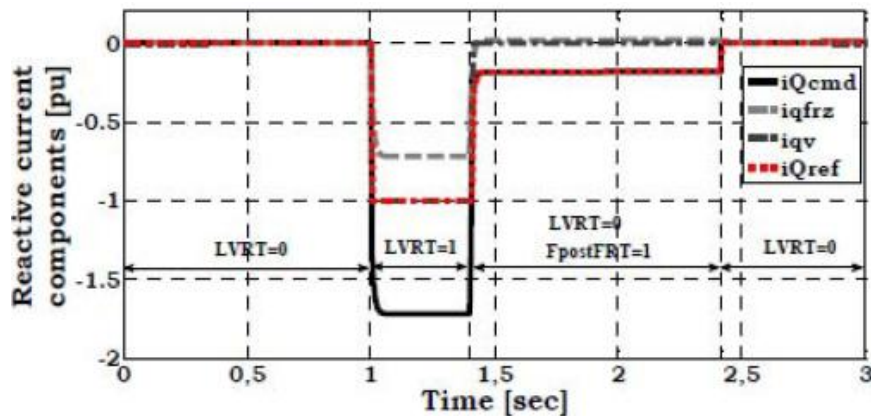


Figure: 7.18. The LVRT and FpostFRT signals during and short after the short circuit.

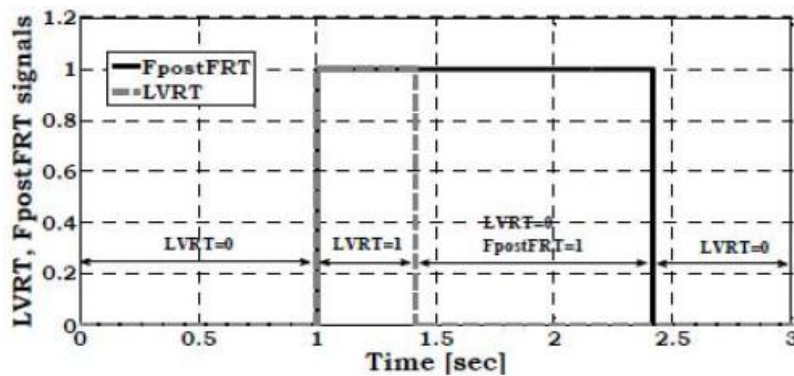


Figure: 7.19. The LVRT and FpostFRT signals during and short after the short circuit.

The active and reactive power response of the WEG is given in Figure 7.20 and 7.21 respectively. Due to the reactive power prioritization, during the voltage dip reactive current is injected as defined in the LVRT strategy applied – see also Section II above –, forcing active power to zero as long as the voltage remains low. At the fault clearance, the sudden increase in the voltage at the WEG terminal leads to a surge of reactive power while in the post fault period, as long as the F_{postFRT} signal remains equal to one, reactive power is injected to the grid offering voltage support to the grid. Before and after the fault, the Power Factor control has been chosen, thus the WEG keeps unity power factor.

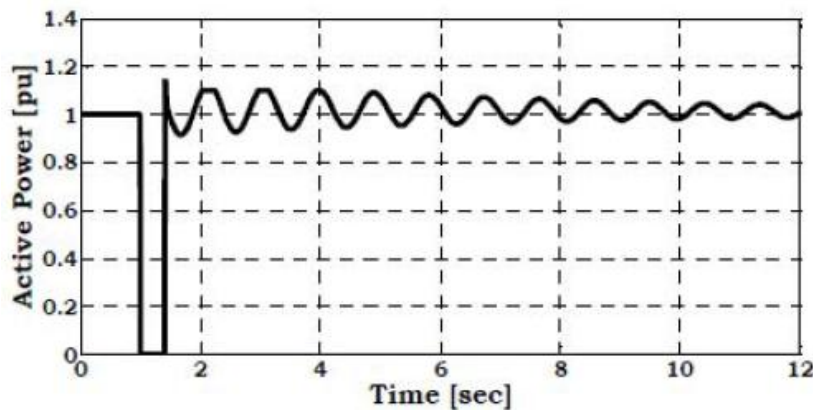


Figure: 7.20. Active power response during and short after the short circuit.

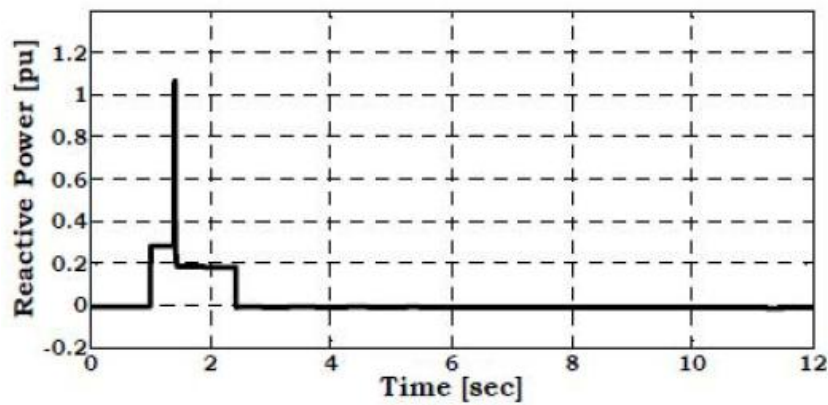


Figure: 7.21. Reactive power response during and short after the short Circuit.

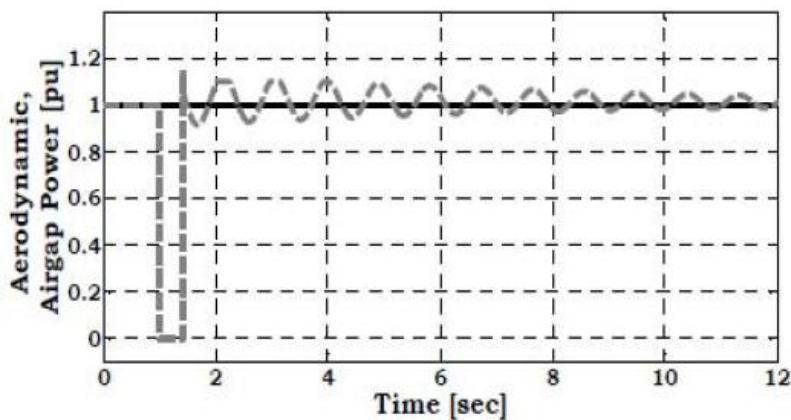


Figure: 7.22. Aerodynamic and airgap power during and short after the short circuit.

Fig. 7.22 shows the results for the aerodynamic and airgap power, which are inputs to the mechanical system of the model. The airgap power is calculated at the generator, thus is equal to the electrical power injected to the grid as no losses are taken into account.

The torsional oscillations, which were simulated using the 2-mass model for the mechanical model, are visible in the rotor speed as well as in the electrical power produced by the WEG, see Figure 7.20 and 7.23. At the fault instant, the low voltage leads to a sudden decrease of the electrical torque resulting in the corresponding increase of the rotor speed as long as the voltage remains low. The oscillation frequency modes of these oscillations can be calculated based on the parameters of the mechanical system [10].

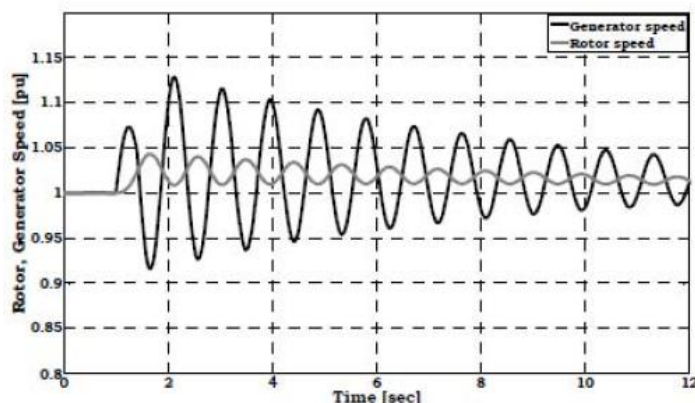


Figure: 7.23. Generator and rotor speed during and short after the short circuit.

7.6 SUMMARY

In this chapter the implementation and performance of the standard IEC proposed Type 3A model for WEGs has been described and the simulation results were presented. The general structure of the standard models defined in Part 1 of the IEC 61400-27 series has been presented. The standard Type 3A model for WEGs includes a constant aerodynamic torque model, the active and reactive power control loop, a 2-mass mechanical model, the generator model including the current limiter with prioritization of active or reactive power and the protection function for under/over voltage and frequency.

The reactive power loop comprises a LVRT control strategy which defines the reactive current output of the controller during and short after a voltage dip at the wind turbine terminals. Results from a short circuit simulated were shown for the main electrical variables of the system and a comparison has been presented to illustrate the prioritization function of active or reactive power, which is part of the current limiter block.

The performance of the model during and short after the voltage dip is considered realistic as compared to field measurements for voltage dips provided by manufacturers in relevant publications. Validation of this standard Type 3A model implemented in Matlab/Simulink and DIgSILENT Power Factory simulation platform against field measurements is further needed to ensure the applicability of this model in power system studies.

Following the validation procedure described in Part 1 of the IEC 61400-27 series, the model will soon be tested against real measurements provided by manufacturers and the parameterization of the model will be thus improved to match a real WEG performance during transient events in the power system e.g. voltage dips.

7.7 REFERENCES

- [1] Prabha Kundur, John Paserba, Venkat Ajjarapu, Göran Andersson, Anjan Bose, Claudio Canizares, Nikos Hatzargyriou, David Hill, Alex Stankovic, Carson Taylor, Thierry Van Cutsem, Vijay Vittal. Definition and Classification of Power System Stability. IEEE/CIGRE Joint Task Force on Stability Terms and Definitions. IEEE Transactions on Power Systems, Vol. 19, No. 2, pp. 1387-1401. May 2004.
- [2] Kristoffersen JR, Christiansen P. Horns rev offshore windfarm: its main controller and remote control system. Wind Eng 2003;27(5):351–66.
- [3] Hansen, A.D.; Sørensen, P.; Iov, F.; Blaabjerg, F., Centralised power control of wind farm with doubly fed induction generators. Renewable Energy (2006) 31 , 935-951.
- [4] A. Ellis, Y. Kazachkov, E. Muljadi, P. Pourbeik and J. Sanchez-Gasca, “Description and Technical Specifications for Generic WTG Models – a status report”, Proceedings of the 2011 IEEE PES PSCE, March 2011, Phoenix, Arizona, USA.
- [5] Jauch, C.; Sørensen, P.; Jensen, B.B., Simulation model of a transient fault controller for an active-stall wind turbine. Wind Eng. (2005) 29 , 33-48.
- [6] J.Fortmann, S. Engelhardt, J. Kretschmann, C. Feltes, M. Janssen, T. Neumann and I. Erlich, “Generic Simulation Model for DFIG and Full Size Converter based Wind Turbines”, Proceedings of the 9th International Workshop on Large-Scale Integration of Wind Power, Quebec/Canada, October 2010.
- [7] Sørensen, Poul Ejnar ; Andresen, Björn ; Bech, John ; Fortmann, Jens ; Pourbeik, Pouyan. Progress in IEC 61400-27. In Proceedings of the 11th International Workshop on Large-Scale Integration of Wind Power into Power Systems as well as on Transmission Networks for Offshore Wind Power Plants, 2012, Lisbon (PT), 13-15 Nov.
- [8] Sørensen, Poul Ejnar ; Andresen, Björn ; Fortmann, Jens ; Johansen, Knud ; Pourbeik, Pouyan. Overview, status and outline of the new IEC 61400 -27 – Electrical simulation models for wind power generation. In Proceedings 10th International Workshop on Large-Scale Integration of Wind Power into Power Systems as well as on Transmission Networks for Offshore Wind Power Plants, 2011, Aarhus (DK), 25-26 Oct.
- [9] IEC 61400-27 Committee Draft, Wind Turbines Part 27-1 Electrical simulation models for wind power generation Wind turbines, IEC Std. Committee Draft(CD)88/424/CD January 2012.
- [10] A. Ellis, Y. Kazachkov, E. Muljadi, P. Pourbeik, and J.Sanchez- Gasca, “Description and technical specifications for generic WTG models-a status report,” in Power Systems Conference and Exposition (PSCE), 2011 IEEE/PES, Mar. 2011, pp. 1–8.
- [11] P. Sørensen, B. Andresen, J. Fortmann, K. Johansen, and P. Pourbeik, “Overview, status and outline of the new iec 61400 -27 electrical simulation models for wind power generation,” in The 10th International Workshop on Large-Scale Integration of Wind Power into Power Systems, Aarhus, Denmark, Oct. 2011.

- [12] V. Akhmatov, "IEC type 1 and type 2 generic wind turbine models: Draft 01," Tech. Rep., Dec. 2010.
- [13] IEC 61400-21 ed. 2, Wind Turbine Generator System–Part 21 Measurement and Assessment of Power Quality Characteristics of Grid Connected Wind Turbines, IEC Std., 2008.
- [14] T.Thiringer and J. Luomi, "Comparison of reduced-order dynamic models of induction machines," Power Systems, IEEE Transactions on, vol. 16, no. 1, pp. 119 –126, Feb 2001.
- [15] S.Chandrasekaran, C. Rossi, D. Casadei , "Modeling and Simulation of Grid Connected Wind Energy Conversion System (WECS) Based on a Doubly Fed Induction Generator (DFIG)", the Third International Renewable Energy Congress, December 20-22, 2011– Hammamet, Tunisia.
- [16] A.D. Hansen, F. Iov, P. Sørensen, N. Cutululis, C. Jaush, and F.Blaabjerg, "Dynamic wind turbine models in power system simulation tool DIgSILENT," Risø National Laboratory, Roskilde, Denmark, Tech. Rep. Risø-R-1400, Aug. 2007.
- [17] P.Sørensen, A. D. Hansen, P. Christensen, M. Mieritz, J. Bech, B. B. Jensen, and H. Nielsen, "Simulation and verification of transient events in large wind power installations," Risø National Laboratory, Roskilde, Denmark, Tech. Rep. Risø-R-1331, Oct. 2003.
- [18] T. Ackermann, Wind power in power systems, 2nd edition, John Wiley & Sons, 2012.
- [19] V. Akhmatov, "Modeling of variable-speed wind turbines with doubly fed induction generators in short-term stability analysis," in Proceedings of the 3rd International Workshop on Transmission Networks for Offshore Wind Farms, Apr. 2002.
- [20] P. Kundur, Power System Stability and Control. McGraw- Hill, 1994.
- [21] NERC IVGTF 1-1, Standard Models for Variable Generation, May 18, 2010, http://www.nerc.com/docs/pc/ivgtf/IVGTF_Report_PhaseII_Task1-1_Fi

CHAPTER 8

SUMMARY

This chapter summarizes the findings of the presented PhD project “Grid Connected Doubly Fed Induction Generator Based Wind Turbine under LVRT”.

- Detailed dynamic modeling of DFIG based Wind Turbine was developed under simulation tools with respect to power system network.
- Power flow analysis of grid connected DFIG based wind turbine under varying wind velocity was studied.
- Decoupling control algorithm was developed so that the active and reactive power can be controlled independently.
- A control strategy of a DFIG wind turbine system equipped with an active crowbar against severe grid faults was proposed.
- In order to reduce the activated time of the crowbar as much as possible, an improved hysteresis control strategy has been proposed.
- Moreover, the reactive power control has been adopted to decrease the oscillations of the transient current both during the voltage dip and after the clearance of the fault. With the help of the proposed control strategy, the WECS kept under control for most of the time during voltage dip.
- Simulation results have shown that an enhanced low voltage ride through capability of the generator can be achieved with the proposed technique.
- To compensate the faulty line voltage DVR was proposed and the results for simulation and experiments are presented.
- VPI controller was proposed to improve the system performance under unbalanced grid condition.
- IEC standard 61400-27-1 for Type 3 machine (Doubly fed induction generator) was developed using Matlab/Simulink. The type 3 machine was simulated and tested under steady state and LVRT.
- The experimental test was carried out on DFIG wind turbine system under steady state and unbalanced grid supply and the best control strategy was highlighted in the table as per grid support capability.

ANNEXURE I

2MW-DFIG WIND TURBINE SIMULATION USING DIGSILENT

In this section, the power flow analysis of 2MW DFIG wind turbine has simulated using power system simulation tool DIGSILENT, power flow analysis can be used to validate the system behavior with respect to different operating condition. Based on the step response analysis, the controller parameter can be designed and optimized and this approach serves to verify the model under different operating conditions. The parameter of 2MW DFIG is shown in Annexure II.

SYSTEM PERFORMANCE UNDER DETERMINISTIC WIND SPEEDS

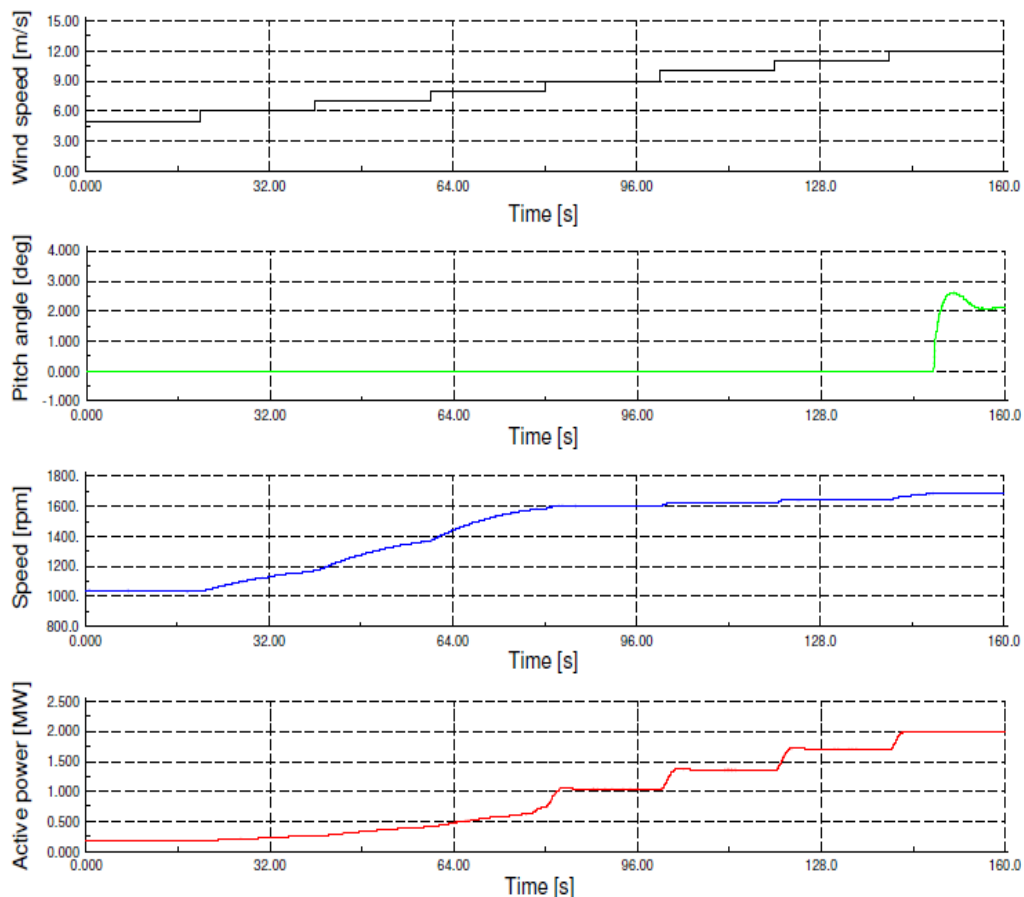


Figure: A.I.1.DFIG wind turbine: Wind speed, pitch angle, generator speed and active power for steps in wind of 1 m/s from 5 m/s up to 12 m/s.

In Figure A.I.1 typical quantities of the DFIG Wind turbine system, as pitch angle, generator speed and power are shown for steps in wind of 1 m/s every 20 seconds. Figure A.I.1 indicates that for lower wind speeds below 12 m/s the pitch mechanism is passive and the pitch angle is kept to its optimal value (i.e. zero for the considered turbine). Meanwhile, the

power controller controls the active power to the active power reference signal provided by the maximum power tracking look-up table. The generator speed is continuously adapted to the wind speed, in such a way that maximum power is extracted out of the wind. Notice that the response time in the steps is bigger at lower wind speeds than at higher wind speeds. When the wind steps up to 12 m/s and exceeds rated wind speed (rated wind speed = 11.8 m/s) and the speed reaches its rated value of 1686 rpm, both speed controller and active power controller are active and the power is limited to the rated value of 2 MW.

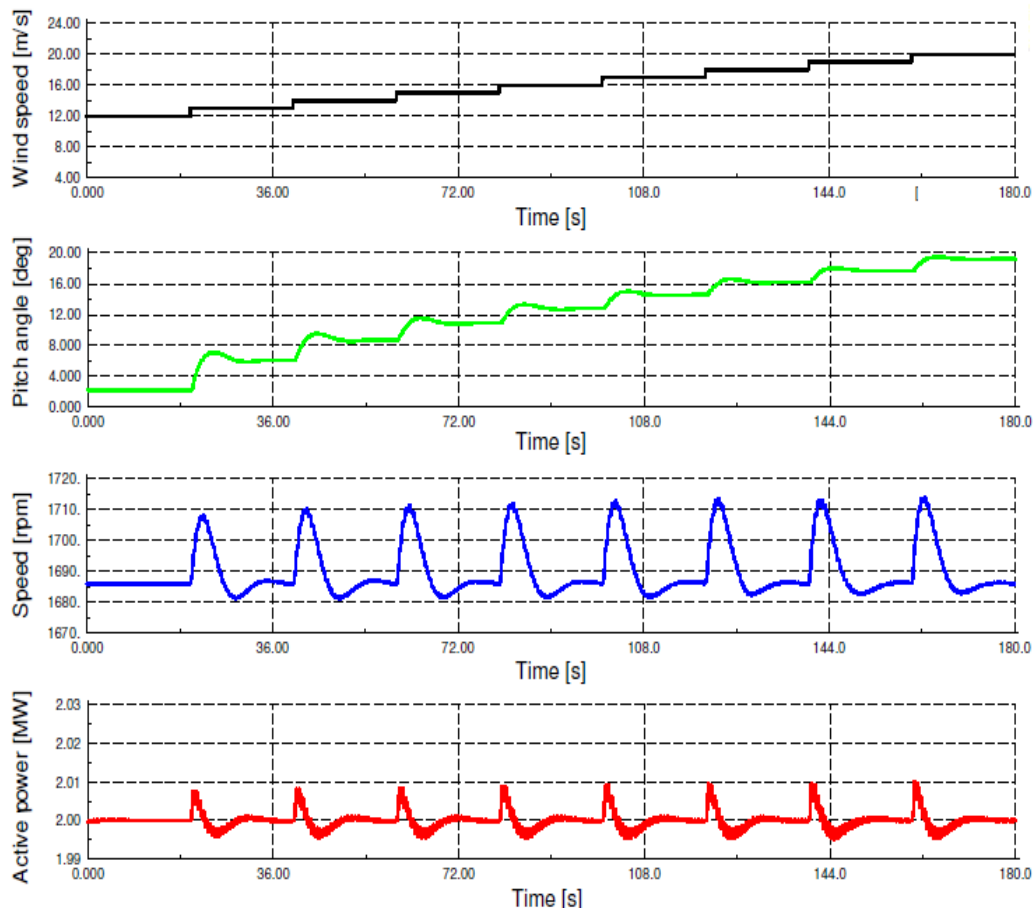


Figure: A.I.2.DFIG wind turbine: Wind speed, pitch angle, generator speed and active power for steps in wind of 1 m/s from 12 m/s up to 20 m/s.

The step response of pitch angle, speed and power for wind speeds higher than 12 m/s is presented in Figure A.I.2. The steps in wind speed yield changes in both the pitch angle and the generator speed. The step response of the pitch angle and generator speed does not present big overshoots and oscillations. Notice, that the response of the generator speed is almost identical over the whole speed range between 12 m/s and 20 m/s, a fact that indicates, that the gain scheduling controller, described in [1-5]. The power controller keeps the active power to 2 MW with a small deviation about 0.5 %. Since the pitch mechanism reacts slowly compared to the power controller, dynamic variations in the generator speed and so in the rotational speed of the turbine rotor are allowed in order to absorb fast wind gusts and to

temporarily store surplus power as rotational power in the turbine's inertia. The simulation results confirm a good dynamic performance of the DFIG wind turbine model and of the developed control strategy during deterministic wind speeds.

SYSTEM PERFORMANCE UNDER STOCHASTIC WIND SPEEDS

In the following, simulations under stochastic wind speeds are performed. Three sets of simulations will be presented:

(i) a simulation with a mean wind speed of 8 m/s, when the turbine operates at partial load only,

(ii) a simulation with a mean wind speed of 12 m/s, when the operation of the turbine changes between partial and full load,

(iii) a simulation with a mean wind speed of 20 m/s, where moreover the ability of the DFIG wind turbine to regulate its power to imposed reference values is underlined.

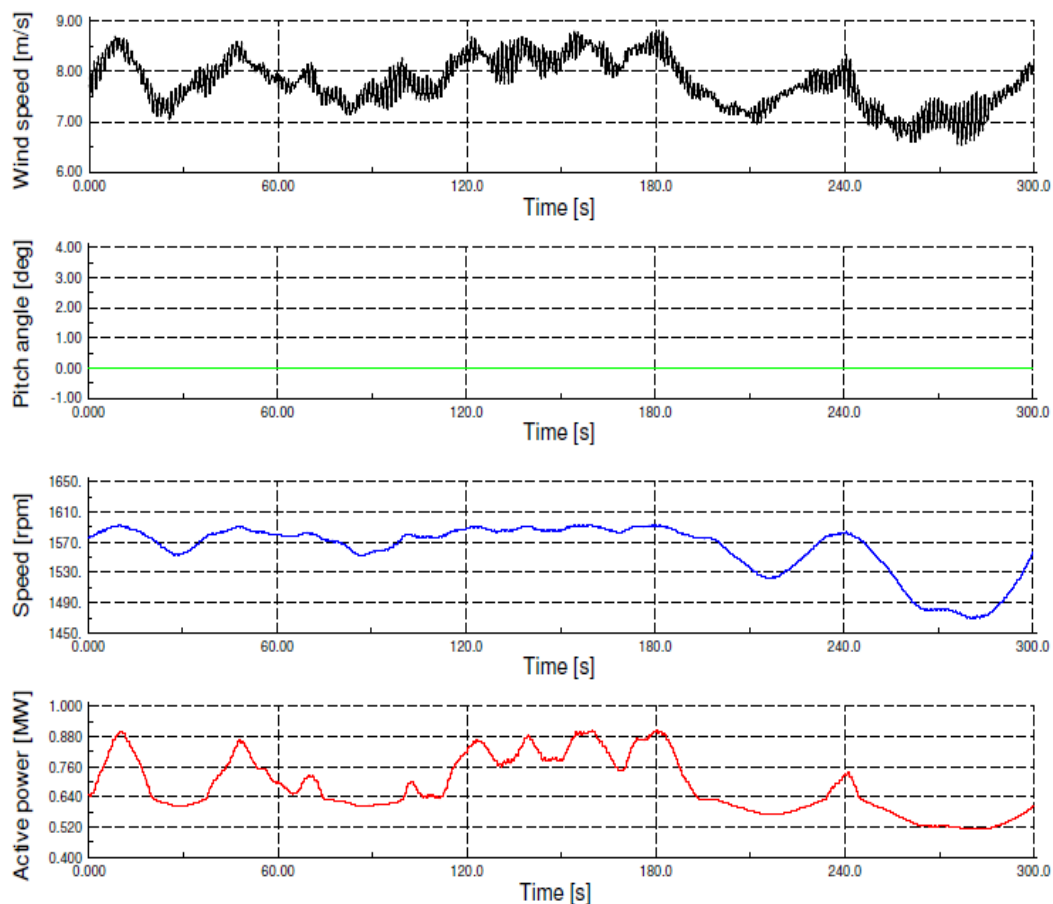


Figure: A.I.3. DFIG wind turbine: Wind speed, pitch angle, generator speed and active power under stochastic wind speed with a mean wind speed of 8 m/s.

Figure A.I.3 shows the turbine quantities pitch angle, rotational speed and active power for a fluctuating wind with a mean wind speed of 8 m/s and a turbulence intensity of 10 %. The turbine operates at partial load only, so that the pitch mechanism is passive. The pitch angle is kept to zero while the speed and the power are adapted to capture the maximal power out of the wind. As expected the speed and the power are tracking the slow variations of the wind speed.

Figure A.I.4 illustrates simulation case (ii) with a mean wind speed of 12 m/s. In this case the pitch mechanism is activated when the speed exceeds its rated value. Notice, that the power is limited to rated power as long as the pitch mechanism is active. Small dynamic variations of the speed above rated speed are allowed to absorb fast wind gusts and to reduce the mechanical stress on turbine and generator system.

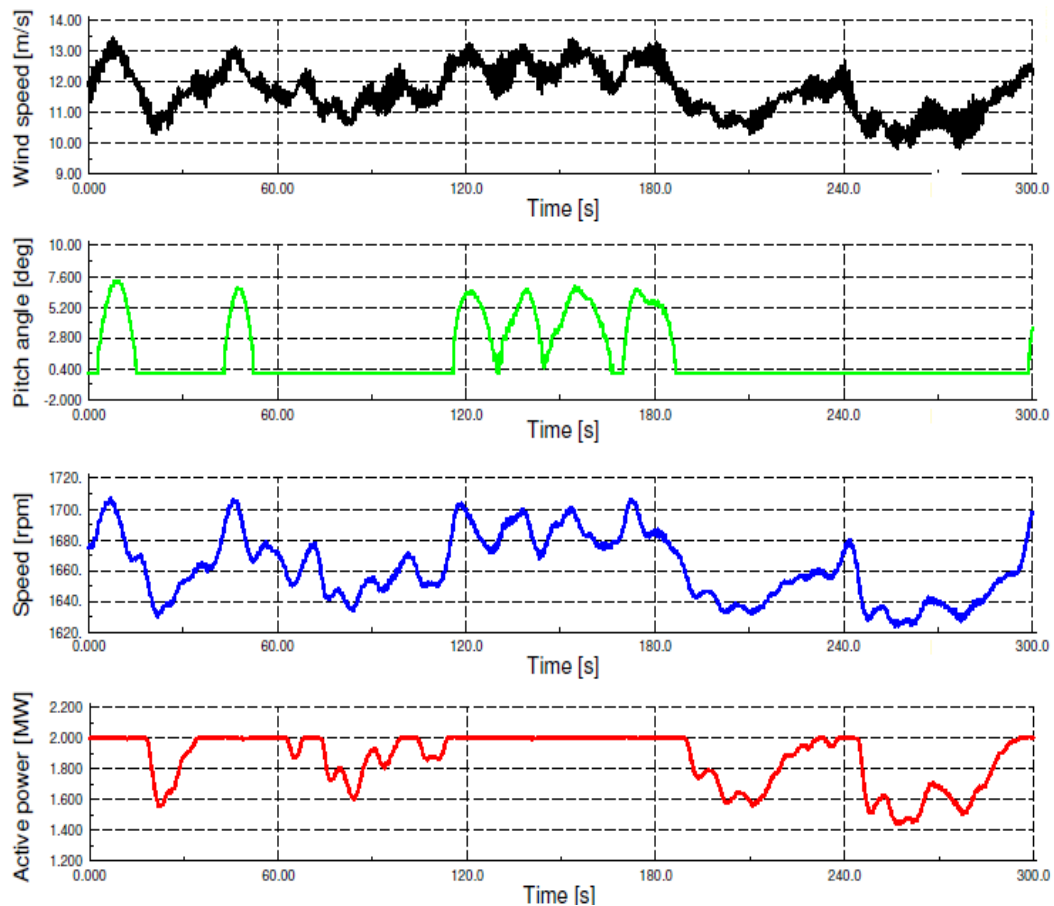


Figure: A.I.4.DFIG wind turbine: Wind speed, pitch angle, generator speed and active power under stochastic wind speed with a mean wind speed of 12 m/s.

Finally, the simulation results of Figure A.I.5 illustrate the ability of the variable speed wind turbine with DFIG to regulate its power production to an imposed reference value and moreover underline the feature of independent active and reactive power control. Figure A.I.5 illustrates the pitch angle, the generator speed as well as the active and reactive power in case of turbulent wind with a mean wind speed of 20 m/s and a turbulence intensity of again 10 %.

The pitch angle signal reflects the stochastic character of the wind and is tracking the slow variations of the wind speed. However, independent of the fluctuations of the wind, the active power can be controlled and limited to 2 MW. The reference power is reduced from 2 MW to 1 MW between 100 and 200 seconds and stepped up back again to 2 MW. Notice that the active power output is following this reference very well. This is however only possible, if the wind speed is sufficiently high. The reduced reference power of 1 MW implies higher pitch angles. The first 250 seconds the reactive power is controlled to zero. Then the same active power control sequence is repeated for a different reactive power reference of 0.5 MVAR. Figure A.I.5 points out, that the designed control strategy of the variable speed wind turbine model with DFIG is able to control active and reactive power independently to specific imposed values, exactly as a conventional power plant does.

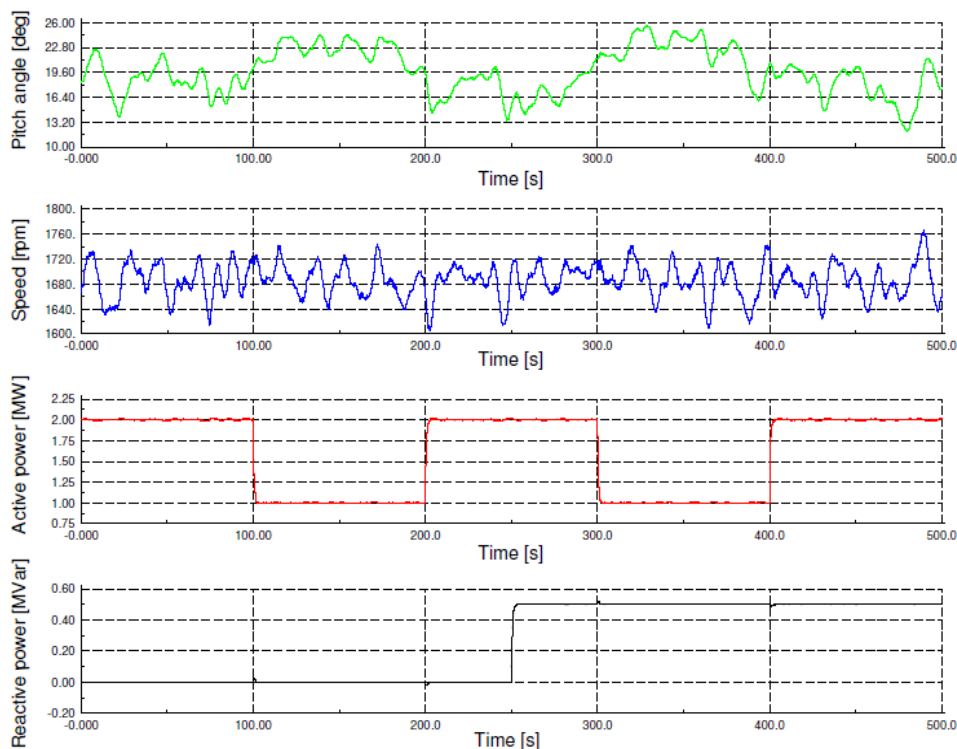


Figure: A.I.5. DFIG wind turbine: Pitch angle, generator speed and active and reactive power production under stochastic wind speed with a mean wind speed of 20 m/s.

The goal of the present work is to develop dynamic simulation models of variable speed wind turbines and to design appropriate control strategies enabling the turbines to act as active components in the power system similar to conventional power plants. Chapter 3 focuses on the design and investigation of the entire control system for a variable speed wind turbine with doubly-fed induction generator, the most commonly used wind turbine concept today. A comprehensive dynamic simulation model is developed in the simulation tool DIGSILENT. In a first step a detailed analysis of the doubly-fed induction generator's steady state behavior is presented.

The steady state power curves of the generator corresponding to different adjusted rotor voltage vectors are illustrated. Different rotor voltage vectors cause a significant change in the shape of the power curves, which in turn enhances the controllability of the generator and the turbine system. In a second step a dedicated control strategy of the DFIG system is designed. The control is realized by vector control technique using appropriate reference frames. The control of the wind turbine is achieved by two coordinated controllers: a speed controller and a power controller. The turbine power is directly controlled by the converter, while the generator speed is regulated by the pitch angle.

The converter control is furthermore subdivided into rotor side converter control and grid side converter control. The rotor side converter controls the generator's active and reactive power production on the grid, while the grid side converter control maintains a constant DC-link voltage and assures converter operation at unity power factor. The controller parameters are designed and optimized based on a set of step response simulations. A set of simulations is performed in order to illustrate that the presented control method successfully controls the variable speed DFIG wind turbine within a range of normal operational conditions.

At wind speeds less than the rated wind speed the converter seeks to maximize the power according to the MPP-tracking. At large wind speeds the speed controller permits a dynamic variation of the generator speed in order to avoid mechanical stresses, while the converter keeps the power to the rated power. The control strategy facilitates furthermore independent control of active and reactive power to imposed reference values at variable speed. However, active power production is still dependent on the actual wind speed. Nevertheless, it can be concluded, that the DFIG wind turbine can operate in a similar manner as a conventional power plant does.

ANNEXURE II

Design of the Mechanical and Electrical system of 2 MW DFIG Wind Turbine

The most relevant data of the aerodynamical and mechanical system of the wind turbine is given in Table A.II.1. The data is valid for DFIG wind turbine and these data are used for Digsilent simulation.

Table A.II.1: Data of the wind turbine's mechanical system.

Rotor diameter	80 m
Rotor inertia	8.6 106 kg m ²
Air density	1.225 kg/m ³
Tip speed ratio	70 m/s
Rotational rotor speed	9...16.7 rpm dyn. 19 rpm
Optimal pitch angle	0 deg
Servo time constant	0.1 s
Pitch angle limits	0...30 deg
Pitch angle rate of change limitation	10 deg/s

The most relevant data of the DFIG wind turbine's electrical system is given in Table A.II.2.

Table A.II.2: Data of the DFIG wind turbine's electrical system.

Apparent power	2.21 MVA
Generator active power (p.u. base)	2 MW
Rating of the IGBT back-to back voltage source converter	0.9 MVA
Stator voltage	690 V
Rated speed	1686 rpm
Synchronous speed (p.u. base)	1500 rpm (= 1p.u.)
Speed range	800 rpm...1686 rpm dynamic limit 1920 rpm
Pole pairs	2
Generator inertia	150.9 kg m ²
Gear ratio	101
DC-link voltage	1.4 kV
DC-link capacitor	1461 μ F

Design of the Mechanical and Electrical system of 1.5 MW DFIG Wind Turbine

The most relevant data of the aerodynamical, mechanical and electrical system of DFIG wind turbine is given in Table A.II.3. The data is valid for DFIG wind turbine and these data are used for Matlab/Simulink/PLECS simulation.

Table A.II.3: Data of the DFIG wind turbines electrical system and DVR .

Rated Power	1.5MW
Rated Voltage(line)	575V
Frequency	50Hz
Stator/rotor turns ratio	1
Stator resistance	0.0014 Ω
Rotor resistance	0.992m Ω
Stator leakage inductance	89.98 μ H
Rotor leakage inductance	82.09 μ H
Magnetizing inductance	1.53mH
Pole pairs	2
Bus capacitance	38mF
Turbine radius	35m
Rated wind speed	12m/s
DVR DC Voltage	560 V
DVR DC Capacitance	7.5mF

Experimental Parameter List

The parameters of experimental setup of DFIG system are shown in Table A.II.4.

Table A.II.4: Data of the DFIG wind turbines electrical system.

Prime Mover	7.5KW	Generator	7.5KW
Converter	5kw	Sw.freq	10kHz
DC	650 V	Phase	3
V/line-line (RMS)	230V	Frequency	50Hz

```

*****
*****M File for 1.5MW DFIG-Wind Turbine*****
*****

%This file is used for initializing the switching simulation
clear all
%Lookup table data for wind turbine torque model
load('TmLookupData.mat');
% Initial conditions with wind speed = 12 m/s
load('DFIGinit_sw_12.mat'); %loads init_val
Vw1 = 12;
Vw2 = 10.5;
% %Initial conditions with wind speed = 10.5 m/s
% load('DFIGinit_sw_10_5.mat'); %loads init_val
% Vw1 = 10.5;
% Vw2 = 8;

%Simulation times
Tstop = 3; %Length of simulation
Tswitch = 1.5; %Time at which wind speed is switched
%Turbine parameters needed for MPT
TSR_opt = 8;
R = 35;
gearbox = 75.7098;

%Grid parameters
Vpp = 470; %peak phase voltage = 575V line rms
f=50;
L = 0.6e-3; %grid side converter inductance
%Rotor converter variables
Udc= 1200;

%Induction Generator Parameters
Rs=0.0014; %ohm
Ls=8.998e-5; %H
Rr=9.9187e-4; %ohm
Lr=8.2088e-5; %H
Lm=1.526e-3; %H
J=5; %or 50 %kgm2
zp=2;
N1=1;
N2=1;
u=1;

%Gain of current loop
kp_i = 0.00003;
ki_i = 0.003;

%Power electronics
fs=10000; %switching frequency - rotor side converter
fs1 = 5000; %switching frequency - grid side converter

```

ANNEXURE III

INTERNATIONAL CONFERENCES AND JOURNALS

S.Chandrasekaran, C.Rossi, D.Casadei, “Modeling and Simulation of Grid Connected Wind Energy Conversion System (WECS) Based on a Doubly Fed Induction Generator (DFIG)”, the Third International Renewable Energy Congress, December 20-22, 2011 – Hammamet, Tunisia.

S.Chandrasekaran, C.Rossi, D.Casadei, A.Tani, “Improved Control Strategy of Wind Turbine with DFIG for Low Voltage Ride Through Capability” International Symposium on Power Electronics, Electrical Drives, Automation and Motion, 2012, Sorrento, Italy.

S.Chandrasekaran, D.Casadei, A.Tani, Poul Sørensen, Frede Blaabjerg, Paul McKeever, “Implementation of Electrical Simulation Model for IEC Standard Type-3A Generator”, European Modelling Symposium(EMS 2013),20-22 November 2013,Manchester,UK.

S.Chandrasekaran, C.Rossi, D.Casadei, Frede Blaabjerg, “Experimental Verification of Power Flow Performance of Grid Connected Doubly Fed Induction Generator”, The 16th European conference on Power Electronics(EPE 2014),Finland(submitted).

S.Chandrasekaran, D.Casadei, C.Rossi, A.Tani, Frede Blaabjerg, “Comparison of Control Strategies for the Active and Reactive Power of DFIG Under Unbalanced Grid Fault”,22nd International Symposium on Power Electronics, Electrical drives, Automation and Motion (SPEEDAM)2014,Italy(submitted).

S.Chandrasekaran, C.Rossi, D.Casadei, A.Tani “Control Algorithm for Grid Code Requirement of DFIG Based Wind Turbine under Fault Ride Through Capability” Electrical & Computer Engineering: An International Journal (ECIJ) ISSN 2201-5957.

S.Chandrasekaran, C.Rossi, D.Casadei, A.Tani “Grid Connected Wind Energy Conversion System based on a Doubly Fed Induction Generator (DFIG)”International Journal of Electrical Engineering-IJOEE.

S.Chandrasekaran, C.Rossi, D.Casadei “Modeling and Simulation of Grid Connected Doubly Fed Induction Generator (DFIG) Based Wind Turbine with Varying Wind Speed” IET Renewable Power Generation Journal, RPG-2012-0280(Acceptedd).

S.Chandrasekaran, C. Rossi, D. Casadei, A.Tani “Improved Control Strategy of DFIG with Wind Turbine for Low Voltage Ride Through Capability” International Journal of Electrical Power & Energy Systems, IJEPES-D-12-01001(Accepted).